



# Regulatory Mechanisms of Bacterial Stress Responses

Dissertation  
zur  
Erlangung des Doktorgrades  
der Naturwissenschaften  
(Dr. rer. nat.)

am Fachbereich der Biologie  
der Philipps-Universität Marburg

vorgelegt von

Hannah Piepenbreier

aus Geseke

(Abschluss: Erste Staatsprüfung für das Lehramt an Gymnasien)

Marburg, Mai 2019

Die Untersuchungen zur vorliegenden Arbeit wurden von Januar 2016 bis Mai 2019 am LOEWE-Zentrum für Synthetische Mikrobiologie (SYNMIKRO) der Philipps-Universität Marburg unter der Leitung von Dr. Georg Fritz durchgeführt.

Vom Fachbereich Biologie der Philipps-Universität Marburg  
als Dissertation angenommen am: 09.05.2019

Erstgutachter: Dr. Georg Fritz

Zweitgutachter: Prof. Dr. Torsten Waldminghaus

Tag der mündlichen Prüfung: 27.06.2019

Hochschulkennziffer: 1180



The studies presented in this dissertation have been published or submitted for publication in the following articles and manuscripts:

**Paper I:** Keppel, M.\*, Piepenbreier, H.\*, Gätgens, C., Fritz, G., and Frunzke, J. (2019) Toxic but tasty - temporal dynamics and network architecture of heme-responsive two-component signaling in *Corynebacterium glutamicum*. *Mol Microbiol* **111**: 1367-1381.  
(\*equal contributions)

**Paper II:** Piepenbreier, H., Diehl, A., and Fritz, G. (2019a) Minimal exposure of lipid II cycle intermediates triggers cell wall antibiotic resistance. *Nat Commun* **10**: 2733.

**Paper III:** Piepenbreier, H., Sim, A., Kobras, C.M., Radeck, J., Mascher, T., Gebhard, S., and Fritz, G. (2019b) (in preparation) From modules to networks: A systems-level analysis of the bacitracin stress response in *Bacillus subtilis*.

**Paper IV:** Piepenbreier, H., Fritz, G., and Gebhard, S. (2017) Transporters as information processors in bacterial signalling pathways. *Mol Microbiol* **104**: 1-15.

## Contents

<b>Zusammenfassung</b> .....	VII
<b>Summary</b> .....	IX
<b>1. Introduction</b> .....	1
1.1 General components of stress response networks.....	2
1.2 Mathematical modelling of bacterial stress response networks .....	5
<b>2. Heme stress response in <i>Corynebacterium glutamicum</i></b> .....	13
2.1 Bacterial responses to heme stress .....	14
2.2 The heme stress response in <i>Corynebacterium glutamicum</i> .....	17
2.3 Paper I: Toxic but tasty – temporal dynamics and network architecture of heme responsive two-component signalling in <i>Corynebacterium glutamicum</i> .....	19
2.4 Conclusion and Outlook.....	20
<b>3. <i>Bacillus subtilis</i> response towards cell wall antibiotics</b> .....	22
3.1 Bacterial response strategies towards antimicrobial compounds .....	24
3.2 The bacterial cell wall as prime target for antibiotic compounds.....	27
3.3 Cell envelope stress response in <i>Bacillus subtilis</i> .....	32
3.4 Paper II: Minimal exposure of lipid II cycle intermediates triggers cell wall antibiotic resistance .....	36
3.5 Paper III: From modules to networks: A systems-level analysis of the bacitracin stress response in <i>Bacillus subtilis</i> .....	40
3.6 Conclusion and Outlook.....	41
<b>4. References</b> .....	45
<b>A. Publications</b> .....	63
A.1 Toxic but tasty – temporal dynamics and network architecture of heme responsive two-component signalling in <i>Corynebacterium glutamicum</i> .....	64
A.2 Minimal exposure of lipid II cycle intermediates triggers cell wall antibiotic resistance .....	107
A.3 From modules to networks: A systems-level analysis of the bacitracin stress response in <i>Bacillus subtilis</i> .....	142
A.4 Transporters as information processors in bacterial signalling pathways .....	180
<b>Acknowledgements</b> .....	196

## List of Figures

Figure 1: Components of bacterial stress response networks.....	3
Figure 2: Mathematical rate laws for complex reaction schemes.....	8
Figure 3: Heme stress response network in <i>C. glutamicum</i> .....	17
Figure 4: Bacterial stress responses towards antimicrobial compounds.....	26
Figure 5: The Gram-positive and Gram-negative cell envelopes.....	28
Figure 6: The lipid II cycle is a prime target for antibiotics in Gram-positive bacteria.....	30
Figure 7: Bacitracin stress response in <i>B. subtilis</i> .....	34
Figure 8: The asymmetric distribution of the lipid II cycle intermediates generates a massive <i>in vivo</i> efficacy gap for lipid II targeting antibiotics.....	37
Figure 9: Prediction of the <i>in vivo</i> efficacy for various cell wall antibiotics in diverse Gram-positive organisms.....	39

## Abbreviations

<b>AMP</b>	Antimicrobial peptide
<b>CESR</b>	Cell envelope stress response
<b>CM</b>	Cell membrane
<b>CW</b>	Cell wall
<b>ECF</b>	Extracytoplasmic function
<b>GlcNAc</b>	N-acetylglucosamine
<b>HK</b>	Histidine kinase
<b>LPS</b>	Lipopolysaccharide
<b>LTA</b>	Lipoteichoic acid
<b>MIC</b>	Minimal inhibitory concentration
<b>MurNAc</b>	N-acetylmuramic acid
<b>ODE</b>	Ordinary differential equation
<b>OM</b>	Outer membrane
<b>PBP</b>	Penicillin-binding protein
<b>PG</b>	Peptidoglycan
<b>RR</b>	Response regulator
<b>TA</b>	Teichoic acid
<b>TCS</b>	Two-component system
<b>UDP</b>	Uridine diphosphate
<b>UP</b>	Undecaprenyl phosphate
<b>UPP</b>	Undecaprenyl pyrophosphate
<b>UppP</b>	Undecaprenyl pyrophosphate phosphatase
<b>WTA</b>	Wall teichoic acid

## Zusammenfassung

Schnelle Anpassungen an ständig wechselnde Umweltbedingungen sind von zentraler Bedeutung für das Wachstum und Überleben von Bakterien. Ausgereifte Stressantwort-Systeme erlauben es Bakterien, Schwankungen in Umweltfaktoren wie pH, Temperatur, Osmolarität, oder Nährstoff- und Schadstoffkonzentrationen sensitiv wahrzunehmen und adäquat darauf zu antworten. Häufig tragen mehrere miteinander gekoppelte Mechanismen, die von einem komplexen Netzwerk aus Signal-Transduktions-Kaskaden, Stoffwechselwegen und Genexpressions-Regulation kontrolliert werden, zur bakteriellen Stressantwort gegenüber einem spezifischen Stressor bei. In dieser Dissertation werden bakterielle Stressantworten gegenüber zwei verschiedenen Stressoren analysiert, wobei ein besonderer Fokus auf den Regulationsmechanismen liegt, die die Gesamtantwort bestimmen.

Der erste Teil dieser Dissertation befasst sich mit der Häm-Stressantwort in *Corynebacterium glutamicum*. Häm ist ein essentieller Cofaktor und alternative Eisenquelle für nahezu alle Bakterien. In hohen Konzentrationen ist Häm jedoch stark giftig, sodass die Häm-Homöostase sehr genau kontrolliert werden muss. Es ist daher eine zentrale Frage, wie Bakterien Häm-Stressantworten regulieren, um Häm nutzen zu können aber sich gleichzeitig vor Vergiftungen zu schützen. Es wird gezeigt, dass *C. glutamicum* einen Mechanismus zur Häm-Entgiftung (gesteuert über den Häm-Exporter HrtBA) und einen Mechanismus zur Häm-Nutzung (gesteuert über die Häm-Oxygenase HmuO) in zeitlicher Hierarchie einleitet, wobei die Entgiftung der Nutzung vorgeschaltet ist. Ein kombinierter Ansatz aus experimentellen Reporter-Messungen und mathematischer Modellierung zeigt auf, wie die unterschiedlichen biochemischen Eigenschaften der beiden Zwei-Komponenten-Systeme, die Häm in *C. glutamicum* detektieren - ChrSA und HrrSA - sowie ein zusätzlicher Regulator (der globale Eisen-Repressor DtxR) diese hierarchische Aktivierung der beiden Stressantwort-Systeme kontrollieren. Diese Analyse beleuchtet die mehrschichtige Häm-Stressantwort, die zur Häm-Homöostase in *C. glutamicum* beiträgt, und verbessert dadurch das Verständnis von bakteriellen Strategien, eine so ambivalente Substanz wie Häm zu beherrschen.

Der zweite Teil dieser Dissertation konzentriert sich auf bakterielle Antwortstrategien gegenüber Zellwand-Antibiotika, die maßgeblich zur Antibiotikaresistenz von Bakterien beigetragen. Um der Resistenzentwicklung entgegenzuwirken, ist es von entscheidender Bedeutung zu verstehen, wie Zellwand-Antibiotika die bakterielle Zellwandbiosynthese stören und welche Strategien Bakterien anwenden, um sich vor Zellwand-Zerstörung zu schützen. Der ersten Frage wird mit Hilfe eines mathematischen Modells nachgegangen, welches den bakteriellen Zellwand-Syntheseweg - den Lipid II Zyklus - sowie dessen Verhalten unter Einfluss von Antibiotika beschreibt. Es zeigt sich, dass die einzelnen Zwischenprodukte innerhalb des Lipid II Zyklus stark ungleichmäßig verteilt sind und dass die Wirksamkeit eines Antibiotikums *in vivo* mit der Verfügbarkeit des Zwischenprodukts, das durch das Antibiotikum gebunden wird, skaliert: Je weniger das Zwischenprodukt vorhanden ist, desto geringer ist die Wirksamkeit eines Antibiotikums, das an dieses Zwischenprodukt bindet, um die Zellwand-Biosynthese zu hemmen. Dies führt dazu, ein neues Prinzip der ‚minimalen Exposition zellulärer Zielstrukturen‘ als intrinsischen Resistenzmechanismus zu formulieren und es wird gezeigt, dass die dadurch hervorgerufene Resistenz vermindert werden kann, wenn Antibiotika kooperativ an ihre Ziele binden. Von diesen Erkenntnissen kann die Entwicklung neuer Medikamente im Kampf gegen Antibiotika-Resistenz deutlich profitieren. Eine experiment-basierte Erweiterung des Modells ermöglicht es schließlich, das Zusammenspiel verschiedener Stressantwort-Mechanismen, die vor einem Antibiotikum schützen, zu analysieren. Hier liegt der Fokus auf der gut untersuchten Antwort von *Bacillus subtilis*

gegenüber dem Zellwand-Antibiotikum Bacitracin. Die Studie zeigt auf, dass das Zusammenspiel zwischen BceAB, der Determinante, die die Stressantwort primär bestimmt und Bacitracin-Entgiftung bewirkt, und BcrC, der Determinante, die sekundär zur Stressantwort beiträgt indem sie die Zellwand-Homöostase schützt, durch die Eigenschaften des Lipid II Zyklus selber kontrolliert wird. Indem diese Analyse Regulationsmechanismen der mehrschichtigen Bacitracin-Stressantwort entschlüsselt, trägt sie zu einem verbesserten Verständnis bakterieller Antibiotikaresistenz bei.

Diese kumulative Dissertation ist wie folgt strukturiert: In Kapitel 1 werden die zentralen Komponenten der Stressantwort-Netzwerke, die in dieser Dissertation untersucht werden, vorgestellt und die Nutzung mathematischer Modelle motiviert, um zugrundeliegende Regulationsmechanismen, die die Gesamtantwort bestimmen, zu verstehen. Daran schließt sich ein kurzer Überblick über die mathematischen Ansätze an, die genutzt wurden, um die Stressantworten in dieser Dissertation zu modellieren. In Kapitel 2 wird die kombinierte Studie aus Theorie und Experiment zur Häm-Stressantwort in *C. glutamicum* vorgestellt. Kapitel 3 präsentiert die quantitative Analyse der Wirkung von Zellwandantibiotika und der Bacitracin-Stressantwort in *B. subtilis*. Die vier Publikationen, die die Grundlage dieser Dissertation bilden, sind im Anhang A zu finden.

## Summary

Bacterial growth and survival critically hinges on the ability to rapidly adapt to ever-changing environmental conditions. Elaborated stress response systems allow bacteria to sensitively detect and adequately respond to fluctuations in environmental conditions, such as pH, temperature, osmolarity, or the concentrations of nutrients and harmful substances. Often, bacterial stress responses towards a specific stressor involve multiple interconnected mechanisms - controlled by a sophisticated network involving signal-transduction cascades, metabolic pathways and gene expression regulation. In this thesis, bacterial stress responses towards two different environmental stressors are analysed; mainly focussing on the regulatory mechanisms that give rise to the overall cellular response.

The first part of this thesis addresses the heme stress response in *Corynebacterium glutamicum*. Heme is an essential cofactor and alternative iron source for almost all bacterial species but can cause severe toxicity when present in elevated concentrations. Consequently, heme homeostasis needs to be tightly controlled. Therefore, one important challenge is to understand how bacteria regulate heme stress responses to both benefit from heme while simultaneously eliminating the associated toxicity. It is shown that *C. glutamicum* induces a heme detoxification mechanism (mediated via the heme exporter HrtBA) and a heme utilization mechanism (mediated via the heme oxygenase HmuO) in a temporal hierarchy, with prioritisation of detoxification over utilization. A combined approach of experimental reporter profiling and computational modelling reveals how differential biochemical properties of the two two-component systems that sense heme in *C. glutamicum* - ChrSA and HrrSA - and an additional regulator (the global iron-regulator DtxR) control this hierarchical expression of the two stress response modules. This analysis sheds light on the multi-layered heme stress response that contributes to overall heme homeostasis in *C. glutamicum* and adds on to the understanding of bacterial strategies to deal with the Janus-faced nature of heme.

The second part of this thesis focusses on bacterial response strategies towards cell wall antibiotics, which play a key role in bacterial antibiotic resistance. To combat resistance evolution, it is important to understand how cell wall antibiotics affect bacterial cell wall biosynthesis and how bacteria orchestrate stress response mechanisms to protect themselves from cell wall damage. The first question is addressed through a comprehensive mathematical model describing the bacterial cell wall synthetic pathway - the lipid II cycle - and its systems-level behaviour under antibiotic treatment. It is found that the lipid II cycle features a highly asymmetric distribution of pathway intermediates and that the efficacy of antibiotics *in vivo* scales directly with the abundance of targeted pathway intermediates: The lower the relative abundance of a lipid II intermediate within the lipid II cycle, the lower the *in vivo* efficacy of an antibiotic targeting this intermediate. This leads to the formulation of a novel principle of 'minimal target exposure' as an intrinsic bacterial resistance mechanism and it is demonstrated that cooperativity in drug-target binding can mitigate the associated resistance. The development of new drugs to counteract antibiotic resistance clearly benefit from these insights. The second question is then addressed by an experimental-based expansion of the model, which allows the analysis of the interplay between multiple stress response mechanisms that protect against a single antibiotic - focussing here on the well-studied response of *Bacillus subtilis* towards the cell wall antibiotic bacitracin. This study reveals that the properties of the lipid II cycle itself control the interaction between the primary bacitracin stress response determinant BceAB mediating bacitracin detoxification, and the secondary determinant BcrC, which contributes to cell wall homeostasis under bacitracin treatment. By

elucidating regulatory mechanisms of the multi-layered response towards bacitracin, this analysis contributes to an advanced understanding of bacterial antibiotic resistance.

This cumulative thesis is structured as follows: In Chapter 1, the basic components of bacterial stress response networks investigated in this thesis are introduced and a motivation why it is beneficial to use computational modelling to understand underlying regulatory mechanisms that give rise to the overall response is given. This is followed by a brief overview of the mathematical approaches used to model the bacterial stress responses in this thesis. In Chapter 2, the combined study of theory and experiment of the heme stress response in *C. glutamicum* is presented. Chapter 3 introduces the quantitative analyses of cell wall antibiotic action and the bacitracin stress response in *B. subtilis*. The full texts of the four publications described within this thesis are attached in Appendix A.



# 1. Introduction

Bacteria thrive in a variety of habitats where growth and survival critically depend on the present environmental conditions. Both the shortage of useful and the presence of harmful substances in the cell's environment as well as deviations in abiotic environmental factors such as temperature, osmolarity, and pH from their optimum can significantly impair bacterial growth and thus, represent distinct stress for the bacterial cell. Consequently, bacteria have evolved a variety of elaborated strategies to sensitively monitor these critical environmental parameters and to respond to variations with appropriate adaptations in cell physiology and metabolism to survive (partly extensive) periods of stress and starvation. These so-called bacterial stress responses are generally controlled by complex networks that involve the interplay of signal-transduction cascades, metabolic pathways and gene expression interactions (Ropers *et al.* 2009). For instance, it is a common strategy to increase the expression of uptake systems of nutrients or osmotic solutes in response to starvation or osmotic stress, respectively, while the expression of specific export or detoxification systems is frequently induced when harmful substances are present. Furthermore, more drastic stress responses, such as the physical movement of motile bacterial cells away from harmful substances (chemotaxis) as well as the formation of dormant, non-reproducing cells (sporulation) that can persist unfavourable environmental conditions for long periods of time, appear in different bacterial species (Moat *et al.*, 2002; Storz and Hengge, 2011). These diverse stress response strategies allow bacteria to survive ever-changing environmental conditions. Thus, in order to understand bacterial physiology, it is an important challenge to uncover *how* bacteria respond to environmental stressors and also *why* they behave this way. It is the aim of this thesis to better understand selected bacterial stress responses that are critical for growth and survival of bacterial organisms - mainly focussing on the underlying networks controlling the cellular stress responses.

In general, even though the various bacterial stress response networks feature high diversity, the fundamental components comprising them are conserved: (i) Signal transduction modules that initially detect a stress signal, process the input signal and subsequently relay it and (ii) the cellular response modules that elicit changes in physiology or metabolism in response to the stress signal (Storz and Hengge, 2011). The network architecture however, can become highly complex. For instance, the integration of several stress signals and the coordination of cellular response mechanisms on multiple levels, which are key to ensure rapid and precise adaptation to the ever-changing environmental conditions, often require intricate regulatory mechanisms. Although many of the individual components of bacterial stress response networks have been identified by experimental approaches, the principles that regulate the interplay between these well-studied components remained mostly elusive. When dealing with networks of the described size and complexity, underlying regulatory mechanisms that give rise to the overall response can not be easily elucidated through experiments. Here, theoretical models - when calibrated by experiments - have been proven as promising tools to overcome the challenge of this complexity and to link the behaviour of a stress system to the interactions between its components. For instance, computational studies revealed important regulatory features of the fine-tuned interplay between diverse modules that impact the decision of sporulation (Bischofs *et al.*, 2009; Gauvry *et al.*, 2019; Iber *et al.*, 2006; Igoshin *et al.*, 2006; Ihekwa *et al.*, 2014; Jabbari *et al.*, 2011; Narula *et al.*, 2012; Schultz *et al.*, 2009) and spore-revival (Mutlu *et al.*, 2018) in response to nutrient availability in *Bacillus subtilis*. Furthermore, they showed the importance of negative feedback mechanisms in the pH stress response and

osmoregulation of *Escherichia coli* (Fritz *et al.*, 2009; Heermann *et al.*, 2014), and deciphered the design principles of the *E. coli* heat shock response network (El-Samad *et al.*, 2005; Kurata *et al.*, 2006). Beyond that, within more global, coarse-grained theoretical frameworks, the dependence of the bacterial growth rate from environmental conditions such as essential nutrients or harmful antibiotics was quantified (Klumpp and Hwa, 2014; Scott and Hwa, 2011; Scott *et al.*, 2010). These studies eventually culminated in the formulation of mathematical relations, referred to as ‘growth laws’, relating the bacterial growth rate to the cellular ribosome content and protein expression, which in turn vary in response to changing environmental conditions (Scott *et al.*, 2010). Jointly, these examples demonstrate the pivotal role of mathematical modelling in understanding complex cellular responses to stressful environmental conditions.

Accordingly, this thesis likewise employs theoretical approaches to study the selected complex bacterial stress response networks and to uncover regulatory mechanisms that determine the cellular stress responses. More precisely, Chapter 2 of this thesis presents a combined study of experiment and theory of a heme stress response system applied by several corynebacterial species, such as *Corynebacterium glutamicum* and *Corynebacterium diphtheriae*. Notably, heme takes here the dual role of a useful and a harmful substance simultaneously: Despite its essentiality for many cellular processes, elevated intracellular heme levels are extremely toxic to the cell, such that uptake, synthesis and utilization have to be carefully balanced (Anzaldi and Skaar, 2010; Choby and Skaar, 2016). A mathematical model elucidates how cells cope with this Janus-faced nature of heme by tightly regulating the expression of a heme detoxification module and a heme utilization module in response to extracellular heme concentrations. Furthermore, in Chapter 3, the cellular response of Gram-positive bacteria to antimicrobial compounds that impair the production of the bacterial cell wall are studied within a theoretical framework. While, on the one hand, bacterial stress responses towards antimicrobial agents ensure growth of competing species in a mixed bacterial population in nature, on the other hand, they also protect pathogenic organisms from getting killed by antibiotics in a medical context and are therefore highly important to understand (Andersson *et al.*, 2016; Bauer and Shafer, 2015; Blair *et al.*, 2015; Nawrocki *et al.*, 2014). A comprehensive model of the bacterial cell wall synthetic pathway deciphers how cell wall antibiotics impair cell wall production and affect cell wall integrity. As will be shown, the cellular pathway itself features important non-trivial emergent properties that influence the degree of stress induced by different cell wall antibiotics. Then, an experiment-based model expansion answered the question how various stress response modules interact to protect the cell wall synthesis and counteract the antibiotic-induced perturbation - focussing here on the stress response towards the cell wall antibiotic bacitracin in the model organism *B. subtilis*. While the respective chapters introduce the precise architecture and characteristics of the investigated stress response networks in detail, the common basic components of these (and many other) bacterial stress response networks as well as the model approaches to describe these quantitatively are reviewed briefly in the following.

## 1.1 General components of stress response networks

### Perception and transduction of external stress signals

To allow for adequate adaptations to environmental stress, one of the major components of bacterial stress response networks are signal transduction modules (Fig. 1, depicted in *blue*)

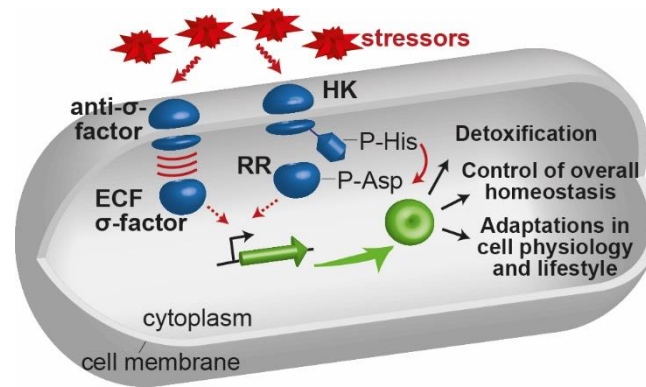


**Figure 1: Components of bacterial stress response networks.** Signal transduction modules (*blue*) perceive the extracellular stress signal and relay information across the cell membrane into the cytoplasm. Upon stress perception, the cytoplasmic regulators of the signal transduction modules stimulate the cellular response (*green*) modules, that is they control the gene expression of target genes, whose gene products participate in the stress response. Cellular response mechanisms are highly diverse. While the stressors considered in this thesis elicit specific detoxification mechanisms to deal with the harmful substances and control mechanisms to maintain overall homeostasis, other stressors induce more general adaptations in the cell's physiology and lifestyle, as they cause for instance sporulation or chemotaxis. For a more detailed mechanistic description of the individual components of the stress response networks please refer to the main text. The figure is adapted from (Piepenbreier *et al.*, 2017).

that sensitively monitor the critical environmental parameters and activate diverse cellular response modules upon stress perception (Moat *et al.*, 2002; Storz and Hengge, 2011). Frequently, the stress signal is present in the cell's environment and thus physically separated from the cytoplasmic response modules by the cell envelope, in particular the cell membrane. The signal transduction modules must therefore relay information about the environmental conditions across this barrier to elicit cellular responses. In general, bacteria employ three different systems that allow transmembrane signal transduction: One-component systems, two-component systems (TCS) and extracytoplasmic function (ECF)  $\sigma$ -factor/transmembrane anti- $\sigma$ -factor units (Butcher *et al.*, 2008; Capra and Laub, 2012; Helmann, 2002; Staroń *et al.*, 2009; Stock *et al.*, 2000; Ulrich *et al.*, 2005). TCS and ECF  $\sigma$ -factor/transmembrane anti- $\sigma$ -factor units are commonly found amongst the signal transduction modules mediating the bacterial response to environmental stressors (Helmann, 2002; Laub, 2011). Central to these two signal transduction modules are membrane-anchored proteins that extend both into the cytoplasmic and the extracytoplasmic space and, therefore, are able to interact with external stress signals and the cytoplasmic regulators of the cellular response modules. The cytoplasmic regulator is usually kept inactive in the absence of an inducing stress signal and becomes activated upon stress perception by the membrane-anchored sensory protein.

In the TCSs relevant for the stress response networks investigated in this thesis, the stimulus perception is performed by a membrane-bound histidine kinase (HK), which interacts with a cytoplasmic response regulator (RR) (Fig. 1) (Capra and Laub, 2012; Mascher *et al.*, 2006; Stock *et al.*, 2000; Zschiedrich *et al.*, 2016). After autophosphorylation at a conserved histidine residue in response to an external stress stimulus, the HK catalyses the transfer of the phosphate group to a conserved aspartate residue of the RR. The RR becomes active by phosphorylation and subsequently acts as a transcriptional regulator, that is it regulates the transcription of target genes by binding to the promoter regions.

The second group of transcriptional regulators that initiate appropriate cellular responses to environmental stresses are the ECF  $\sigma$ -factors (Fig. 1). They can associate with the bacterial RNA polymerase to subsequently guide it to their target promoters (Davis *et al.*, 2017; Helmann and Chamberlin, 1988), thereby regulating the transcription of their target gene. Without the respective stimulus, the ECF  $\sigma$ -factor interacts physically with a (mostly) membrane-anchored

anti- $\sigma$ -factor and is kept inactive (Brown and Hughes, 1995; Helmann, 1999; Kazmierczak *et al.*, 2005). The recognition of the external stress signal by the respective anti- $\sigma$ -factor induces the release and thereby activation of the ECF  $\sigma$ -factor, caused either by conformational change or by regulated proteolysis of the anti- $\sigma$ -factor (Brooks and Buchanan, 2008; Hastie *et al.*, 2013; Paget, 2015; Schöbel *et al.*, 2004).

### **Adaptations in gene expression in response to stress**

The genes, whose expression is controlled by the diverse signal transduction modules, and their respective gene products that protect the bacterial cell from environmental stressors represent the second major component of bacterial stress response networks, namely the cellular response modules (Fig. 1, depicted in *green*). The overall cellular response to a specific environmental stressor, however, involves often not only the regulation of one target gene and is far more complex. In many cases, multiple cellular response modules with varying functions are induced to protect the cell from environmental stress. For instance, both *E. coli* (Arsène *et al.*, 2000; Nonaka *et al.*, 2006) and *B. subtilis* (Helmann *et al.*, 2001; Schumann, 2003) upregulate the expression of a variety of genes in response to high temperatures. These genes encode so-called heat-shock proteins with several different functions, many of which play a key role in preventing protein misfolding under elevated temperatures (Arsène *et al.*, 2000). Furthermore, the pH stress response in *E. coli* comprises multiple mechanisms including adaptations in metabolism and increased production of ion transporters (Maurer *et al.*, 2005; Tucker *et al.*, 2002), which enable the cell to cope with changes in pH. Additionally, it has been shown that bacterial responses towards cell envelope stress often involve mechanisms that actively remove the stressor from the envelope as well as mechanisms that control the cell envelope homeostasis (Jordan *et al.*, 2008; Radeck *et al.*, 2016). As another widespread feature of bacterial stress responses networks, signal transduction modules also regulate their own expression via a positive feedback loop, such that the number of signal transduction modules is increased in response to the stress stimulus (Goulian, 2010; Groisman, 2016; Mitrophanov and Groisman, 2008). In addition, it appears that multiple stress-dependent regulators control the expression of the same target gene, such that several stress input signals need to be integrated at the target gene promoter (Ishihama, 2010). As will be shown, the heme stress response in *C. glutamicum* critically depends on the integration of different stress input signals (Frunzke *et al.*, 2011). Ultimately, cellular response modules themselves can reduce the levels of the stress input signal and thereby influence their own expression pattern via negative feedback, as known for example for transporters that remove harmful substances from the cell (Fritz *et al.*, 2015).

Indeed, these non-linear interactions between signal transduction and cellular response modules, and especially the illustrated feedback loops, significantly influence the overall cellular response to environmental stressor (Brandman and Meyer, 2008; Groisman, 2016; Mitrophanov and Groisman, 2008). For example, negative feedback mechanisms can lead to transient gene expression kinetics and an enduring homeostatic control of the target gene expression in the long term (Fritz *et al.*, 2009). Moreover, positive feedback loops can for instance influence the response time and the response levels of the auto-regulated signalling systems (Mitrophanov *et al.*, 2010; Shin *et al.*, 2006).

Taken together, stress response networks often feature a distinct degree of complexity and involve a variety of non-trivial regulatory mechanisms, which can not be readily understood without theoretical frameworks.

## 1.2 Mathematical modelling of bacterial stress response networks

The complex architecture of the bacterial stress response networks investigated here motivates the use of mathematical modelling to study how the interplay between the individual components of the respective systems give rise to the overall cellular stress response. Of note, every mathematical model is not a faithful copy of the reality but a simplified representation adapted to the biological question being answered with the model. Thus, instead of using a single modelling approach, often multiple modelling techniques are combined to capture the different aspects of the modelled system. In the following, the most important model techniques used to describe the individual components of the stress response networks are reviewed, following closely the book by Ingalls (Ingalls, 2013).

In general, mathematical modelling is usually employed to study time-dependent changes in the abundance of individual molecular species within the system of interest – the system's dynamic behaviour – as this provides insight into existing dependencies of individual molecular species from others within the system. The individual molecular species can represent for instance reactants participating in a chemical reaction, enzymes catalysing biochemical reactions, metabolites of a metabolic network or individual cells interacting within a population. Likewise, the computational studies in this thesis aim to monitor the dynamic changes in the concentrations of the individual molecules involved in the stress response networks to be investigated, such as the transcription factors controlling gene expression or the gene products contributing to the overall stress response. Models that address these kind of questions by describing the time-dependent behaviour of the modelled system are referred to as dynamic mathematical models. Here, the various factors that affect these dynamics, for example environmental conditions or biochemical properties of the molecular species of the system, enter the model as parameters, as will be explained in detail in the course of this section. Within this class of mathematical models, two fundamentally different model approaches exist: (i) Deterministic and (ii) stochastic models. Stochastic models are suitable for describing systems with random interactions between their individual molecular species, that is the system's dynamic behaviour is influenced both by defined conditions and by unpredictable forces (Zheng and Sriram, 2010). Thus, stochastic model approaches are used to investigate processes that depend on small numbers of molecules and can be strongly affected by stochastic fluctuations in the molecule abundances, such as gene expression regulation on single-cell level (Booth *et al.*, 2007; Choudhary *et al.*, 2014; Hasty *et al.*, 2001; Mettetal *et al.*, 2006, Schultz *et al.*, 2007). Furthermore, they are applied to study cell-to-cell variations in growth (Alonso *et al.*, 2014; Thomas *et al.*, 2018) and metabolism (Tonn *et al.*, 2019). Stochastic modelling therefore usually requires elaborated and time-consuming experiments quantifying the abundances of the molecular species involved in the modelled system on a single-cell level, such as microfluidics or microscopy (Kutalik *et al.*, 2005; Potvin-Trottier *et al.*, 2018). However, in many biological processes a large number of molecules are involved, such that stochastic fluctuations in molecule abundances are insignificant and the system's dynamic behaviour is instead dependent on the average numbers of the individual molecules (Zheng and Sriram, 2010). Here, deterministic models provide an adequate approximation of the biological system. They are based on the assumption that the behaviour of the modelled system is exclusively dependent on a defined set of conditions and certain interactions between the involved molecular species and therefore exactly reproducible when conditions are identical. Deterministic models are often applied to study complex biological reaction systems comprising multiple individual molecular species, such as bacterial stress response networks (Bischofs *et al.*, 2009; El-Samad *et al.*, 2005; Hahl and Kremling, 2016; Igoshin *et*

*al.*, 2006; Ihekwaba *et al.*, 2014; Ropers *et al.*, 2009). These systems are frequently investigated within bacterial populations to quantify the population-averaged number of involved molecules without accounting for single-cell variations. These data can be acquired through high-throughput cell-culture experiments and allow for a comprehensive analysis of the complex systems. Accordingly, in this thesis, a deterministic model approach is applied to understand the general principles that shape the population-averaged cellular responses to several environmental stressors.

One of the most frequently used deterministic model approaches consists of ordinary differential equations (ODEs), which describe - in a general sense - the production and decay rates of the individual molecular species of the system. Let  $x(t) = (x_1(t), \dots, x_n(t))$  the vector of the concentrations of the individual molecular species of the modelled system at time point  $t$ , and  $p = (p_1, \dots, p_m)$  the vector of all model parameters that determine the system's behaviour. Then, the dynamic changes in the concentrations of the individual molecular species can be quantitatively described by a set of ordinary differential equations having the following general form:

$$\frac{d}{dt}x_i(t) = f_i(x(t), t, p), \quad i \in \{1, \dots, n\}$$

where  $\frac{d}{dt}x_i(t)$  represents the rate of changes in  $x_i(t)$  and  $f_i(\cdot)$  is a (usually highly) nonlinear function that relates the rate of changes in  $x_i(t)$  to the time-dependent concentrations of all individual molecular species and the model parameters (Ropers *et al.*, 2009, Zheng and Sriram, 2010). This so-called 'rate-equation' approach<sup>1</sup> and has been applied to a wide range of biological systems, for example the description of metabolism (Kremling *et al.*, 2007), signalling (Groban *et al.*, 2009, Kremling *et al.*, 2004; Rowland and Deeds, 2014; Shinar *et al.*, 2007) or gene regulation (reviewed e.g. in Mackey *et al.*, 2004; Vilar *et al.*, 2003). Central to this modelling approach, however, is to define the functions  $f_i(\cdot)$ , that is to find a mathematical expression for the rate of each reaction of the modelled system, which critically depends on the type and complexity of the reaction itself. Here, some general principles allowed the mathematical description of the reaction rates of many standard biological reactions, as reviewed in the following. They eventually guide the quantification of more complex reaction schemes, as illustrated in Figure 2, and also represent the basis for the computational models of the stress response networks developed in this thesis.

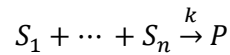
## Derivation of mathematical rate equations

The simplest and most fundamental quantification of reaction rates is formulated in the law of mass action, which was first postulated by Gulberg (1836-1903) and Waage (1833-1900) (Voit *et al.*, 2015). It is based on the assumption that the probability of a reaction occurring is proportional to the probability of the reactants colliding in the reaction volume with one another. Accordingly, the law of mass action states that the rate of a reaction is proportional to the

---

<sup>1</sup> The 'rate-equation' approach is based on two fundamental assumptions: (i) All molecules are equally distributed in the space where the reactions occurs (e.g. the cell, a specific cell compartment etc.) (referred to as spatial homogeneity), so that the rate of a reaction is independent of position and space where the reaction occurs (ii) Each individual molecule species is abundant in a high number. This assumption allows the approximation of discrete changes in numbers of the species by continuous changes in concentrations of the species (based on the continuum hypothesis).

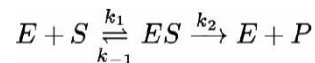
product of the concentrations of the reactants. Thus, for a simple chemical reaction involving  $n$  different reactants  $S_1, \dots, S_n$  that form a product  $P$



the rate equation describing the changes in the concentration of  $P$  is given by

$$\frac{d}{dt}p(t) = k \prod_{i=1}^n s_i(t),$$

where  $s_i(t)$  and  $p(t)$  represent the concentration of the reactant  $S_i$  and the product  $P$  at time  $t$ , respectively, and  $k$  is the constant of proportionality, referred to as rate constant in the mass action formalism (Murray, 2002). In the first instance, this law provides a mathematical description for simple reactions that are independent from regulation or from assistance by enzymes, which are also part of bacterial stress response networks (e.g. the spontaneous decay of molecules). Beyond that, the law of mass action also represents the basis for the description of the much more complex reaction schemes (Voit *et al.*, 2015). For instance, the quantitative framework of an enzyme-catalysed reaction can be derived by applying the law of mass action. The individual events involved in the conversion of a substrate  $S$  to a product  $P$  catalysed by an enzyme  $E$  can be written as



For simplification, henceforward the time-dependent concentrations of the individual reactants are denoted by  $[\cdot]$ . Applying the law of mass action, the rate equations take the form

$$\begin{aligned} \frac{d}{dt}[S] &= -k_1[S][E] + k_{-1}[ES] \\ \frac{d}{dt}[E] &= -k_1[S][E] + k_{-1}[ES] + k_2[ES] \\ \frac{d}{dt}[ES] &= k_1[S][E] - k_{-1}[ES] - k_2[ES] \\ \frac{d}{dt}[P] &= k_2[ES] \end{aligned}$$

Under the assumptions that (i) the first reaction is fast and rapidly in equilibrium ( $\frac{d}{dt}[ES] \approx 0$ ) and (ii) the enzyme is not consumed in this reaction, that is the total enzyme concentration  $[E_{TOT}]$  is constant ( $[E_{TOT}] = [E] + [ES]$ ) (Murray, 2002), the system of differential equations can be condensed to a single rate equation describing the production rate of product  $P$

$$\frac{d}{dt}[P] = [E_{TOT}] * k_{cat} * \frac{[S]}{K_M + [S]}.$$

The arising rate equation is the well-known Michaelis-Menten equation with the Michaelis constant  $K_M = \frac{k_{-1} + k_2}{k_1}$  and  $k_{cat} = k_2$ , referred to as enzyme's catalytic constant (Michaelis and Menten, 1913). Of note, the rate of enzyme-catalysed reactions approaches a limit defined as the maximal velocity  $V_{max} = [E_{TOT}] * k_{cat}$ , which is caused by enzyme saturation. This basic Michaelis-Menten rate equation can be modified and expanded to describe much more complex enzyme-catalysed reactions involving multiple substrates, such as the Ping-Pong mechanism (Stein, 2011; Voet, D. and Voet, J., 2011), which is analysed in Figure 2A.



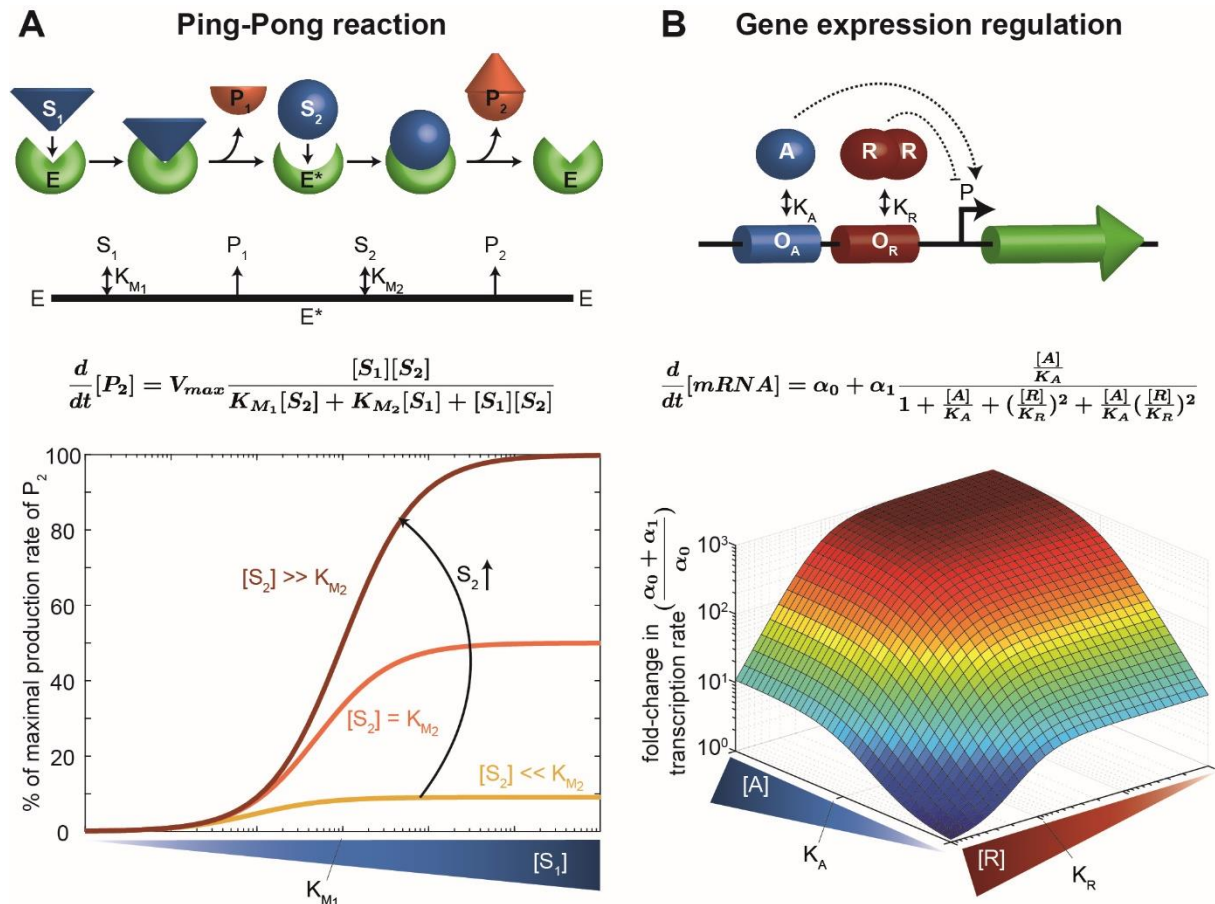


**Figure 2: Mathematical rate laws for complex reaction schemes.** The quantification of complex reaction schemes, involving multiple reactants and regulation, are explained through example systems. All parameters are chosen arbitrary and the scales of the plots are expressed relative to these parameters. **(A)** Ping-Pong or double displacement enzyme reactions involve multiple substrates, where one (or more) products are released before all substrates are bound. In these reactions, the enzyme change into an intermediate form after a first substrate-to-product reaction and is then able to bind a second substrate and catalyse conversion. In the illustrated example, the first substrate ( $S_1$ ) binds to the standard form of the enzyme ( $E$ ) with Michaelis constant  $K_{M_1}$ . The enzyme catalyses the conversion to the first product ( $P_1$ ) and remains in a modified state ( $E^*$ ), which can be bound by the second substrate ( $S_2$ ) with Michaelis constant  $K_{M_2}$ . The modified form of the enzyme eventually catalyses the formation of the second product ( $P_2$ ) and is thereby restored to its initial form. The production rate of  $P_2$  is given by a modified Michaelis-Menten term (Voet, D. and Voet, J., 2011), which reveals that the rate is determined by the concentrations of both substrates and the respective Michaelis constants. As the log-plot for varying concentrations of  $S_1$  and several fixed concentrations of  $S_2$  illustrates, the maximal rate  $V_{max}$  can only be achieved when both substrates are present at saturating concentrations, that is  $[S_i] \gg K_{M_i}$ . Enzymes featuring such Ping-Pong mechanisms are frequently found in bacteria and, for instance, fulfil diverse roles in *E. coli* (Axley and Grahame, 1991; Goodenough-Lashua and Garcia, 2003; Gyamerah and Willetts, 1997; Pejchal *et al.*, 2005) - to list only some examples. **(B)** Gene expression regulation by a transcriptional activator ( $A$ , blue) and a dimeric repressor ( $R$ , red). Both regulators can bind either individually or simultaneously to their respective operator sites ( $O_A$  and  $O_R$ , respectively) on the promoter  $P$  of the gene (depicted in green) with dissociation constants  $K_A$  and  $K_R$ . If the repressor  $R$  is bound, only basal transcription at rate  $\alpha_0$  occurs. The activated state of the promoter results from exclusive binding of the activator  $A$  to the promoter, such that the maximal transcription rate ( $\alpha_0 + \alpha_1$ ) is reached when the promoter is saturated with activator  $A$  and no repressor  $R$  is bound, as illustrated in the three-dimensional log-log-plot. The colour codes for the fold-change in the transcription rate, which is given by  $\frac{\alpha_0 + \alpha_1}{\alpha_0}$ . An increase in repressor concentration leads to a more pronounced decrease in the transcription rate than a decrease in the activator concentration due to the dimeric nature of the repressor. A gene regulation scenario as illustrated here is found in the heme stress response in *C. glutamicum* (Frunzke *et al.*, 2011; Wennerhold and Bott, 2006).



All enzyme-catalysed reactions involved in the stress responses that will be analysed in this work are quantified by applying Michaelis-Menten-like kinetics.

In contrast to the reactions considered so far, which are independent from any regulation, the majority of biological reactions are regulated. Their reaction rates depend not only on the concentrations of the reactants but also on the presence/absence of the regulators. As demonstrated in the previous section, regulatory mechanisms are key to bacterial stress responses, both on a genetic level as well as on protein level, such as the regulation of enzyme activity. Thus, in the remainder of this section, the mathematical framework for describing regulated reactions, which again is based on the application of a mass-action formalism, is introduced. As a common mechanism, regulation in the selected stress response networks is mediated by regulator molecules that bind to specific sites on the regulated structure. In case of the regulation of enzyme activity, regulator molecules bind either to the active site (competitive inhibition) or to the allosteric site (allosteric regulation) of the enzyme and thereby control the rate of substrate conversion (Voet, D. and Voet, J., 2011). Likewise, the regulation at the genetic level is mediated through transcription factors, which bind to so-called operator sites on the promoter of the regulated gene and thereby modulate the binding efficiency of the RNA polymerase to the promoter and thus the rate of gene transcription (Balleza *et al.*, 2008; Ishihama, 2010). Consequently, the rate of a regulated reaction critically depends on whether a regulator is bound to the respective binding site or not and is thus determined by the fractional occupancy of the binding sites of the regulated structures, that is the fraction of binding sites that are occupied by regulators compared to the total number of binding sites (Bintu *et al.*, 2005b; Voet, D. and Voet, J., 2011). More precisely, dependent on the function of the regulator (activator or repressor), the rate of a regulated reaction is either proportional to the fraction of bound regulators (in case of activation) or proportional to the fraction of unbound regulators (in case of repression) (Bintu *et al.*, 2005b). Applied to enzyme regulation, this means that the reaction rate of a regulated enzyme-catalysed reaction is given by a Michaelis-Menten term, which is scaled by a factor that quantifies the fractional occupancy of the regulation sites of the enzyme (Voet, D. and Voet, J., 2011). For example, when considering the regulation of an enzyme by an allosteric inhibitor, which binds independently from the substrate, the reaction occurs on maximal rate when the inhibitor is unbound and accordingly, the production rate of product P of the enzyme-catalysed reaction is given by

$$\frac{d}{dt}[P] = V_{max} * \frac{[S]}{K_M + [S]} * \frac{1}{1 + \frac{[I]}{K_I}}$$

Here, the fractional occupancy of the allosteric site is determined by both, the inhibitor concentration  $[I]$  and the affinity of the inhibitor to the allosteric site of the enzyme  $K_I$ . Of note, the Michaelis-Menten term itself also contains a description of fractional occupancy, namely the fractional occupancy of the enzyme's active site by the substrate, which actually determines the reaction rate of an unregulated reaction. In the context of gene expression regulation, the rate of gene transcription scales with the fractional occupancy of the promoter by transcription factors, as this determines the probability that the RNA polymerase is bound to the promoter of the gene (Bintu *et al.*, 2005a; Bintu *et al.*, 2005b)<sup>2</sup>. Accordingly, the

<sup>2</sup> The quantitative description of gene expression dependent on the occupancy of the different promoter regulation sites is generally termed 'thermodynamic modelling' (Bintu *et al.*, 2005a; Bintu *et al.*, 2005b). The approach introduced here combines thermodynamic modelling to describe promoter-transcription factor-interaction with differential equation modelling to describe dynamic changes in levels of molecules involved in gene expression and gene products.

transcription rate of a gene controlled by a transcription activator A, that is the rate of production of the respective mRNA, is given by

$$\frac{d}{dt}[mRNA] = \alpha_0 + \alpha_1 \frac{\frac{[A]}{K_A}}{1 + \frac{[A]}{K_A}},$$

while a repressor R affects the transcription rate as follows

$$\frac{d}{dt}[mRNA] = \alpha_0 + \alpha_1 \frac{1}{1 + \frac{[R]}{K_R}}.$$

Here  $[A]$  and  $[R]$  display the concentration of the activator and repressor, respectively, and  $K_A$  and  $K_R$  are the corresponding dissociation constants of promoter binding.  $[mRNA]$  denotes the concentration of the mRNA of the transcribed gene. Furthermore, the basal transcription rate<sup>3</sup> without regulation is given by  $\alpha_0$ , while  $\alpha_0 + \alpha_1$  represents the maximal rate of transcription. However, since the rate of activated transcription  $\alpha_1$  is usually unknown and it is rather possible to determine the fold-change between basal and maximal transcription rate, a modified expression is commonly used to quantify transcriptional activation:

$$\frac{d}{dt}[mRNA] = \alpha_0 \left( \frac{1 + \omega \frac{[A]}{K_A}}{1 + \frac{[A]}{K_A}} \right),$$

at which the fold-change is defined by  $\omega = \frac{\alpha_0 + \alpha_1}{\alpha_0}$  (Bintu *et al.*, 2005b).<sup>4</sup> Finally, to account for multiple regulators with different functions (activator or repressor) acting on the same target structure (promoter or enzyme), all possible binding states are considered and the reaction rate is proportional to the fraction of binding sites that are in an activated state compared to the total number of binding sites (Bintu *et al.*, 2005b). For instance, two independent transcription activators  $A_1$  and  $A_2$ , which bind to non-overlapping binding sites on a promoter with dissociation constants  $K_{A_1}$  and  $K_{A_2}$ , affect the of transcription rate as follows:

$$\frac{d}{dt}[mRNA] = \alpha_0 + \alpha_1 * \frac{\frac{[A_1]}{K_{A_1}} + \frac{[A_2]}{K_{A_2}} + \frac{[A_1][A_2]}{K_{A_1}K_{A_2}}}{1 + \frac{[A_1]}{K_{A_1}} + \frac{[A_2]}{K_{A_2}} + \frac{[A_1][A_2]}{K_{A_1}K_{A_2}}}.$$

Here, both, the individual binding of  $A_1$  and  $A_2$  and the combination can activate the transcription. This theoretical framework represents the basis for the mathematical description of arbitrarily complex regulation scenarios, one of which is part of the heme stress response network of *C. glutamicum* and is discussed as an example in Fig. 2B. To mention further impressive examples, the complex regulation of the *E. coli lac*-operon as well as the control of several promoters of phage  $\lambda$  were also studied analogously (Bintu *et al.*, 2005a). All these examples demonstrate the power of this model approach to study complex bacterial regulatory

<sup>3</sup> In case of transcriptional repression,  $\alpha_0$  represents the 'leak' of the promoter, as absolute repression can never be achieved.

<sup>4</sup> The modified expression arise from the previous one as follows:

$$\alpha_0 + \alpha_1 \frac{\frac{[A]}{K_A}}{1 + \frac{[A]}{K_A}} = \frac{\alpha_0 \left(1 + \frac{[A]}{K_A}\right) + \alpha_1 \frac{[A]}{K_A}}{1 + \frac{[A]}{K_A}} = \frac{\alpha_0 + (\alpha_1 + \alpha_0) \frac{[A]}{K_A}}{1 + \frac{[A]}{K_A}} = \alpha_0 \frac{1 + \frac{\alpha_1 + \alpha_0}{\alpha_0} \frac{[A]}{K_A}}{1 + \frac{[A]}{K_A}} = \alpha_0 \frac{1 + \omega \frac{[A]}{K_A}}{1 + \frac{[A]}{K_A}}$$

networks, featuring not only multiple, but also interacting regulators. Hence, all regulatory mechanisms involved in the stress response networks, including gene and protein regulation, are quantified based on the demonstrated approach.

In summary, the model techniques introduced here represent the set of tools that guide the development of the ODE-based mathematical models of the stress response networks in this thesis. Of note, complex, non-trivial interaction networks such as stress response networks are usually described by a large systems of ODEs, which cannot be solved analytically. Instead, numerical simulations are used to approximate the exact solution.

### Calibration of mathematical models

The value of any mathematical model depends critically on how precise the real biological scenario is represented by the theoretical description - in other words, on the accuracy of the parameters. As briefly mentioned above, model parameters represent the physiological conditions of the systems being analysed, such as environmental parameters or biochemical properties of molecule species that are part of the system. Therefore, it is one of the major tasks of mathematical modelling to find appropriate parameter values for the model, referred to as model calibration. Sometimes, model parameters can be measured directly by experiments. For instance, degradation rates of the proteins can be determined from observations of half-lives and enzyme assays reveal the kinetic parameters of an enzyme. However, various model parameters are not directly accessible by experiments and need to be assigned by so-called parameter fitting approaches instead. Parameter fitting generally aims to find the values for the model parameters for which the model simulations best match available experimental data of the system of interest - in other words, values for which the model most likely describes the system's behaviour (Press *et al.*, 1999). For instance, measured time-course data as well as steady-state concentrations of the individual molecule species of a system can be mimicked by a model and an optimal set of model parameters should minimize the deviation between the model predictions and experimental data (Geier *et al.*, 2012). One of the most commonly used methods for parameter calibration is least-squares fitting. The method of least squares is based on maximum likelihood estimation (Press *et al.*, 1999). In maximum likelihood estimation, the likelihood of a parameter set is given by the probability of observing the available experimental data in the model (Jaqaman and Danuser, 2006). Thus, the most likely and therefore optimal parameter set is obtained by maximizing this likelihood. Consider a system involving  $n$  individual molecule species, whose behaviour depends on  $m$  parameters,  $p = (p_1, \dots, p_m)$ .  $y = (y_1, \dots, y_n)$  represents a vector of population-averaged experimental data (see above for details) and  $x(p) = (x_1(p), \dots, x_n(p))$  is the vector of the corresponding model data. As every experiment is generally subject to inevitable uncertainties, for example regarding the preparation procedure or laboratory conditions, each data point  $y_i$  has a certain measurement error  $\epsilon_i$  (Geier *et al.*, 2012). Supposing these measurement errors are uncorrelated and normally distributed<sup>5</sup>, the likelihood  $L$  of the parameter set  $p$  is given by the probability to observe the data set  $y$  in the model:

$$L(p|y) = \prod_{i=1}^n \frac{1}{\sqrt{2\pi\sigma_i^2}} \exp\left(-\frac{(y_i - x_i(p))^2}{2\sigma_i^2}\right),$$

<sup>5</sup> These assumptions apply in many practical settings (Geier *et al.*, 2012).

where  $\sigma_i^2$  indicates the variance in the measurement errors of  $y_i$  (Jaqaman and Danuser, 2006). Maximizing  $L$  is equivalent to maximizing its logarithm, or minimizing the negative of its logarithm<sup>6</sup>

$$-\log(L(p|y)) = \sum_{i=1}^n \log\left(\sqrt{2\pi\sigma_i^2}\right) + \frac{(y_i - x_i(p))^2}{2\sigma_i^2}.$$

Since the term  $\log\left(\sqrt{2\pi\sigma_i^2}\right)$  is independent of  $p$ , minimizing the negative log likelihood is equivalent to minimizing the weighted sum of squared residuals  $\chi^2$  (Geier *et al.*, 2012, Press *et al.*, 1999)

$$\chi^2(p) = \sum_{i=1}^n \frac{(y_i - x_i(p))^2}{\sigma_i^2}$$

and least-square fitting essentially aims to find the values of  $p$  that minimize this function:

$$\min_p(\chi^2(p)).$$

The optimal set of parameters  $p^*$  can be found by numerical function-minimizing techniques (Geier *et al.*, 2012; Press *et al.*, 1999)<sup>7</sup>. In this thesis, a trust-region reflective Newton algorithm imbedded in MATLAB (MATLAB, The MathWorks. Inc) is applied for the parameter fitting problems.

All mathematical models presented in this thesis involve data from multiple experiments, which either determine model parameters directly or allow for indirect determination by parameter fitting following the least-squares approach presented here.

---

<sup>6</sup>  $\log(L(p|y)) = \log\left(\prod_{i=1}^n \frac{1}{\sqrt{2\pi\sigma_i^2}} \exp\left(-\frac{(y_i - x_i(p))^2}{2\sigma_i^2}\right)\right) = \sum_{i=1}^n \log\left(\frac{1}{\sqrt{2\pi\sigma_i^2}} \exp\left(-\frac{(y_i - x_i(p))^2}{2\sigma_i^2}\right)\right) = \sum_{i=1}^n -\log\left(\sqrt{2\pi\sigma_i^2}\right) - \frac{(y_i - x_i(p))^2}{2\sigma_i^2}$

<sup>7</sup> For further reading please refer to (Moles *et al.*, 2003; Press *et al.*, 1999)

## 2. Heme stress response in *Corynebacterium glutamicum*

*‘All things are poison, and nothing is without poison, the dosage alone makes it so a thing is not a poison’ (Paracelsus, 1493-1541)*

*Part of the work described in this chapter was published (Keppel et al., 2019). The full article is attached in the Appendix A.1 (Paper I).*

Bacterial life in ever-changing environmental conditions demands both the protection against harmful substances and the optimal utilization of useful substances that support growth, such as nutrients. The distinction between harmful and useful substances, however, is not always a clear-cut matter. As already emphasized by the Swiss physician and founder of modern toxicology, Paracelsus (1493-1541), ‘*all things are poison, nothing is without poison, the dosage alone makes it so a thing is not a poison*’ (Paracelsus). According to this central maxim, nutrients that naturally support cell growth and survival, can cause severe toxicity when present in elevated concentrations in the cell. Bacterial response mechanisms towards nutrient excess are therefore key to a cell’s survival and a robust regulation of the interplay between detoxification mechanisms and mechanisms for nutrient consumption is essential for optimal cell growth, as has been shown for example for calcium, copper, iron and manganese (Argüello et al., 2013; Chandrangu et al., 2017; Cornelis et al., 2011; Juttukonda and Skaar, 2015; Rosch et al., 2008). One further paradigm that features this Janus-faced nature is the organic molecule heme, which is essential to most bacterial organisms but toxic at high concentrations at the same time. In particular, virtually all bacterial pathogens require heme to cause infections and, accordingly, have evolved elaborated strategies to acquire host-synthesized heme and simultaneously eliminate heme toxicity (Anzaldi and Skaar, 2010; Choby and Skaar, 2016). Thus, as heme stress responses are of such high relevance for bacteria, it is an important challenge to understand how they balance heme uptake, utilization and detoxification to control heme homeostasis, which is essential for growth.

The work presented in this chapter focusses on the heme stress response in the soil bacterium *Corynebacterium glutamicum* and arose in fruitful collaboration with the group of Prof. Dr. Julia Frunzke (Institute of Bio- und Geosciences, IBG-1: Biotechnology, Forschungszentrum Jülich). The heme stress response in *C. glutamicum* comprises the expression of a heme exporter (HrtBA) for detoxification as well as a heme oxygenase (HmuO) for utilization of heme and is regulated by two paralogous heme-responsive TCSs (ChrSA and HrrSA). Interestingly, the dedication of two paralogous TCSs for regulating the response towards heme appears as a unique theme among the *Corynebacteriaceae* family (Bibb et al., 2007; Bott and Brocker, 2012; Burgos and Schmitt, 2016; Frunzke et al., 2011; Heyer et al., 2012). In addition, it has been shown that the TCSs of *C. glutamicum* feature significant cross-talk (Hentschel et al., 2014), that is each of the two HKs is able to phosphorylate both RRs. These observations motivate extensive experimental efforts to decipher the precise role of the two TCSs in the response towards heme in *Corynebacteriaceae*.

Here, we addressed this question through a combined experimental and modelling approach, aiming at a comprehensive quantitative description of the individual components of the heme stress response network in *C. glutamicum* (Paper I). The developed theory was used to analyse the dynamics of the detoxification and utilization module under varying heme levels, both in a wildtype background and when considering several mutations in the TCSs. In

combination with comprehensive reporter assays of the TCSs target promoters, this allowed for the identification of some crucial regulatory mechanisms that shape the heme stress response in *C. glutamicum*, such as negative feedback of the target structures on the stress stimulus and the integration of different input signals on a genetic level. During the course of this thesis, further research has focussed on the precise characterization of the stimulus perception and signal transduction mechanisms of the two TCSs and the impact of every individual TCS on the overall heme stress response (Hentschel *et al.*, 2014; Keppel *et al.*, 2018). The results presented here add to this by shedding light on the mechanisms that regulate the interplay between heme detoxification and heme utilization and the importance of different properties of the TCSs in this context and thereby advance our understanding of heme stress responses in bacteria.

This chapter will start with a brief presentation of the role of heme in bacterial physiology and an overview of the different mechanism bacteria employ to cope with heme toxicity (Section 2.1). Subsequently, the individual components of the heme stress response network in *C. glutamicum* are introduced in detail, with a special focus on the regulatory role of the TCSs, serving as the basis for the formulation of the mathematical model (Section 2.2). Then, the central results of Paper I on the regulation of the interplay between the stress response modules are presented (Section 2.3). Finally, an outlook on possible further applications of the developed model in studying heme stress responses in bacterial organisms is given (Section 2.4).

## 2.1 Bacterial responses to heme stress

### The role of heme in bacterial physiology

Heme, a porphyrin ring complexed with iron, is a versatile molecule that is important for various cellular processes of most bacterial species. For instance, it functions as an electron shuttle in enzymes of the electron transport chain, is required for cellular respiration and plays a crucial role in oxygen metabolism (Choby and Skaar, 2016). In addition, cells critically rely on heme for the function of many important enzymes including cytochromes, hydroxylases, catalases, peroxidases, and hemoglobins (Layer *et al.*, 2010; Poulos, 2007). Moreover, heme represents an important alternative source of iron, which itself is - with only few exceptions - essential to nearly all living organisms (Andrews *et al.*, 2003). In particular, the greatest reservoir of iron for pathogens within human hosts is in the form of host-synthesized heme as a cofactor of hemoproteins, such as the well-known haemoglobin (Contreras *et al.*, 2014; Maresso *et al.*, 2008; Marvig *et al.*, 2014; Pishchany *et al.*, 2010). In the absence of iron, however, also non-pathogenic bacteria rely on the salvage of heme-bound iron, highlighting the physiological relevance of heme for virtually all bacteria.

According to the illustrated importance of heme for bacterial physiology, many bacteria are capable of synthesizing heme endogenously (Choby and Skaar, 2016; Panek and O'Brian, 2002). Beyond that, most pathogenic organisms have evolved elaborated strategies to acquire heme from host sources, ranging from surface receptors to secreted proteins that bind either heme or hemoproteins and induce heme uptake (reviewed e.g. in Anzaldi and Skaar, 2010; Choby and Skaar, 2016; Tong and Guo, 2009). Once inside the cell, heme is either degraded to release free iron or used intact for the functions mentioned above. In most bacteria, the degradation of heme depends on heme oxygenases that catalyse the conversion of heme to biliverdin, thereby liberating iron (Unno *et al.*, 2004; Wilks, 2002). Various members of this

class of enzymes have been characterized for many bacterial species, such as the heme oxygenase HmuO identified in diverse corynebacterial species (Frunzke *et al.*, 2011; Kunkle and Schmitt, 2007; Schmitt, 1997; Wilks and Schmitt, 1998), the *Pseudomonas aeruginosa* PfgA heme oxygenase (Ratliff *et al.*, 2001) and the HemO heme oxygenase of various *Neisseria* spp. (Zhu *et al.*, 2000a; Zhu *et al.*, 2000b) - to list only some examples.

Paradoxically, despite its importance for a variety of cellular processes, heme also has the potential to cause toxicity at high intracellular concentrations. Although the toxicity of heme towards bacteria has been observed for a long time (Anzaldi and Skaar, 2010; Everse and Hsia, 1997; Nitzan *et al.*, 1987; van Heyningen, 1948), the mechanism of how this molecule interferes with bacterial physiology is not conclusively unravelled. However, several studies showed that the heme toxicity is likely the result of a combination of membrane disruption, membrane protein and lipid oxidation, and DNA damage (Anzaldi and Skaar, 2010; Choby and Skaar, 2016; Imlay *et al.*, 1988; Nir *et al.*, 1991; Wakeman *et al.*, 2012). Thus, bacteria employ various strategies to tightly regulate the intracellular concentration of heme and overcome heme toxicity, as will be introduced in the following paragraph.

### **Bacterial strategies to cope with heme toxicity**

As common for bacterial stress responses, the responses towards toxic concentrations of heme comprise of both the sensing of heme concentrations and appropriate cellular response mechanisms. While the cellular response mechanisms towards toxic concentrations of heme will be introduced in a first instance, bacterial heme sensing mechanisms are discussed in the subsequent paragraph.

Bacteria employ several diverse strategies to avoid heme toxicity, ranging from preventive mechanisms, such as the control of heme biosynthesis and uptake, to detoxification mechanisms, such as heme export, sequestration, and degradation (Anzaldi and Skaar, 2010). In the following, the detoxification mechanisms will be discussed in greater detail.

As a first well-conserved heme detoxification strategy, heme export systems have been identified in both Gram-positive and Gram-negative bacteria and three systems have been described: HrtBA, PefAB/CD and MtrCDE. The heme-regulated transporter HrtBA is assumed to export heme from the bacterial cytoplasm and is required for resistance to heme toxicity in diverse bacterial species including *Staphylococcus aureus* (Stauff *et al.*, 2008; Torres *et al.*, 2007), *Bacillus anthracis* (Stauff and Skaar, 2009a), *Lactobacillus lactis* (Joubert *et al.*, 2014; Lechardeur *et al.*, 2012), *Streptococcus agalactiae* (Fernandez *et al.*, 2010) and *C. diphtheriae*. (Bibb and Schmitt, 2010). Furthermore, putative Hrt systems can also be found in other Gram-positive pathogens, suggesting that these systems may have evolved to protect pathogens from heme toxicity in their host (Anzaldi and Skaar, 2010). In addition to HrtBA, a second system that mediates heme export has been identified in *S. agalactiae*, comprising of the two putative heme efflux pumps PefAB and PefCD (Fernandez *et al.*, 2010). Finally, it has been shown that the multiple-transferable-resistance efflux system MtrCDE, which provides resistance to hydrophobic agents in *Neisseria gonorrhoeae*, also contributes to resistance to heme stress (Bozja *et al.*, 2004; Hagman *et al.*, 1995).

Sequestration of excess heme is a second strategy to overcome heme toxicity. The best example of heme sequestration is in the eukaryotic parasite *Plasmodium* spp., which has the capability to sequester heme into a nontoxic, highly insoluble substance called hemozoin (Fitch, 1998; Jani *et al.*, 2008). Furthermore, several proteins have been found to bind and

sequester heme and thereby contribute to resistance to heme toxicity in diverse bacterial species (Anzaldi and Skaar, 2010; Choby and Skaar, 2016).

Finally, as a third strategy, the heme oxygenase-mediated degradation of heme outlined as part of heme utilization can also contribute to the reduction of heme toxicity. Although in bacteria most heme oxygenases are implicated primarily in iron acquisition, some have been identified to alleviate heme toxicity (Skaar *et al.*, 2006; Zhu *et al.*, 2000b).

As will be illustrated in the next section, *C. glutamicum* combines a heme export mechanism with a heme degradation mechanism to protect itself from toxic heme concentrations and the interplay of both mechanisms is studied in Paper I.

### Heme sensing in bacteria

Many of the mechanisms involved in the bacterial heme stress responses are not constitutively active but rather induced in response to heme toxicity signals. In Gram-positive species, TCSs appear to be the predominant form of heme sensory systems (Stauff and Skaar, 2009b), which initiate the cellular responses to protect from heme intoxication. *S. aureus* and *B. anthracis*, for instance, both utilize the heme sensory system HssRS to detect toxic heme concentrations and subsequently activate the expression of the *hrtBA* operon (Stauff and Skaar, 2009a; Stauff and Skaar, 2009b; Stauff *et al.*, 2007). Furthermore, as a common theme, *Corynebacteriaceae* dedicate two paralogous TCSs for heme sensing and the appropriate regulation of heme homeostasis, referred to as ChrSA and HrrSA (Bibb *et al.*, 2007; Bott and Brocker, 2012; Burgos and Schmitt, 2016; Frunzke *et al.*, 2011; Heyer *et al.*, 2012). These TCSs coordinate the expression of genes involved in heme biosynthesis, heme detoxification (*hrtBA*) and heme utilization (*hmuO*) amongst others. In contrast to the central role of TCSs in Gram-positive species, an ECF  $\sigma$ -factor controls the heme utilization in the Gram-negative bacterium *Bordetella avium* (Kirby *et al.*, 2004). Here, the membrane-anchored heme sensor protein RhuR interacts with extracellular heme and activates the  $\sigma$ -factor RhuI, which in turn controls the expression of a system involved in heme utilization (*bhuRSTUV*).

In addition to these membrane-anchored heme sensing systems, also intracellular regulators were described to be involved in the control of heme homeostasis and heme stress responses. For instance, the introduced heme detoxification system PefAB/CD in *S. agalactiae* is regulated by the MarR superfamily repressor PefR (Fernandez *et al.*, 2010). While PefR inhibits the expression of the two respective operons *pefAB* and *pefRCD* under low heme conditions, elevated concentrations of intracellular heme induce binding of heme to PefR, which alleviates the inhibition. Moreover, heme homeostasis was also shown to be under control of iron-dependent regulators. Such a mechanism was observed in corynebacterial species, where the master regulator of iron homeostasis, DtxR, integrates information on iron availability into the network controlling heme homeostasis. More precisely, DtxR was shown to repress the expression of *hmuO* heme oxygenase among others under high iron conditions (Schmitt, 1997; Wennerhold and Bott, 2006). In Paper I, the role of DtxR in the heme stress response of *C. glutamicum* is investigated in detail.



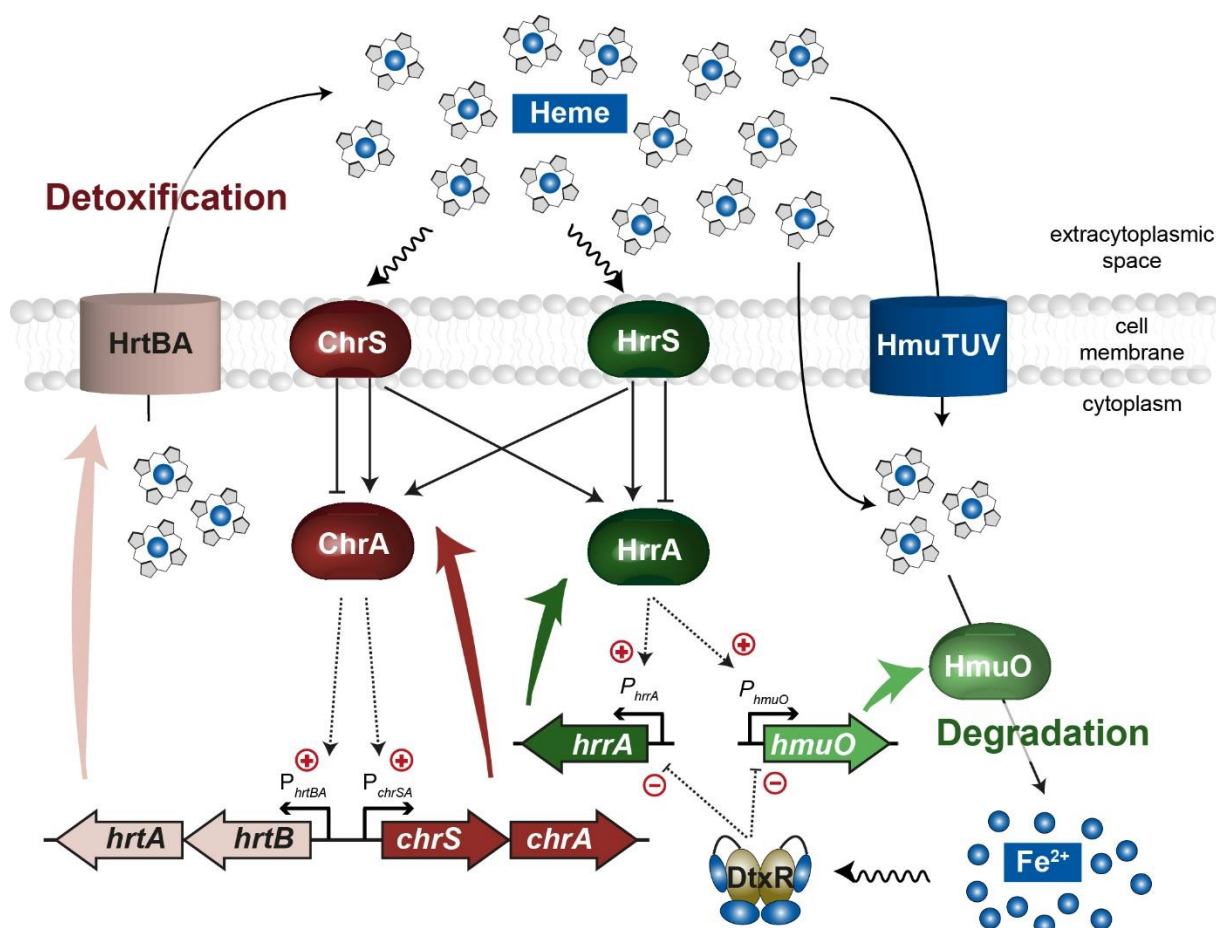


**Figure 3: Heme stress response network in *C. glutamicum*.** For a detailed description please refer to the main text.

## 2.2 The heme stress response in *Corynebacterium glutamicum*

The central components of the heme stress response network in *Corynebacterium glutamicum* are the heme transporter HrtBA and the heme oxygenase HmuO as well as the two TCSs ChrSA and HrrSA and the iron-repressor DtxR (see Fig. 3). Figure 3 also depicts the HmuTUV heme uptake system, which is not part of the heme stress response system but assists transport of heme into the cell (Drazek *et al.*, 2000; Frunzke *et al.*, 2011). In addition, heme can diffuse over the cell membrane into the cell and both processes affect the intracellular heme concentration. The ABC transporter HrtBA is assumed to export excessive heme from the cytoplasm to the extracytoplasmic space, thereby inducing detoxification (Anzaldi and Skaar, 2010). The heme oxygenase HmuO degrades intracellular heme to liberate iron (Anzaldi and Skaar, 2010; Choby and Skaar, 2016) and is therefore relevant for both, heme detoxification as well as the usage of heme as an alternative iron source, as described above. Together, HrtBA and HmuO reduce the intracellular heme concentration and thereby contribute to heme homeostasis and resistance to heme toxicity at the same time.

The expression of the introduced heme stress response modules is regulated by the two paralogous TCSs ChrSA and HrrSA (Bott and Brocker, 2012; Frunzke *et al.*, 2011; Heyer *et al.*, 2012). As the group of Prof. Dr. Julia Frunzke could show, the stimulus perception of both TCSs is mediated by a direct interaction with the input molecule heme (Keppel *et al.*, 2018). Interestingly, this particular setup is the first example of two paralogous TCSs sensing the same stimulus and is not only found in *C. glutamicum* but also in the human pathogen *C. diphtheriae* (Bibb *et al.*, 2007; Burgos and Schmitt, 2016; Schmitt, 1997). Upon recognition of

heme, the HKs ChrS and HrrS of both TCSs undergo autophosphorylation and subsequently catalyse phosphotransfer to their cognate RRs ChrA and HrrA, which are thereby activated. In addition, significant cross-phosphorylation was observed between these two systems (Hentschel *et al.*, 2014), that is both HKs can phosphorylate the non-cognate RR of the other TCS. In the absence of the heme stimulus, ChrS and HrrS feature phosphatase activity and catalyse the dephosphorylation of ChrA and HrrA, respectively. Dephosphorylation of RRs is in general crucial for the termination of the cellular stress response and the reset to the initial, inactivated state after stimulus decline (Mascher *et al.*, 2006; Stock *et al.*, 2000; Zschiedrich *et al.*, 2016). In contrast to the kinase activity, the phosphatase activity of ChrS and HrrS has been shown to be highly specific, such that both HKs can only dephosphorylate their cognate RR (Hentschel *et al.*, 2014). It was previously suggested that this specific dephosphorylation of HrrA and ChrA may counteract the cross-phosphorylation and prevent the inadvertent activation of these regulators, thereby maintaining the specificity of each HK-RR pair in the heme stress response (Hentschel *et al.*, 2014). The question of how the phosphatase activity of the two TCSs affects the dynamics of the two cellular stress response modules in *C. glutamicum* is addressed in Paper I.

Once activated by phosphorylation, the activated RRs bind to the promoters of their target genes and activate the expression of the respective heme stress modules. While HrrA is responsible for the activation of *hmuO* expression, ChrA positively regulates the expression of *hrtBA* (Frunzke *et al.*, 2011; Heyer *et al.*, 2012). Interestingly, despite the identical genetic setup of the TCSs, different regulation was observed in *C. diphtheria* compared to *C. glutamicum*: While *hrtBA* is exclusively regulated by ChrSA in both species alike, *hmuO* was proposed to be controlled by both HrrSA and ChrSA in *C. diphtheriae*, with ChrA being the predominant regulator of *hmuO* expression (Bibb and Schmitt, 2010; Bibb *et al.*, 2005; Bibb *et al.*, 2007). Beyond the regulation of the stress response target genes, it was postulated that the regulons of both RRs comprise several additional genes in *C. glutamicum*. For ChrSA, significant autoregulation was observed (Heyer *et al.*, 2012), that is activated ChrA upregulates the expression of the *chrSA* operon in a positive feedback loop and thereby increases the abundance of ChrSA heme sensory systems under heme stress. In contrast to the small and very specific regulon of ChrSA, HrrSA seems to coordinate a global, homeostatic response to heme and features a much bigger regulon. Genes encoding proteins involved in heme biosynthesis (*hemE*, *hemH* and *hemA*), the respiratory chain (*ctaD* and *ctaE*) and further cellular functions are controlled by activated HrrA (Frunzke *et al.*, 2011). During the course of this thesis, the group of Prof. Dr. Julia Frunzke continued studying the HrrSA regulon and revealed HrrA binds to more than 250 different genomic targets encoding proteins involved in heme homeostasis and a variety of other cellular processes (J. Frunzke, personal communication). In addition, activated HrrA was also suggested to auto-regulate its own expression (Hentschel *et al.*, 2014; Heyer *et al.*, 2012). However, as HrrS and HrrA are not encoded in one operon, they do not feature a co-regulated expression and HrrS is rather assumed to be expressed in a constitutive, heme-independent manner (Heyer *et al.*, 2012).

Ultimately, information on iron availability are also integrated into the heme stress response in *C. glutamicum*. Since the degradation of heme leads to the liberation of iron and iron itself is also toxic to the cell in elevated intracellular concentrations (Andrews *et al.*, 2003; Cornelis *et al.*, 2011), heme degradation needs to be tightly regulated to prevent a toxic iron concentration. Therefore, in *C. glutamicum*, the expression of both *hrrA* and its target gene *hmuO* is repressed by the key regulator of iron homeostasis, DtxR, as indicated above (Wennerhold and Bott, 2006). Upon binding of iron ( $\text{Fe}^{2+}$  ion), DtxR dimerizes and binds to the respective promoters, where it counteracts the heme-dependent target gene activation via HrrA. Several further

corynebacterial species, including *C. diphtheriae*, feature this integration of information on iron concentrations into the network controlling heme homeostasis via DtxR (Schmitt, 1997). Paper I analyses how the integration of these opposing signals on the  $P_{hrrA}$  and  $P_{hmuO}$  promoter dictates the dynamic expression of the heme oxygenase.

In the end, all components presented here are taken into account for the formulation of a quantitative mathematical model of the heme stress response in *C. glutamicum*, which is used to study the regulatory dynamics within the system (Section 2.3).

### **2.3 Paper I: Toxic but tasty – temporal dynamics and network architecture of heme responsive two-component signalling in *Corynebacterium glutamicum***

In the paper ‘Toxic but tasty – temporal dynamics and network architecture of heme-responsive two-component signalling in *Corynebacterium glutamicum*’ by Marc Keppel\*, Hannah Piepenbreier\*, Cornelia Gätgens, Georg Fritz and Julia Frunzke (\*equal contributions) (Keppel *et al.*, 2019), we set out to decipher the factors that shape the dynamic response to heme in *C. glutamicum* by combining experimental reporter profiling with computational modelling. When experimentally monitoring the response of *C. glutamicum* to heme in iron-limiting conditions, we found a temporal hierarchy between the two heme stress response modules: While the detoxification response via HrtBA is nearly instantaneously initiated after stimulus addition and features a transient dynamics, activation of HmuO-mediated heme degradation and utilization is significantly delayed. In fact, the time point of both, deactivation of *hrtBA* expression and activation of *hmuO* expression correlate with the levels of heme in the cell’s environment. To analyse the origin of this temporal hierarchy, we introduced a comprehensive mathematical model for both heme stress modules, including a description of (i) heme-dependent cell growth based on the uptake of extracellular heme and intracellular consumption (ii) the dynamics within the TCSs ChrSA and HrrSA in response to heme, (iii) the regulation of the target gene expression by the activated RRs and DtxR, respectively, and (iv) the effect of HrtBA and HmuO on the extracellular and intracellular heme concentrations. When calibrated with experimental data, we found that this model accurately captures the response characteristics of both heme response modules. By analysing the dynamics of all individual components of the heme stress network, we uncovered that the timing of the shut-off of the detoxification response is causally related to the depletion of external heme concentrations. Supported by growth experiments under varying heme concentrations, we showed that the cellular consumption of external heme, which enables growth under the given iron-limitation, reduces the stress stimulus and thus dictates deactivation of *hrtBA* expression via a negative feedback loop. Thereby, higher initial heme concentrations lead to heme exhaustion at a later time-point compared to lower ones and, consequently, elicit a prolonged induction of the heme detoxification response.

Furthermore, our quantitative analyses and experimental screening of single and double mutants of ChrSA and HrrSA and mutants lacking the phosphatase activity of the HKs further demonstrated that the characteristics of the TCSs critically co-determine the dynamics of both heme stress modules. The transient dynamics and especially the rapid shut-off of the HrtBA response are mainly determined by a strong phosphatase activity of ChrS, which implies immediate dephosphorylation and thereby inactivation of ChrA upon stimulus decline. In contrast, a comparable minor phosphatase activity of HrrS on HrrA can explain the delayed

activation of *hmuO* expression by phosphorylated HrrA RRs despite incipient reduction of the heme stimulus.

Moreover, our results indicate that DtxR decisively contributes to the observed biphasic induction of *hmuO* by initially inhibiting *hmuO* expression within the first hours when intracellular concentrations of heme and iron are high. A decline of internal heme and iron concentrations over time (by heme export via HrtBA and heme and iron consumption) eventually reduces the levels of activated DtxR repressor, so that HrrA-dependent activation of *hmuO* expression takes over as soon as the DtxR concentration drops below a critical threshold.

Taken together, the combination of theory and experiment allowed us to decipher the general principle of the heme stress response in *C. glutamicum*, namely the prioritisation of a detoxification response over heme degradation and utilization, as well as the factors that control this hierarchical activation. The predicted hierarchy between the response strategies is in agreement with reported variations in heme sensitivity of the two heme sensing systems, more precisely a higher sensitivity of ChrSA towards small changes in extracellular heme concentrations than of HrrSA (Keppel *et al.*, 2018). Our study thus illustrates how *C. glutamicum* carefully balances heme detoxification and utilization to account for the Janus-faced nature of heme as a useful and toxic substance at the same time.

## 2.4 Conclusion and Outlook

Most nutrients, which are essential for bacteria, can cause severe toxicity when present in elevated concentrations, as already emphasized by Paracelsus in the 16<sup>th</sup> century. Thus, it is of vital importance for bacterial growth and survival to tightly control the intracellular concentrations of such substances and to initiate proper stress responses when concentrations become critically high. Within this chapter, a comprehensive systems-level characterization of the stress response towards toxic concentrations of one of such Janus-faced nutrients, namely heme, was presented. The results of this study shed light on the regulating factors that shape a temporal hierarchy between the different modules contributing to the heme stress response in *C. glutamicum*. Interestingly, we deciphered how two TCSs, which actually respond to the same stimulus but feature different biochemical properties, and the integration of an additional regulatory system can elicit such a multi-layered, hierarchical physiological response. Variations in phosphorylation and dephosphorylation activities of the histidine kinases as well as the tight control of one of the TCSs and its target gene by an iron-dependent repressor determine the cellular response to a multifaceted stimulus such as heme. These regulatory insights were essentially provided by the theoretical model, as this was able to predict the dynamic changes in the concentrations of active response regulators ChrA and HrrA, which were not accessible by experiments yet – neither in *C. glutamicum* in the lab of Prof. Dr. Julia Frunzke nor in its relative *C. diphtheriae* (Burgos and Schmitt, 2016).

The physiological relevance of the strict prioritisation of heme detoxification over heme utilization can be understood when looking more closely at the process of heme degradation via HmuO. Since degradation of heme liberates iron, which is just as harmful as heme in elevated concentrations, it seems highly plausible that *C. glutamicum* initially employs the detoxification transporter HrtBA to reduce elevated heme concentrations and permits heme degradation by HmuO only after intracellular heme concentrations drop below a critical threshold. Thus, the iron-dependent inhibition of *hmuO* expression may protect the cell from

intoxication by iron when aiming to reduce high heme concentrations by degradation. Ultimately, the complex regulation of heme degradation – in particular the integration of an activating and a repressing signal – illustrates how bacteria manage to benefit from nutrients while simultaneously eliminating the associated toxicity.

Finally, as detailed before (Section 2.2), several other experimental studies in *C. glutamicum* could show that the heme stress response systems presented here are part of a much broader heme homeostasis network, comprising for instance systems for heme uptake and heme biosynthesis. Since several of these systems are regulated simultaneously by *hrrA*, it is likely that they mutually affect each other. Thus, on the one hand, it will be interesting to further investigate the individual components of the heme homeostasis network experimentally to address remaining questions, as for instance, whether the uptake of heme is also regulated in a heme- or iron-dependent manner to control heme homeostasis. On the other hand, it will be worthwhile to expand the mathematical model based on these new experimental results to get further insights into the mechanisms that regulate the interplay between all individual components of the heme homeostasis network.

In the end, analogous quantitative studies in pathogens could reveal important insights in how these organisms orchestrate different heme stress modules to deal with high concentrations of heme in the human host. As introduced above (Section 2.1), both heme degradation systems and heme export systems are widespread in bacteria to control heme homeostasis and it would be of interest to investigate if a similar hierarchy between these modules as observed in *C. glutamicum* can be found in other organisms. In particular, as HrtBA-like transporters were found in many Gram-positive pathogens (Anzaldi and Skaar, 2010; Choby and Skaar, 2016) and several of them are likewise controlled by TCSs, it is important to study if these organisms employ similar regulatory mechanisms as *C. glutamicum* to control the interplay between heme export and further detoxification strategies. As a first step into this, it would be interesting to adapt the existing mathematical model to the known regulatory properties of the heme stress response in *C. diphtheriae* (as described in Section 2.2). Actually, it is likely that the here presented results for *C. glutamicum* will be - at least partially - transferable to *C. diphtheriae* due to the similar architecture of the stress response systems. A model adaptation to the specific features of the stress response network of *C. diphtheriae* could help to identify the appropriate adaptations of the two relatives to the particular environmental conditions of their natural habitats (soil in the case of *C. glutamicum* and the upper respiratory system of a host in case of *C. diphtheriae*).

### 3. *Bacillus subtilis* response towards cell wall antibiotics

Part of the work described in this chapter was (Piepenbreier *et al.*, 2017; Piepenbreier *et al.* 2019a) or will be published (Piepenbreier *et al.* 2019b). The full articles are attached in Appendices A.2 (Paper II), A.3 (Paper III) and A.4 (Paper IV), respectively.

Environmental habitats are usually populated by a multitude of different microorganism. Since all environmental resources within such a habitat are finite, resident microorganisms frequently compete for limited resources, such as essential nutrients, in order to survive. Different strategies that provide a competitive advantage in this race have thus evolved in microorganisms. The production of antimicrobial compounds is one of the most prominent strategies, as discovered for the first time by Alexander Fleming in 1928, who found that the growth of staphylococci was significantly impaired in a culture accidentally contaminated with a mould fungus (Fleming, 1929). In mixed microbial habitats, antimicrobial compounds can kill or significantly impair the growth of competitors and are therefore beneficial for the compound-producing microbial species but represent severe stress for all other species within the same habitat. Bacteria, which are frequently faced with such antimicrobial compounds, have consequently entered the arms race by employing various stress response mechanisms against antimicrobial compounds.

In fact, these stress response mechanisms to antimicrobial compounds pose one of the major threats to human health today. In medicine, a multitude of antimicrobial compounds have been established as antibiotics to treat pathogen-caused diseases. However, elaborated strategies to protect against antibiotics have quickly evolved in pathogenic organisms, such that currently the majority (>70%) of bacterial pathogens that cause fatal infections are likely to be resistant to at least one of the clinically relevant antibiotics (Hassan *et al.*, 2012)<sup>8</sup> and more and more multi-resistant pathogens are emerging<sup>9</sup>. To combat this alarming development, a detailed understanding of the mechanisms that bacteria employ to become resistant to antibiotics is of critical importance, as this can guide the development of urgently needed novel classes of antibiotic agents and new treatment strategies for pathogenic infections.

This chapter focusses on bacterial stress responses towards cell wall antibiotics, which represent one of the most important classes of clinically used antibiotic compounds but which are becoming increasingly less effective due to a variety of stress response mechanisms that are protecting bacteria. Cell wall antibiotics interfere with the integrity or biosynthesis of the bacterial cell envelope - the vital cellular protection barrier - and thereby provoke growth arrest or cell lysis (Bugg *et al.*, 2011; Kohanski *et al.*, 2010; Silver, 2003; Silver, 2006; Tomasz, 1979). A common target of most cell wall antibiotics is the lipid II cycle, which represents the essential cellular pathway of cell wall biosynthesis conserved amongst bacteria (as will be introduced in detail in Section 3.2 and illustrated in Fig. 6). Many lipid II cycle-active antibiotics are capable of binding molecules involved in the lipid II cycle, thereby perturbing the progression of the cycle and consequently, the synthesis of the bacterial cell wall (Breukink and Kruijff, 2006; Oppedijk *et al.*, 2016; Schneider and Sahl, 2010). Strikingly, for several of these antibiotics, there are vast differences between their *in vivo* efficacy (Hiron *et al.*, 2011; Mota-Meira *et al.*, 2000; Shaaly *et al.*, 2013; Staroń *et al.*, 2011; Tiyanont *et al.*, 2006; Yoshida *et al.*, 2011)

---

<sup>8</sup> Reported in 2004 by the Infection Disease Society of America (IDSA) (Hassan *et al.*, 2012).

<sup>9</sup> In 2017, the World Health Organisation (WHO) published a list of antibiotic-resistant pathogens that pose the greatest threat to human health and for which new antibiotics are urgently needed ('WHO priority pathogens list for research and development of new antibiotics') (WEB: <https://www.who.int/news-room/detail/27-02-2017-who-publishes-list-of-bacteria-for-which-new-antibiotics-are-urgently-needed>)

compared to their *in vitro* binding affinity to their molecular targets (Beauregard *et al.*, 1997; Hu *et al.*, 2003; Wiedemann *et al.*, 2001) - even in bacterial strains that feature none of the known stress response mechanisms that can protect from antibiotic attack and thereby reduce antibiotic potency *in vivo*. Furthermore, for a specific class of cell wall antibiotics, the so-called glycopeptides, it has been found but not yet conclusively understood that compounds binding in a cooperative manner to their targets have much higher *in vivo* efficacy than variants that are unable to multimerize (Jia *et al.*, 2013; Loll *et al.*, 1998; Wang *et al.*, 2018). Hence, before focussing on stress response mechanisms related to cell wall antibiotics, it is first important to understand (i) how binding of an antibiotic to its target within the lipid II cycle affects the overall progression of cell wall biosynthesis and, accordingly, (ii) what determines - beyond the *in vitro* binding affinity to the cellular target - the *in vivo* efficacy of cell wall antibiotics. In a second step, it is then interesting to address the question (iii) how stress response mechanisms counteract the antibiotic-induced perturbation of the lipid II cycle to protect cell wall biosynthesis. A well-studied example of a sophisticated response towards cell wall antibiotics is the bacitracin stress response in the model organism *B. subtilis*. Three major response modules involved in both detoxification and control of overall homeostasis of cell wall synthesis mediate the response to bacitracin stress in *B. subtilis* (reviewed in Radeck *et al.*, 2017): The bacitracin transporter BceAB, the UPP phosphatase BcrC, and the phage-shock proteins LiaI and LiaH. Interestingly, it has been demonstrated that these modules vary in both, sensitivity towards bacitracin and response intensity (Rietkötter *et al.*, 2008) and a hierarchy among these modules was found, with BceAB representing the primary layer and BcrC and LiaI/H are the secondary layer of the bacitracin stress response (Radeck *et al.*, 2016). However, the mechanisms that regulate this hierarchical induction of the different stress modules and thereby give rise to the overall response towards bacitracin have not yet been conclusively unravelled.

The work presented in this chapter of the thesis approaches all these questions from a quantitative perspective by applying a theoretical model for the cell wall biosynthesis and cell wall stress response in *B. subtilis* (Paper II and III). In Paper II, we first examined the system-level behaviour of the lipid II cycle under antibiotic treatment without stress response systems. Based on a multitude of published biochemical data, we developed a comprehensive mathematical model that quantitatively describes the individual cycle reactions and their interactions, which determine the overall production of the bacterial cell wall. When studying the effect of antibiotic binding on the progression of the lipid II cycle, we found that the *in vivo* efficacy of cell wall antibiotics critically depends on *which* intermediate molecule of the lipid II cycle is bound by the antibiotic and *how* binding occurs (in terms of cooperativity). We were able to attribute this phenomenon to the cyclic nature of the lipid II cycle and a highly asymmetric distribution of intermediates within the cycle, and thereby provided the first mechanistic explanation for the reduced *in vivo* efficacy of many cell wall antibiotics. Thus, this theoretical study contributes significantly to a systems-level understanding of cell wall antibiotic action and uncovers a novel principle of 'minimal target exposure' as an intrinsic resistance strategy towards this class of antibiotics. In Paper III, we eventually sought to examine how *B. subtilis* orchestrates the multiple stress response modules to protect the lipid II cycle from bacitracin-induced perturbations and therefore expanded our model through a detailed quantitative description of the bacitracin stress response network. In combination with quantitative gene expression measurements, we identified mechanisms that control the multi-layered bacitracin stress response and uncovered an important homeostasis mechanism by which cells compensate for a loss of one of the stress modules. Thus, this study adds on an advanced understanding of bacterial antibiotic resistance by shedding light on the regulatory

interplay between the individual stress response modules that mediate bacitracin resistance in *B. subtilis*.

In the course of this chapter, first of all, the role of antimicrobial compounds in nature and medicine is briefly discussed and general strategies of bacteria to respond to antimicrobial compound stress are reviewed (Section 3.1). The subsequent section (Section 3.2) describes the architecture of the bacterial cell envelope and the cell wall biosynthesis and introduces diverse cell wall active antibiotics. Then, an overview about the *B. subtilis* cell envelope stress response network is given, with a special focus on the modules that contribute to the bacitracin stress response (Section 3.3). Ultimately, the central results of Paper II on the quantitative impact of cell wall antibiotics on the lipid II cycle are discussed (Section 3.4), followed by a presentation of our findings of Paper III on the regulatory mechanisms of the bacitracin stress response (Section 3.5). At the end of the chapter, further applications of the theory developed here to study bacterial stress responses towards antibiotics are depicted (Section 3.6).

### 3.1 Bacterial response strategies towards antimicrobial compounds

#### Antimicrobial compounds in nature and medicine

Antimicrobial compounds are capable of both suppressing the growth of microbial organisms and killing them, and therefore fulfil an essential role in resource competition in mixed bacterial populations. Bacterial rivals fighting for limited essential resources, such as nutrients, can produce a variety of antimicrobial compounds to harm competitors. A well-studied and widespread class of such substances, which give a competitive advantage to the producer, are antimicrobial peptides (AMP). AMPs are oligopeptides with a varying number of amino acids, which kill cells by disrupting cell envelope integrity, by inhibiting proteins, DNA and RNA synthesis, or by interacting with other various intracellular targets (Bahar and Ren, 2013; Pfalzgraff *et al.*, 2018; Zhang and Gallo, 2016). Most AMPs produced by bacteria feature a cationic and amphipathic nature (Peschel and Sahl, 2006), providing them the capability to bind to lipid components (hydrophobic region) and phospholipid groups (hydrophilic region), which both represent the major components of the bacterial cell membrane and cell wall. Usually, bacterial AMPs are active against other bacteria of the same species or across genera (Cotter *et al.*, 2005), dependent on the species composition in the producer's local environment. Notably, to protect themselves from self-killing, AMP producer species simultaneously express genes that confer immunity to the produced AMPs. For instance, the production of dedicated immunity proteins that interact with the cognate AMP and the synthesis of specialized transporters that export the AMP out of the producer are known immunity strategies (Draper *et al.*, 2008; Dubois *et al.*, 2009; Ellermeier *et al.*, 2006; Gebhard, 2012; González-Pastor *et al.*, 2003; Stein *et al.*, 2003). The production of AMPs, however, is not limited to bacteria but is rather a widespread phenomenon amongst all kingdoms of life, including fungi, plants and animals (Bahar and Ren, 2013; Bauer and Shafer, 2015; Zhang and Gallo, 2016). In higher organisms, such as humans, AMPs are also referred to as 'host defence peptides', as they are part of the front-line of defence against harmful microorganisms and contribute to innate immunity (Bahar and Ren, 2013).

Beyond their natural role, antimicrobial compounds have become of vital importance in medicine, as they are used as antibiotics to kill harmful bacteria. The described observation of Fleming, which actually led to the discovery of the world's first antibiotic, penicillin, set the starting point for the development and establishment of a variety of antibiotic substances used



to treat pathogenic infections. In fact, most of the medically used antibiotics are either derived from natural products or are produced by the synthetic modification of natural products (Overbye and Barrett, 2005) and AMPs especially have come into the focus as source for the development of new antibiotics in the recent years (Pfalzgraff *et al.*, 2018; Hassan *et al.*, 2012). The mechanisms by which antibiotics kill bacteria are actually as diverse as the mechanisms of naturally occurring antimicrobial compounds, whereas a large group of clinically used antibiotics interfere with the bacterial cell wall. These so-called cell wall antibiotics are the focus of this chapter.

As they impair growth and survival, antimicrobial compounds represent a distinct stressor for bacteria and, consequently, a variety of stress response mechanisms that protect them from antimicrobial compounds have evolved. While these stress response mechanisms are beneficial for the bacterial organisms, they massively threaten human health when present in pathogens. Indeed, they at first enable infection of the host, when pathogenic organisms can cope with the host-produced antimicrobial compounds, and they furthermore impede the treatment of those infections by antibiotics, when pathogens feature stress response mechanisms against the medically used substances. Especially, the stress responses to medically used antibiotics represent a major problem, since they make pathogens resistant to antibiotic treatment. The general strategies bacteria use to protect themselves from antimicrobial compounds are briefly introduced in the following paragraph.

### **Bacterial stress responses towards antimicrobial compounds**

As a general principle, to protect themselves from the harmful effect of antimicrobial compounds, bacteria aim to avoid interaction between the antibiotic compound and the respective cellular target. They achieve this by different defence strategies (Fig. 4) reviewed below, following (Andersson *et al.*, 2016; Bauer and Shafer, 2015; Blair *et al.*, 2015; Joo *et al.*, 2016; Nawrocki *et al.*, 2014).

As a first line of defence, bacteria have evolved extracellular mechanisms that inactivate the antimicrobial compound before interacting with the cell. For instance, it was found that many bacteria produce proteins that degrade antimicrobial compounds. These proteins can be attached to the bacterial cell surface or secreted into the local environment (Fig. 4, point 1). A paradigm of such proteins are  $\beta$ -lactamases, which protect against so-called  $\beta$ -lactam antibiotics (see Section 3.2) and mediate  $\beta$ -lactam-resistance in various bacterial organisms (Bush, 2010; Bush and Bradford, 2019; Lakshmi *et al.*, 2014). Another mechanism is the production of extracellular or surface-linked proteins that directly bind to the antimicrobial compound and sequester them, which thereby blocks their access to the cell (Fig. 4, point 2).

Once antimicrobial compounds have reached the cell surface, the second defence strategy is to modify the properties of the cell envelope to shield the cellular targets from the antimicrobial compounds. Usually, the bacterial cell envelope of both Gram-positive and Gram-negative organisms, has a negative surface charge. As many antimicrobial compounds are positively charged and therefore attracted by the negatively charged cell envelope, it is a common strategy to alter the components of the cell envelope to reduce the negative charge and thereby induce electrostatic repulsion between the antimicrobial compounds and the bacterial cell envelope (Fig. 4, point 4). In many Gram-positive bacterial genera, such as *Staphylococcus*,

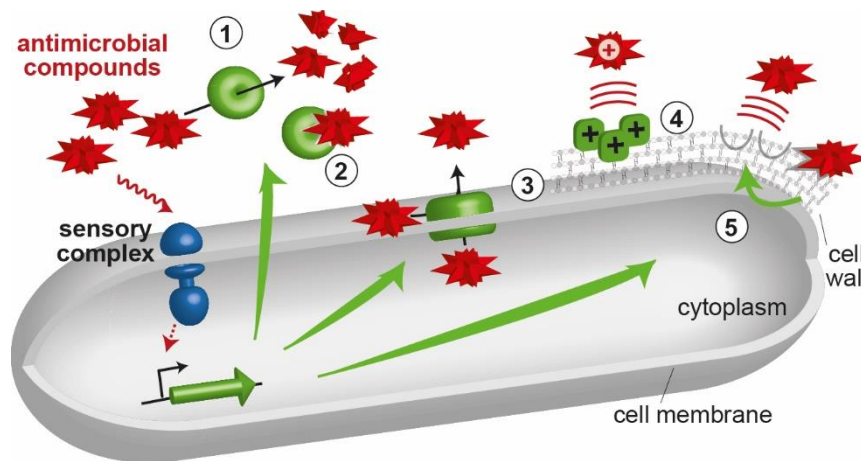


**Figure 4: Bacterial stress responses towards antimicrobial compounds.** Bacteria protect themselves from antimicrobial compounds by preventing interactions with the respective cellular target. The most common strategies to achieve this include the inactivation of the antimicrobial compound by degradation (1) or sequestration (2), the active removal of antimicrobial compounds from the cell (3), the addition of positive charges to the cell envelope - here depicted for the cell wall - to provoke electrostatic repulsion from the antimicrobial compounds (4) and the alteration of the cellular target structure of the antimicrobial compound (5), here depicted for cell wall-located targets. The expression of the various stress response determinants is activated by diverse sensory complexes upon sensing of antimicrobial compounds in the cell's environment. The figure is adapted from (Piepenbreier *et al.*, 2017).

*Listeria*, *Enterococcus*, *Bacillus*, *Clostridium*, *Streptococcus* and *Lactobacillus*, this reduction of the negative charge of the cell envelope is mediated by the DltABCD proteins (Neuhaus and Baddiley, 2003; Reichmann *et al.*, 2013; Revilla-Guarinos *et al.*, 2014). These proteins add a positive charge to the so-called teichoic acids, which cause the negative charge of the Gram-positive cell wall, as will be introduced in detail in Section 3.2. In addition to charge alteration, the modification of the teichoic acids by the Dlt proteins also leads to an increased surface rigidity, which decreases the permeability of the cell wall and thereby additionally protects the cell from antimicrobial compounds (Revilla-Guarinos *et al.*, 2014). Moreover, many Gram-positive organisms exploit strategies to modify the negative charge of their cell membrane (Ernst and Peschel, 2011). In contrast, in Gram-negative bacteria, electrostatic repulsion of antimicrobial compounds from the cell envelope can be elicited by adding positive charges to the outer membrane, in particular to the anionic lipopolysaccharides (LPS), which represent the outermost leaflet of the cell envelope in Gram-negatives (see Section 3.2).

As a third strategy to protect against antimicrobial compounds, bacteria employ a variety of efflux pumps to actively remove the harmful substances from the cell (Fig. 4, point 3). Such efflux systems play a crucial role in the defence against antimicrobial compounds in both Gram-positive and Gram-negative bacteria, and have been shown to be essential to antibiotic resistance in many pathogens (Delmar *et al.*, 2014; Gebhard, 2012). In Gram-positive bacteria, the majority of such efflux pumps constitute two-component ABC transporters. Many of these two-component ABC-transporter systems belong to the so-called BceAB group, which has been shown to protect bacterial species against a wide range of antimicrobial compounds produced by other bacteria, fungi or mammals (Nawrocki *et al.*, 2014). Prominent examples from the long list of this transporter type are BceAB and PsdAB from *B. subtilis*, BraAB, VraDE and VraFE from *S. aureus*, AnrAB from *Listeria monocytogenes* and MbrAB from *Streptococcus mutans* (Gebhard, 2012). As will be discussed in detail in Section 3.3, BceAB-like transporters also play a crucial role in the stress response to cell envelope active antimicrobial compounds in *B. subtilis*.

Ultimately, the last strategy bacteria use to protect themselves from antimicrobial compounds is the modification of the cellular target to reduce the affinity of the antimicrobial compound and

prevent binding (Fig. 4, point 5). A prime example is the modification of lipid II - the central molecule involved in bacterial cell wall synthesis (as introduced in detail in the subsequent section) - in the pathogen *Enterococcus* spp., which leads to an insensitivity against the antibiotic agent vancomycin (Cetinkaya *et al.*, 2000).

The different response mechanisms to antimicrobial compounds presented here are genetically encoded and bacteria acquire these stress response genes in two different ways: (i) Spontaneous beneficial mutations in their own genome, which are typically the origin of permanent target modifications and (ii) horizontal gene transfer, which allows for the exchange of stress response genes between different bacterial organisms (Björkman and Andersson, 2000; Hassan *et al.*, 2012; Lerminiaux and Cameron, 2019; Overbye and Barrett, 2005; Wintersdorff *et al.*, 2016). In fact, it is assumed that genes responsible for the self-protection against AMPs are transferred from the AMP producer strain to non-producing strains, such that self-immunity mechanism become widespread stress response mechanisms used by many bacteria (Gebhard, 2012; Peterson and Kaur, 2018; Schneider and Sahl, 2010). For instance, it was suggested that enterococci acquire the described vancomycin-insensitivity through the transfer of the genes responsible for the lipid II modification from vancomycin-producing strains and it has additionally been shown that they can transmit these genes to further Gram-positive pathogens (Bourgeois-Nicolaos *et al.*, 2006; Niederhäusern *et al.*, 2011; Palmer *et al.*, 2010; Schneider and Sahl, 2010). The dissemination of resistance genes by horizontal gene transfer, even across different genera, is the primary reason for the rapid evolution of antibiotic resistance in bacteria.

### 3.2 The bacterial cell wall as prime target for antibiotic compounds

The cell envelope is an indispensable structure for the bacterial cell, as it not only protects the cell from harmful substances in the environment, but also determines the cell shape, counteracts the high internal turgor pressure and mediates the controlled exchange of material between the cell's cytoplasm and the environment (Delcour *et al.*, 1999; Höltje, 1998). However, due to this essentiality and its easy accessibility, the cell envelope represents a prime target for numerous antimicrobial compounds, in particular antibiotics. The architecture of the cell envelope, its synthesis as well as cell wall active antibiotics are introduced in the following.

#### The bacterial cell envelope

To fulfil all its essential tasks, the bacterial cell envelope features a sophisticated and complex structure, which is however fundamentally different between Gram-positive and Gram-negative bacteria (Fig. 5). As the work presented in this chapter focusses on Gram-positive bacteria, a detailed introduction into the components of the Gram-positive cell envelope will be given below, while the architecture of the Gram-negative cell envelope is only briefly outlined<sup>10</sup>.

---

<sup>10</sup> See (Silhavy *et al.*, 2010) for more detailed information about the Gram-negative cell envelope.

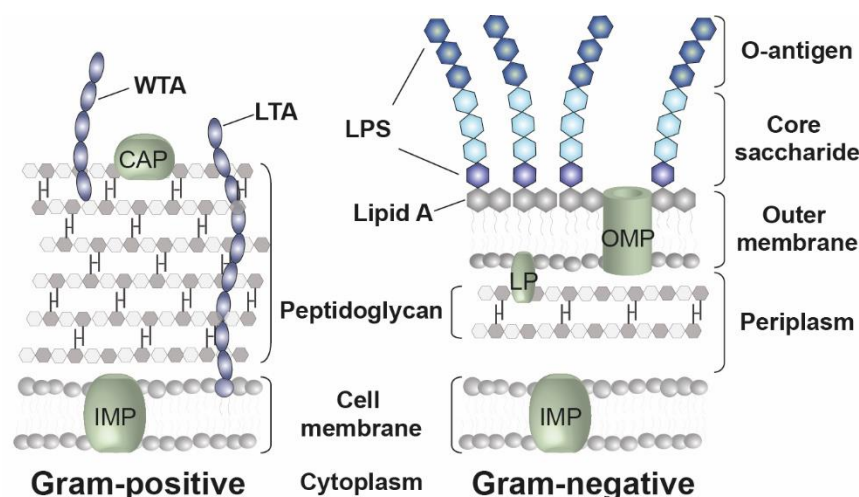


**Figure 5: The Gram-positive and Gram-negative cell envelopes.** CAP = covalently attached protein; IMP = integral membrane protein; LP = lipoprotein; LPS = lipopolysaccharide; LTA = lipoteichoic acids; OMP = outer membrane protein; WTA = wall teichoic acids. The figure is adapted from (Silhavy *et al.*, 2010).

The cell envelope of Gram-negative bacteria consists of three principal layers, starting from the inside and proceeding outward: (i) The cytoplasmic or cell membrane (CM), (ii) a thin peptidoglycan cell wall (CW) above and (iii) the outer membrane (OM) containing lipopolysaccharides (LPS) as the outermost layer (Silhavy *et al.*, 2010). The LPSs cover around 75% of the whole cell surface and cause the negative surface charge (Joo *et al.*, 2016). The two concentric membranes delimit the periplasm (Silhavy *et al.*, 2010). Please refer to Figure 5 for a detailed depiction of the components of the Gram-negative cell envelope.

The Gram-positive cell envelope features key differences from its Gram-negative counterpart. First and foremost, Gram-positive bacteria lack the OM but have a substantially thicker peptidoglycan cell wall as its outermost layer (Breukink and Kruijff, 2006; Silhavy *et al.*, 2010). In addition, long anionic polymers, called teichoic acids, are attached to the peptidoglycan in most Gram-positive organisms, which results in the negative net charge of the cell wall (Brown *et al.*, 2013; Swoboda *et al.*, 2010). The three-dimensional net-like layer of peptidoglycan (PG) is made up of repeating units of a disaccharide of N-acetylglucosamine (GlcNAc) and N-acetylmuramic acid (MurNAc) (Harz *et al.*, 1990; Schleifer and Kandler, 1972; Vollmer *et al.*, 2008). The MurNAc subunits are cross-linked by short peptide bridges, which contribute to the rigid but nevertheless elastic structure of the PG network (Vollmer *et al.*, 2008). Teichoic acids (TA), which intersperse the PG layer, are linear polymers composed largely of glycerol phosphate, glucosyl phosphate, or ribitol phosphate repeats (Brown *et al.*, 2013; Swoboda *et al.*, 2010). One class of TAs, referred to as wall teichoic acids (WTA), are coupled to the peptidoglycan, while another class, the lipoteichoic acids (LTA), are anchored to the cell membrane and are threaded through the layers of peptidoglycan (Neuhaus and Baddiley, 2003). Although some bacterial species show modification in the composition or cross-linking of the glycan strands (Münch and Sahl, 2015), the overall structure of the cell wall, as presented here, is similar in most Gram-positive bacteria. Due to its rigid structure, the cell wall fulfils the role of protection from environmental stressors and cell shape determination.

The inner layer of the Gram-positive cell envelope, the bacterial cell membrane, is a phospholipid bilayer, which surrounds the cytosol of the cell. Multiple different proteins that function for instance in energy production, lipid biosynthesis, protein secretion and transport of various kind of molecules, are located in the cell membrane (Silhavy *et al.*, 2010). The cell membrane controls the permeability of the cell, allows the formation of a membrane potential

and is platform for interactions between the intra- and extracellular space of the cell (Hurdle *et al.*, 2011), to list just a few functions. Indeed, also the machinery responsible for the production of the bacterial cell wall is partially located at the cell membrane, as will be introduced in detail in the next paragraph.

Both membrane and cell wall composition can actively be changed by bacteria in response to environmental conditions, as illustrated for instance in some of the response strategies to antimicrobial compounds introduced in Section 3.1. Due to the lack of the outer membrane, which displays an essential protection barrier in Gram-negative organisms, Gram-positives are particularly sensitive to cell wall active antimicrobial compounds. Most of them interfere with the synthesis of the Gram-positive cell wall, in particular the production of peptidoglycan, as will be detailed in the following.

### Cell wall biosynthesis

The synthesis of the bacterial PG cell wall comprises of different steps (Fig. 6), including (i) the cytoplasmic synthesis of the PG building blocks GlcNAc and MurNAc, (ii) the subsequent attachment of these PG precursors to lipid carrier molecules anchored in the cell membrane, and (iii) their transport across the membrane and subsequent incorporation into the existing cell wall.

The cytoplasmic production of the PG precursors (reviewed e.g. in Barreteau *et al.*, 2008; Mengin-Lecreulx *et al.*, 1982; van Heijenoort, 2007) initiates with the conversion of fructose-6-phosphate to GlcNAc. GlcNAc is subsequently activated by the addition of a uridine diphosphate (UDP), giving rise to the first PG precursor UDP-GlcNAc. The second PG precursor, UDP-MurNAc-pentapeptide, is eventually produced by the conversion of UDP-GlcNAc to UDP-MurNAc and the subsequent attachment of the pentapeptide chain, catalysed by the MurA-F ligases.

The major pathway shuttling the PG precursors across the membrane is the lipid II cycle (reviewed e.g. in Breukink and Kruijff, 2006; Kruijff *et al.*, 2008; Schneider and Sahl, 2010; van Heijenoort, 1996), which will be introduced in detail below. After cytoplasmic production, as a first step of the lipid II cycle, UDP-MurNAc-pentapeptide is attached to the membrane-bound lipid carrier undecaprenyl phosphate (UP) via the translocase MraY, giving rise to the lipid I intermediate. Subsequently, the MurG transferase loads UDP-GlcNAc onto lipid I, which leads to the production of lipid II. Lipid II is then translocated to the outer leaflet of the cell membrane via various flippases, where penicillin-binding proteins (PBPs) incorporate the supplied PG subunits into the nascent PG layer. The phosphorylated state of the lipid carrier, undecaprenyl pyrophosphate (UPP), remains and is recycled by dephosphorylation via UPP phosphatases (UppPs), yielding the initial lipid carrier UP for another round of PG subunit transport. Since the step of UPP dephosphorylation likely occurs at the outer leaflet of the membrane (Chang *et al.*, 2014; Tatar *et al.*, 2007), carrier recycling requires UP translocation to the internal leaflet of the membrane by a yet unknown mechanism (Manat *et al.*, 2015; Touzé *et al.*, 2008). Finally, cytoplasmic *de novo* synthesis of UPP balances the growth-dependent dilution of lipid carrier and supplies new carrier to the cycle. However, the translocation mechanism required to present UPP to the externally acting phosphatases is yet unknown as well.

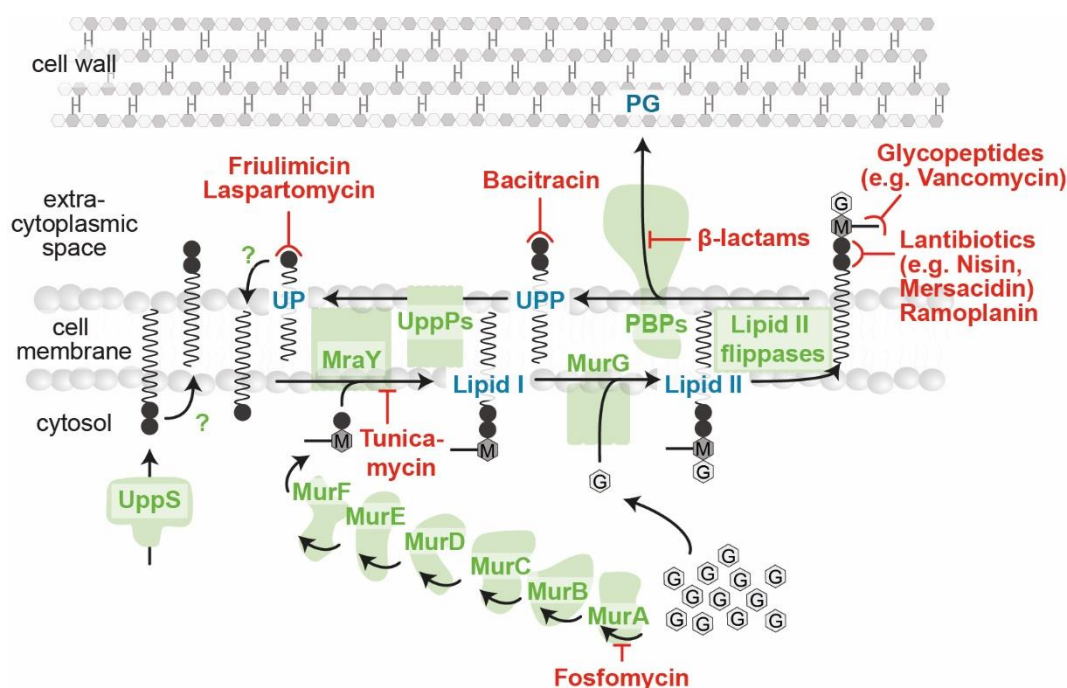


**Figure 6: The lipid II cycle is a prime target for antibiotics in Gram-positive bacteria.** For a detailed description of the lipid II cycle and lipid II cycle-inhibiting antibiotics please refer to the main text. Antibiotic inhibition is indicated by the T-shaped red lines. M = UDP-MurNAc-pentapeptide; G =UDP-GlcNAc; UP = undecaprenyl phosphate; UPP = undecaprenyl pyrophosphate; PG = peptidoglycan; PBPs = penicillin-binding proteins; UppPs = UPP phosphatases.

The central lipid II cycle, as presented here, is highly conserved throughout the bacterial world and thus represents a prime target for antibiotic attack. Some prominent classes of cell wall antibiotics targeting the lipid II cycle are presented in the next paragraph.

## Cell wall antibiotics

Although few antibiotics have been reported that target the production of WTA (Campbell *et al.*, 2012) or even reach the cell's cytoplasm and impair production of PG precursor (Kahan *et al.*, 1974; Lambert and Neuhaus, 1972), most cell wall antibiotics interfere with the lipid II cycle. Diverse classes will be introduced above, following (Breukink and Kruijff, 2006; Oppedijk *et al.*, 2016; Schneider and Sahl, 2010). Nearly all steps of the lipid II cycle are prone to antibiotic attack (as depicted in Fig. 6) and two general mechanisms can be distinguished. One common mechanism of lipid II cycle active antibiotics is the direct inhibition of the enzymes catalysing the individual reactions of the lipid II cycle. The most important class of enzyme-inhibiting antibiotics are  $\beta$ -lactams, which include the prominent examples penicillin and cephalosporin. By mimicking their actual substrate,  $\beta$ -lactams are recognised and bound by PBPs (Fernandes *et al.*, 2013). Upon  $\beta$ -lactam binding, PBPs are inactivated and thus no longer able to catalyse the appropriate incorporation of PG precursors into the cell wall. Another group of enzyme-inhibiting antibiotics represent the sugar substrate analogues resembling the UDP-activated sugars, such as tunicamycin that impairs the attachment of PG precursor UDP-MurNAc to lipid carrier UP by binding to *MraY* (Brandish *et al.*, 1996). Since enzyme-inhibiting antibiotics are not the focus of this thesis, it will be left at this brief overview<sup>11</sup> and the antibiotics following the second inhibition mechanism will be introduced in more detail.

<sup>11</sup> For a more detailed introduction into diverse classes of enzyme-inhibiting antibiotics please refer to (Schneider and Sahl, 2010).



The second way by which antibiotics successfully perturb the lipid II cycle is the interaction with the lipid intermediates of the cycle (UPP, UP, lipid I and lipid II). Antibiotic binding to an individual lipid II cycle intermediate prevents enzyme-catalysed conversion and thereby blocks the appropriate reaction in the lipid II cycle. Different classes of these substrate-inhibiting antibiotics are found to bind all lipid intermediates that are accessible at the outer face of the cell membrane (UPP, UP and lipid II), making crossing of the cell membrane therefore not necessary. Amongst these, antibiotics that target lipid II represent by far the largest group.

Antibiotic binding to lipid II can occur at various molecular moieties but it generally inhibits the PBP-catalysed incorporation of PG precursors into the existing cell wall layer. One important and well-studied class of lipid II-binding antibiotics are glycopeptides, such as vancomycin or teicoplanin. The antibiotic activity of these compounds relies on their binding to the pentapeptide side chain of lipid II, in particular to the 4<sup>th</sup> and 5<sup>th</sup> position of the peptide (D-Ala-D-Ala terminus) (Reynolds, 1989), which is involved in peptidoglycan cross-linking. Glycopeptide antibiotics are frequently used as last-resort antibiotics for the treatment of Gram-positive pathogens, which already feature resistance against other antibiotics, such as MRSA (Methicillin-resistant Staphylococcus aureus) (Choo and Chambers, 2016). The usage of alternative versions of the pentapeptide side chain of lipid II, however, significantly reduces the affinity for some glycopeptides and leads to insensitivity against these antibiotics, as demonstrated in Section 3.1 for vancomycin (Cetinkaya *et al.*, 2000). Lantibiotics represent a second major class of lipid II-targeting antibiotics, whose members are structurally highly diverse. One subgroup of these, referred to as nisin-like lantibiotics, combine inhibition of cell wall biosynthesis with membrane disruption. By using lipid II as a docking molecule, they are able to form pores in the cell membrane and thereby permeabilise it (Breukink *et al.*, 1999). A well-studied member of this subgroup is nisin, which is commonly used as a food preservative (Hansen, 1994). The other subgroup of lantibiotics, so-called mersacidin-like lantibiotics, do not feature the pore-formation ability and exclusively act by binding to lipid II, such as mersacidin or actagardine (Bierbaum and Sahl, 2009). As a common theme, all lantibiotics appear to bind to the sugar-pyrophosphate moiety of lipid II (Breukink and Kruijff, 2006). A further well-known example of a lipid II-binding antibiotic interacting mainly with the pyrophosphate moiety of lipid II is the cyclic lipodepsipeptide ramoplanin, which is also used as last-resort antibiotic against resistant pathogens (Fang *et al.*, 2006).

Beyond these lipid II-targeting compounds, there are also cell wall antibiotics binding extracellularly accessible UPP and UP. A well-studied antibiotic, which blocks the recycling of the lipid carrier by forming a complex with UPP, is the cyclic dodecylpeptide bacitracin (Storn and Strominger, 1973). Bacitracin is mainly used for treatment of skin infections caused by Gram-positive bacteria (Schneider and Sahl, 2010). Ultimately, further cyclic lipopeptide antibiotics, such as friulimicin or laspartomycin (Borders *et al.*, 2007; Kleijn *et al.*, 2016; Kleijn *et al.*, 2017), have been reported to bind to UP and thereby inhibit *MraY*-dependent production of lipid I. Of note, virtually all of the substrate-inhibiting lipid II cycle antibiotics presented here are derived from naturally occurring antimicrobial compounds, produced by diverse bacterial species (Schneider and Sahl, 2010).

Extensive experimental studies have helped to characterise most of these cell wall antibiotics concerning their cellular targets, their *in vitro* antibiotic-target binding affinities and their minimal inhibitory concentrations (MICs), that is the antibiotic concentrations necessary to fully inhibit bacterial population growth *in vivo* (e.g. Beauregard *et al.*, 1997; Gebhard *et al.*, 2014; Hiron *et al.*, 2011; Hu *et al.*, 2003; Mota-Meira *et al.*, 2000; Radeck *et al.*, 2016; Shaaly *et al.*, 2013; Staroń *et al.*, 2011; Storm and Strominger, 1973; Tyanont *et al.*, 2006; Wecke *et al.*,

2009; Wiedemann *et al.*, 2001; Yoshida *et al.*, 2011). However, it is not yet understood comprehensively why many cell wall active antibiotics are less potent *in vivo* than suggested by the antibiotic-target binding affinity *in vitro*. This question is addressed in Paper II of this thesis by studying the quantitative effect of cell wall antibiotic binding on the progression of the lipid II cycle within a theoretical framework (Section 3.4).

In the end, most of the stress response strategies to antimicrobial compounds presented in Section 3.1 confer bacterial resistance to diverse cell wall-active antibiotics. The soil bacterium *B. subtilis*, which is an important Gram-positive model organism, orchestrates in fact multiple stress response modules to cope with antibiotic-induced cell envelope stress, as introduced in the next section.

### 3.3 Cell envelope stress response in *Bacillus subtilis*

The integrity of the bacterial cell envelope can not only be affected by antibiotic attack, as introduced before, but also by other environmental stressors such as heat or osmotic shock. In the broadest sense, thus, cell envelope stress responses (CESR) encompass all mechanisms that protect cells from the various envelope perturbing conditions (Jordan *et al.*, 2008). Here, the CESR network in *B. subtilis* will be introduced, which in fact mainly comprises response mechanisms against cell wall active antimicrobial compounds. The CESR in *B. subtilis* is mediated by a signalling network of four TCS and (at least) three ECF  $\sigma$ -factors, which orchestrate cellular responses on various levels, including the production of specific stress determinants and the control of the overall cell envelope homeostasis.

Three out of the four CES-inducible TCSs, namely BceRS, PsdRS and YxdJK, are part of paralogous systems, referred to as Bce-like systems. Each of these systems consists of the respective TCS and an ABC transporter regulated by it, both of which are encoded by two neighbouring operons (Staroń *et al.*, 2011). Together, they form specific detoxification modules that efficiently remove diverse antimicrobial compounds from their site of action and thereby mediate high levels of resistance against these compounds (Dintner *et al.*, 2011; Mascher *et al.*, 2003). The best-understood example of the Bce-like systems is BceRS-BceAB, which responds primarily to bacitracin and will be therefore introduced in detail below. Furthermore, the PdsRS-PsdAB system is preferentially triggered by a number of lantibiotics, including nisin and actagardine, while the YxdJK-YxdLM system responds to the human AMP LL-37 (Joseph *et al.*, 2004; Pietiäinen *et al.*, 2005; Staroń *et al.*, 2011). BceRS-like TCSs are highly conserved and widely distributed in *Firmicutes* bacteria and as an example contribute to resistance against cell wall antibiotics in *S. aureus* and *E. faecalis* (Hiron *et al.*, 2011; Gebhard *et al.*, 2014).

The fourth TCS, which is part of the CESR in *B. subtilis*, is LiaRS. In contrast to the narrow inducer spectrum of the other TCSs, LiaRS strongly responds to various cell wall active antibiotics, such as bacitracin, vancomycin, ramoplanin and diverse lantibiotics (Jordan *et al.*, 2006; Mascher *et al.*, 2004; Pietiäinen *et al.*, 2005; Wecke *et al.*, 2009). Additionally, it is induced by a number of more unspecific stimuli, such as alkaline shock, detergents and ethanol, although to a weaker extent (Mascher *et al.*, 2004; Pietiäinen *et al.*, 2005; Petersohn *et al.*, 2001; Tam *et al.*, 2006; Wiegert *et al.*, 2001). Moreover, it has been shown that LiaRS is intrinsically induced by the YydF peptide produced by *B. subtilis* itself (Butcher *et al.*, 2007). The LiaRS TCS interacts with a membrane-anchored inhibitor protein LiaF, which keeps the HK LiaS inactive under non-inducing conditions (Jordan *et al.*, 2006). LiaRSF-like systems are



also widespread in *Firmicutes* bacteria and homologous systems are for example involved in general CESRs in streptococci and staphylococci (Schrecke *et al.*, 2012). In *B. subtilis*, LiaFSR regulates the expression of the *liaIH* operon, encoding the phage-shock-proteins LiaI and LiaH. Although the precise stress response mechanism mediated by LiaIH remains elusive, it was shown that the LiaFSR-LiaIH system contributes to bacitracin resistance in *B. subtilis* (Radeck *et al.*, 2016), as will be discussed in more detail below.

Ultimately, in contrast to the specific TCS-dependent responses, the three major ECF  $\sigma$ -factors involved in the CCSR of *B. subtilis* -  $\sigma^M$ ,  $\sigma^W$  and  $\sigma^X$  - orchestrate more complex and highly diverse mechanisms by regulating a variety of different genes (reviewed in Helmann, 2016). The first ECF  $\sigma$ -factors,  $\sigma^M$ , regulates the expression of ~60 genes, which are involved in cell wall synthesis, cell shape determination and cell division, amongst others (Eiamphungporn and Helmann, 2008; Zhao *et al.*, 2019). It has been shown that  $\sigma^M$  contributes to *B. subtilis* resistance against bacitracin (Cao and Helmann, 2002).  $\sigma^M$  activity is controlled by the anti- $\sigma$ -factor complex YhdLK (Horsburgh and Moir, 1999; Yoshimura *et al.*, 2004), which releases the  $\sigma$ -factors in response to more general stimuli such as acidic pH, heat, salt as well as to specific cell wall antibiotics such as bacitracin, friulimicin or vancomycin (Cao *et al.*, 2002b; Mascher *et al.*, 2003; Thackray and Moir, 2003).  $\sigma^W$ , the second CES-inducible ECF  $\sigma$ -factor, also controls approximately 60 genes, summarized as the 'antibiosis regulon', with many of them encoding proteins involved in stress response against antimicrobial compounds, especially membrane-targeting ones (Cao *et al.*, 2002a; Helmann, 2006; Huang *et al.*, 1999; Kingston *et al.*, 2013). The activation of  $\sigma^W$  is based on the proteolytic degradation of its cognate membrane-anchored anti- $\sigma$ -factor RsiW (Schöbel *et al.*, 2004), which is induced by a number of cell wall active compounds such as vancomycin or cephalosporin C (Cao *et al.*, 2002a), but also by alkaline shock (Wiegert *et al.*, 2001).  $\sigma^X$  features the smallest regulon with ~30 genes (most of which are also regulated by another ECF  $\sigma$ -factor,  $\sigma^V$ ), whose gene products are mainly involved in cell envelope composition and cell surface modification (Cao and Helmann, 2004). For instance, one of the targets of  $\sigma^X$  is the *dltABCDE* operon, which is responsible for reducing the overall negative charge of the Gram-positive cell envelope in response to positively charged antimicrobial compounds (Neuhaus and Baddiley, 2003), as introduced in Section 3.1. The corresponding anti- $\sigma$ -factor of  $\sigma^X$  is RsiX, which responds for instance to bacitracin (Cao and Helmann, 2002). Overall, the three ECF  $\sigma$ -factors involved in CCSR of *B. subtilis* significantly overlap in their regulons, with many genes regulated by two or even all three of the ECF  $\sigma$ -factors (Mascher *et al.*, 2007). Moreover, individual cell wall antibiotics activate all three ECF  $\sigma$ -factors simultaneously, as has been shown for bacitracin (Mascher *et al.*, 2003). Thus, it is expected that the ECFs of *B. subtilis* orchestrate more general protective measures and homeostatic adaptations to envelope stress, whereas the TCSs regulate more inducer-specific mechanisms (Radeck *et al.*, 2017). The *B. subtilis* stress response to bacitracin, in fact, combines both of these strategies and is introduced in detail the following.

### Bacitracin stress response network in *B. subtilis*

By forming a tight complex with the lipid II cycle intermediate UPP, bacitracin blocks UPP dephosphorylation and thereby impairs the overall progression of the lipid II cycle (Economou *et al.*, 2013; Storm and Strominger, 1973). To cope with this stress, *B. subtilis* has evolved a multi-layered response towards bacitracin, including (i) the BceRS-BceAB system, (ii) the Lia-system and (iii)  $\sigma^M$ -dependent control of cell wall synthesis genes (depicted in detail in Fig. 7).

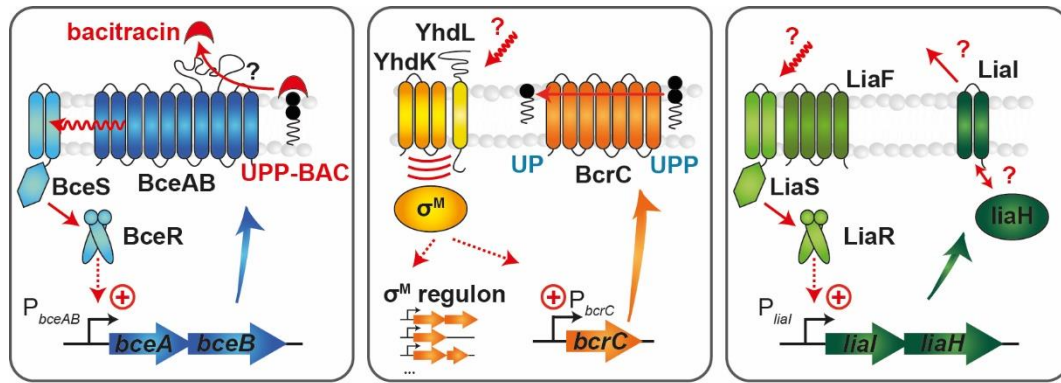


**Figure 7: Bacitracin stress response in *B. subtilis*.** The primary bacitracin stress response module, BceRS-BceAB, is depicted in *blue*. The ABC transporter BceAB removes bacitracin from its cellular target UPP employing a so far unknown mechanism. Transport activity serves as a stimulus for the BceRS TCS, which upregulates *bceAB* expression in response to high transport activity (flux-sensing mechanism) (Fritz *et al.*, 2015). The secondary bacitracin stress response modules, the  $\sigma^M$ -dependent regulation of BcrC and the Lia-system, are depicted in *orange* and *green*, respectively. A yet unknown stimulus triggers the release of  $\sigma^M$  from its cognate anti- $\sigma$ -factor YhdLK into the cytoplasm, where it activates the expression of *bcrC* and regulates the expression of a variety of other genes. The RR LiaR of the LiaFSR sensory complex activates the expression of the *liaIH* operon in response to cell envelope damage. The precise physiological stimulus sensed by the LiaFS complex as well as the protective role of LiaIH are yet unknown. The figure is adapted from (Radeck *et al.*, 2017)

The BceRS-BceAB system (Fig. 7, *blue*) is strongly induced by bacitracin and also contributes significantly to resistance towards this compound in *B. subtilis* (Mascher *et al.*, 2003; Ohki *et al.*, 2003; Rietkötter *et al.*, 2008). It is assumed that the protective effect of the ABC transporter BceAB relies on clearing UPP from its inhibitory antibiotic compound (Fritz *et al.*, 2015). The expression of the BceAB transporter is controlled by the RR BceR of the cognate TCS (Ohki *et al.*, 2003). However, experimental evidence suggested that the transporter itself is involved in the signalling process (Bernard *et al.*, 2007; Rietkötter *et al.*, 2008) and it has been shown that the permease BceB of the transporter forms a complex with the histidine kinase BceS of the TCS (Dintner *et al.*, 2011; Dintner *et al.*, 2014). A computational model has finally brought these observations together and postulated a flux-sensing mechanism for the BceRS-BceAB system (Fritz *et al.*, 2015). Here, the activity of the histidine kinase BceS depends on the transport activity of BceAB, that is the physical interaction between BceS and BceB serves to measure the bacitracin flux per transporter. The expression of new transporters is thus adapted to the current capability of the cell to deal with the bacitracin challenge, and a high transport activity of individual transporters induces the production of more BceAB transporters. The elevated number of transporters then alleviates the transport activity of each individual transporter, such that BceAB regulates its own expression in a negative feedback loop. This flux-sensing mechanism allows the precise adaptation of the stress response to the current stress level of the cell. As discussed in detail in the review ‘Transporters as information processors in bacterial signalling pathways’ by Hannah Piepenbreier, Georg Fritz and Susanne Gebhard (Piepenbreier *et al.*, 2017) (**Paper IV**), which is part of this thesis, tandems of transporters and signalling systems, referred to as ‘flux-sensors’, are often found to be involved in bacterial signalling processes. Actually, according to the high conservation of Bce like-systems in *Firmicutes*, flux-sensing is expected to represent a widespread regulatory principle to control cell envelope stress within this group (Piepenbreier *et al.*, 2017; Radeck *et al.*, 2017).

The second bacitracin stress response module, the Lia-system (Fig. 7, *green*), has been originally discovered and described in the course of bacitracin resistance (Mascher *et al.*, 2003). Although it has been recognized that the Lia-system is induced in response to a variety of cell wall active antimicrobial compounds (Jordan *et al.*, 2006; Mascher *et al.*, 2004; Pietiäinen *et al.*, 2005; Wecke *et al.*, 2009), the precise stimulus perceived by LiaFSR has not

been deciphered so far. Instead of detecting the antimicrobial compound directly, it is suggested that the LiaFSR sensory complex senses downstream effects and might thus act as an indirect, damage-sensing system (Radeck *et al.*, 2017), in line with the broad inducer spectrum including also other cell envelope stressors different from antimicrobial compounds. The role of its target genes, *liaIH*, in protecting *B. subtilis* from bacitracin-induced stress has also not yet been conclusively unravelled. It has been demonstrated that LiaI is a small membrane protein, which serves as an anchor for the phage-shock protein A homolog, LiaH, upon cell envelope stress (Domínguez-Escobar *et al.*, 2014). Together, all experimental evidences support a model in which the LiaFSR sensory complex scans for envelope perturbations and activates *liaIH* expression upon detection. LiaI inserts into the membrane and recruits LiaH to presumably counteract the cell envelope damage (Domínguez-Escobar *et al.*, 2014).

The  $\sigma^M$ -dependent upregulation of a specific cell wall synthesis gene, *bcrC*, is the third layer of bacitracin stress response in *B. subtilis* (Fig. 7, orange). BcrC fulfils the crucial role of an UPP-phosphatase in the lipid II cycle of *B. subtilis* and catalyses, together with a second enzyme, UppP, the recycling of lipid carrier UPP. The corresponding gene, *bcrC*, is under control of  $\sigma^M$ -regulation (Cao and Helmann, 2002; Eiamphungporn and Helmann, 2008) and its expression is upregulated in response to bacitracin (Bernard *et al.*, 2005; Cao and Helmann, 2002; Ohki *et al.*, 2003). An elevated number of BcrC results in a more efficient dephosphorylation of UPP to UP, which diminishes the UPP concentration and thus the number of bacitracin target molecules. Hence, the  $\sigma^M$ -dependent upregulation of *bcrC* expression can be understood as a more general response that promotes the progression of the lipid II cycle and ensures cell wall homeostasis. The precise stimulus that triggers the release of  $\sigma^M$  from its anti- $\sigma$ -factor YhdLK and elicits the upregulation of *bcrC* expression, however, has yet not been identified (Asai, 2018; Zhao *et al.*, 2019).

Indeed, the three stress response modules differ significantly in both their sensitivity and response characteristics towards bacitracin (Rietkötter *et al.*, 2008) as well as their contribution to the overall protection against bacitracin. A recent study demonstrated a clear-cut hierarchy between them, with BceAB representing the primary stress response module against bacitracin, and LiaIH and BcrC contributing secondarily to protection against this compound (Radeck *et al.*, 2016). BceAB confers high-level resistance towards bacitracin and a loss of this primary resistance module increases the susceptibility towards bacitracin ~85-fold, as MIC measurements in a *B. subtilis* wild type and a *bceAB* mutant showed. In contrast, LiaIH does not play a role in bacitracin resistance in the wildtype and BcrC also contributes only moderately to bacitracin resistance here. However, their actual impact becomes visible in a *B. subtilis bceAB* deletion strain, where the presence of LiaIH reduces the susceptibility towards bacitracin ~6-fold and the presence of BcrC even ~24-fold. Together, these results suggest that the BceRS-BceAB stress module contributes most to bacitracin resistance in *B. subtilis* and is already induced by low amounts of bacitracin. As BceAB removes bacitracin from its target, it functions as a detoxification module and protects the lipid II cycle from perturbation up to a certain degree. The other two modules probably contribute to cell wall homeostasis under higher bacitracin concentrations and can - at least partially - compensate for a loss in the primary resistance module.

Based on the discovery of this clear-cut hierarchy, further important questions arise: What regulates the multi-layered response towards bacitracin and how do the different response modules interact to shape the overall response to bacitracin? These questions are addressed

in Paper III by a systems approach, combining mathematical modelling with quantitative gene expression measurements.

### 3.4 Paper II: Minimal exposure of lipid II cycle intermediates triggers cell wall antibiotic resistance

In the Paper ‘Minimal exposure of lipid II cycle intermediates triggers cell wall antibiotic resistance’ by Hannah Piepenbreier, Angelika Diehl and Georg Fritz (Piepenbreier *et al.*, 2019a), we studied the perturbation of cell wall biosynthesis by cell wall antibiotics from a quantitative perspective. To the best of our knowledge, we here developed the first comprehensive computational model of the lipid II cycle in *B. subtilis* by incorporating published biochemical data quantifying enzyme activities and concentrations of lipid II cycle intermediates (Barreteau *et al.* 2009; Brandish *et al.* 1996; Crouvoisier *et al.* 2007; Geis and Plapp 1978; Mengin-Lecreux *et al.* 1982; Mengin-Lecreux *et al.* 1983; Mengin-Lecreux and van Heijenoort 1985; Schwartz *et al.*, 2002; Touzé *et al.*, 2008; van Heijenoort *et al.* 1992). When doing so, we interestingly found that the individual lipid II cycle intermediates are distributed highly asymmetrically within the cycle with high concentrations of UPP, medium UP concentrations and low concentrations of lipid I and II (Figure 8A-D). As we aimed to use this model to study the systems-level behaviour of the core lipid II cycle under antibiotic treatment, stress response modules that confer antibiotic resistance were not included yet. Rather, the model described the individual reaction of the lipid II cycle in detail and used the rate of peptidoglycan synthesis, defined as  $j_{PG}$ , as a quantitative measure for the overall progression of the cycle.

$$j_{PG} = [PBPs] * k_{cat}^{PBPs} * \frac{[Lipid II_{OUT}]}{K_M^{PBPs} + [Lipid II_{OUT}]}$$

Here,  $[PBPs]$  represents the concentration of penicillin-binding proteins catalysing the incorporation of PG into the growing cell wall layer, while  $k_{cat}^{PBPs}$  and  $K_M^{PBPs}$  define the catalytic constant and the Michaelis-Menten constant for the PBP reaction, respectively.  $[Lipid II_{OUT}]$  describes the concentration of lipid II present at the outer leaflet of the cell membrane after flipping, which represents the substrate for the PG incorporation reaction. The reduction of the rate of PG synthesis by antibiotic binding was monitored and the antibiotic concentration that provokes a reduction by 50% was defined as  $IC_{50}$  and served as a quantitative measurement for the antibiotic’s efficacy in our theory. When simulating the binding of five different cell wall antibiotics (bacitracin, friulimicin, ramoplanin, vancomycin and nisin) to their targets within the lipid II cycle, we found that this  $IC_{50}$  partially equals the *in vitro* antibiotic-target dissociation constant,  $K_D$ , and partially massively exceeds this value - in line with the previous experimental observations (Fig. 9). Indeed, the model-predicted  $IC_{50}$  values closely resemble experimentally determined MICs for all five antibiotics in *B. subtilis* strains lacking major antibiotic resistance determinants (Mota-Meira *et al.*, 2000; Radeck *et al.*, 2016; Staroń *et al.*, 2011; Tiyanont *et al.*, 2006; Wecke *et al.*, 2009), indicating that our theory precisely describes the *in vivo* efficacy of these cell wall antibiotics (Fig. 9). Strikingly, it turned out that the discrepancy between *in vitro* dissociation constant and *in vivo* efficacy clearly depends on the antibiotic target. While both values are similar for bacitracin (targeting UPP) and only slightly different for friulimicin (targeting UP), especially the lipid II-binding antibiotics nisin, ramoplanin and vancomycin, feature a distinctly higher  $IC_{50}$  compared to their *in vitro*  $K_D$ , suggesting that they are significantly less active *in vivo* than *in vitro*.

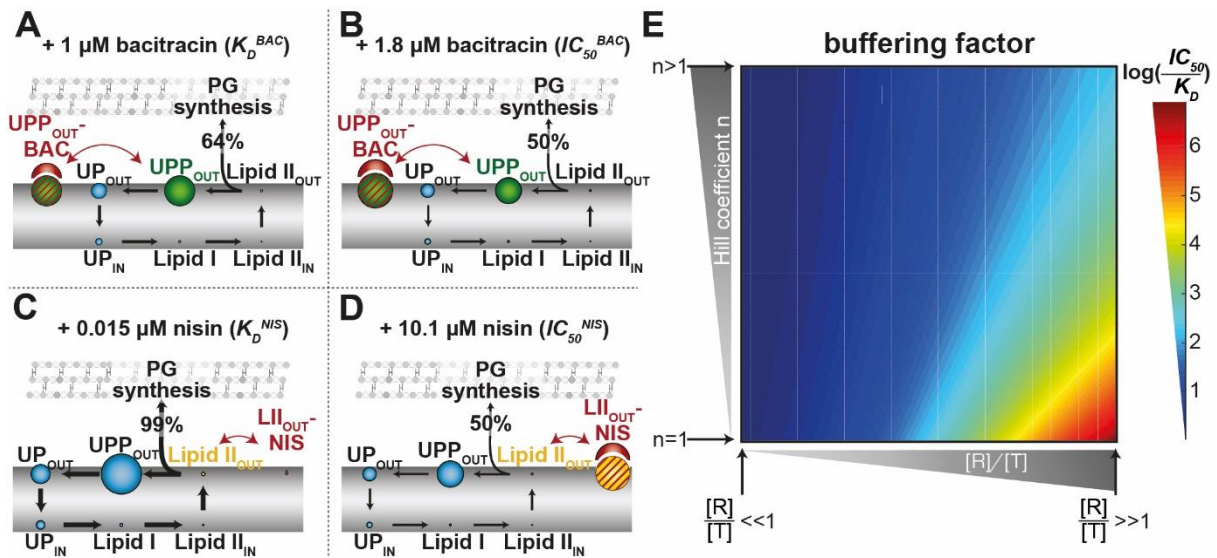


**Figure 8: The asymmetric distribution of lipid II cycle intermediates generates a massive *in vivo* efficacy gap for lipid II-targeting antibiotics.** The intermediates within the lipid II cycle feature a highly asymmetric distribution with high concentrations of externally accessible UPP (UPP<sub>OUT</sub>) and comparable tiny concentrations of externally accessible lipid II (Lipid II<sub>OUT</sub>). The size of the circles in A-D correlates with the concentrations of the different intermediates. The thickness of the black arrows is proportional to the reaction rates of the individual lipid II cycle reactions. The cell membrane is depicted in grey. **(A)** Efficient binding of external UPP by bacitracin (BAC) commences at its *in vitro*  $K_D$  value ( $K_D^{BAC} = 1\mu\text{M}$ ; Storm and Strominger, 1973) and reduces the pool of free UPP to its half-maximum. As UPP is the most abundant intermediate in the lipid II cycle, this implies the sequestration of high levels of lipid intermediates from the cycle, thereby decreasing the concentrations of all free cycle intermediates, especially lipid II. Since the lipid II concentration determines the PG synthesis rate, this already reduces the rate to a level of 64% of its maximum. **(B)** Only slightly higher bacitracin concentrations are required to reduce the free lipid II pool and thereby the rate of PG synthesis to 50% ( $IC_{50}^{BAC} = 1.8\mu\text{M}$ ) **(C)** In contrast, although nisin (NIS) - at concentrations around the  $K_D$  ( $K_D^{NIS} = 0.015\mu\text{M}$ ; Wiedemann *et al.*, 2001) - binds 50% of the free lipid II pool, this only sequesters ~1% of all lipid intermediates from the cycle. As the remaining lipid intermediates function as a reservoir and quickly replenish the free form of lipid II molecules by on-going cycling, the rate of PG synthesis is not reduced significantly (99% of maximum). **(D)** Only when increasing the nisin-concentration markedly ( $IC_{50}^{NIS} = 10.1\mu\text{M}$ ), ~50% of the total lipid II cycle intermediates are sequestered into the nisin-lipid II complexes (LII<sub>OUT</sub>-NIS) and the pool of free lipid II and thus the rate of PG synthesis are reduced to 50% of its maximal value. **(E)** A reduced model for the lipid II cycle rationalizes the *in vivo* efficacy gap by quantifying the ratio between  $IC_{50}$  and  $K_D$ , which is defined as 'buffering factor', by a mathematical equation  $\frac{IC_{50}}{K_D} \approx \sqrt[n]{1 + \left(\frac{[R]}{[T]}\right)}$ .  $[T]$  denotes the concentration of the antibiotic target and  $[R]$  summarizes the concentrations of all non-target lipid II cycle intermediates, referred to as bactoprenol pool.  $n$  represents the Hill coefficient describing cooperativity in antibiotic-target interaction. The colour in the log-log plot codes for  $\log\left(\frac{IC_{50}}{K_D}\right)$ , where a high buffering factor indicates a large *in vivo* efficacy gap. The buffering factor and thus the *in vivo* efficacy gap increases for increasing bactoprenol reservoir size relative to the target pool (*horizontal axis*). The two arrows indicate the scenarios for UPP ( $[T] \gg [R]$ ) and lipid II ( $[T] \ll [R]$ ) binding. The buffering factor scales additionally with  $n$ , whereas higher  $n$  reduce the ratios between  $IC_{50}$  and  $K_D$  (*vertical axis*). This reduction of the *in vivo* efficacy gap by increases cooperativity is most pronounced for large ratios between  $[R]$  and  $[T]$ , as for lipid II binding antibiotics.

In fact, our developed theory allowed us for the first time to decipher that this apparent '*in vivo* efficacy gap' of lipid II-binding antibiotics is an emergent property of the lipid II cycle and can be explained by the cyclic nature of this pathway and the observed highly asymmetric distribution of lipid intermediates within this cyclic reaction network. When analysing the effect of antibiotic binding not only on the target lipid intermediate but also on all other intermediates in the cycle, we found that a reduction of the overall rate of peptidoglycan synthesis by 50% correlates with a reduction of the concentration of externally present lipid II to ~50%. We further demonstrated that this reduction of the lipid II pool was achieved only if the total amount of lipid intermediates is significantly reduced (Fig. 8A-D). Accordingly, the efficacy of an antibiotic depends on its ability to reduce the total amount of lipid II cycle intermediates by binding. Binding of the by far most-abundant lipid intermediate UPP by bacitracin actually leads to an efficient sequestration of lipid intermediates already at the *in vitro*  $K_D$ , where 50% of the target

and thereby a significant portion of the total amount of lipid intermediates is bound (Fig. 8A), resulting in similar values for the  $IC_{50}$  of bacitracin and the *in vitro*  $K_D$  (Fig. 8B). In contrast, the concentration of extracellularly presented lipid II is ~two orders of magnitude lower and the reduction of this concentration to 50% by antibiotic binding, e.g. by nisin, at the *in vitro*  $K_D$  leads to a negligible reduction of the total amount of lipid intermediates (Fig. 8C). Here, the high-abundant lipid intermediates serve as a reservoir and the ongoing circular flux of lipid intermediates quickly replenish the lipid II pool when it is diminished by antibiotic binding. The antibiotic concentration that causes a distinct reduction of total amount of lipid intermediates and thereby provokes a half-maximal rate of peptidoglycan synthesis, consequently, has to exceed the  $K_D$  significantly (Fig. 8D). Thus, the reduced *in vivo* efficacy of lipid II-targeting antibiotics result from the fact that the concentration of extracellularly accessible lipid II is much lower than the concentration of other intermediates of the lipid II cycle.

Eventually, beyond this mechanistic explanation for the *in vivo* efficacy gap, we also aimed to rationalize this phenomenon and find a mathematical equation describing how the antibiotic efficacy depends on the abundance of its cellular target. Here, an in-depth analysis of a reduced model version enabled us to find an analytical expression for the  $IC_{50}$ , which clearly revealed the factors that affect the *in vivo* efficacy of cell wall antibiotics:

$$IC_{50} \approx K_D \left( 1 + \frac{[R]}{[T]} \right)$$

$[T]$  represents the concentration of the antibiotic target and  $[R]$  describes the sum over all concentrations of the other (non-target) lipid intermediates, referred to as bactoprenol reservoir. We defined  $\left( 1 + \frac{[R]}{[T]} \right)$  as ‘buffering factor’, which quantifies the discrepancy between  $IC_{50}$  and  $K_D$ . According to this equation, the  $IC_{50}$  and thereby the *in vivo* efficacy of a lipid II cycle-active antibiotic not only depends on its *in vitro* activity but also on the relative abundance of its target intermediate compared to the sum of all other intermediates (Fig. 8E, *horizontal axis*). For antibiotics that target the most-abundant intermediate UPP, such as bacitracin, the bactoprenol reservoir is small and  $\frac{[R]}{[T]} \ll 1$ , such that  $IC_{50} \approx K_D$ . In contrast, for lipid II-binding antibiotics, the massive bactoprenol reservoir leads to a significant shift of the  $IC_{50}$  compared to the  $K_D$  ( $\frac{[R]}{[T]} \gg 1$ ) and the observed large *in vivo* efficacy gap. Hence, our results clearly showed that the reduction in the *in vivo* efficacy is most pronounced for lipid II-binding antibiotics. As they represent a large group within the cell wall antibiotics, it is plausible that bacteria have evolved to minimize the concentration of extracellularly accessible lipid II and we suggested this novel principle of ‘minimal target exposure’ as an intrinsic resistance mechanisms towards cell wall antibiotics.

However, as a second major result, our theory predicted that this intrinsic resistance can be circumvented - at least partially - by antibiotics that cooperatively bind their targets and thereby provides the first quantitative explanation for the pivotal role of cooperative binding for the efficiency of vancomycin and other glycopeptide antibiotics (Jia *et al.*, 2013; Loll *et al.*, 1998; Wang *et al.*, 2018). When expanding our model analysis to cooperative binding antibiotics, we were able to find a generalized mathematical expression describing how antibiotic efficacy additionally depends on the cooperativity in antibiotic-target interactions, quantified by the Hill coefficient  $n$ :



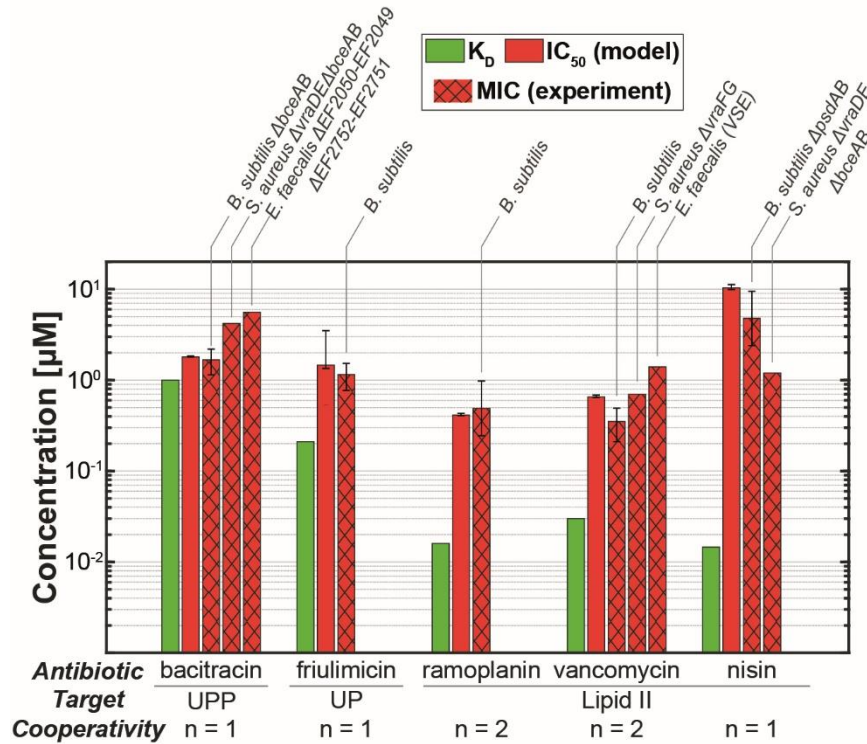


**Figure 9: Prediction of the *in vivo* efficacy for various cell wall antibiotics in diverse Gram-positive organisms.** The developed theory predicts the *in vivo* efficacy ( $IC_{50}$ , red solid bars) exclusively from the antibiotics *in vitro* dissociation constant ( $K_D$ , green bars) and available information about the cooperativity in antibiotic-target-interaction. The model predictions are in good agreement with experimental data for *B. subtilis* (Mota-Meira *et al.*, 2000; Radeck *et al.*, 2016; Staroń *et al.*, 2011; Tiyanont *et al.*, 2006; Wecke *et al.*, 2009), *S. aureus* (Hiron *et al.*, 2011; Yoshida *et al.*, 2011) and *E. faecalis* (Gebhard *et al.*, 2014, Shaaly *et al.*, 2013) strains deleted for the known resistance determinants against the different antibiotics (MIC, red dashed bars), highlighting the universality of the theoretical model for various Gram-positive organisms. Error bars of literature MIC values represent standard deviations from multiple measurements, when available. Error bars for the model predictions of  $IC_{50}$  values represent confidence intervals propagated from uncertainties in the model parameters.

$$IC_{50} \approx K_D \sqrt[n]{1 + \frac{[R]}{[T]}}$$

This equation demonstrates that the Hill coefficient  $n$  attenuates the buffering factor that shifts the  $IC_{50}$  according to the relative abundance of the antibiotic target via the  $n^{\text{th}}$ -root. Thus, the higher the cooperativity  $n$  in antibiotic-target interaction, the lower the buffering factor and the smaller the discrepancy between  $IC_{50}$  and  $K_D$  (Fig. 8E, vertical axis). Obviously, this effect is particularly pronounced if the buffering factor is large, as for lipid II-binding antibiotics. Hence, our results demonstrated that cooperative binding can significantly boost the *in vivo* efficacy of lipid II-binding antibiotics.

To summarize, the theory presented here correctly predicted the *in vivo* efficacy of five different cell wall antibiotics against the Gram-positive model organism *B. subtilis* and deciphered the factors that determine this efficacy. Thereby, it resolved the longstanding conundrum of a significantly reduced *in vivo* efficacy of lipid II-binding antibiotics, which is explained by the low abundance of intermediate lipid II in the lipid II cycle. Since the model was based on cumulative information about the lipid II cycle in diverse bacterial species, we hypothesized that it might serve as a universal description of the essential pathway of cell wall biosynthesis and expected the discovered principles to apply to other Gram-positive bacteria as well, including pathogens. In fact, experimental studies of Gram-positive pathogens revealed similar *in vivo* efficacy gaps for lipid II-binding antibiotics as observed and analysed for *B. subtilis* (Fig. 9) (Gebhard *et al.*,

2014; Hiron *et al.*, 2011; Yoshida *et al.*, 2011), letting us suggest that the asymmetric distribution of lipid II cycle intermediates is conserved amongst Gram-positive organisms and the principle of minimal target exposure might be a common intrinsic resistance strategy.

### 3.5 Paper III: From modules to networks: A systems-level analysis of the bacitracin stress response in *Bacillus subtilis*

In the manuscript 'From modules to networks: A systems-level analysis of the bacitracin stress response in *Bacillus subtilis*' by Hannah Piepenbreier, Andre Sim, Carolin M. Kobras, Jara Radeck, Thorsten Mascher, Susanne Gebhard and Georg Fritz (Piepenbreier *et al.*, 2019b), we followed up on the systems-level analysis of cell wall antibiotic action, this time focussing on the role of cell envelope stress response systems in protecting cell wall biosynthesis from antibiotic-induced perturbations. Combining quantitative gene expression experiments with computational modelling, we sought to decipher regulatory mechanisms of the multi-layered bacitracin stress response in *B. subtilis*. More precisely, we studied how the primary bacitracin resistance determinant, BceAB, and the secondary resistance layer, BcrC, interact to combat bacitracin-induced perturbations of the lipid II cycle. To address this question, we first experimentally monitored cell growth and gene expression of both stress response modules in *B. subtilis* wildtype and mutant strains deficient for one or even both modules under varying bacitracin concentrations. The experimental results revealed quantitative differences in bacitracin sensitivity and response intensity of the two modules and demonstrated how the loss of one or both modules affects *B. subtilis* bacitracin resistance, confirming the previously postulated hierarchy (Radeck *et al.*, 2016). To understand how the individual modules confer resistance in mutants in which the other module is missing and how they interact to shape the wildtype response towards bacitracin, we aimed for a quantitative description of the whole bacitracin stress response network. To this end, we expanded the previously developed model of the lipid II cycle (Piepenbreier *et al.*, 2019a) by a theoretical description of the  $\sigma^M$ -control of BcrC expression and incorporated additionally a pre-existing theory of the Bce-system (Fritz *et al.*, 2015). When calibrating this model with the quantitative experimental data describing the response characteristics of the individual modules towards bacitracin, we correctly predicted the susceptibility of the *B. subtilis* wildtype towards bacitracin. As our theory did not include any additional layers of regulation, we concluded from these results that the properties of the lipid II cycle itself contribute to control the interplay between both bacitracin stress response determinants in the wildtype.

In addition, by studying the diverse mutant scenarios within our theory in detail, we were also able to formulate the hypothesis that *B. subtilis* compensates for a loss of BcrC by an increased total number of intermediates in the lipid II cycle. In a  $\Delta bcrC$  mutant strain, not only the secondary bacitracin stress response determinant but also an important lipid II cycle enzyme is lacking, leading to a reduced dephosphorylation of UPP and accordingly, UPP accumulation and depletion of all other lipid intermediate pools. An increased total amount of lipid intermediates would counterbalance this depletion of all other lipid intermediate pools, thereby contributing to a homeostasis in cell wall synthesis. Testing this hypothesis by relative quantitative RT-PCR (qPCR), we indeed found higher transcript levels for some  $\sigma^M$ -controlled genes involved in the *de novo* production of lipid carrier UPP in a  $\Delta bcrC$  mutant compared to the wildtype, letting us conclude that *B. subtilis* upregulates the UPP synthesis to raise the total amount of lipid intermediates in response to a loss of BcrC. In the end, we demonstrated that the significantly higher UPP levels caused by the increased production and accumulation in a



$\Delta bcrC$  mutant strain can also explain the increased activation of the primary resistance determinant BceAB when BcrC is lacking.

Taken together, the theory presented in this paper precisely captured the response characteristics of the two bacitracin stress response modules and correctly predicted the susceptibility of *B. subtilis* wildtype and single or double mutants towards bacitracin. Thus, it not only provides a comprehensive quantitative description of the bacitracin stress response in *B. subtilis* but also enabled us to uncover principles that control the interplay between bacitracin detoxification via BceAB and maintenance of lipid II cycle homeostasis via BcrC. Interestingly, we were able to explain the stronger induction of  $\sigma^M$  in  $\Delta bcrC$  mutant strains (Zhao *et al.*, 2016) by a secondary role of this regulator in the homeostatic control of lipid intermediate concentrations when BcrC is lacking.

### 3.6 Conclusion and Outlook

A detailed understanding of both the effect of antibiotic action on bacterial growth and the strategies bacteria employ to protect against antibiotics is crucial to combat the alarming evolution of antibiotic-resistant bacteria, as this can guide the development of novel antibiotics and alternative treatment strategies. Within this chapter, an in-depth analysis of the perturbation of cell wall synthesis by cell wall antibiotics and the protective role of cell envelope stress responses in this context was presented.

The first study presented here shed light on the systems-level behaviour of the lipid II cycle under antibiotic perturbations. While benefiting greatly from experimental insights into the cellular concentrations of the intermediates and kinetic constants of involved enzymes, the first quantitative computational model of the lipid II cycle in *B. subtilis* was developed and the antibiotic binding to lipid II cycle intermediates was studied. The theory revealed a highly asymmetric distribution of lipid intermediates and uncovered that the cell wall antibiotic's *in vivo* efficacy scales with the relative abundance of the targeted lipid II cycle intermediate. Thus, a novel principle of 'minimal target exposure' was postulated as an intrinsic resistance mechanism to counteract cell wall antibiotic attack, not only relevant for in *B. subtilis* but also other Gram-positive pathogenic bacteria. In contrast to the traditional stress response strategies towards antimicrobial compounds, this principle of minimal target exposure is not an inducible stress response but can rather be understood as an 'evolutionary stress response'. Bacteria may have evolved this highly asymmetric distribution of lipid II cycle intermediates and especially the reduced abundance of lipid II in response to frequent cell envelope stress caused by lipid II-binding antibiotics in nature and medicine. Although the permanent modification of the pentapeptide chain is a known strategy to combat vancomycin attack (Cetinkaya *et al.*, 2000), it is plausible that a complex and essential molecule such as lipid II can hardly be modified completely - especially not in the core components as the pyrophosphate and the carbohydrate moieties, which represent the binding sites for most other lipid II-binding antibiotics. Thus, the reduction of the target exposure can be seen as an effective alternative resistance strategy towards lipid II-binding antibiotics that is compatible with the pivotal role of the target molecule in the biosynthetic pathway. As the success of this strategy critically depends on the cyclic nature of the lipid II cycle, it is plausible that the principle of minimal target exposure also applies to other cyclic biosynthetic pathways that are attacked by antibiotics, such as the cyclic biosynthesis of the second cell wall component, WTA (Brown *et al.*, 2013; Swoboda *et al.*, 2010). Obviously, the development of new antibiotics

clearly benefit from these findings, as they suggest the most effective perturbation of cyclic biosynthetic pathways is by antibiotics that bind to highly abundant intermediates. If only low-abundant intermediates are accessible, cooperative binding should be considered to boost antibiotic potency, as our study also showed.

A model expansion with the experimentally well-characterized *B. subtilis* bacitracin stress response network then revealed that the properties of the lipid II cycle not only determine the efficacy of cell wall antibiotics but also contribute to the regulation of the overall stress response to the cell wall antibiotic bacitracin in *B. subtilis*. Here, it would be worthwhile to investigate - both from an experimental and theoretical perspective - if a perturbation of the lipid II cycle additionally to the bacitracin-induced one, such as by further cell wall antibiotics, would impair the regulatory role of the cycle and unbalance the interplay between the two resistance modules. Controlling the interplay between stress response modules that protect the same biosynthetic pathway by properties of the pathway itself appears as a cost-efficient regulation strategy and thus, it would furthermore be interesting to study if this strategy also applies to additional stress response networks.

Besides, the study of the bacitracin stress response network in *B. subtilis* uncovered  $\sigma^M$ -dependent upregulation of lipid carrier production in response to a *bcrC* deletion, as the lack of BcrC induces UPP accumulation and depletion of all other intermediates of the lipid II cycle. Interestingly, activation of  $\sigma^M$  has also been previously noted in strains carrying further mutations that affect the abundance or distribution of lipid II cycle intermediates. For instance, a mutation that reduces the expression of UppS, the undecaprenol pyrophosphate synthetase catalysing the final step of UPP synthesis, leads to a modest induction of the  $\sigma^M$  regulon (Lee and Helmann, 2013). Furthermore, upregulation of the  $\sigma^M$  regulon was also observed in strains affected in WTA biogenesis (D'Elia *et al.*, 2009). Like PG synthesis, WTA synthesis requires UP as a carrier to ferry precursors across the cell membrane and depends on UPP production and dephosphorylation (Brown *et al.*, 2013; Swoboda *et al.*, 2010). A perturbation of WTA synthesis consequently affects the availability of UPP and UP as lipid carriers for PG synthesis and thereby can cause re-distribution and shortage of intermediates in the lipid II cycle. In fact, it was shown that mutations in the later steps of WTA synthesis are lethal, presumably due to the sequestration of the limiting lipid carrier on dead-end products (D'Elia *et al.*, 2006). Together, the previous results and the new insights suggest that one important role of  $\sigma^M$  as cell wall homeostasis regulator is to control the abundance and (correct) distribution of lipid II cycle intermediates to ensure progression of PG synthesis under cell wall-perturbing conditions - elicited both by cell wall antibiotics and the lack of important cell wall synthesis enzymes. The regulation of lipid II cycle intermediate balance can occur at different tuning knobs, dependent on which pathway is perturbed, as enzymes involved in UPP synthesis and WTA synthesis and also enzymes that provide a backup for key-steps in PG synthesis are part of the  $\sigma^M$  regulon (Eiamphungporn and Helmann, 2008; Helmann, 2016). According to this function of  $\sigma^M$ , one could speculate that the cognate anti- $\sigma$ -factor YhdLK might release  $\sigma^M$  in response to changes in the distribution of lipid II cycle intermediates and that the physiological stimulus might be the accumulation or depletion of a specific lipid II cycle intermediate. To further investigate this, it would be worthwhile to continue experiments testing the connection between perturbations of PG, WTA and UPP synthesis caused by mutations in important steps and  $\sigma^M$  activation.

Both studies clearly confirm theoretical modelling approaches as powerful tools to study bacterial stress responses towards antibiotics. The mathematical models reconciled *in vitro* and *in vivo* experiments and thereby deciphered complex features of the modelled systems,

which were not accessible by experimentation alone, such as the non-trivial emergent properties of the lipid II cycle as well as the regulatory interplay in the bacitracin stress response network in *B. subtilis*. Of note, the study on the systems-level response of the lipid II cycle towards cell wall antibiotics has benefitted two-fold from theoretical modelling: While model simulations demonstrated *how* the lipid II cycle behaves under antibiotic treatment, the in-depth model analyses of the reduced model deciphered *why* it behaves as it does. Analogous theoretical studies provided important insights into the bacterial responses towards other important classes of antibiotics, such as ribosome-targeting antibiotics (Deris *et al.*, 2013; Greulich *et al.*, 2015; Greulich *et al.*, 2017) or DNA-replication inhibitors (Bollenbach *et al.*, 2009), and also  $\beta$ -lactams (Murphy *et al.*, 2008). From all these results, it is clearly visible that theoretical modelling has the potential to unravel complex, non-trivial principles of bacterial stress responses towards antibiotics. However, key to the success of modelling are certainly the incorporation of experimental data as well as the validation of the model predictions by experiments, such that it is worthwhile to follow up on combined approaches in the fight against antibiotic-resistant bacteria.

As a next step on this way, the theory of cell wall biosynthesis developed here can serve as a basis for further applications that can augment our understanding of cell wall antibiotic action in Gram-positive bacteria. For instance, an analogous study of the second class of cell wall antibiotics, the substrate-inhibiting compounds, can be performed within the existing theoretical framework. In addition, the developed model also allows the study of the effect of antibiotic combinations on the progression of the lipid II cycle, particularly combinations of antibiotics that feature different inhibition mechanisms (substrate-binding vs. enzyme-binding), which might shed light on promising drug-drug combinations for treatment of pathogen infections. Moreover, by expanding the model with a detailed quantitative description of the PG precursor synthesis pathway, the effect of additional cell wall antibiotics targeting this pathway, such as fosfomicin (Kahan *et al.*, 1974), can be investigated. This, however, clearly requires a seamless biochemical characterization of the enzymes involved in PG precursor production by further experimental studies.

To advance our knowledge of the regulation of bacterial stress responses towards cell wall antibiotics in wildtype cells, the theory of cell wall biosynthesis should be expanded with 'mathematical building blocks' describing CESR modules for further cell wall antibiotics (as illustrated in Section 3.3) - analogous to the procedure demonstrated here for the bacitracin resistance network in *B. subtilis*. Moreover, the addition of a detailed description of WTA biosynthesis and UPP production pathway could also allow the investigation of the role of  $\sigma^M$  in controlling the interplay between PG, WT and UPP synthesis in response to cell wall antibiotics (as detailed above) from a theoretical perspective. As several of these CESR modules are highly conserved in *Firmicutes* bacteria (Gebhard, 2012; Revilla-Guarinos *et al.*, 2014), it is conceivable that these broader studies uncover general regulatory mechanisms of bacterial resistance against cell wall antibiotics.

It would also be worthwhile to couple the existing theories with the bacterial growth laws describing the basic physiology of bacterial growth (Klumpp and Hwa, 2014; Scott and Hwa, 2011; Scott *et al.*, 2010) to study physiological adaptations to cell wall antibiotics. Since it was previously described that cells adapt their cell physiology and reduce their growth rate in response to antibiotic treatment (Balaban *et al.*, 2004; Brauner *et al.*, 2016; Lewis, 2007), it is of great importance to study from a quantitative perspective how the bacterial growth rate affects antibiotic efficacy. For instance, for the group of ribosome-targeting antibiotics, non-trivial efficacy-growth rate relations have been observed and were attributed to growth-rate

dependent variations in cellular ribosome content and the ribosome binding kinetics of the antibiotic by mathematical modelling (Greulich *et al.*, 2015). Likewise, it would be important to investigate how growth rate-dependent adaptations in the lipid II cycle affect the cycle properties and thereby the efficacy of cell wall antibiotics. Here, experimental determinations of both, concentration of lipid II cycle enzymes and lipid intermediates as well as antibiotic MICs under different growth rates could guide a model expansion to decipher efficacy-growth rate relations for cell wall antibiotics. Moreover, it will be important to analyse growth-rate dependent variations in the expression of specific resistance determinants experimentally, as they can certainly affect the efficacy-growth rate relation. From a theoretical perspective, it would be then interesting to study the interplay between the specific resistance mechanisms and the adaptations in cell physiology that ultimately shapes the overall cellular response towards cell wall antibiotics and determines bacterial antibiotic resistance.

## 4. References

- Alonso, A.A., Molina, I., and Theodoropoulos, C. (2014) Modeling bacterial population growth from stochastic single-cell dynamics. *Appl Environ Microbiol* **80**: 5241-5253.
- Andersson, D.I., Hughes, D., and Kubicek-Sutherland, J.Z. (2016) Mechanisms and consequences of bacterial resistance to antimicrobial peptides. *Drug Resist Updat* **26**: 43-57.
- Andrews, S.C., Robinson, A.K., and Rodríguez-Quifones, F. (2003) Bacterial iron homeostasis. *FEMS Microbiol Rev* **27**: 215-237.
- Anzaldi, L.L., and Skaar, E.P. (2010) Overcoming the heme paradox: heme toxicity and tolerance in bacterial pathogens. *Infect and Immun*, **78**: 4977-4989.
- Argüello, J.M., Raimunda, D., and Padilla-Benavides, T. (2013) Mechanisms of copper homeostasis in bacteria. *Front Cell Infect Microbiol* **3**: 73.
- Arsène, F., Tomoyasi, T., and Bukau, B. (2000) The heat shock response of *Escherichia coli*. *Int J Food Microbiol* **55**: 3-9.
- Asai, K. (2018) Anti-sigma factor-mediated cell surface stress responses in *Bacillus subtilis*. *Genes Genet Syst* **92**: 223-234.
- Axley, M.J., and Grahame, D.A. (1991) Kinetics for formate dehydrogenase of *Escherichia coli* formate-hydrogenlyase. *J Biol Chem* **266**: 13731-13736.
- Bahar, A.A., and Ren, D. (2013) Antimicrobial peptides. *Pharmaceuticals (Basel)*, **28**: 1543-1575.
- Balaban, N.Q., Merrin, J., Chait, R., Kowalik, L., and Leibler, S. (2004) Bacterial persistence as a phenotypic switch. *Science* **305**: 1622-1625.
- Balezza, E., López-Bojorquez, L.N., Martínez-Antibio, A., Resendis-Antonio, O., Lozada-Chávez, I., Balderas-Martínez, Y.I., Encarnación, A., and Collado-Vides, J. (2009) Regulation by transcription factors in bacteria: Beyond description. *FEMS Microbiol Rev* **33**: 133-151.
- Barreteau, H., Kovac, A., Boniface, A., Sova, M., Gobec, S., and Blanot, D. (2008) Cytoplasmic steps of peptidoglycan biosynthesis. *FEMS Microbiol Rev* **32**: 168-207.
- Barreteau, H., Magnet, S., El Ghachi, M., Touzé, T., Arthur, M., Mengin-Lecreulx, D., and Blanot, D. (2009) Quantitative high-performance liquid chromatography analysis of the pool levels of undecaprenyl phosphate and its derivatives in bacterial membranes. *J Chromatogr B Analyt Technol Biomed Life Sci* **877**: 213-220.
- Bauer, M.E., and Shafer, W.M. (2015) On the *in vivo* significance of bacterial resistance to antimicrobial peptides. *Biochim Biophys Acta* **1848**: 3101-3111.
- Beauregard, D.A., Maguire, A.J., Williams, D.H., and Reynolds, P.E. (1997) Semiquantitation of cooperativity in binding of vancomycin-group antibiotics to vancomycin-susceptible and -resistant organisms. *Antimicrob Agents Chemother* **41**: 2418-2423.
- Bernard, R., El Ghachi, M., Mengin-Lecreulx, D., Chippaux, M., and Denizot, F. (2005) BcrC from *Bacillus subtilis* acts as an undecaprenyl pyrophosphate phosphatase in bacitracin resistance. *J Biol Chem* **280**: 28852-28857.

- Bernard, R., Guiseppi, A., Chippaux, M., Foglino, M., and Denizot, F. (2007) Resistance to bacitracin in *Bacillus subtilis*: unexpected requirement of the BceAB ABC transporter in the control of expression of its own structural genes. *J Bacteriol* **189**: 8636-8642.
- Bibb, L.A., King, N.D., Kunkle, C.A., and Schmitt, M.P. (2005) Analysis of a heme-dependent signal transduction system in *Corynebacterium diphtheriae*: Deletion of the *chrAS* genes results in heme sensitivity and diminished heme-dependent activation of the *hmuO* promoter. *Infect Immun* **73**: 7406-7412.
- Bibb, L.A., Kunkle, C.A., and Schmitt, M.P. (2007) The ChrA-ChrS and HrrA-HrrS signal transduction systems are required for activation of the *hmuO* promoter and repression of the *hemA* promoter in *Corynebacterium diphtheriae*. *Infect Immun* **75**: 2421-2431.
- Bibb, L.A., and Schmitt, M.P. (2010) The ABC transporter HrtAB confers resistance to hemin toxicity and is regulated in a hemin-dependent manner by the ChrAS two-component system in *Corynebacterium diphtheriae*. *J Bacteriol* **192**: 4606-4617.
- Bierbaum, G., and Sahl, H.G. (2009) Lantibiotics: Mode of action, biosynthesis and bioengineering. *Curr Pharm Biotechnol* **10**: 2-18.
- Bintu, L., Buchler, N.E., Garcia, H.G., Gerland, U., Hwa, T., Kondev, J., Kuhlman, T., and Phillips, R. (2005a) Transcriptional regulation by the numbers: applications. *Curr Opin Genet Dev* **15**: 125-135.
- Bintu, L., Buchler, N.E., Garcia, H.G., Gerland, U., Hwa, T., Kondev, J., and Phillips, R. (2005b) Transcriptional regulation by the numbers: models. *Curr Opin Genet Dev* **15**: 116-124.
- Bischofs, I.B., Hug, J.A., Liu, A.W., Wolf, D.M., and Arkin, A.P. (2009) Complexity in bacterial cell-cell communication: Quorum signal integration and subpopulation signaling in the *Bacillus subtilis* phosphorelay. *Proc Natl Acad Sci U S A* **106**: 6459-6464.
- Björkman, J., and Andersson, D.I. (2000) The cost of antibiotic resistance from a bacterial perspective. *Drug Resist Updat* **3**: 237-245.
- Blair, J.M.A., Webber, M.A., Baylay, A.J., Ogbolu, D.O., and Piddock, L.J.V. (2015) Molecular mechanisms of antibiotic resistance. *Nat Rev Microbiol* **13**: 42-51.
- Bollenbach, T., Quan, S., Chait, R., and Kishony, R. (2009) Nonoptimal microbial response to antibiotics underlies suppressive drug interactions. *Cell* **139**: 707-718.
- Booth H.S., Burden C.J., Hegland M., Santoso L. (2007) A Stochastic Model of Gene Regulation Using the Chemical Master Equation. In *Mathematical Modeling of Biological Systems, Volume I*. Deutsch A., Bruschi L., Byrne H., Vries G., and Herzog H. (eds.). Birkhäuser Boston, pp. 71-81.
- Borders, D.B., Leese, R.A., Jarolmen, H., Francis, N.D., Fantini, A.A., Falla, T., Fiddes, J.C., and Aumelas, A. (2007) Laspartomycin, an acidic lipopeptide antibiotic with a unique peptide core. *J Nat Prod* **70**: 443-446.
- Bott, M., and Brocker, M. (2012) Two-component signal transduction in *Corynebacterium glutamicum* and other corynebacteria: on the way towards stimuli and targets. *Appl Microbiol Biotechnol* **94**: 1131-1150.
- Bourgeois-Nicolaos, N., Moubareck, C., Mangeney, N., Butel, M.-J., and Doucet-Populaire, F. (2006) Comparative study of *vanA* gene transfer from *Enterococcus faecium* to *Enterococcus faecalis* and to *Enterococcus faecium* in the intestine of mice. *FEMS Microbiol Lett* **254**: 27-33.

- Bozja, J., Yi, K., Shafer, W.M., and Stojilkovic, I. (2004) Porphyrin-based compounds exert antibacterial action against the sexually transmitted pathogens *Neisseria gonorrhoeae* and *Haemophilus ducreyi*. *Int J Antimicrob Agents* **24**: 578-584.
- Brandish, P.E., Burnham, M.K., Lonsdale, J.T., Southgate, R., Inukai, M., and Bugg, T.D.H. (1996) Slow binding inhibition of phospho-N-acetylmuramyl-pentapeptide-translocase (*Escherichia coli*) by mureidomycin A. *J Biol Chem* **271**: 7609-7614.
- Brandish, P.E., Kimura, K.I., Inukai, M., Southgate, R., Lonsdale, J.T., and Bugg, T.D.H. (1996) Modes of action of tunicamycin, liposidomycin B, and mureidomycin A: Inhibition of phosphor-N-acetylmuramyl-pentapeptide translocase from *Escherichia coli*. *Antimicrob Agents Chemother* **40**: 1640-1644.
- Brandman, O., and Meyer, T. (2008) Feedback loops shape cellular signals in space and time. *Science* **332**: 390-395.
- Brauner, A., Fridman, O., Gefen, O., and Balaban, N.Q. (2016) Distinguishing between resistance, tolerance and persistence to antibiotic treatment. *Nat Rev Microbiol* **14**: 320-330.
- Breukink, E., and de Kruijff, B. (2006) Lipid II as a target for antibiotics. *Nat Rev Drug Discov* **5**: 321-332.
- Breukink, E., Wiedemann, I., van Kraaij, C., Kuipers, O.P., Sahl, H.G., and de Kruijff, B. (1999) Use of cell wall precursor lipid II by a pore-forming peptide antibiotic. *Science* **286**: 2361-2364.
- Brooks, B.E. and Buchanan, S.K. (2008) Signaling mechanisms for activation of extracytoplasmic function (ECF) sigma factors. *Biochim Biophys Acta* **1778**: 1930-1945.
- Brown, K.L., and Hughes, K.T. (1995) The role of anti-sigma factors in gene regulation. *Mol Microbiol* **16**: 397-404.
- Brown, S., Santa Maria, J.P., and Walker, S. (2013) Wall teichoic acids of Gram-positive bacteria. *Annu Rev Microbiol* **67**: 313-336.
- Bugg, T.D.H., Braddick, D., Dowson, C.G., and Roper, D.I. (2011) Bacterial cell wall assembly: still an attractive antibacterial target. *Trends Biotechnol* **29**: 167-173.
- Burgos, J.M., and Schmitt, M.P. (2016) The ChrSA and HrrSA two-component systems are required for transcriptional regulation of the *hemaA* promoter in *Corynebacterium diphtheriae*. *J Bacteriol* **198**: 2419-2430.
- Bush, K. (2010) Bench-to-bedside review: The role of  $\beta$ -lactamases in antibiotic-resistant Gram-negative infections. *Crit Care* **14**: 224.
- Bush, K., and Bradford, P.A. (2019) Interplay between  $\beta$ -lactamases and new  $\beta$ -lactamase inhibitors. *Nat Rev Microbiol* **17**: 295-306.
- Butcher, B.G., Lin, Y.-P., and Helmann, J.D. (2007) The *yydFGHIJ* operon of *Bacillus subtilis* encodes a peptide that induces the LiaRS two-component system. *J Bacteriol* **189**: 8616-8625.
- Butcher, B.G., Mascher, T., and Helmann, J.D. (2008) Environmental Sensing and the Role of Extracytoplasmic Function Sigma Factors. In *Bacterial Physiology*. El-Sharoud, W. (ed). Berlin, Heidelberg: Springer Berlin Heidelberg, pp. 233–261.
- Campbell, J., Singh, A.K., Swoboda, J.G., Gilmore, M.S., Wilkinson, B.J., and Walker, S. (2012) An antibiotic that inhibits a late step in wall teichoic acid biosynthesis induces the

- cell wall stress stimulon in *Staphylococcus aureus*. *Antimicrob Agents Chemother* **56**: 1810-1820.
- Cao, M., and Helmann, J.D. (2002) Regulation of the *Bacillus subtilis* *bcrC* bacitracin resistance gene by two Extracytoplasmic Function  $\sigma$  factors. *J Bacteriol* **184**: 6123-6129.
- Cao, M., and Helmann, J.D. (2004) The *Bacillus subtilis* Extracytoplasmic-Function  $\sigma^X$  factor regulates modification of the cell envelope and resistance to cationic antimicrobial peptides. *J Bacteriol* **186**: 1136-1146.
- Cao, M., Kobel, P.A., Morshedi, M.M., Wu, M.F.W., Paddon, C., and Helmann, J.D. (2002a) Defining the *Bacillus subtilis*  $\sigma^W$  regulon: A comparative analysis of promoter consensus search, run-off transcription/microarray analysis (ROMA), and transcriptional profiling approaches. *J Mol Biol* **316**: 443-457.
- Cao, M., Wang, T., Ye, R., and Helmann, J.D. (2002b) Antibiotics that inhibit cell wall biosynthesis induce expression of the *Bacillus subtilis*  $\sigma^W$  and  $\sigma^M$  regulons. *Mol Microbiol* **45**: 1267-1276.
- Capra, E.J., and Laub, M.T. (2012) Evolution of two-component signal transduction systems. *Annu Rev Microbiol* **66**: 325-347.
- Cetinkaya, Y., Falk, P., and Mayhall, C.G. (2000) Vancomycin-resistant enterococci. *Clin Microbiol Rev*, **13**: 686-707.
- Chandrangsu, P., Rensing, C., and Helmann, J.D. (2017) Metal homeostasis and resistance in bacteria. *Nat Rev Microbiol* **15**: 338-350.
- Chang, H.-Y., Chou, C.-C., Hsu, M.-F., and Wang, A.H.J. (2014) Proposed carrier lipid-binding site of undecaprenyl pyrophosphate phosphatase from *Escherichia coli*. *J Biol Chem* **289**: 18719-18735.
- Choby, J.E., and Skaar, E.P. (2016) Heme synthesis and acquisition in bacterial pathogens. *J Mol Biol* **428**: 3408-3428.
- Choo, E.J., and Chambers, H.F. (2016) Treatment of Methicillin-Resistant *Staphylococcus aureus* Bacteremia. *Infect Chemother* **48**: 267-273.
- Choudhary, K., Oehler, S., and Narang, A. (2014) Protein distribution from a stochastic model of the *lac* operon of *E. coli* with DNA looping: Analytical solution and comparison with experiments. *PLoS One* **9**: e102580.
- Contreras, H., Chim, N., Credali, A., and Goulding, C.W. (2014) Heme uptake in bacterial pathogens. *Curr Opin Chem Biol* **19**: 34-41.
- Cornelis, P., Wei, Q., Andrews, S.C., and Vinckx, T. (2011) Iron homeostasis and management of oxidative stress response in bacteria. *Metallomics* **3**: 540-549.
- Cotter, P.D., Hill, C., and Ross, R.P. (2005) Bacteriocins: developing innate immunity for food. *Nat Rev Microbiol* **3**: 777-788.
- Crouvoisier, M., Auger, G., Blanot, D., and Mengin-Lecreulx, D. (2007) Role of the amino acid invariants in the active site of MurG as evaluated by site-directed mutagenesis. *Biochimie* **89**: 1498-1508.
- Davis, M.C., Kesthely, C.A., Franklin, E.A., and MacLellan, S.R. (2017) The essential activities of the bacterial sigma factor. *Can J Microbiol* **63**: 89-99.



- De Kruijff, B., van Dam, V., and Breukink, E. (2008) Lipid II: a central component in bacterial cell wall synthesis and a target for antibiotics. *Prostaglandins Leukot Essent Fatty Acids* **79**: 117-121.
- Delcour, J., Ferain, T., Deghorain, M., Palumbo, E., and Hols, P. (1999) The biosynthesis and functionality of the cell-wall of lactic acid bacteria. *Antonie vVan Leeuwenhoek* **76**: 159–184.
- D’Elia, M.A., Millar, K.E., Beveridge, T.J., and Brown, E.D. (2006) Wall teichoic acid polymers are dispensable for cell viability in *Bacillus subtilis*. *J Bacteriol* **188**: 8313-8316.
- D’Elia, M.A., Millar, K.E., Bhavsar, A.P., Tomljenovic, A.M., Hutter, B., Schaab, C., Moreno-Hagelsieb, G., and Brown, E.D. (2009) Probing teichoic acid genetics with bioactive molecules reveals new interactions among diverse processes in bacterial cell wall biogenesis. *Chem Biol* **16**: 548-556.
- Delmar, J.A., Su, C.-C., and Yu, E.W. (2014) Bacterial multidrug efflux transporters. *Annu Rev Biophys* **43**: 93-117.
- Deris, J.B., Kim, M., Zhang, Z., Okano, H., Hermsen, R., Groisman, A., and Hwa, T. (2013) The innate growth bistability and fitness landscapes of antibiotic-resistant bacteria. *Science* **342**: 1237435.
- Dintner, S., Heermann, R., Fang, C., Jung, K., and Gebhard, S. (2014) A sensory complex consisting of an ATP-binding cassette transporter and a two-component regulatory system controls bacitracin resistance in *Bacillus subtilis*. *J Biol Chem* **289**: 27899-27910.
- Dintner, S., Staron, A., Berchtold, E., Petri, T., Mascher, T., and Gebhard, S. (2011) Coevolution of ABC transporters and two-component regulatory systems as resistance modules against antimicrobial peptides in *Firmicutes* Bacteria. *J Bacteriol* **193**: 3851-3862.
- Domínguez-Escobar, J., Wolf, D., Fritz, G., Höfler, C., Wedlich-Söldner, R., and Mascher, T. (2014) Subcellular localization, interactions and dynamics of the phage-shock protein-like Lia response in *Bacillus subtilis*. *Mol Microbiol* **92**: 716-732.
- Draper, L.A., Ross, R.P., Hill, C., and Cotter, P.D. (2008) Lantibiotic immunity. *Cure Protein Pept Sci* **9**: 39–49.
- Drazek, E.S., Hammack, C.A., and Schmitt, M.P. (2000) *Corynebacterium diphtheriae* genes required for acquisition of iron from haemin and haemoglobin are homologous to ABC haemin transporters. *Mol Microbiol* **36**: 68-84.
- Dubois, J.-Y.F., Kouwen, T.R.H.M., Schurich, A.K.C., Reis, C.R., Ensing, H.T., Trip, E.N., Zweers, J.C., and van Dijl, J.M. (2009) Immunity to the bacteriocin sublancin 168 is determined by the SunI (YoIF) protein of *Bacillus subtilis*. *Antimicrob Agents Chemother* **53**: 651-661.
- Economou, N.J., Cocklin, S., and Loll, P.J. (2013) High-resolution crystal structure reveals molecular details of target recognition by bacitracin. *Proc Natl Acad Sci U S A* **110**: 14207-14212.
- Eiamphungporn, W., and Helmann, J.D. (2008) The *Bacillus subtilis*  $\sigma^M$  regulon and its contribution to cell envelope stress responses. *Mol Microbiol* **67**: 830-848.
- Ellermeier, C.D., Hobbs, E.C., González-Pastor, J.E., and Losick, R. (2006) A three-protein signaling pathway governing immunity to a bacterial cannibalism toxin. *Cell* **124**: 549-559.

- El-Samad, H., Kurata, H., Doyle, J.C., Gross, C.A., and Khammash, M. (2005) Surviving heat shock: control strategies for robustness and performance. *Proc Natl Acad Sci U S A* **102**: 2736-2741.
- Ernst, C.M., and Peschel, A. (2011) Broad-spectrum antimicrobial peptide resistance by MprF-mediated aminoacylation and flipping of phospholipids. *Mol Microbiol* **80**: 290-299.
- Everse, J., and Hsia, N. (1997) The toxicities of native and modified hemoglobins. *Free Radic Biol Med* **22**: 1075–1099.
- Fang, X., Tiyanont, K., Zhang, Y., Wanner, J., Boger, D., and Walker, S. (2006) The mechanism of action of ramoplanin and enduracidin. *Mol Biosyst* **2**: 69-76.
- Fernandes, R., Amador, P, and Prudêncio, C. (2013)  $\beta$ -lactams: Chemical structure, mode of action and mechanisms of resistance. *Rev Med Microbiol* **24**: 7-17.
- Fernandez, A., Lechardeur, D., Derré-Bobillot, A., Couvé, E., Gaudu, P., and Gruss, A. (2010) Two coregulated efflux transporters modulate intracellular heme and protoporphyrin IX availability in *Streptococcus agalactiae*. *PLoS Pathog* **6**: e1000860.
- Fitch, C.D. (1998) Involvement of heme in the antimalarial action of chloroquine. *Trans Am Clin Climatol Assoc* **109**: 97–106.
- Fleming, A. (1929) On the antibacterial action of cultures of a penicillium, with special reference to their use in the isolation of *B. influenzae*. *Br J Exp Pathol* **10**: 226–236.
- Fritz, G., Dintner, S., Treichel, N.S., Radeck, J., Gerland, U., Mascher, T., and Gebhard, S. (2015) A new way of sensing: Need-based activation of antibiotic resistance by a flux-sensing mechanism. *mBio* **6**: e00975.
- Fritz, G., Koller, C., Burdack, K., Tetsch, L., Haneburger, I., Jung, K., and Gerland, U. (2009) Induction kinetics of a conditional pH stress response system in *Escherichia coli*. *J Mol Biol* **393**: 272-286.
- Frunzke, J., Gätgens, C., Brocker, M., and Bott, M. (2011) Control of heme homeostasis in *Corynebacterium glutamicum* by the two-component system HrrSA. *J Bacteriol* **193**: 1212-1221.
- Gauvry, E., Mathot, A.-G., Couvert, O., Leguériel, I., Jules, M., and Coroller, L. (2019) Differentiation of vegetative cells into spores: A kinetic model applied to *Bacillus subtilis*. *Appl Environ Microbiol* **85**: e00322.
- Gebhard, S. (2012) ABC transporters of antimicrobial peptides in *Firmicutes* bacteria - phylogeny, function and regulation. *Mol Microbiol* **86**: 1295-1317.
- Gebhard, S., Fang, C., Shaaly, A., Leslie, D.J., Weimar, M.R., Kalamorz, F., Carne, A., and Cook, G.M. (2014) Identification and characterization of a bacitracin resistance network in *Enterococcus faecalis*. *Antimicrob Agents Chemother* **58**: 1425-1433.
- Geier, F., Fengos, G., Felizzi, F., and Iber, D. (2010) Analysing and constraining signalling networks: Parameter estimation for the user. In *Computational Modeling of Signaling Networks. Methods in Molecular Biology*. Liu, X., and Betterton, M. (eds.). Totowa, NJ: Humana Press, pp. 23-39.
- Geis, A., and Plapp, R. (1978) Phospho-N-acetylmuramoyl-pentapeptide-transferase of *Escherichia coli* K12. Properties of the membrane-bound and the extracted and partially purified enzyme. *Biochim Biophys Acta* **527**: 414–424.

- González-Pastor, J.E., Hobbs, E.C., and Losick, R. (2003) Cannibalism by sporulating bacteria. *Science* **301**: 510-513.
- Goodenough-Lashua, D.M. and Garcia, G.A. (2003) tRNA-guanine transglycosylase from *E. coli*: A ping-pong kinetic mechanism is consistent with nucleophilic catalysis. *Bioorg Chem* **31**: 311-344.
- Goulian, M. (2010) Two-component signaling circuit structure and properties. *Curr Opin Microbiol* **13**: 184-189.
- Greulich, P., Doležal, J., Scott, M., Evans, M.R., and Allen, R.J. (2017) Predicting the dynamics of bacterial growth inhibition by ribosome-targeting antibiotics. *Phys Biol* **14**: 065005.
- Greulich, P., Scott, M., Evans, M.R., and Allen, R.J. (2015) Growth-dependent bacterial susceptibility to ribosome-targeting antibiotics. *Mol Syst Biol* **11**: 796.
- Groban, E.S., Clarke, E.J., Salis, H.M., Miller, S.M., and Voigt, C.A. (2009) Kinetic buffering of cross talk between bacterial two-component sensors. *J Mol Biol* **390**: 380-393.
- Groisman, E.A. (2016) Feedback control of two-component regulatory systems. *Annu Rev Microbiol* **70**: 103-124.
- Gyamerah, M., and Willetts, A.J. (1997) Kinetics of overexpressed transketolase from *Escherichia coli* JM107/pQR700. *Enzyme Microb Technol* **20**: 127-134.
- Hagman, K.E., Pan, W., Spratt, B.G., Balthazar, J.T., Judd, R.C., and Shafer, W.M. (1995) Resistance of *Neisseria gonorrhoeae* to antimicrobial hydrophobic agents is modulated by the *mtrRCDE* efflux system. *Microbiology* **141**: 611-622.
- Hahl, S.K., and Kremling, A. (2016) A comparison of deterministic and stochastic modeling approaches for biochemical reaction systems: On fixed points, means, and modes. *Front Genet* **7**: 157.
- Hansen, J.N. (1994) Nisin as a model food preservative. *Crit Rev Food Sci Nutr* **34**: 69-93.
- Harz, H., Burgdorf, K., and Höltje, J.V. (1990) Isolation and separation of the glycan strands from murein of *Escherichia coli* by reversed-phase high-performance liquid chromatography. *Anal Biochem* **190**: 120-128.
- Hassan, M., Kjos, M., Nes, I.F., Diep, D.B., and Lotfipour, F. (2012) Natural antimicrobial peptides from bacteria: characteristics and potential applications to fight against antibiotic resistance. *J Appl Microbiol* **113**: 723-736.
- Hastie, J.L., Williams, K.B., and Ellermeier, C.D. (2013) The activity of  $\sigma^V$ , an extracytoplasmic function  $\sigma$  factor of *Bacillus subtilis*, is controlled by regulated proteolysis of the anti- $\sigma$ -factor RsiV. *J Bacteriol* **195**: 3135-3144.
- Hasty, J., McMillen, D., Isaacs, F., and Collins, J.J. (2001) Computational studies of gene regulatory networks: *In numero* molecular biology. *Nat Rev Genet* **2**: 268-279.
- Heermann, R., Zigann, K., Gayer, S., Rodriguez-Fernandez, M., Banga, J.R., Kremling, A., and Jung, K. (2014) Dynamics of an interactive network composed of a bacterial two-component system, a transporter and K<sup>+</sup> as mediator. *PLoS One* **9**: e89671.
- Helmann, J.D. (1999) Anti-sigma factors. *Curr Opin Microbiol* **2**: 135-141.
- Helmann, J.D. (2002) The extracytoplasmic function (ECF) sigma factors. *Adv Microb Physiol* **46**: 47-110.

- Helmann, J.D. (2006) Deciphering a complex genetic regulatory network: The *Bacillus subtilis*  $\sigma^W$  protein and intrinsic resistance to antimicrobial compounds. *Sci Prog* **89**: 243–266.
- Helmann, J.D. (2016) *Bacillus subtilis* extracytoplasmic function (ECF) sigma factors and defense of the cell envelope. *Curr Opin Microbiol* **30**: 122-132.
- Helmann, J.D., and Chamberlin, M.J. (1988) Structure and function of bacterial sigma factors. *Annu Rev Biochem* **57**: 839-872.
- Helmann, J.D., Wu, M.F., Kobel, P.A., Gamo, F.J., Wilson, M., Morshedi, M.M., Navre, M., and Paddon, C. (2001) Global transcriptional response of *Bacillus subtilis* to heat shock. *J Bacteriol* **183**: 7318-7328.
- Hentschel, E., Mack, C., Gätgens, C., Bott, M., Brocker, M., and Frunzke, J. (2014) Phosphatase activity of the histidine kinases ensures pathway specificity of the ChrSA and HrrSA two-component systems in *Corynebacterium glutamicum*. *Mol Microbiol* **92**: 1326-1342.
- Heyer, A., Gätgens, C., Hentschel, E., Kalinowski, J., Bott, M., and Frunzke, J. (2012) The two-component system ChrSA is crucial for haem tolerance and interferes with HrrSA in haem-dependent gene regulation in *Corynebacterium glutamicum*. *Microbiology* **158**: 3020-3031.
- Hiron, A., Falord, M., Valle, J., Débarbouillé, M., and Msadek, T. (2011) Bacitracin and nisin resistance in *Staphylococcus aureus*: A novel pathway involving the BraS/BraR two-component system (SA2417/SA2418) and both the BraD/BraE and VraD/VraE ABC transporters. *Mol Microbiol* **81**: 602-622.
- Höltje, J.-V. (1998) Growth of the stress-bearing and shape-maintaining murein sacculus of *Escherichia coli*. *Microbiol Molecular Biol Rev* **62**: 181–203.
- Horsburgh, M.J., and Moir, A. (1999)  $\sigma^M$ , an ECF RNA polymerase sigma factor of *Bacillus subtilis* 168, is essential for growth and survival in high concentrations of salt. *Mol Microbiol* **32**: 41-50.
- Hu, Y., Helm, J.S., Chen, L., Ye, X.-Y., and Walker, S. (2003) Ramoplanin inhibits bacterial transglycosylases by binding as a dimer to lipid II. *J Am Chem Soc* **125**: 8736-8737.
- Huang, X., Gaballa, A., Cao, M., and Helmann, J.D. (1999) Identification of target promoters for the *Bacillus subtilis* extracytoplasmic function  $\sigma$  factor,  $\sigma^W$ . *Mol Microbiol* **31**: 361–371.
- Hurdle, J.G., O'Neill, A.J., Chopra, I., and Lee, R.E. (2011) Targeting bacterial membrane function: an underexploited mechanism for treating persistent infections. *Nat Rev Microbiol* **9**: 62-75.
- Iber, D., Clarkson, J., Yudkin, M.D., and Campbell, I.D. (2006) The mechanism of cell differentiation in *Bacillus subtilis*. *Nature* **441**: 371-374.
- Igoshin, O.A., Price, C.W., and Savageau, M.A. (2006) Signalling network with a bistable hysteretic switch controls developmental activation of the sigma transcription factor in *Bacillus subtilis*. *Mol Microbiol* **61**: 165-184.
- Ihekwa, A.E.C., Mura, I., and Barker, G.C. (2014) Computational modelling and analysis of the molecular network regulating sporulation initiation in *Bacillus subtilis*. *BMC Syst Biol* **8**: 119.
- Imlay, J.A., Chin, S.M., and Linn, S. (1988) Toxic DNA damage by hydrogen peroxide through the Fenton reaction *in vivo* and *in vitro*. *Science* **240**: 640–642.

- Ingalls, B.P. (2013) *Mathematical modeling in systems biology. An introduction*. Cambridge, Mass.: MIT Press.
- Ishihama, A. (2010) Prokaryotic genome regulation: Multifactor promoters, multitarget regulators and hierarchic networks. *FEMS Microbiol Rev* **34**: 628-645.
- Jabbari, S., Heap, J.T., and King, J.R. (2011) Mathematical modelling of the sporulation-initiation network in *Bacillus subtilis* revealing the dual role of the putative quorum-sensing signal molecule PhrA. *Bull Math Biol* **73**: 181-211.
- Jani, D., Nagarkatti, R., Beatty, W., Angel, R., Slebodnick, C., Andersen, J., Kumar, S., and Rathore, D. (2008) HDP-a novel heme detoxification protein from the malaria parasite. *PLoS Pathog* **4**: e1000053.
- Jaqaman, K., and Danuser, G. (2006) Linking data to models: data regression. *Nat Rev Mol Cell Biol* **7**: 813-819.
- Jia, Z., O'Mara, M.L., Zuegg, J., Cooper, M.A., and Mark, A.E. (2013) Vancomycin: ligand recognition, dimerization and super-complex formation. *FEBS J* **280**: 1294-1307.
- Joo, H.-S., Fu, C.-I., and Otto, M. (2016) Bacterial strategies of resistance to antimicrobial peptides. *Philos Trans R Soc Lon B Biol Sci* **371**: 20150292.
- Jordan, S., Hutchings, M.I., and Mascher, T. (2008) Cell envelope stress response in Gram-positive bacteria. *FEMS Microbiol Rev* **32**: 107-146.
- Jordan, S., Junker, A., Helmann, J.D., and Mascher, T. (2006) Regulation of LiaRS-dependent gene expression in *Bacillus subtilis*: Identification of inhibitor proteins, regulator binding sites, and target genes of a conserved cell envelope stress-sensing two-component system. *J Bacteriol* **188**: 5153-5166.
- Joseph, P., Guiseppi, A., Sorokin, A., and Denizot, F. (2004) Characterization of the *Bacillus subtilis* YxdJ response regulator as the inducer of expression for the cognate ABC transporter YxdLM. *Microbiology* **150**: 2609-2617.
- Joubert, L., Derré-Bobillot, A., Gaudu, P., Gruss, A., and Lechardeur, D. (2014) HrtBA and menaquinones control haem homeostasis in *Lactococcus lactis*. *Mol Microbiol* **93**: 823-833.
- Juttukonda, J.L., and Skaar, E.P. (2015) Manganese homeostasis and utilization in pathogenic bacteria. *Mol Microbiol* **97**: 216-228.
- Kahan, F.M., Kahan, J.S., Cassidy, P.J., and Kropp, H. (1974) The mechanism of action of fosfomycin (phosphonomycin). *Ann N Y Acad Sci* **235**: 364-386.
- Kazmierczak, M.J., Wiedmann, M., and Boor, K.J. (2005) Alternative sigma factors and their roles in bacterial virulence. *Microbiol Mol Biol Rev* **69**: 527-543.
- Keppel, M., Davoudi, E., Gätgens, C., and Frunzke, J. (2018) Membrane topology and heme binding of the histidine kinases HrrS and ChrS in *Corynebacterium glutamicum*. *Front Microbiol* **9**: 183.
- Keppel, M., Piepenbreier, H., Gätgens, C., Fritz, G., and Frunzke, J. (2019) Toxic but tasty - temporal dynamics and network architecture of heme-responsive two-component signaling in *Corynebacterium glutamicum*. *Mol Microbiol* **111**: 1367-1381.
- Kingston, A.W., Liao, X., and Helmann, J.D. (2013) Contributions of the  $\sigma^W$ ,  $\sigma^M$  and  $\sigma^X$  regulons to the lantibiotic resistome of *Bacillus subtilis*. *Mol Microbiol* **90**: 502-518.

- Kirby, A.E., King, N.D., and Connell, T.D. (2004) RhuR, an Extracytoplasmic Function sigma factor activator, is essential for heme-dependent expression of the outer membrane heme and hemoprotein receptor of *Bordetella avium*. *Infect Immun* **72**: 896-907.
- Kleijn, L.H.J., Oppedijk, S.F., 't Hart, P., van Harten, R.M., Martin-Visscher, L.A., Kemmink, J., Breukink, E., and Martin, N.I. (2016) Total synthesis of laspartomycin C and characterization of its antibacterial mechanism of action. *J Med Chem* **59**: 3569-3574.
- Kleijn, L.H.J., Vlieg, H.C., Wood, T.M., Sastre Toraño, J., Janssen, B.J.C., and Martin, N.I. (2017) A high-resolution crystal structure that reveals molecular details of target recognition by the calcium-dependent lipopeptide antibiotic laspartomycin C. *Angew Chem Int Ed Engl* **56**: 16546-16549.
- Klumpp, S., and Hwa, T. (2014) Bacterial growth: global effects on gene expression, growth feedback and proteome partition. *Curr Opin Biotechnol* **28**: 96-102.
- Kohanski, M.A., Dwyer, D.J., and Collins, J.J. (2010) How antibiotics kill bacteria: from targets to networks. *Nat Rev Microbiol* **8**: 423-435.
- Kremling, A., Bettenbrock, K., and Gilles, E.D. (2007) Analysis of global control of *Escherichia coli* carbohydrate uptake. *BMC Syst Biol* **1**: 42.
- Kremling, A., Heermann, R., Centler, F., Jung, K., and Gilles, E.D. (2004) Analysis of two-component signal transduction by mathematical modeling using the KdpD/KdpE system of *Escherichia coli*. *Biosystems* **78**: 23-37.
- Kunkle, C.A., and Schmitt, M.P. (2007) Comparative analysis of *hmuO* function and expression in *Corynebacterium* species. *J Bacteriol* **189**: 3650-3654.
- Kurata, H., El-Samad, H., Iwasaki, R., Ohtake, H., Doyle, J.C., Grigorova, I., Gross, C.A., and Khammash, M. (2006) Module-based analysis of robustness tradeoffs in the heat shock response system. *PLoS Comput Biol* **2**: e59.
- Kutalik, Z., Razaz, M., Elfwing, A., Ballagi, A., and Baranyi, J. (2005) Stochastic modelling of individual cell growth using flow chamber microscopy images. *Int J Food Microbiol* **105**: 177-190.
- Lakshmi, R., Nusrin, K.S., Georgy, S.A., and Sreelakshmi, K.S. (2014) Role of beta lactamases in antibiotic resistance: A review. *Int Res J Pharm* **5**: 37-40.
- Lambert, M.P., and Neuhaus, F.C. (1972) Mechanism of D-cycloserine action: alanine racemase from *Escherichia coli* W. *J Bacteriol* **110**: 978-987.
- Laub, M. (2011) The role of two-component signal transduction systems in bacterial stress responses. In *Bacterial stress responses*. Storz, G., and Hengge, R. (eds). Washington, DC: ASM Press, pp. 45-58
- Layer, G., Reichelt, J., Jahn, D., and Heinz, D.W. (2010) Structure and function of enzymes in heme biosynthesis. *Protein Sci* **19**: 1137-1161.
- Lechardeur, D., Cesselin, B., Liebl, U., Vos, M.H., Fernandez, A., Brun, C., Gruss, A., and Gaudu, P. (2012) Discovery of intracellular heme-binding protein HrtR, which controls heme efflux by the conserved HrtB-HrtA transporter in *Lactococcus lactis*. *J Biol Chem* **287**: 4752-4758.
- Lee, Y.H., and Helmann, J.D. (2013) Reducing the level of undecaprenyl pyrophosphate synthase has complex effects on susceptibility to cell wall antibiotics. *Antimicrob Agents Chemother* **57**: 4267-4275.

- Lerminiaux, N.A., and Cameron, A.D.S. (2019) Horizontal transfer of antibiotic resistance genes in clinical environments. *Can J Microbiol* **65**: 34-44.
- Lewis, K. (2007) Persister cells, dormancy and infectious disease. *Nat Rev Microbiol* **5**: 48-56.
- Loll, P.J., Miller, R., Weeks, C.M., and Axelsen, P.H. (1998) A ligand-mediated dimerization mode for vancomycin. *Chem Biol* **5**: 293–298.
- Mackey, M.C., Santillán, M., and Yildirim, N. (2004) Modeling operon dynamics: the tryptophan and lactose operons as paradigms. *C R Biol* **327**: 211-224.
- Manat, G., El Ghachi, M., Auger, R., Baouche, K., Olatunji, S., and Kerff, F., *et al.* (2015) Membrane topology and biochemical characterization of the *Escherichia coli* BacA undecaprenyl-pyrophosphate phosphatase. *PLoS One* **10**: e0142870.
- Maresso, A.W., Garufi, G., and Schneewind, O. (2008) *Bacillus anthracis* secretes proteins that mediate heme acquisition from hemoglobin. *PLoS Pathog* **4**: e1000132.
- Marvig, R.L., Damkiær, S., Khademi, S.M.H., Markussen, T.M., Molin, S., and Jelsbak, L. (2014) Within-host evolution of *Pseudomonas aeruginosa* reveals adaptation toward iron acquisition from hemoglobin. *mBio* **5**: e00966.
- Mascher, T., Hachmann, A.-B., and Helmann, J.D. (2007) Regulatory overlap and functional redundancy among *Bacillus subtilis* Extracytoplasmic Function  $\sigma$  factors. *J Bacteriol* **189**: 6919-6927.
- Mascher, T., Helmann, J.D., and Uden, G. (2006) Stimulus perception in bacterial signal-transducing histidine kinases. *Microbiol Mol Biol Rev* **70**: 910-938.
- Mascher, T., Margulis, N.G., Wang, T., Ye, R.W., and Helmann, J.D. (2003) Cell wall stress responses in *Bacillus subtilis*: The regulatory network of the bacitracin stimulon. *Mol Microbiol* **50**: 1591-1604.
- Mascher, T., Zimmer, S.L., Smith, T.-A., and Helmann, J.D. (2004) Antibiotic-inducible promoter regulated by the cell envelope stress-sensing two-component system LiaRS of *Bacillus subtilis*. *Antimicrob Agents Chemother* **48**: 2888-2896.
- Maurer, L.M., Yohannes, E., Bondurant, S.S., Radmacher, M., and Slonczewski, J.L. (2005) pH regulates genes for flagellar motility, catabolism, and oxidative stress in *Escherichia coli* K-12. *J Bacteriol* **187**: 304-319.
- Mengin-Lecreulx, D., Flouret, B., and van Heijenoort, J. (1982) Cytoplasmic steps of peptidoglycan synthesis in *Escherichia coli*. *J Bacteriol* **151**: 1109–1117.
- Mengin-Lecreulx, D., Flouret, B., and van Heijenoort, J. (1983) Pool levels of UDP N-acetylglucosamine and UDP N-acetylglucosamine-enolpyruvate in *Escherichia coli* and correlation with peptidoglycan synthesis. *J Bacteriol* **154**: 1284–1290.
- Mengin-Lecreulx, D., and van Heijenoort, J. (1985) Effect of growth conditions on peptidoglycan content and cytoplasmic steps of its biosynthesis in *Escherichia coli*. *J Bacteriol* **163**: 208–212.
- Mettetal, J.T., Muzzey, D., Pedraza, J.M., Ozbudak, E.M., and van Oudenaarden, A. (2006) Predicting stochastic gene expression dynamics in single cells. *Proc Natl Acad Sci U S A* **103**: 7304-7309.
- Michaelis, L., and Menten, M.L. (1913) Die Kinetik der Invertinwirkung. *Biochem Z* **49**: 333-369.

- Mitrophanov, A.Y., and Groisman, E.A. (2008) Positive feedback in cellular control systems. *Bioessays* **30**: 542-555.
- Mitrophanov, A.Y., Hadley, T.J., and Groisman, E.A. (2010) Positive autoregulation shapes response timing and intensity in two-component signal transduction systems. *J Mol Biol* **410**: 671-680.
- Moat, A.G., Foster, J.W., and Spector, M.P. (2002) Microbial Stress Responses. In *Microbial Physiology*. Moat, A.G., Foster, J.W., and Spector, M.P. (eds). Hoboken, NJ, USA: John Wiley & Sons, Inc, pp. 582–611.
- Moles, C.G., Mendes, P., and Banga, J.R. (2003) Parameter estimation in biochemical pathways: A comparison of global optimization methods. *Genome Res* **13**: 2467-2474.
- Mota-Meira, M., Lapointe, G., Lacroix, C., and Lavoie, M.C. (2000) MICs of mutacin B-Ny266, nisin A, vancomycin, and oxacillin against bacterial pathogens. *Antimicrob Agents Chemother* **44**: 24–29.
- Münch, D., and Sahl, H.-G. (2015) Structural variations of the cell wall precursor lipid II in Gram-positive bacteria - Impact on binding and efficacy of antimicrobial peptides. *Biochim Biophys Acta* **1848**: 3062-3071.
- Murphy, J.T., Walshe, R., and Devocelle, M. (2008) A computational model of antibiotic-resistance mechanisms in methicillin-resistant *Staphylococcus aureus* (MRSA). *J Theor Biol* **254**: 284-293.
- Murray, J.D. (2002) *Mathematical Biology: I. An Introduction*. NY: Springer-Verlag New York.
- Mutlu, A., Trauth, S., Ziesack, M., Nagler, K., Bergeest, J.-P., and Rohr, K., *et al.* (2018) Phenotypic memory in *Bacillus subtilis* links dormancy entry and exit by a spore quantity-quality tradeoff. *Nat Commun* **9**: 69.
- Narula, J., Devi, S.N., Fujita, M., and Igoshin, O.A. (2012) Ultrasensitivity of the *Bacillus subtilis* sporulation decision. *Proc Natl Acad Sci U S A* **109**: E3513-E3522.
- Nawrocki, K.L., Crispell, E.K., and McBride, S.M. (2014) Antimicrobial peptide resistance mechanisms of Gram-positive bacteria. *Antibiotics* **3**: 461-492.
- Neuhaus, F.C., and Baddiley, J. (2003) A continuum of anionic charge: Structures and functions of D-alanyl-teichoic acids in Gram-positive bacteria. *Microbiol Mol Biol Rev* **67**: 686-723.
- Niederhäusern, S. de, Bondi, M., Messi, P., Iseppi, R., Sabia, C., Manicardi, G., and Anacarso, I. (2011) Vancomycin-resistance transferability from VanA enterococci to *Staphylococcus aureus*. *Curr Microbiol* **62**: 1363-1367.
- Nir, U., Ladan, H., Malik, Z., and Nitzan, Y. (1991) *In vivo* effects of porphyrins on bacterial DNA. *J Photochem Photobiol B* **11**: 295-306.
- Nitzan, Y., Ladan, H., and Malik, Z. (1987) Growth-inhibitory effect of hemin on staphylococci. *Curr Microbiol* **14**: 279-284.
- Nonaka, G., Blankschien, M., Herman, C., Gross, C.A., and Rhodius, V.A. (2006) Regulon and promoter analysis of the *E. coli* heat-shock factor,  $\sigma^{32}$ , reveals a multifaceted cellular response to heat stress. *Genes Dev* **20**: 1776-1789.
- Ohki, R., Giyanto, Tateno, K., Masuyama, W., Moriya, S., Kobayashi, K., and Ogasawara, N. (2003) The BceRS two-component regulatory system induces expression of the bacitracin transporter, BceAB, in *Bacillus subtilis*. *Mol Microbiol* **49**: 1135–1144.



- Oppedijk, S.F., Martin, N.I., and Breukink, E. (2016) Hit 'em where it hurts: The growing and structurally diverse family of peptides that target lipid-II. *Biochim Biophys Acta* **1858**: 947-957.
- Overbye, K., and Barrett, J. (2005) Antibiotics: Where did we go wrong? *Drug Discov Today* **10**: 45-52.
- Paget, M.S. (2015) Bacterial sigma factors and anti-sigma factors: Structure, function and distribution. *Biomolecules* **5**: 1245-1265-
- Palmer, K.L., Kos, V.N., and Gilmore, M.S. (2010) Horizontal gene transfer and the genomics of enterococcal antibiotic resistance. *Curr Opin Microbiol* **13**: 632-639.
- Panek, H., and O'Brian, M.R. (2002) A whole genome view of prokaryotic haem biosynthesis. *Microbiology* **148**: 2273-2282.
- Paracelsus Die dritte Defension wegen des Schreibens der neuen Recepte. In *Paracelsus (Hg.) 1965 - Septem Defensiones*, pp. 508–513.
- Pejchal, R., Sargeant, R., and Ludwig, M.L. (2005) Structures of NADH and CH<sub>3</sub>-H<sub>4</sub>folate complexes of *Escherichia coli* methylenetetrahydrofolate reductase reveal a Spartan strategy for a ping-pong reaction. *Biochemistry* **44**: 11447-11457.
- Peschel, A., and Sahl, H.-G. (2006) The co-evolution of host cationic antimicrobial peptides and microbial resistance. *Nat Rev Microbiol* **4**: 529-536.
- Petersohn, A., Brigulla, M., Haas, S., Hoheisel, J.D., Völker, U., and Hecker, M. (2001) Global analysis of the general stress response of *Bacillus subtilis*. *J Bacteriol* **183**: 5617-5631.
- Peterson, E., and Kaur, P. (2018) Antibiotic resistance mechanisms in bacteria: Relationships between resistance determinants of antibiotic producers, environmental bacteria, and clinical pathogens. *Front Microbiol* **9**: 2928.
- Pfalzgraff, A., Brandenburg, K., and Weindl, G. (2018) Antimicrobial peptides and their therapeutic potential for bacterial skin infections and wounds. *Front Pharmacol* **9**: 281.
- Piepenbreier, H., Diehl, A., and Fritz, G. (2019a) Minimal exposure of lipid II cycle intermediates triggers cell wall antibiotic resistance. *Nat Commun* **10**: 2733.
- Piepenbreier, H., Fritz, G., and Gebhard, S. (2017) Transporters as information processors in bacterial signalling pathways. *Mol Microbiol* **104**: 1-15.
- Piepenbreier, H., Sim, A., Kobras, C.M., Radeck, J., Mascher, T., Gebhard, S., and Fritz, G. (2019b) (in preparation) From modules to networks: A systems-level analysis of the bacitracin stress response in *Bacillus subtilis*.
- Pietiäinen, M., Gardemeister, M., Mecklin, M., Leskelä, S., Sarvas, M., and Kontinen, V.P. (2005) Cationic antimicrobial peptides elicit a complex stress response in *Bacillus subtilis* that involves ECF-type sigma factors and two-component signal transduction systems. *Microbiology* **151**: 1577-1592.
- Pishchany, G., McCoy, A.L., Torres, V.J., Krause, J.C., Crowe, J.E., Fabry, M.E., and Skaar, E.P. (2010) Specificity for human hemoglobin enhances *Staphylococcus aureus* infection. *Cell Host Microbe* **8**: 544-550.
- Potvin-Trottier, L., Luro, S., and Paulsson, J. (2018) Microfluidics and single-cell microscopy to study stochastic processes in bacteria. *Curr Opin Microbiol* **43**: 186-192.
- Poulos, T.L. (2007) The Janus nature of heme. *Nat Prod Rep* **24**: 504-510.

- Press, W.H., Teukolsky, S.A., and Vetterling, W.T. (1999) *Numerical Recipes in C. The Art of Scientific Computing*. Cambridge: University Press
- Radeck, J., Fritz, G., and Mascher, T. (2017) The cell envelope stress response of *Bacillus subtilis*: From static signaling devices to dynamic regulatory network. *Curr Genet* **63**: 79-90.
- Radeck, J., Gebhard, S., Orchard, P.S., Kirchner, M., Bauer, S., Mascher, T., and Fritz, G. (2016) Anatomy of the bacitracin resistance network in *Bacillus subtilis*. *Mol Microbiol* **100**: 607-620.
- Ratliff, M., Zhu, W., Deshmukh, R., Wilks, A., and Stojiljkovic, I. (2001) Homologues of neisserial heme oxygenase in Gram-negative bacteria: Degradation of heme by the product of the *pigA* gene of *Pseudomonas aeruginosa*. *J Bacteriol* **183**: 6394-6403.
- Reichmann, N.T., Cassona, C.P., and Gründling, A. (2013) Revised mechanism of D-alanine incorporation into cell wall polymers in Gram-positive bacteria. *Microbiology* **159**: 1868-1877.
- Revilla-Guarinos, A., Gebhard, S., Mascher, T., and Zúñiga, M. (2014) Defence against antimicrobial peptides: Different strategies in *Firmicutes*. *Environ Microbiol* **16**: 1225-1237.
- Reynolds, P.E. (1989) Structure, biochemistry and mechanism of action of glycopeptide antibiotics. *Eur J Clin Microbiol Infect Dis* **8**: 943-950.
- Rietkötter, E., Hoyer, D., and Mascher, T. (2008) Bacitracin sensing in *Bacillus subtilis*. *Mol Microbiol* **68**: 768-785.
- Ropers, D., Jong, H. de, and Geiselman, J. (2009) Mathematical Modeling of Genetic Regulatory Networks: Stress Responses in *Escherichia coli*. In *Systems Biology and Synthetic Biology*. Fu, P., and Panke, S. (eds). Hoboken, NJ, USA: John Wiley & Sons, Inc, pp. 235–271.
- Rosch, J.W., Sublett, J., Gao, G., Wang, Y.D., and Tuomanen, E.I. (2008) Calcium efflux is essential for bacterial survival in the eukaryotic host. *Mol Microbiol* **70**: 435-444.
- Rowland, M.A., and Deeds, E.J. (2014) Crosstalk and the evolution of specificity in two-component signaling. *Proc Natl Acad Sci U S A* **111**: 5550-5555.
- Schleifer, K.H., and Kandler, O. (1972) Peptidoglycan types of bacterial cell walls and their taxonomic implications. *Bacteriol Rev* **36**: 407–477.
- Schmitt, M.P. (1997) Transcription of the *Corynebacterium diphtheriae hmuO* gene is regulated by iron and heme. *Infect Immun* **65**: 4634–4641.
- Schneider, T., and Sahl, H.-G. (2010) An oldie but a goodie - cell wall biosynthesis as antibiotic target pathway. *Int J Med Microbiol* **300**: 161-169.
- Schöbel, S., Zellmeier, S., Schumann, W., and Wiegert, T. (2004) The *Bacillus subtilis*  $\sigma^W$  anti-sigma factor RsiW is degraded by intramembrane proteolysis through YluC. *Mol Microbiol* **52**: 1091-1105.
- Schrecke, K., Staroń, A., and Mascher, T. (2012) Two-component signaling in the Gram-positive envelope stress response: intramembrane-sensing histidine kinases and accessory membrane proteins. In *Two Component Systems in Bacteria*. Gross, R., and Beier, D. (eds). Hethersett, Norwick, UK: Horizon Scientific Press, pp. 199–229.
- Schultz, D., Ben Jacob, E., Onuchic, J.N., and Wolynes, P.G. (2007) Molecular level stochastic model for competence cycles in *Bacillus subtilis*. *Proc Natl Acad Sci U S A* **104**: 17582-17587.

- Schultz, D., Wolynes, P.G., Ben Jacob, E., and Onuchic, J.N. (2009) Deciding fate in adverse times: sporulation and competence in *Bacillus subtilis*. *Proc Natl Acad Sci U S A* **106**: 21027-21034.
- Schumann, W. (2003) The *Bacillus subtilis* heat shock stimulon. *Cell Stress Chaperones* **8**: 207-217.
- Schwartz, B., Markwalder, J.A., Seitz, S.P., Wang, Y., and Stein, R.L. (2002) A kinetic characterization of the glycosyltransferase activity of *Escherichia coli* PBP1b and development of a continuous fluorescence assay. *Biochemistry* **41**: 12552–12561.
- Scott, M., Gunderson, C.W., Mateescu, E.M., Zhang, Z., and Hwa, T. (2010) Interdependence of cell growth and gene expression: Origins and consequences. *Science* **330**: 1099-1102.
- Scott, M., and Hwa, T. (2011) Bacterial growth laws and their applications. *Curr Opin Biotechnol* **22**: 559-565.
- Shaaly, A., Kalamorz, F., Gebhard, S., and Cook, G.M. (2013) Undecaprenyl pyrophosphate phosphatase confers low-level resistance to bacitracin in *Enterococcus faecalis*. *J Antimicrob Chemother* **68**: 1583-1593.
- Shin, D., Lee, E.-J., Huang, H., and Groisman, E.A. (2006) A positive feedback loop promotes transcription surge that jump-starts *Salmonella* virulence circuit. *Science* **314**: 1607-1609.
- Shinar, G., Milo, R., Martínez, M.R., and Alon, U. (2007) Input output robustness in simple bacterial signaling systems. *Proc Natl Acad Sci U S A* **104**: 19931-19935.
- Silhavy, T.J., Kahne, D., and Walker, S. (2010) The bacterial cell envelope. *Cold Spring Harb Perspect Biol* **2**: a000414.
- Silver, L.L. (2003) Novel inhibitors of bacterial cell wall synthesis. *Curr Opin Microbiol* **6**: 431-438.
- Silver, L.L. (2006) Does the cell wall of bacteria remain a viable source of targets for novel antibiotics? *Biochem Pharmacol* **71**: 996-1005.
- Skaar, E.P., Gaspar, A.H., and Schneewind, O. (2006) *Bacillus anthracis* IldG, a heme-degrading monooxygenase. *J Bacteriol* **188**: 1071-1080.
- Staroń, A., Finkeisen, D.E., and Mascher, T. (2011) Peptide antibiotic sensing and detoxification modules of *Bacillus subtilis*. *Antimicrob Agents Chemother* **55**: 515-525.
- Staroń, A., Sofia, H.J., Dietrich, S., Ulrich, L.E., Liesegang, H., and Mascher, T. (2009) The third pillar of bacterial signal transduction: Classification of the Extracytoplasmic Function (ECF)  $\sigma$  factor protein family. *Mol Microbiol* **74**: 557-581.
- Stauff, D.L., Bagaley, D., Torres, V.J., Joyce, R., Anderson, K.L., Kuechenmeister, L., Dunman, P.M., and Skaar, E.P. (2008) *Staphylococcus aureus* HrtA is an ATPase required for protection against heme toxicity and prevention of a transcriptional heme stress response. *J Bacteriol* **190**: 3588-3596.
- Stauff, D.L., and Skaar, E.P. (2009a) *Bacillus anthracis* HssRS signalling to HrtAB regulates haem resistance during infection. *Mol Microbiol* **72**: 763-778.
- Stauff, D.L., and Skaar, E.P. (2009b) The heme sensor system of *Staphylococcus aureus*. *Contrib Microbiol* **16**: 120-135.

- Stauff, D.L., Torres, V.J., and Skaar, E.P. (2007) Signaling and DNA-binding activities of the *Staphylococcus aureus* HssR-HssS two-component system required for heme sensing. *J Biol Chem* **282**: 26111-26121.
- Stein, R.L. (2011) Kinetics of Two-Substrate Enzymatic Reactions. In *Kinetics of Enzyme Action*. Stein, R.L. (ed). Hoboken, NJ, USA: John Wiley & Sons, Inc, pp. 141–168.
- Stein, T., Heinzmann, S., Solovieva, I., and Entian, K.-D. (2003) Function of *Lactococcus lactis* nisin immunity genes *nisl* and *nisFEG* after coordinated expression in the surrogate host *Bacillus subtilis*. *J Biol Chem* **278**: 89-94.
- Stock, A.M., Robinson, V.L., and Goudreau, P.N. (2000) Two-component signal transduction. *Annu Rev Biochem* **69**: 183-215.
- Storm, D.R., and Strominger, J.L. (1973) Complex formation between bacitracin peptides and isoprenyl pyrophosphates. The specificity of lipid-peptide interactions. *J Biol Chem* **248**: 3940–3945.
- Storz, G., and Hengge, R. (2011) *Bacterial stress responses*. Washington, DC: ASM Press.
- Swoboda, J.G., Campbell, J., Meredith, T.C., and Walker, S. (2010) Wall teichoic acid function, biosynthesis, and inhibition. *ChemBiochem* **11**: 35-45.
- Tam, L.T., Eymann, C., Albrecht, D., Sietmann, R., Schauer, F., Hecker, M., and Antelmann, H. (2006) Differential gene expression in response to phenol and catechol reveals different metabolic activities for the degradation of aromatic compounds in *Bacillus subtilis*. *Environ Microbiol* **8**: 1408-1427.
- Tatar, L.D., Marolda, C.L., Polischuk, A.N., van Leeuwen, D., and Valvano, M.A. (2007) An *Escherichia coli* undecaprenyl-pyrophosphate phosphatase implicated in undecaprenyl phosphate recycling. *Microbiology* **153**: 2518-2529.
- Thackray, P.D., and Moir, A. (2003) SigM, an Extracytoplasmic Function sigma factor of *Bacillus subtilis*, is activated in response to cell wall antibiotics, ethanol, heat, acid, and superoxide stress. *J Bacteriol* **185**: 3491-3498.
- Thomas, P., Terradot, G., Danos, V., and Weiße, A.Y. (2018) Sources, propagation and consequences of stochasticity in cellular growth. *Nat Commun* **9**: 4528.
- Tiyanont, K., Doan, T., Lazarus, M.B., Fang, X., Rudner, D.Z., and Walker, S. (2006) Imaging peptidoglycan biosynthesis in *Bacillus subtilis* with fluorescent antibiotics. *Proc Natl Acad Sci U S A* **103**: 11033-11038.
- Tomasz, A. (1979) The mechanism of the irreversible antimicrobial effects of penicillins: How the beta-lactam antibiotics kill and lyse bacteria. *Annu Rev Microbiol* **33**: 11-137.
- Tong, Y., and Guo, M. (2009) Bacterial heme-transport proteins and their heme-coordination modes. *Arch Biochem Biophys* **481**: 1-15.
- Tonn, M, Thomas, P., Barahona, M., and Oyarzún, D. (2019) Stochastic modelling reveals mechanism of metabolic heterogeneity. *Commun Biol* **2**: 108
- Torres, V.J., Stauff, D.L., Pishchany, G., Bezbradica, J.S., Gordy, L.E., and Iturregui, J., *et al.* (2007) A *Staphylococcus aureus* regulatory system that responds to host heme and modulates virulence. *Cell Host Microbe* **1**: 109-119.
- Touzé, T., Blanot, D., and Mengin-Lecreux, D. (2008) Substrate specificity and membrane topology of *Escherichia coli* PgpB, an undecaprenyl pyrophosphate phosphatase. *J Biol Chem* **283**: 16573-16583.

- Tucker, D.L., Tucker, N., and Conway, T. (2002) Gene expression profiling of the pH response in *Escherichia coli*. *J Bacteriol* **184**: 6551-6558.
- Ulrich, L.E., Koonin, E.V., and Zhulin, I.B. (2005) One-component systems dominate signal transduction in prokaryotes. *Trends Microbiol* **13**: 52-56.
- Unno, M., Matsui, T., Chu, G.C., Couture, M., Yoshida, T., Rousseau, D.L., Olson, J.S., and Ikeda-Saito, M. (2004) Crystal structure of the dioxygen-bound heme oxygenase from *Corynebacterium diphtheriae*: Implications for heme oxygenase function. *J Biol Chem* **279**: 21055-21061.
- van Heijenoort, J. (1996) Murein synthesis. In *Escherichia coli and Salmonella*. Neidhardt, F.C., Curtiss, R., Ingraham, J.L., Lin, E.C.C., Brooks Low, K., Magasanik, B., et al. (ed). Washington, DC: ASM Press, pp. 1025–1034.
- van Heijenoort, J. (2007) Lipid intermediates in the biosynthesis of bacterial peptidoglycan. *Microbiol Mol Biol Rev* **71**: 620-635.
- van Heijenoort, Y., Gómez, M., Derrien, M., Ayala, J., and van Heijenoort, J. (1992) Membrane intermediates in the peptidoglycan metabolism of *Escherichia coli*: Possible roles of PBP 1b and PBP 3. *J Bacteriol*, **174**: 3549–3557.
- van Heyningen, W.E. (1948) Inhibition of aerobic sporing bacilli by Hæmatin. *Nature* **162**: 114
- Vilar, J.M.G., Guet, C.C., and Leibler, S. (2003) Modeling network dynamics: The *lac* operon, a case study. *J Cell Biol* **161**: 471-476.
- Voet, D., and Voet, J.G. (2011) Rates of enzymatic reactions In *Biochemistry*. Voet, D., and Voet, J.G. (eds.). Hoboken, NJ, USA: John Wiley & Sons, Inc, pp. 482–505.
- Voit, E.O., Martens, H.A., and Omholt, S.W. (2015) 150 years of the mass action law. *PLoS Comput Biol* **11**: e1004012.
- Vollmer, W., Blanot, D., and Pedro, M.A. de (2008) Peptidoglycan structure and architecture. *FEMS Microbiol Rev* **32**: 149-167.
- Wakeman, C.A., Hammer, N.D., Stauff, D.L., Attia, A.S., Anzaldi, L.L., Dikalov, S.I., Calcutt, M.W., and Skaar, E.P. (2012) Menaquinone biosynthesis potentiates haem toxicity in *Staphylococcus aureus*. *Mol Microbiol* **86**: 1376-1392.
- Wang, F., Zhou, H., Olademehin, O.P., Kim, S.J., and Tao, P. (2018) Insights into key interactions between vancomycin and bacterial cell wall structures. *ACS Omega* **3**: 37-45.
- Wecke, T., Zühlke, D., Mäder, U., Jordan, S., Voigt, B., and Pelzer, S., et al. (2009) Daptomycin versus friulimicin B: In-depth profiling of *Bacillus subtilis* cell envelope stress responses. *Antimicrob Agents Chemother* **53**: 1619-1623.
- Wennerhold, J., and Bott, M. (2006) The DtxR regulon of *Corynebacterium glutamicum*. *J Bacteriol* **188**: 2907-2918.
- Wiedemann, I., Breukink, E., van Kraaij, C., Kuipers, O.P., Bierbaum, G., de Kruijff, B., and Sahl, H.G. (2001) Specific binding of nisin to the peptidoglycan precursor lipid II combines pore formation and inhibition of cell wall biosynthesis for potent antibiotic activity. *J Biol Chem* **276**: 1772-1779.
- Wiegert, T., Homuth, G., Versteeg, S., and Schumann, W. (2001) Alkaline shock induces the *Bacillus subtilis*  $\sigma^W$  regulon. *Mol Microbiol* **41**: 59-71.

- Wilks, A. (2002) Heme oxygenase: Evolution, structure, and mechanism. *Antioxid Redox Signal* **4**: 603-614.
- Wilks, A., and Schmitt, M.P. (1998) Expression and characterization of a heme oxygenase (HmuO) from *Corynebacterium diphtheriae*. *J Biol Chem* **273**: 837-841.
- Wintersdorff, C.J.H. von, Penders, J., van Niekerk, J.M., Mills, N.D., Majumder, S., van Alphen, L.B., Savelkoul, P.H.M., and Wolffs, P.F.G. (2016) Dissemination of antimicrobial resistance in microbial ecosystems through horizontal gene transfer. *Front Microbiol* **7**: 173.
- Yoshida, Y., Matsuo, M., Oogai, Y., Kato, F., Nakamura, N., Sugai, M., and Komatsuzawa, H. (2011) Bacitracin sensing and resistance in *Staphylococcus aureus*. *FEMS Microbiol Lett* **320**: 33-39.
- Yoshimura, M., Asai, K., Sadaie, Y., and Yoshikawa, H. (2004) Interaction of *Bacillus subtilis* Extracytoplasmic Function (ECF) sigma factors with the N-terminal regions of their potential anti-sigma factors. *Microbiology* **150**: 591-599.
- Zhang, L.-J., and Gallo, R.L. (2016) Antimicrobial peptides. *Curr Biol* **26**: R14-R19.
- Zhao, H., Roistacher, D.M., and Helmann, J.D. (2019) Deciphering the essentiality and function of the anti- $\sigma^M$  factors in *Bacillus subtilis*. *Mol Microbiol* [ahead of print].
- Zhao, H., Sun, Y., Peters, J.M., Gross, C.A., Garner, E.C., and Helmann, J.D. (2016) Depletion of undecaprenyl pyrophosphate phosphatases disrupts cell envelope biogenesis in *Bacillus subtilis*. *J Bacteriol* **198**: 2925-2935.
- Zheng, Y., and Sriram, G. (2010) Mathematical modeling: Bridging the gap between concept and realization in synthetic biology. *J Biomed Biotechnol* **2010**: 541609.
- Zhu, W., Hunt, D.J., Richardson, A.R., and Stojiljkovic, I. (2000a) Use of heme compounds as iron sources by pathogenic *Neisseriae* requires the product of the *hemO* gene. *J Bacteriology* **182**: 439-447.
- Zhu, W., Wilks, A., and Stojiljkovic, I. (2000b) Degradation of heme in Gram-Negative bacteria: The product of the *hemO* gene of *Neisseriae* is a heme oxygenase. *J Bacteriol* **182**: 6783-6790.
- Zschiedrich, C.P., Keidel, V., and Szurmant, H. (2016) Molecular mechanisms of two-component signal transduction. *J Mol Biol* **428**: 3752-3775.

## A. Publications

*The following four papers (Paper I-IV) are subject of my thesis. The full texts of these articles are attached below.*

**Paper I:** Keppel, M.\*, Piepenbreier, H.\*, Gätgens, C., Fritz, G., and Frunzke, J. (2019) Toxic but tasty - temporal dynamics and network architecture of heme-responsive two-component signaling in *Corynebacterium glutamicum*. *Mol Microbiol* **111**: 1367-1381.  
(\*equal contributions)

**Paper II:** Piepenbreier, H., Diehl, A., and Fritz, G. (2019a) Minimal exposure of lipid II cycle intermediates triggers cell wall antibiotic resistance. *Nat Commun* **10**: 2733


**Paper III:** Piepenbreier, H., Sim, A., Kobras, C.M., Radeck, J., Mascher, T., Gebhard, S., and Fritz, G. (2019b) (in preparation) From modules to networks: A systems-level analysis of the bacitracin stress response in *Bacillus subtilis*.

**Paper IV:** Piepenbreier, H., Fritz, G., and Gebhard, S. (2017) Transporters as information processors in bacterial signalling pathways. *Mol Microbiol* **104**: 1-15.

**A.1 Toxic but tasty – temporal dynamics and network architecture of heme responsive two-component signalling in *Corynebacterium glutamicum*.**



# Toxic but tasty – temporal dynamics and network architecture of heme-responsive two-component signaling in *Corynebacterium glutamicum*

Marc Keppel,<sup>1†</sup> Hannah Piepenbreier,<sup>2†</sup>  
Cornelia Gätgens,<sup>1</sup> Georg Fritz <sup>2\*</sup> and  
Julia Frunzke<sup>1\*</sup>

<sup>1</sup>Institute of Bio- und Geosciences, IBG-1:  
Biotechnology, Forschungszentrum Jülich, Jülich,  
52425, Germany.

<sup>2</sup>LOEWE-Zentrum für Synthetische  
Mikrobiologie, Philipps-Universität Marburg, Marburg,  
35032, Germany.

## Summary

Heme is an essential cofactor and alternative iron source for almost all bacterial species but may cause severe toxicity upon elevated levels and consequently, regulatory mechanisms coordinating heme homeostasis represent an important fitness trait. A remarkable scenario is found in several corynebacterial species, e.g. *Corynebacterium glutamicum* and *Corynebacterium diphtheriae*, which dedicate two paralogs, heme-responsive two-component systems, HrrSA and ChrSA, to cope with the *Janus nature* of heme. Here, we combined experimental reporter profiling with a quantitative mathematical model to understand how this particular regulatory network architecture shapes the dynamic response to heme. Our data revealed an instantaneous activation of the detoxification response (*hrtBA*) upon stimulus perception and we found that kinase activity of both kinases contribute to this fast onset. Furthermore, instant deactivation of the  $P_{hrtBA}$  promoter is achieved by a strong ChrS phosphatase activity upon stimulus decline. While the activation of detoxification response is uncoupled from further factors, heme utilization is additionally governed by the global iron regulator DtxR integrating information on iron availability into

the regulatory network. Altogether, our data provide comprehensive insights how TCS cross-regulation and network hierarchy shape the temporal dynamics of detoxification (*hrtBA*) and utilization (*hmuO*) as part of a global homeostatic response to heme.

## Introduction

‘All things are poison, and nothing is without poison, the dosage alone makes it so a thing is not a poison’ – Paracelsus (1493–1541)

Heme represents an important iron source for almost all bacterial species (Andrews *et al.*, 2003) and is a ubiquitous cofactor of a variety of enzymes (Poulos, 2007). Elevated cellular concentrations of heme can, however, cause severe toxicity. But this is basically true for all nutrients as already emphasized by the Swiss physician and founder of modern toxicology, Paracelsus (Paracelsus, 1965; Borzelleca, 2000). Consequently, a robust regulation of homeostasis is key to the cell's survival and typically, sophisticated regulatory mechanisms are engaged in maintaining optimal intracellular conditions and tolerance to environmental fluctuations.

Once inside the cell, most bacteria rely on heme oxygenases to catalyze the conversion of heme to biliverdin, thereby salvaging the central iron atom with the concomitant release of carbon monoxide (Wilks, 2002). One early-characterized example for this class of enzymes is HmuO, a heme oxygenase of *Corynebacterium diphtheriae* that was found to be essential for the utilization of free and hemoglobin-bound heme (Schmitt, 1997; Wilks and Schmitt, 1998). An ortholog of HmuO was also identified in *Corynebacterium glutamicum*, where the deletion of the corresponding gene led to reduced growth on hemin as sole iron source (Frunzke *et al.*, 2011). In Gram-negative pathogens, including *Neisseria* spp. and *Pseudomonas aeruginosa*, proteins of the HemO/PigA family were found to catalyze the cleavage of the porphyrin ring structure, but do not share significant sequence similarity with HmuO of Gram-positive species (Zhu *et al.*, 2000b; Ratliff *et al.*,

Accepted 11 February, 2019. \*For correspondence. E-mails georg.fritz@synmikro.uni-marburg.de; Tel. +49 6421 28 22582 (Georg Fritz); j.frunzke@fz-juelich.de; Tel. +49 2461 615430; Fax +49-6421 28 24430 (Julia Frunzke).

<sup>†</sup>These authors contributed equally to this work.

2001). The cost and benefit of using heme as an alternative iron source, however, needs to be carefully considered by the cell. Corynebacterial species, for example, employ the master regulator of iron homeostasis, DtxR, to feed information on iron availability into the network controlling heme homeostasis. DtxR was shown to repress *hmuO* under iron-replete conditions and thereby adds an additional layer of regulation to the physiological response to heme (Schmitt, 1997; Wennerhold and Bott, 2006).

Due to the reactive nature of the heme molecule, high levels are readily toxic to microbial cells (Imlay et al., 1988; Nir et al., 1991; Anzaldi and Skaar, 2010; Wakeman et al., 2012). Consequently, organisms have evolved a variety of mechanisms to minimize toxic effects. Whereas some bacteria rely mostly on their oxygenase to degrade excess heme, such as *Neisseria gonorrhoeae* (Zhu et al., 2000a) or *Clostridium perfringens* (Hassan et al., 2010), an alternative strategy can be found in the eukaryotic parasite *Plasmodium* spp. which is capable to sequester excess heme in an insoluble substance called hemozoin (Fitch, 1998; Jani et al., 2008; Anzaldi and Skaar, 2010). While several bacterial species harbor bacterioferritins, which can store iron in the form of heme molecules, other forms of sequestration are not well described so far (Andrews et al., 2003; Anzaldi and Skaar, 2010). A third class of detoxification systems are heme exporters, such as HrtBA which have been described for several Gram-positive species including *Staphylococcus aureus* (Torres et al., 2007; Stauff and Skaar, 2009a), *Bacillus anthracis* (Stauff and Skaar, 2009a), *Streptococcus agalactiae* (Fernandez et al., 2010) and can also be found in corynebacterial species (Bibb and Schmitt, 2010; Heyer et al., 2012).

Bacterial two-component systems (TCS), consisting of a membrane bound histidine kinase (HK) and a cytoplasmatic response regulator (RR) (Mascher et al., 2006; Zschiedrich et al., 2016), play a central role as transient heme sensor systems in Gram-positive species (Stauff and Skaar, 2009b). This is known from bacteria such as *Staphylococcus aureus* and *Bacillus anthracis*, both utilizing the heme sensor system HssRS to react to heme as extracellular stimulus (Stauff and Skaar, 2009a; 2009b). A common theme among *Corynebacteriaceae* appears to be the dedication of two paralogous TCS for the regulation of heme homeostasis (Bibb et al., 2007; Frunzke et al., 2011; Bott and Brocker, 2012; Heyer et al., 2012; Burgos and Schmitt, 2016). Here, the HrrSA and ChrSA systems coordinate the expression of genes involved in heme biosynthesis, heme detoxification (*hrtBA*), respiratory chain and the heme oxygenase (*hmuO*). While in *C. glutamicum* it was suggested that both TCS have partially overlapping regulons, HrrSA was shown to play an important role in the utilization of heme as an alternative iron source by activating expression of *hmuO*, whereas ChrSA is crucial for the activation of the *hrtBA*

operon encoding a heme exporter (Frunzke et al., 2011; Heyer et al., 2012). Furthermore, previous studies of our group revealed significant cross-phosphorylation between these TCS but a highly specific phosphatase activity of the HKs toward their cognate RR (Hentschel et al., 2014). Previous studies focused mostly on the identification of target genes, which were confirmed by different *in vivo* and *in vitro* assays. However, the systemic understanding of this homeostatic network, maintaining balance between heme detoxification and utilization, demands the analysis of temporal dynamics and requires comprehensive insights in the particular network architecture.

In this study, we have conducted an analysis of reporter assays of HrrSA and ChrSA target promoters in the background of the wild-type strain, as well as in mutant strains lacking single components of the two TCSs. These data were integrated in a quantitative mathematical model, which was used to test functional hypotheses and to simulate distinct differences in autoregulation and ON/OFF kinetics of target promoters. Finally, by studying the impact of the iron regulator DtxR on *hrrA* and *hmuO* expression at temporal resolution our data as well as the model revealed that DtxR adds an important additional regulatory level ensuring the appropriate timing of heme utilization.

## Results

### *Temporal hierarchy in the heme utilization and detoxification response*

Under iron-limiting conditions, the growth of *C. glutamicum* is significantly impaired, but can be restored by the presence of heme in the medium. Provided that excess heme is toxic to the cells, we wondered which strategy *C. glutamicum* uses to regulate the balance between its heme utilization and detoxification modules. To this end, we studied the expression dynamics of the two major components responsible for heme utilization (*hmuO*) and detoxification (*hrtBA*) in response to an extracellular heme stimulus, by monitoring promoter-reporter fusions for the two systems (Hentschel et al., 2014). Interestingly, a wild-type strain of *C. glutamicum* transformed with plasmids carrying the reporter constructs (pJC1\_P<sub>*hmuO*</sub>-*eyfp* or pJC1\_P<sub>*hrtBA*</sub>-*eyfp*) revealed highly distinct response profiles and a temporal hierarchy in reporter output of the P<sub>*hmuO*</sub> and P<sub>*hrtBA*</sub> promoters (Fig. 1): While we observed a nearly instant but transient response for the heme detoxification module *hrtBA* to 4 μM extracellular heme (Fig. 1, red line), the heme utilization module *hmuO* displayed higher initial expression levels compared to *hrtBA* and experienced an expression boost after a delay of about 5 h (Fig. 1, green line). This increase in *hmuO* expression temporally coincides with a declining *hrtBA* expression.

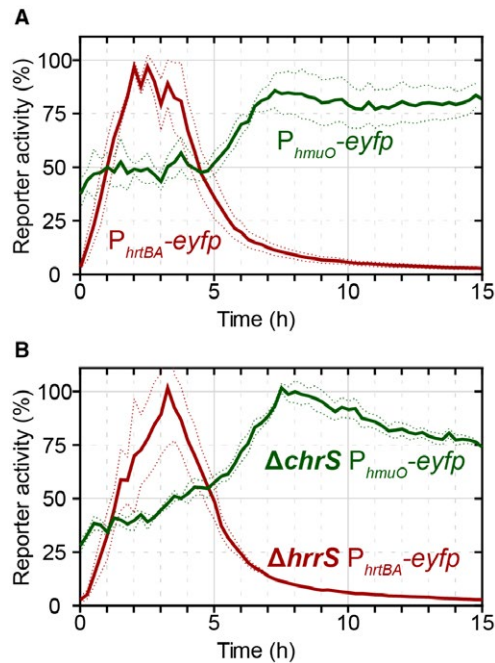


**Fig. 1.** Activation of  $P_{hmuO}$  and  $P_{hrtBA}$  in response to extracellular heme addition.

A. The *C. glutamicum* wild-type strain was transformed with one of the target gene reporters pJC1\_  $P_{hmuO}$ -eyfp or pJC1\_  $P_{hrtBA}$ -eyfp. Iron-deprived cells were subsequently cultivated in a microbioreactor system (Biolector) in CGXII minimal medium with 2% (w/v) glucose containing 4  $\mu$ M hemin. The eYFP fluorescence was measured as the output of target promoter activation, and backscatter values were recorded to monitor biomass formation. The specific fluorescence (fluorescence/backscatter) was normalized according to material and methods and the reporter activity (%) was calculated with the maximum reporter output. B. *C. glutamicum*  $\Delta chrS$ /pJC1\_  $P_{hmuO}$ -eyfp and  $\Delta hrrS$ /pJC1\_  $P_{hrtBA}$ -eyfp grown as described in (A). Non-cognate sensor kinases do not significantly affect the response profile. [Colour figure can be viewed at [wileyonlinelibrary.com](http://wileyonlinelibrary.com)]

From a physiological perspective, these antagonistic expression profiles seem plausible and impressively demonstrate the urgency of detoxification over utilization after first contact with the stimulus.

How does *C. glutamicum* implement appropriate timing of detoxification and utilization using two paralogous TCS responsive to the same stimulus? In this study, we formulated three distinct questions and addressed those by experiments described in the following:

1. How does cross-regulation between ChrSA and HrrSA affect *hrtBA* and *hmuO* expression respectively?
2. Does the differential interpretation of their common stimulus, i.e. the external heme concentration, impact the response?
3. How does regulatory hierarchy and network architecture affect the response profile?

To test the first hypothesis, we tested two mutant strains deleted for either one of the HKs ( $\Delta chrS$  and

$\Delta hrrS$ ) and transformed them with a reporter plasmid carrying the non-cognate target promoter ( $\Delta chrS$ /pJC1\_  $P_{hmuO}$ -eyfp and  $\Delta hrrS$ /pJC1\_  $P_{hrtBA}$ -eyfp). Strikingly, despite some quantitative differences (as discussed below), neither of the deletions changed the qualitative response of the non-cognate target promoter toward heme (Fig. 1B), that is the  $P_{hrtBA}$ -eyfp response was still transient in a  $\Delta hrrS$  mutant and the  $P_{hmuO}$ -eyfp response was still delayed in a  $\Delta chrS$  mutant, indicating that cross-regulation between the TCS cannot explain the antagonistic regulation strategy in *C. glutamicum*.

#### Modeling of heme uptake and consumption

Therefore, we wanted to test whether the depletion of external heme could serve as a joint trigger to cause opposing regulation of heme utilization and detoxification systems. However, before turning to this question, we first asked how long it would take to deplete heme in our experiments? To this end, we considered a simple mathematical model describing the uptake and consumption of heme, assuming that the reproduction of *C. glutamicum* requires  $\sim 5 \times 10^6$   $Fe^{2+}$  molecules per single cell (see Supplementary Text for details). Since this number sets a constraint on the growth kinetics of *C. glutamicum* in the heme-supplied medium, we studied the availability of heme per cell during bacterial growth. At the given final biomass and at the experimentally determined growth rate in our medium (Fig. 2A and B), the model predicts a depletion of the total heme levels per cell (levels of cytoplasmic heme and portion of extracytoplasmic heme in the medium per cell) approx. 3–5 h after the start of the experiment (Fig. 2E), depending on the initial heme concentrations in the medium. Experimental measurements of the levels of cell-associated heme (see Experimental procedures for experimental details) (Fig. 2D), which correspond to the model predictions of the heme levels per cell, confirm these dynamics and point out that the availability of heme in the medium dictates the growth dynamics of *C. glutamicum*. Hence, when comparing the experimental growth curves (Fig. 2A) with the theoretical predictions, the time points when cytoplasmic heme pools are depleted (Fig. 2C), in fact correlate with the cease of growth of the cultures in experiment and theory (Fig. 2A and B). Also the time point of growth cessation can be tuned by adding different initial heme concentrations (1–4  $\mu$ M) to the medium (Fig. 2A), as predicted by our model (Fig. 2B).

#### Transient expression of the *C. glutamicum* *hrtBA* detoxification module

Next, we asked whether the depletion of heme could also explain the transient activity of the *hrtBA* promoter. To this end, we extended our mathematical model to

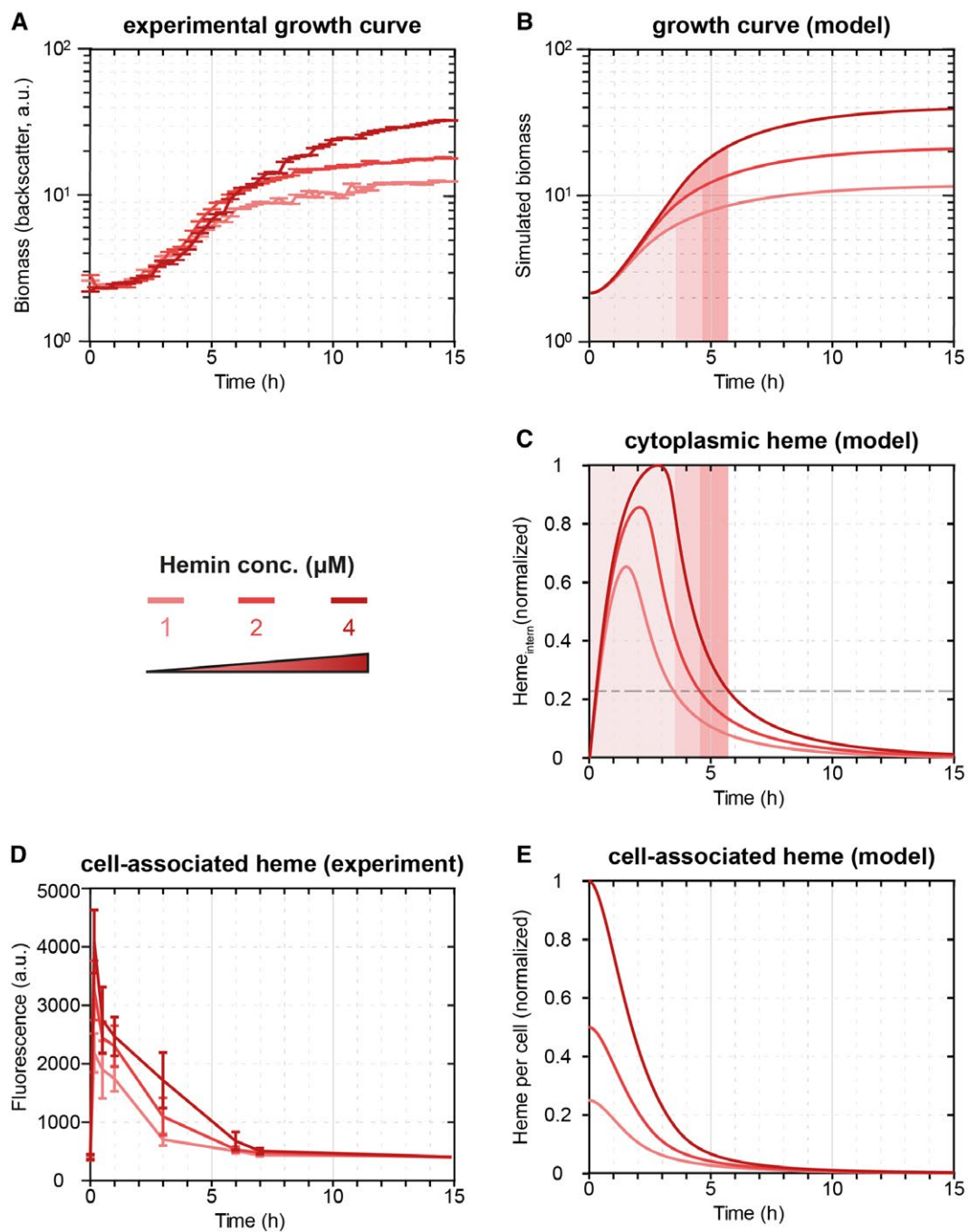


**Fig. 2.** The mathematical model reproduces the experimental growth curves quantitatively.

A. Growth curves of the *C. glutamicum* wild-type strain under increasing hemin concentrations (1  $\mu\text{M}$ , 2  $\mu\text{M}$  and 4  $\mu\text{M}$ ).

B. The mathematical model can reproduce the average growth behavior (left).

C. The mathematical model predicts the consumption of cytoplasmic heme required for growth.

D. The depletion of cell-associated heme (sum of internal heme and external heme adhering to the cell) dictates the bacterial growth. The experimental data align with (E) the model predictions of total heme levels per cell (cytoplasmic heme and the portion of external heme per cell). [Colour figure can be viewed at [wileyonlinelibrary.com](http://wileyonlinelibrary.com)]

describe stimulus perception and regulation within the two TCSs, as well as the dynamical response of the *chrSA* and *hrtBA* operons (for details, the reader is referred to the Supplementary text). Briefly, the

model considers sensing of externally added heme and subsequent autophosphorylation of ChrS and HrrS (Keppel *et al.*, 2018), (cross-)phosphorylation of ChrA by phosphorylated HKs (ChrS~P and HrrS~P) and



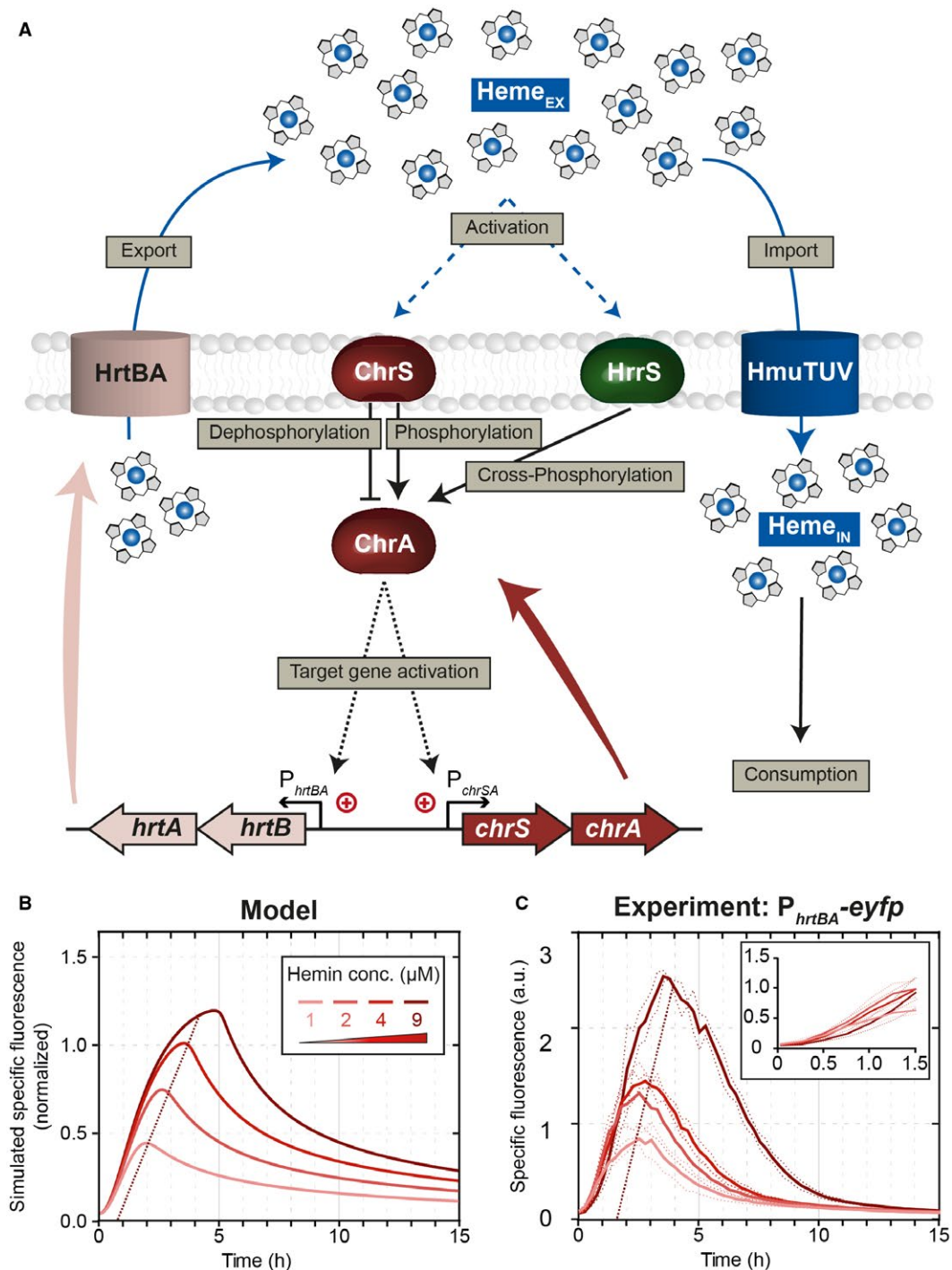


**Fig. 3.** Regulatory scheme and dynamic response of the *C. glutamicum* heme detoxification module.

**A.** Scheme of the regulatory interactions considered in the mathematical model for the heme detoxification module. Uptake of external heme molecules via HmuTUV and subsequent consumption/incorporation via diverse enzymes is crucial for bacterial growth under iron starvation. The fine-tuned response to heme in order to avoid intoxication is mainly based on the two TCSs ChrSA and HrrSA. The two kinases ChrS and HrrS are autophosphorylated in response to external hemin. After activation, they (cross-)phosphorylate the response regulator ChrA. In addition, the non-phosphorylated form of ChrS functions as a phosphatase on the phosphorylated response regulator ChrA. The phosphorylated response regulator activates expression of its target genes *hrtBA* and *chrSA*. The gene product of *hrtBA* is a heme exporter that transports internal heme to the extracellular space.

**B.** Dynamical response of our computational model for the detoxification module (Supplementary Text; Model equations M1) toward different external heme levels, as given by the simulation of specific fluorescence of a  $P_{hrtBA}$ -*eyfp* reporter, normalized to the maximal specific fluorescence at 4  $\mu\text{M}$  heme.

**C.** Experimental dynamical response of a  $P_{hrtBA}$ -*eyfp* reporter in wild-type *C. glutamicum* cells toward different heme concentrations supplied in the medium at  $t = 0$  h. [Colour figure can be viewed at [wileyonlinelibrary.com](http://wileyonlinelibrary.com)]

promoter activation of  $P_{chrSA}$  and  $P_{hrtBA}$  by phosphorylated response regulator  $\text{ChrA}\sim\text{P}$  (Fig. 3A). Simulations of the model predict that the depletion of external heme dictates the time point of deactivation of  $P_{hrtBA}$ , leading to a prolonged promoter activity and higher overall HrtBA production at higher initial heme concentrations (Fig. 3B). In fact, when experimentally supplying different heme concentrations (1–9  $\mu\text{M}$ ) to the medium, we found that both the strength as well as the duration of  $P_{hrtBA}\text{-eyfp}$  expression increased with increasing amounts of supplied heme (Fig. 3C). In the light of a bifunctional ChrS kinase/phosphatase, exhaustion of external heme is sufficient to explain the transient response dynamics of  $P_{hrtBA}\text{-eyfp}$  expression.

Interestingly, our experimental data also showed that for all heme concentrations, the initial response (within the first hour) of the reporter  $P_{hrtBA}\text{-eyfp}$  was almost identical (Fig. 3C) and that the overall peak height is only modulated by the time point of stimulus decline. This suggests that either (i) despite varying levels of  $\text{ChrA}\sim\text{P}$ , the  $P_{hrtBA}$  promoter is nearly fully saturated or (ii) the applied heme concentrations lead to saturation of the sensor kinase, i.e. maximal phosphorylation ( $[\text{ChrS}\sim\text{P}]/[\text{ChrS}_{\text{TOT}}] \approx 1$ ), and thus to similar phosphorylation levels of ChrA. In order to discriminate between these scenarios, we sought to

increase  $\text{ChrA}\sim\text{P}$  levels in the cell and test whether the  $P_{hrtBA}$  will be more active than in the wild type. To this end, we analyzed a *chrS* phosphatase-OFF mutant (*chrSQ191A*) still harboring its kinase activity (Hentschel *et al.*, 2014), supposedly leading to higher  $\text{ChrA}\sim\text{P}$  levels. Interestingly, the *chrSQ191A* phosphatase mutant strain displayed a sevenfold increased  $P_{hrtBA}\text{-eyfp}$  output (Fig. 4A), as incurred by a higher and more sustained promoter activity within the first 4 h of incubation when compared to the wild type (Fig. 4A inset). A similar behavior can also be observed in our computational models, in which the maximal phosphorylation level of ChrA is 25% in the wild type as compared to 100% in the phosphatase mutant (Fig. S5B), leading in our model to a stronger initial promoter activity in the latter case (Figs. 4B and S5C). The predicted increase of initial promoter activity is, however, more prominent in the model than in our experimental data, in which the kinase mutant showed a wild-type-like behavior for around 1 h before reaching a stronger promoter activity (Fig. 4A inset). Within the model, the time point of differentiation between the reporter output of the wild type and the phosphatase-OFF mutant – induced by stimulus decline and accordingly divergent  $\text{ChrA}\sim\text{P}$  levels (Fig. S5B) – is reached after  $\approx 15$  min (Fig. S5C). This discrepancy emphasized that saturation of kinase activity

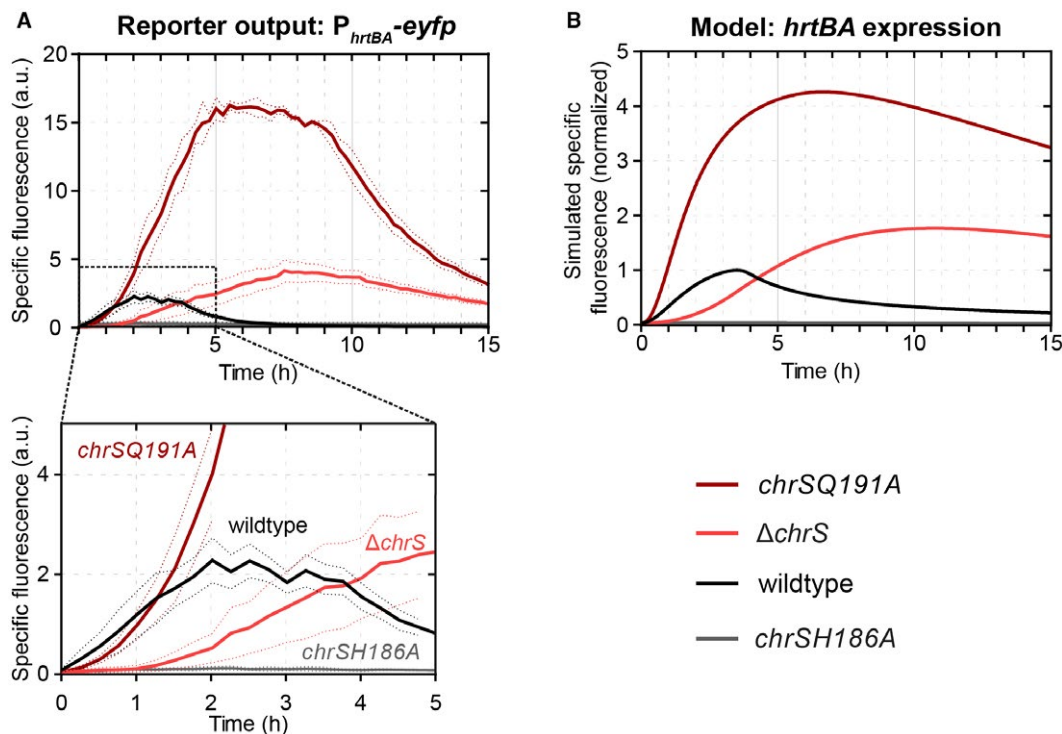


**Fig. 4.** Kinase and phosphatase activity of ChrS shape the *hrtBA* response.

A. Reporter output of *C. glutamicum* wild type and mutant strains carrying the vector pJC1- $P_{hrtBA}\text{-eyfp}$ . Cells were inoculated in CGXII minimal medium with 2% (w/v) glucose containing 4  $\mu\text{M}$  hemin as iron source.

B. Simulated specific fluorescence of the *C. glutamicum* wild-type strain and in the mutant strains *chrSQ191A* (phosphatase = off), *chrSH186A* (kinase = off) and  $\Delta\text{chrS}$ . [Colour figure can be viewed at [wileyonlinelibrary.com](http://wileyonlinelibrary.com)]

is not sufficient to explain the experimental data and that instantaneous promoter occupancy by phosphorylated response regulator may contribute to the fast onset of the detoxification response (see 'Memoryless activation of the *hrtBA* detoxification module').

Finally, another interesting feature of the model is that the depletion of external heme leads to a quick dephosphorylation of ChrA~P and promoter shut-off in the wild type. In contrast, in the phosphatase mutant, ChrA~P is only slowly diluted and/or degraded by growth or spontaneous dephosphorylation (Fig. S5B), leading to a significantly delayed promoter shut-off about 1 h after external heme depletion. Thus, the strong phosphatase activity of ChrS is important in wild type cells in order to quickly turn off *hrtBA* expression once external heme is depleted.

#### Both kinases, ChrS and HrrS, contribute to a fast onset of the $P_{hrtBA}$ promoter

Next, we wanted to study the response of the heme detoxification module in a strain featuring reduced ChrA~P levels. However, a *chrS* mutant deficient in its kinase activity (*chrSH186A*) was unable to activate the  $P_{hrtBA}$  promoter altogether (Fig. 4A; grey line), suggesting that ChrSH186A retains its strong phosphatase activity and likely reduces ChrA~P below a level required to activate  $P_{hrtBA}$ . Instead, our model predicted that in a  $\Delta chrS$  mutant, which lacks both kinase and phosphatase activity from ChrS, the non-cognate HrrS sensor kinase should be able to slowly, but gradually phosphorylate ChrA~P (Hentschel *et al.*, 2014) and thus activate  $P_{hrtBA}$  (Fig. 4B; light red). Indeed, the experimental kinetics of the  $P_{hrtBA}$ -*eyfp* reporter showed a weaker activation during the first 2 h, but also displayed a more sustained and eventually a stronger expression peak compared to the wild type (Fig. 4A). Within our computational model, this sustained response is again caused by the slow rate of dilution and/or dephosphorylation of ChrA~P after heme depletion, given the lack of phosphatase activity in the  $\Delta chrS$  mutant (Fig. 4B). Taken together, these data show that in the absence of ChrS, the non-cognate kinase HrrS is sufficient to activate the promoter of the detoxification module,  $P_{hrtBA}$ .

This provoked the question as to whether the non-cognate kinase HrrS also has an effect on the induction kinetics of  $P_{hrtBA}$  in wild-type cells. Interestingly, when measuring the  $P_{hrtBA}$ -*eyfp* reporter activity in a  $\Delta hrrS$  mutant, the mutant indeed showed a delayed promoter activation and was about 20–30 min slower than the wild type (Fig. 5). This suggests that HrrS acts as a 'kick-starter' in order to speed up the induction of the detoxification system. The additional kinase activity conferred by HrrS might in fact be needed as a support for ChrS to achieve higher ChrA phosphorylation levels, given that

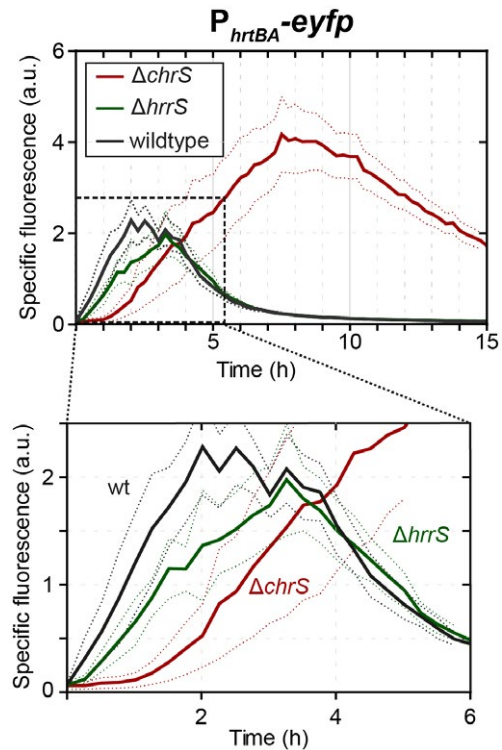


**Fig. 5.** HrrS-mediated cross-phosphorylation of ChrA might act as a kick-start impulse contributing to a fast ON-set of the  $P_{hrtBA}$  response. Reporter output of *C. glutamicum* wild-type cells and the mutant strains  $\Delta hrrS$  and  $\Delta chrS$ , carrying the vector pJC1\_  $P_{hrtBA}$ -*eyfp* and cultivated in CGXII minimal medium with 2% (w/v) glucose containing 4  $\mu$ M hemin as iron source. [Colour figure can be viewed at [wileyonlinelibrary.com](http://wileyonlinelibrary.com)]

our analysis above suggested that ChrS is already fully in its kinase state for all heme concentrations applied here.

#### Memoryless activation of the *hrtBA* detoxification module

Above-described results suggested that a high promoter occupancy by ChrA~P may contribute to the fast onset of the detoxification response. Considering this scenario, we would not expect memory in the  $P_{hrtBA}$  response if two heme pulses were applied at subsequent times. Theoretically, our model predicted nearly identical levels of promoter saturation for different heme levels, suggesting that the application of a second heme pulse should not lead to a faster response and no priming effect on the output should be observable.

While lag phase cells (growth depicted in Fig. S1) needed up to 35 min to reach maximum promoter activity following a heme pulse, promoter activity was nearly instantaneously observable after an additional heme pulse in the early exponential phase (Fig. 6A). Here, cells did respond equally fast irrespective of whether the cells were primed first, but a slightly higher maximal activity

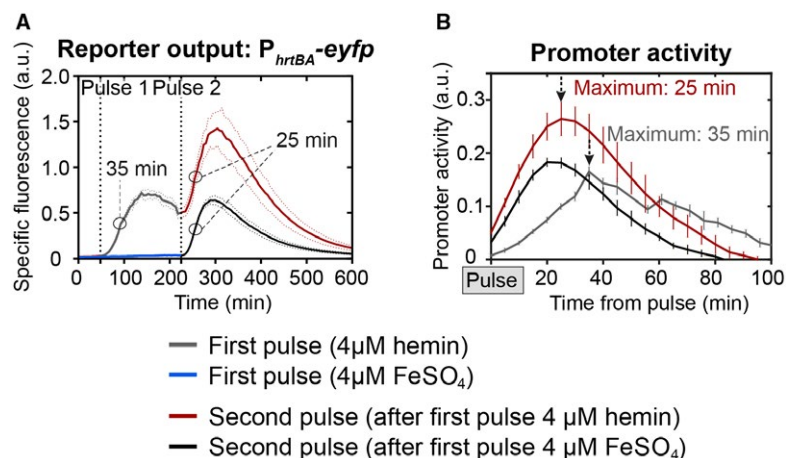


**Fig. 6.** Additional heme pulses do not ‘prime’ the  $P_{hrtBA}$  output.

A. *C. glutamicum* wild type cells were transformed with the target gene reporter pJC1\_  $P_{hrtBA}$ -*eyfp* and starved from iron overnight as described in material and methods. Subsequently, the cells were inoculated in CGXII minimal medium without iron source and eYFP fluorescence (=reporter output) and backscatter (biomass) was measured every 5 min. After 45 min, hemin (A, grey line) or  $FeSO_4$  (A, black line) was added to a final concentration of 4  $\mu M$ . A second pulse of 4  $\mu M$  hemin was applied to both conditions after 225 min. B. Promoter activities (calculated as derivative of the fluorescence intensity ( $I$ ) over time ( $t$ ), divided by the cell’s biomass (backscatter), that is  $\frac{dI(t)}{dt}/backscatter(t)$ ) of (A) in relation to the first or second pulse. [Colour figure can be viewed at [wileyonlinelibrary.com](http://wileyonlinelibrary.com)]

was observed after cells were primed with a heme pulse (Fig. 6A, red line) in comparison to an iron pulse (Fig. 6A, black line). Furthermore, the time point of the second heme pulses did not affect the onset of the  $P_{hrtBA}$  response (Fig. S2). Please note that the higher amplitude of the second pulse (Fig. 6A) is a result of cells already containing eYFP molecules and a ‘reactivation’ of ChrSA (and thus  $P_{hrtBA}$ ) leads to formation of additional eYFP molecules. The total increase is comparable to the increase in the first 4  $\mu M$  hemin pulse. Overall, this data supports the hypothesis that promoter saturation by phosphorylated response regulator contributes as a significant determinant of response kinetics.

#### Heme utilization is co-regulated by DtxR integrating information on iron availability

While a detoxification response must be fast and rather uncoupled from other regulatory interference, utilization of a particular nutrient has to be carefully considered in the light of the current physiological status of the cell: As shown above, the activation of the detoxification module *hrtBA* is solely influenced by the amount of heme in the medium. In contrast, for a decision on heme utilization as an alternative iron source, information on general iron availability needs to be incorporated into the network controlling *hmuO* expression. In this context, it was already revealed by the previous studies that both *hrrA* and *hmuO* are repressed by the iron regulator DtxR in response to iron availability (Wennerhold and Bott, 2006).

Given that DtxR repression and HrrA activation seem to have opposing effects on the timing of *hmuO* expression,

we asked how these signals are prioritized at the  $P_{hmuO}$  promoter. To investigate the impact of both regulators on the activation of the heme utilization system, we developed a second mathematical model that focuses on HrrSA and DtxR as main regulators of the  $P_{hmuO}$  and  $P_{hrrA}$  activity (Fig. 7A). Like before, in this model the description of the non-cognate two-component system (ChrSA) was limited to the cross-phosphorylation of ChrS on HrrA. In addition, we made the simplifying assumption that the activation of DtxR is proportional to the internal heme levels, based on the fact that the iron availability is proportional to the conversion of the internal heme pool under our experimental (iron-limiting) conditions. Activated DtxR and phosphorylated HrrA bind to both  $P_{hmuO}$  and  $P_{hrrA}$  promoters, where they repress and activate gene expression respectively. Ultimately, increased production of the heme oxygenase HmuO contributes to heme consumption (Frunzke *et al.*, 2011) (see Supplementary Text; Model equations M2 for all details).

Simulations of this computational model revealed a biphasic induction pattern of the  $P_{hmuO}$  promoter with a quick activation within the first hour after heme addition, followed by a significantly delayed expression boost at approx. 4–5 h (for 4  $\mu M$  heme) (Fig. 7B), very similar to the experimental dynamics observed before (Fig. 1). The initial activation of  $P_{hmuO}$  within the model is induced by an instantaneous increase in HrrA~P levels (Fig. 7D) in response to external heme. Since the dynamics of the active form DtxR~ $Fe^{2+}$  indirectly depends on the increase in cytoplasmic heme (which is converted to intracellular iron) (Fig. 2C), the DtxR-mediated repression of  $P_{hmuO}$ , which counteracts the promoter activation by HrrA~P, initiates not before DtxR~ $Fe^{2+}$  exceeds a certain



threshold – approximately after 1 h – in the model (Fig. 7D). However, low basal levels of endogenously synthesized heme, which are not reflected in the mathematical

model, as well as trace amounts of iron (resulting from the pre-cultivation of the cells, see Experimental Procedures) probably lead to a basal level of activated DtxR in the

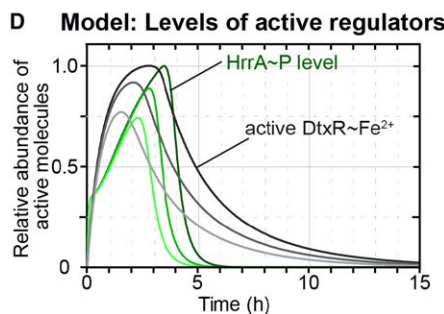
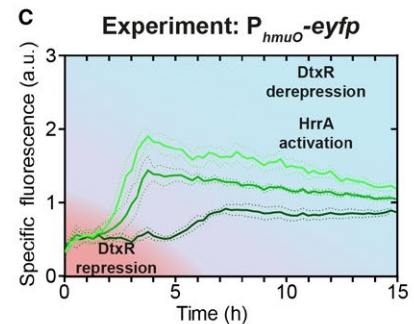
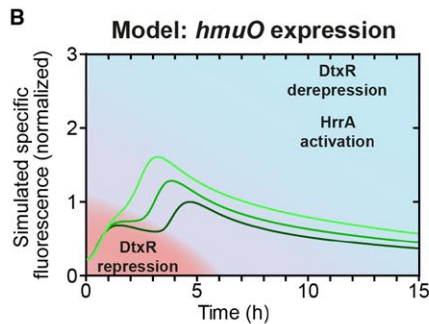
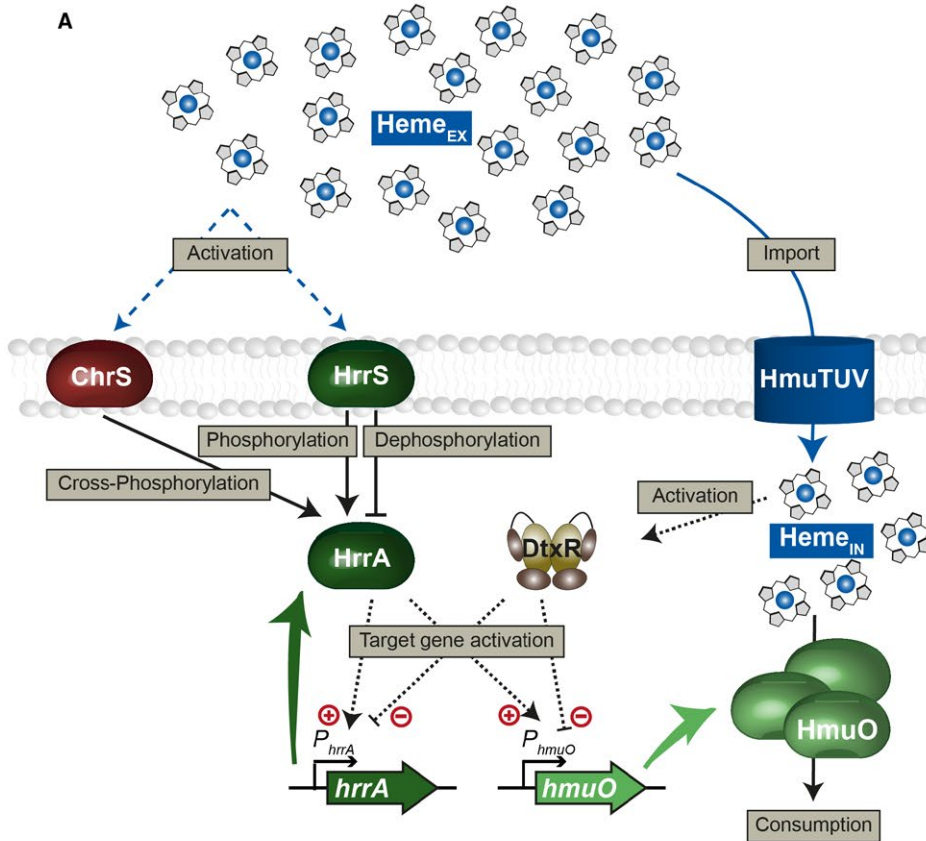


**Fig. 7.** Information on iron availability is integrated into the HrrSA-regulated utilization module *hmuO* via DtxR.

A. The mathematical model of the heme utilization module in *C. glutamicum* shares many basic assumptions with the model of heme detoxification (for description see Fig. 3). Here, heme consumption is assumed to be supported by the heme oxygenase HmuO, whose production is regulated by the phosphorylated response regulator HrrA~P and the iron repressor DtxR. The activation of DtxR is expected to be influenced by internal heme levels. DtxR repression and HrrA activation shape the delayed response of the heme utilization module *hmuO*.

B. The  $P_{hmuO}$  promoter is activated by the phosphorylated response regulator HrrA~P after a significant time delay of 3–5 h. Higher heme concentrations lead to a prolonged delay and a lower *hmuO* expression in general.

C. The mathematical model of the heme utilization network in *C. glutamicum* could reproduce this behavior and gave an explanation regarding.

D. The temporal dynamics of both regulators on  $P_{hmuO}$ . Levels of the activated iron repressor DtxR increase immediately after addition of heme and repress the promoter activation of  $P_{hmuO}$ , proportional to stimulus strength. However, HrrA~P levels increase with a short time delay in response to the stimulus and activate the promoter to a certain extent at the beginning and with increasing intensity upon DtxR dissociation [Colour figure can be viewed at [wileyonlinelibrary.com](http://wileyonlinelibrary.com)]

experimental scenario. These basal levels of DtxR might reduce the initial activation of HrrA~P on  $P_{hmuO}$  *in vivo*, leading to a less-pronounced initial increase and a more prominent plateau in the experimental data (Fig. 7C) of the  $P_{hmuO}$ -*eyfp* reporter output compared to the model prediction (Fig. 7B). Interestingly, when lowering the initial heme concentration, the model predicts an earlier onset of  $P_{hmuO}$  activation. Strikingly, when experimentally tuning the initial heme levels, we found this exact hierarchy in the activation of the heme utilization module (Fig. 7C): A short delay of 3 h at 1  $\mu$ M heme and a longer delay of 5 h at 4  $\mu$ M heme.

As such, this biphasic induction of *hmuO* strikingly differs from *hrtBA* activation by ChrSA and is governed by the influence of the iron repressor DtxR on *hmuO* expression (Fig. 8). Upon depletion of internal heme (and thus iron-levels) below a critical threshold, DtxR dissociates from its target promoters and allows their activation (Fig. 7B and D). Accordingly, lower initial heme concentrations within the medium do also shift the time point of heme exhaustion to earlier times, thereby rationalizing the earlier induction of gene expression in the heme utilization module. From a physiological perspective, this again seems very plausible, suggesting that high levels of the heme utilization system are only required under iron limitation when external heme sources are available.

Regarding the regulatory hierarchy of HrrA and DtxR on  $P_{hmuO}$  activity, one can think of two potential scenarios: either (i) HrrA is a *bona fide* activator of *hmuO* expression or (ii) HrrA-binding competes with the binding of the repressor DtxR thereby acting as an activator by derepressing *hmuO*, as might be suggested by the close proximity of their binding sites within the  $P_{hmuO}$  promoter (Fig. 8A). Altogether, our experimental data are clearly in favor for HrrA acting as a *bona fide* activator. While  $P_{hmuO}$  activity is completely abolished in a *hrrA* mutant (twofold lower reporter output than the WT), it is strongly increased in mutant lacking the *dtxR* gene (Fig. 8B). Furthermore, we tested different triplet mutations in the HrrA binding site in their ability to disrupt HrrA binding. In EMSA-studies, an AAC::TTG mutation in the middle of the HrrA operator completely abolished *in vitro* binding of HrrA to  $P_{hmuO}$  (Fig. S3). Subsequently, this mutation was

inserted to the  $pJC1\_P_{hmuO}$ -*eyfp* reporter, resulting in the  $pJC1\_P_{hmuO}$ -*eyfp*<sup>AAC::TTG</sup> plasmid (Fig. 8A). Irrespective of whether it was introduced to the wild-type strain or the  $\Delta dtxR$  strain, disruption of HrrA binding decreased the activity of the  $P_{hmuO}$  reporter to background levels (Figs. 8B and S4). To further validate our findings, we tested the wild type strain carrying the  $P_{hmuO}$  reporter under different heme and iron conditions (high-iron/low-heme; low-iron/high-heme, etc). As also revealed by our model (Fig. 7B and C), the results shown in Figure S8 indicate the intimate link between the iron and the heme pool. Due to the basal expression of the heme oxygenase (see Fig. 1 or Fig. 8, WT versus  $\Delta hrrA$ ) addition of heme will also impact the bioavailable iron pool, thereby affecting DtxR-mediated repression of *hmuO*. Thus, according to our current model, HrrA represents an essential activator of *hmuO*, which is required for a basal level of *hmuO* expression (and likely also required for the turnover of the endogenously synthesized heme). DtxR repression places an additional threshold on *hmuO* activation, which is only released when the intracellular iron pool is depleting. Then DtxR dissociates from the *hmuO* promoter allowing full activation by HrrA.

## Discussion

Orchestration of heme homeostasis and detoxification of excess heme appears to be of utmost importance for *Corynebacteriaceae*, as remarkably, several species dedicate two paralogous TCS to this regulatory task (Bott and Brocker, 2012). Here, we provide comprehensive insights into the temporal dynamics of *hmuO* and *hrtBA* expression modulated by HrrSA and ChrSA in *C. glutamicum*. Similar regulatory setups, with two paralogous, exclusively heme-dedicated systems are, for example, found in *C. diphtheria*, *Corynebacterium pseudotuberculosis* and *Corynebacterium lipophiloflavum* (Trost *et al.*, 2010; Bott and Brocker, 2012), where the corresponding sequence identities and a conserved genomic synteny suggest a similar role of these systems in the coordinated control of heme detoxification and utilization (Bibb

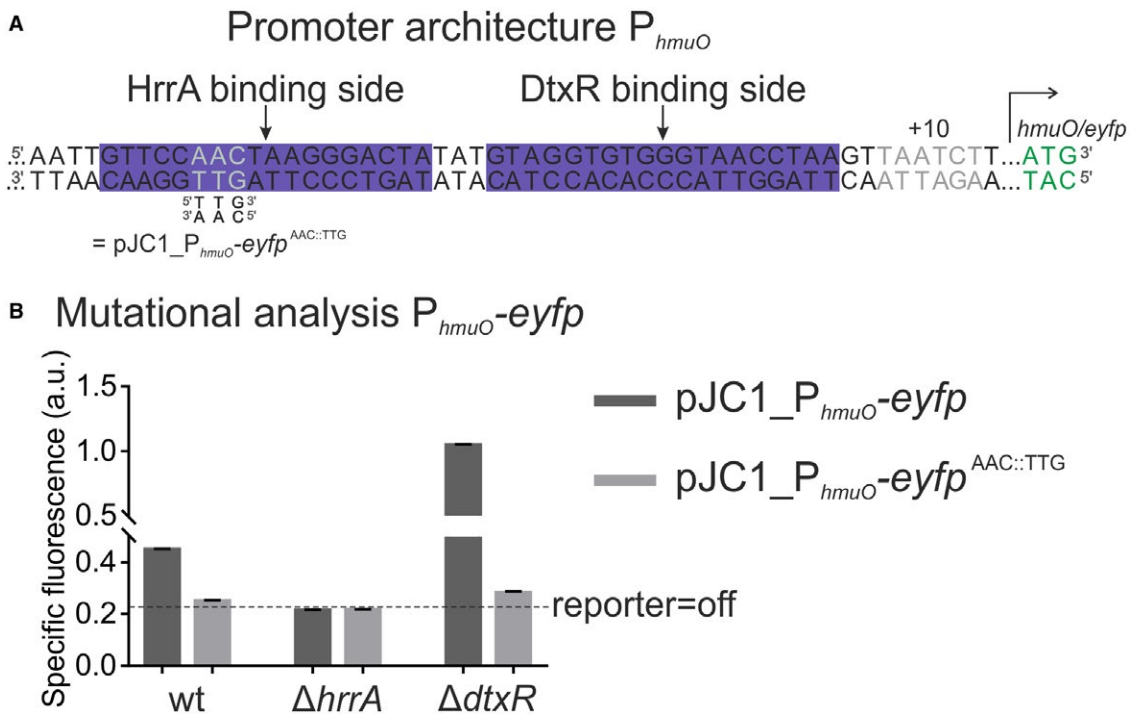


**Fig. 8.** HrrA and DtxR cooperate to control *hmuO* expression in response to iron and heme availability.

A. Promoter architecture of *hmuO*. The DtxR binding site was published previously (Wennerhold and Bott, 2006). The AAC::TTG mutation (grey letters) was shown to disrupt HrrA binding to  $P_{hmuO}$  in vitro (Fig. S3).

B. Mutational analysis of  $P_{hmuO}$ . HrrA binding was abolished by introducing the AAC::TTG mutation into the  $P_{hmuO}$ -eyfp reporter. All strains were grown in BHI complex medium supplemented with 4  $\mu$ M hemin as the  $\Delta dtxR$  strain grows poorly in CGXII medium. After iron starvation overnight, the three strains (wild type,  $\Delta hrrA$  and  $\Delta dtxR$ ) were inoculated in BHI and the specific fluorescence (eYFP-fluorescence/backscatter) was recorded in 15 min intervals. The graph shows the specific fluorescence after 20 h. Full reporter outputs are shown in the supplementary Fig. S4. [Colour figure can be viewed at [wileyonlinelibrary.com](http://wileyonlinelibrary.com)]

*et al.*, 2007; Bibb and Schmitt, 2010). To our knowledge, these systems represent the first example studied in detail, where two paralogous systems coordinate a complex physiological response by perceiving the same stimulus: heme.

As a general principle, the integrative signaling pathway design appears to be especially beneficial if a multifaceted stimulus requires different regulatory and appropriately timed outputs. The response of *C. glutamicum* to extracellular heme sets an interesting example for this, as the physiological adaptation is shaped by a fast-reacting ChrSA system-regulating expression of the detoxification module and the HrrSA system contributing to a layered dynamic regulation of heme utilization. In a recent study, we could show that the HKs of both TCS, HrrS and ChrS, slightly differ regarding their responsiveness and their general mode of heme-protein interaction (Keppel *et al.*, 2018). One obvious difference is, for example, a higher basal activity of the HrrSA system as reflected by the significantly higher output of a *hmuO* reporter compared to *hrtBA* in cells grown on  $\text{FeSO}_4$ . This basal activation is likely triggered by the endogenously synthesized heme pool. In contrast to ChrSA, which is required to counteract

toxic heme levels, HrrSA has an important role in maintaining heme homeostasis by balancing the synthesis of heme proteins, heme degradation and heme biosynthesis (Frunzke *et al.*, 2011; Hentschel *et al.*, 2014). In this context, it becomes apparent that this system is sensitive toward endogenous heme levels of the cells.

However, kinase activity is not the only factor influencing differential target gene activation. While the  $P_{chrSA}$  promoter and the divergently located  $P_{hrtBA}$  promoter are positively autoregulated from one-centered ChrA binding site (Fig. 3A), *hrrS* and *hrrA* are controlled from two distinct promoters. For *hrrA* as well as *hmuO*, the global iron regulator DtxR adds an additional regulatory layer, thereby integrating information on general iron availability in the cell (Wennerhold and Bott, 2006; Frunzke *et al.*, 2011). Experiments under different iron and heme conditions, furthermore, illustrated the intimate link between these cellular pools (Fig. S8), which is based on the activity of the heme oxygenase – degrading heme to release iron. Here, we could show that HrrA does not simply displace DtxR on the promoter of *hmuO* but is in fact an essential activator, also in the absence of DtxR repression (Fig. 8B). By this means, information on heme (stimulus of HrrS)

and Fe<sup>2+</sup> (co-repressor of DtxR) is directly integrated at the level of *hmuO* expression and RR (HrrA) synthesis.

In contrast, ChrSA-mediated activation of *hrtBA* expression is solely influenced by heme availability, as expected for a detoxification system. Here, our data suggested an instantaneous saturation of the ChrS kinase and strong activation of P<sub>*hrtBA*</sub> in response to exogenous heme – independent of the applied heme concentrations tested in our setup (Fig. 3). Our model and experiments revealed that the overall strength of *hrtBA* expression was determined solely by the duration of the response, as governed by the timescale of heme exhaustion in the medium. Thus, it seems that the comparable levels of P<sub>*hrtBA*</sub> promoter occupancy independent from stimulus strength ensure an effective detoxification response even for low-toxic heme concentrations, as claimed for a detoxification module.

Another important factor in the maintenance of intracellular heme homeostasis is the previously reported cross-phosphorylation between HrrSA and ChrSA (Hentschel *et al.*, 2014). While deletion of *chrS* did not significantly influence the P<sub>*hmuO*</sub> activation pattern in our reporter studies (Fig. 1B), deletion of *hrrS* resulted in a delayed P<sub>*hrtBA*</sub> activation in response to heme (Fig. 5). These findings suggest a role of HrrSA as a ‘kick-start’ system of *chrSA*, thereby giving *C. glutamicum* a competitive edge by shortening the reaction time to mount the detoxification response. Furthermore, the bifunctionality of ChrS ensures efficient proof-reading of ChrA~P counteracting cross-phosphorylation by HrrS under non-inducing conditions where ChrS is dominantly in its phosphatase state.

Physiologically relevant cross phosphorylation between TCSs was, for example, shown in *Bacillus anthracis* (Mike *et al.*, 2014). In this case, the heme responsive HssRS system was shown to cross interact with HitRS, which is activated by cell envelope stress. Cross-regulation between HssRS and HitRS thereby enables an integrated response of *B. anthracis* to heme and to heme-induced cell envelope damage (Mike *et al.*, 2014). Interestingly, HrrSA and ChrSA as well as HssRS and HitRS are among the closest-related TCS in the particular species reflecting that duplication and subsequent specialization represents an evolutionary driver of TCS signaling toward the integration of multiple signals and the creation of a multifaceted response to complex stimuli. A similar scenario is found with the NarPQ and NarXL systems regulating the response to nitrate and nitrite in *Escherichia coli* (Rabin and Stewart, 1993). For these closely related systems, significant cross phosphorylation appears to play a role in the modulation of target gene activation and maintenance of nitrogen homeostasis (Noriega *et al.*, 2010).

The regulatory setup shaping the response to heme may also have considerable impact on heme tolerance of the particular species. Already decades ago, van

Heyningen reported on the differential sensitivity of *Bacillus* species to heme (Van Heyningen, 1948). Mike and co-workers correlated an increased tolerance, as observed for *B. anthracis*, with the employment of two cross-regulating TCS coordinating heme export (HssRS) and cell envelope stress (HitRS) (Mike *et al.*, 2014). Therefore, it might be conceivable that the employment of two heme-responsive TCSs by some corynebacterial species enables a more robust control of heme homeostasis compared to the regulation by a single system. Remarkably, while the HrtBA exporter is conserved among many Gram-positive species, the TCS systems ‘in charge’ do not share significant sequence similarity – especially not in their membrane-embedded sensor domains (Stauff and Skaar, 2009b; Keppel *et al.*, 2018). This overall scenario of two cross-regulating TCSs modulating heme homeostasis and detoxification underlines a favorable concept nature employs to respond to the multifaceted stimulus heme.

In summary, we have approached the regulatory interplay between the heme-responsive HrrSA and ChrSA TCSs of *C. glutamicum* by a comprehensive screening of various mutant strains carrying different target promoters. Generation of a mathematical model based on this data set revealed the underlying mechanisms triggering the antagonistic temporal dynamics in TCS signaling, which shape the cellular response toward the ‘toxic, but tasty’ heme molecule. We believe that the approach of combining time-resolved monitoring of gene expression and systems-level modeling of the underlying regulatory networks is key to understanding the logic behind complex homeostatic responses in bacteria.

## Experimental procedures

### *Bacterial strains and growth conditions*

Bacterial strains used in this study are listed in Table S1. *C. glutamicum* strain ATCC 13032 was used as wild type (Kalinowski *et al.*, 2003) and either cultivated in BHI (brain heart infusion, Difco BHI, BD, Heidelberg, Germany) as complex medium or CGXII (Keilhauer *et al.*, 1993) containing 2% (w/v) glucose as minimal medium. All cultivations were performed at 30°C and, if necessary, 25 µg/ml kanamycin was added to the medium for selection. For standard cloning applications, *E. coli* DH5α was cultivated in Lysogeny Broth (Difco LB, BD, Heidelberg, Germany) medium at 37°C in a rotary shaker and for selection, 50 µg/ml kanamycin was added to the medium.

### *Recombinant DNA work and cloning techniques*

Standard cloning and other molecular methods were performed according to the standard protocols (Sambrook and Russell, 2001). For most applications, chromosomal DNA of *C. glutamicum* ATCC 13032 was used as a



template for PCR amplification of DNA fragments and was prepared as described previously (Eikmanns *et al.*, 1994). All sequencing and synthesis of oligonucleotides was performed by Eurofins Genomics (Ebersberg, Germany). For the construction of plasmids, the DNA regions of interest were amplified from chromosomal *C. glutamicum* DNA with oligonucleotides listed in Table S2 and ligated into the plasmid backbone (see Table S3) via restriction sites indicated in the same table. Genomic integrations and/or deletions were performed using the pK19mobsacB plasmid and the two-step homologous recombination method described earlier (Niebisch and Bott, 2001). Point mutations for the integration of kinase mutants or construction of a mutated reporter plasmid were introduced via 'QuickChange Lightning' site-directed mutagenesis according to the supplier's manual (Agilent Technologies, Inc., Santa Clara, USA).

### Reporter assays

For reporter studies, *C. glutamicum* wild type or one of the mutant strains were transformed with a reporter plasmid (Table S3). A preculture in BHI medium (25 µg/ml kanamycin) was inoculated from a fresh BHI agar plate and incubated for 8–10 h at 30°C in a rotary shaker. After that, cells were transferred into a second preculture in CGXII medium (Keilhauer *et al.*, 1993) containing 2% (w/v) glucose and 0 µM FeSO<sub>4</sub> to starve the cells from iron. However, protocatechuic acid (PCA) was present in the preculture, allowing the uptake of trace amounts of iron. After growth overnight, the main culture was inoculated to an OD<sub>600</sub> of 1 in CGXII medium and cultivated in 48-well Flowerplates (m2p-labs GmbH, Aachen, Germany) at 30°C, 95% humidity, 1200 rpm. For the hemin stock solution, hemin (Sigma Aldrich, Munich, Germany) was dissolved in 20 mM NaOH to a concentration of 2.5 mM and, as an iron source, added to the medium in the desired concentrations. Growth of the cells (biomass production) was recorded as the backscattered light intensity of sent light with a wavelength of 620 nm (signal gain factor of 12). For the measurement of eYFP fluorescence, the culture was excited at 510 nm and emission was measured at 532 nm (signal gain factor of 50). Measurements were performed in 15 min intervals.

### Electrophoretic mobility shift assays

To characterize the operator sequence of HrrA, the protein was produced in *E. coli* BL21 and purified as His<sub>6</sub>-tagged variant from cells as described previously (Frunzke *et al.*, 2011). As ligand, 30 bp DNA fragments with triplet mutations were amplified and subsequently, 100 ng of the fragments were incubated with 0x, 10x and 30x excess of HrrA in in EMSA buffer (250 mM Tris-HCl pH 7.5, 25 mM MgCl<sub>2</sub>, 200 mM KCl, 25% (v/v) glycerol). After 30 min at room temperature, the samples were loaded to a native 12% polyacrylamide gel (TBE-based, TBE (89 mM Tris base, 89 mM boric acid, 2 mM Na<sub>2</sub>EDTA, loading dye: 0.01% (w/v) xylene cyanol dye, 0.01% (w/v) bromophenol blue dye, 20% (v/v) glycerol, 1 × TBE). Electrophoresis was carried out for

60 min at 160 V. DNA was subsequently stained with SYBR Green I (Sigma Aldrich, Munich, Germany).

### Measurement of cell-associated heme levels

The protocol for the fluorescent measurement of (total) cell-associated heme was derived from an assay described by Sassa (1976). A preculture containing *C. glutamicum* wild-type cells was inoculated in BHI medium from a fresh BHI agar plate and incubated for 8–10 h at 30°C in a rotary shaker. After that, cells were transferred into a second preculture in CGXII medium containing 2% (w/v) glucose and 0 µM FeSO<sub>4</sub> to starve the cells from iron. After growth for 12–16 h, the main culture was inoculated to an optical density (OD<sub>600</sub>) of 1 in CGXII medium. Before addition of 4 µM hemin, as well as 5 min, 30 min, 1, 3, 6, 7 and 23 h after hemin addition, samples were taken for the determination of cell-associated heme. For that, cells corresponding to an OD<sub>600</sub> of 2 in 250 µl were harvested and washed once in 250 µl PBS. Subsequently, the pellet was resuspended in 250 µl 20 mM oxalic acid and stored at 4°C for max 5–6 h. Then, 250 µl of 2 M oxalic acid were added and each sample was heated to 98°C for 30 min. For the measurement, 200 µL of each sample were transferred to a 96-well microtiter plate and the fluorescence was recorded on a Tecan (Tecan Trading AG, Switzerland) Microplate Reader (excitation at 400 nm and emission at 608 nm). The values for each sample were normalized to the emission of an unheated control sample (cells before hemin addition in 1 M oxalic acid).

### Mathematical models and mutant simulation

Two mathematical models were developed to assess the determining factors of the dynamics of the heme detoxification and utilization modules (see Supplementary Text; Model equations M1 and M2). A set of ordinary differential equations (ODEs) describes the time-dependent changes in the different components of the two networks under varying heme concentrations as stimulus of both systems. The interactions between the kinases and the response regulators of the two TCSs were described based on the modeling approach by Groban and co-workers (2009), while thermodynamic modeling (Bintu *et al.*, 2005) was used to describe the target gene regulation in both systems. The dynamics of the individual components were simulated for wild-type conditions as well as different mutant strains. The numerical solution of the ODEs as well as the individual simulations were performed with MATLAB<sup>TM</sup> software (The MathWorks, Inc.).

### Acknowledgements

We would like to thank Ulrike Viets for excellent technical support, Eva Davoudi for critical proof-reading and discussion and Dominik Wolf for his help with the EMSA experiments. This work was financially supported by the Deutsche Forschungsgemeinschaft (DFG SPP 1617; grant FR3673/1-2 and grant FR 2759/4-1) and the Helmholtz Association (W2W3-096).

## Conflict of interest

The authors declare that the research was conducted in the absence of any commercial or financial relationships that could be construed as a potential conflict of interest.

## Author contributions

MK, HP, GF and JF conceived the study; MK and CG performed the experiments; MK, HP, GF and JF analyzed the data; HP and GF generated the models; MK, HP, GF and JF wrote the manuscript.

## References

- Andrews, S.C., Robinson, A.K. and Rodriguez-Quinones, F. (2003) Bacterial iron homeostasis. *FEMS Microbiology Reviews*, **27**, 215–237.
- Anzaldi, L.L. and Skaar, E.P. (2010) Overcoming the heme paradox: heme toxicity and tolerance in bacterial pathogens. *Infection and Immunity*, **78**, 4977–4989.
- Bibb, L.A. and Schmitt, M.P. (2010) The ABC transporter HrtAB confers resistance to hemin toxicity and is regulated in a hemin-dependent manner by the ChrAS two-component system in *Corynebacterium diphtheriae*. *Journal of Bacteriology*, **192**, 4606–4617.
- Bibb, L.A., Kunkle, C.A. and Schmitt, M.P. (2007) The ChrA-ChrS and HrrA-HrrS signal transduction systems are required for activation of the *hmuO* promoter and repression of the *hemA* promoter in *Corynebacterium diphtheriae*. *Infection and Immunity*, **75**, 2421–2431.
- Bintu, L., Buchler, N.E., Garcia, H.G., Gerland, U., Hwa, T., Kondev, J. and Phillips, R. (2005) Transcriptional regulation by the numbers: models. *Current Opinion in Genetics & Development*, **15**, 116–124.
- Borzelleca, J.F. (2000) Paracelsus: herald of modern toxicology. *Toxicological Sciences: An Official Journal of the Society of Toxicology*, **53**, 2–4.
- Bott, M. and Brocker, M. (2012) Two-component signal transduction in *Corynebacterium glutamicum* and other corynebacteria: on the way towards stimuli and targets. *Applied Microbiology and Biotechnology*, **94**, 1131–1150.
- Burgos, J.M. and Schmitt, M.P. (2016) The ChrSA and HrrSA two-component systems are required for transcriptional regulation of the *hemA* promoter in *Corynebacterium diphtheriae*. *Journal of Bacteriology*, **198**, 2419–2430.
- Eikmanns, B.J., Thum-Schmitz, N., Eggeling, L., Ludtke, K.U. and Sahm, H. (1994) Nucleotide sequence, expression and transcriptional analysis of the *Corynebacterium glutamicum* *gltA* gene encoding citrate synthase. *Microbiology (Reading, England)*, **140**(Pt 8), 1817–1828.
- Fernandez, A., Lechardeur, D., Derre-Bobillot, A., Couve, E., Gaudu, P. and Gruss, A. (2010) Two coregulated efflux transporters modulate intracellular heme and protoporphyrin IX availability in *Streptococcus agalactiae*. *PLoS Pathogens*, **6**, e1000860.
- Fitch, C.D. (1998) Involvement of heme in the antimalarial action of chloroquine. *Transactions of the American Clinical and Climatological Association*, **109**, 97–106.
- Frunzke, J., Gatgens, C., Brocker, M. and Bott, M. (2011) Control of heme homeostasis in *Corynebacterium glutamicum* by the two-component system HrrSA. *Journal of Bacteriology*, **193**, 1212–1221.
- Groban, E.S., Clarke, E.J., Salis, H.M., Miller, S.M. and Voigt, C.A. (2009) Kinetic buffering of cross talk between bacterial two-component sensors. *Journal of Molecular Biology*, **390**, 380–393.
- Hassan, S., Ohtani, K., Wang, R., Yuan, Y., Wang, Y., Yamaguchi, Y. and Shimizu, T. (2010) Transcriptional regulation of hemO encoding heme oxygenase in *Clostridium perfringens*. *Journal of Microbiology (Seoul, Korea)*, **48**, 96–101.
- Hentschel, E., Mack, C., Gatgens, C., Bott, M., Brocker, M. and Frunzke, J. (2014) Phosphatase activity of the histidine kinases ensures pathway specificity of the ChrSA and HrrSA two-component systems in *Corynebacterium glutamicum*. *Molecular Microbiology*, **92**, 1326–1342.
- Heyer, A., Gatgens, C., Hentschel, E., Kalinowski, J., Bott, M. and Frunzke, J. (2012) The two-component system ChrSA is crucial for haem tolerance and interferes with HrrSA in haem-dependent gene regulation in *Corynebacterium glutamicum*. *Microbiology (Reading, England)*, **158**, 3020–3031.
- Imlay, J.A., Chin, S.M. and Linn, S. (1988) Toxic DNA damage by hydrogen peroxide through the Fenton reaction in vivo and in vitro. *Science*, **240**, 640–642.
- Jani, D., Nagarkatti, R., Beatty, W., Angel, R., Slebodnick, C., Andersen, J., et al. (2008) HDP – A novel heme detoxification protein from the malaria parasite. *PLoS Pathogens*, **4**, e1000053.
- Kalinowski, J., Bathe, B., Bartels, D., Bischoff, N., Bott, M., Burkovski, A., et al. (2003) The complete *Corynebacterium glutamicum* ATCC 13032 genome sequence and its impact on the production of L-aspartate-derived amino acids and vitamins. *Journal of Biotechnology*, **104**, 5–25.
- Keilhauer, C., Eggeling, L. and Sahm, H. (1993) Isoleucine synthesis in *Corynebacterium glutamicum*: molecular analysis of the *ilvB-ilvN-ilvC* operon. *Journal of Bacteriology*, **175**, 5595–5603.
- Keppel, M., Davoudi, E., Gätgens, C. and Frunzke, J. (2018) Membrane topology and heme binding of the histidine kinases HrrS and ChrS in *Corynebacterium glutamicum*. *Frontiers in Microbiology*, **9**, 183, doi:10.3389/fmicb.2018.00183
- Mascher, T., Helmann, J.D. and Uden, G. (2006) Stimulus perception in bacterial signal-transducing histidine kinases. *Microbiology and Molecular Biology Reviews*, **70**, 910–938.
- Mike, L.A., Choby, J.E., Brinkman, P.R., Olive, L.Q., Dutter, B.F., Ivan, S.J., et al. (2014) Two-component system cross-regulation integrates *Bacillus anthracis* response to heme and cell envelope stress. *PLoS Pathogens*, **10**, e1004044.
- Niebisch, A. and Bott, M. (2001) Molecular analysis of the cytochrome *bc<sub>1</sub>-aa<sub>3</sub>* branch of the *Corynebacterium glutamicum* respiratory chain containing an unusual diheme cytochrome *c<sub>1</sub>*. *Archives of Microbiology*, **175**, 282–294.
- Nir, U., Ladan, H., Malik, Z. and Nitzan, Y. (1991) In vivo effects of porphyrins on bacterial DNA. *Journal of Photochemistry and Photobiology B, Biology*, **11**, 295–306.

- Noriega, C.E., Lin, H.Y., Chen, L.L., Williams, S.B. and Stewart, V. (2010) Asymmetric cross-regulation between the nitrate-responsive NarX-NarL and NarQ-NarP two-component regulatory systems from *Escherichia coli* K-12. *Molecular Microbiology*, **75**, 394–412.
- Paracelsus. (1965) Die dritte defension wegen des Schreibens der neuen Rezepte. *Septem Defensiones*, **1538**, 508–513.
- Poulos, T.L. (2007) The Janus nature of heme. *Natural Product Reports*, **24**, 504–510.
- Rabin, R.S. and Stewart, V. (1993) Dual response regulators (NarL and NarP) interact with dual sensors (NarX and NarQ) to control nitrate- and nitrite-regulated gene expression in *Escherichia coli* K-12. *Journal of Bacteriology*, **175**, 3259–3268.
- Ratliff, M., Zhu, W., Deshmukh, R., Wilks, A. and Stojiljkovic, I. (2001) Homologues of neisserial heme oxygenase in gram-negative bacteria: degradation of heme by the product of the *pigA* gene of *Pseudomonas aeruginosa*. *Journal of Bacteriology*, **183**, 6394–6403.
- Sambrook, J. and Russell, D. W. (2001) *Molecular Cloning: A Laboratory Manual*, 3rd edition. New York, NY: Cold Spring Harbor Laboratory Press
- Sassa, S. (1976) Sequential induction of heme pathway enzymes during erythroid differentiation of mouse Friend leukemia virus-infected cells. *Journal of Experimental Medicine*, **143**, 305–315.
- Schmitt, M.P. (1997) Transcription of the *Corynebacterium diphtheriae hmuO* gene is regulated by iron and heme. *Infection and Immunity*, **65**, 4634–4641.
- Stauff, D.L. and Skaar, E.P. (2009a) *Bacillus anthracis* HssRS signalling to HrtAB regulates haem resistance during infection. *Molecular Microbiology*, **72**, 763–778.
- Stauff, D.L. and Skaar, E.P. (2009b) The heme sensor system of *Staphylococcus aureus*. *Contributions to Microbiology*, **16**, 120–135.
- Torres, V.J., Stauff, D.L., Pishchany, G., Bezbradica, J.S., Gordy, L.E., Iturregui, J., *et al.* (2007) A *Staphylococcus aureus* regulatory system that responds to host heme and modulates virulence. *Cell Host & Microbe*, **1**, 109–119.
- Trost, E., Ott, L., Schneider, J., Schroder, J., Jaenicke, S., Goesmann, A., *et al.* (2010) The complete genome sequence of *Corynebacterium pseudotuberculosis* FRC41 isolated from a 12-year-old girl with necrotizing lymphadenitis reveals insights into gene-regulatory networks contributing to virulence. *BMC Genomics*, **11**, 728, doi:10.1186/1471-2164-11-728
- Van Heyningen, W.E. (1948) Inhibition of aerobic sporing bacilli by haematin. *Nature*, **162**, 114–115.
- Wakeman, C.A., Hammer, N.D., Stauff, D.L., Attia, A.S., Anzaldi, L.L., Dikalov, S.I., *et al.* (2012) Menaquinone biosynthesis potentiates haem toxicity in *Staphylococcus aureus*. *Molecular Microbiology*, **86**, 1376–1392.
- Wennerhold, J. and Bott, M. (2006) The DtxR regulon of *Corynebacterium glutamicum*. *Journal of Bacteriology*, **188**, 2907–2918.
- Wilks, A. (2002) Heme oxygenase: evolution, structure, and mechanism. *Antioxidants & Redox Signaling*, **4**, 603–614.
- Wilks, A. and Schmitt, M.P. (1998) Expression and characterization of a heme oxygenase (HmuO) from *Corynebacterium diphtheriae*. Iron acquisition requires oxidative cleavage of the heme macrocycle. *The Journal of Biological Chemistry*, **273**, 837–841.
- Zhu, W., Hunt, D.J., Richardson, A.R. and Stojiljkovic, I. (2000a) Use of heme compounds as iron sources by pathogenic *Neisseriae* requires the product of the *hemO* gene. *Journal of Bacteriology*, **182**, 439–447.
- Zhu, W., Wilks, A. and Stojiljkovic, I. (2000b) Degradation of heme in gram-negative bacteria: the product of the *hemO* gene of *Neisseriae* is a heme oxygenase. *Journal of Bacteriology*, **182**, 6783–6790.
- Zschiedrich, C.P., Keidel, V. and Szurmant, H. (2016) Molecular mechanisms of two-component signal transduction. *Journal of Molecular Biology*, **428**, 3752–3775.

### Supporting Information

Additional supporting information may be found online in the Supporting Information section at the end of the article

## Supplementary Information

### **Toxic but tasty - Temporal dynamics and network architecture of heme-responsive two-component signalling in *Corynebacterium glutamicum***

Marc Keppel<sup>1#</sup>, Hannah Piepenbreier<sup>2#</sup>, Cornelia Gätgens<sup>1</sup>, Georg Fritz<sup>2\*</sup> and Julia Frunzke<sup>1\*</sup>

<sup>1</sup>Institute of Bio- und Geosciences, IBG-1: Biotechnology, Forschungszentrum Jülich, 52425 Jülich, Germany

<sup>2</sup>LOEWE-Zentrum für Synthetische Mikrobiologie, Philipps-Universität Marburg, 35032 Marburg, Germany

\*Corresponding authors:

Georg Fritz; Email: [georg.fritz@synmikro.uni-marburg.de](mailto:georg.fritz@synmikro.uni-marburg.de); Phone: +49 6421 28 22582

Julia Frunzke; Email: [j.frunzke@fz-juelich.de](mailto:j.frunzke@fz-juelich.de); Phone: +49 2461 615430

#These authors contributed equally to this work.



## Content

**Figure S1:** Growth curves after application of additional heme pulses.

**Figure S2:** Additional heme pulses do not prime  $P_{hrtBA}$ .

**Figure S3:** Electrophoretic Mobility Shift Assays (EMSAs) reveal crucial nucleotides for HrrA binding to the operator.

**Figure S4:** Control of  $P_{hmuO}$  by HrrA and DtxR.

**Figure S5:** Dephosphorylation of the response regulator ChrA determines the dynamics of the target gene activation in the wildtype and a *chrSQ191A* phosphatase mutant.

**Figure S6:** The *in vitro* data suggest a cross-phosphatase activity of HrrS which did not result in a model that quantitatively fits to the behavior of the  $\Delta chrS$  mutant *in vivo* data

**Figure S7:** An increased phosphatase activity of HrrS prevents a delayed  $P_{hmuO}$  activation by HrrA~P.

**Figure S8:**  $P_{hmuO}$ -*eyfp* screening under different environmental conditions.

**General supplement file S1:** In depth description of the mathematical models and equations

**Table S1:** Bacterial strains used in this study.

**Table S2:** Oligonucleotides used in this study.

**Table S3:** Plasmids used in this study.

**Table S4:** Parameters used in the mathematical model of the *C. glutamicum* heme detoxification module.

**Table S5:** Additional parameters used in the mathematical model of the *C. glutamicum* heme utilization module.

**Table S6:** Transformation of the units within the mathematical models.

## Pulsing experiments, biomass

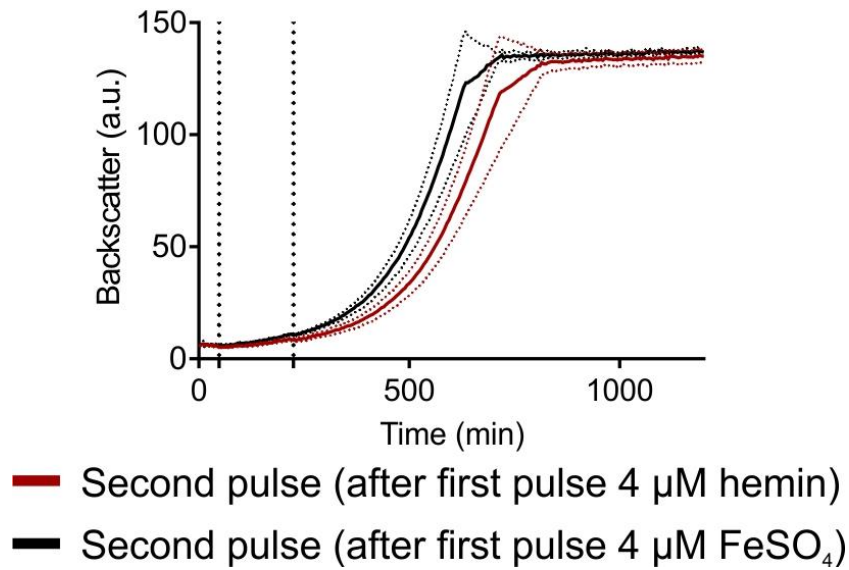


**Figure S1: Growth curves after application of additional heme pulses**

*C. glutamicum* cells were transformed with the target gene reporter  $p\text{JC1\_P}_{hrt\text{BA-eYfp}}$  and starved from iron overnight as described in material and methods. Subsequently, the cells were inoculated in CGXII minimal medium with 2% (w/v) glucose containing no iron source and transferred to the microbioreactor system (Biolector) where eYfp fluorescence (=reporter output) and backscatter (biomass) was measured in 5 minutes intervals. After 45 min, hemin (red line) or  $\text{FeSO}_4$  (black line) was added to a final concentration of 4  $\mu\text{M}$ . A second pulse of 4  $\mu\text{M}$  hemin was applied to both cultures after 225 min.

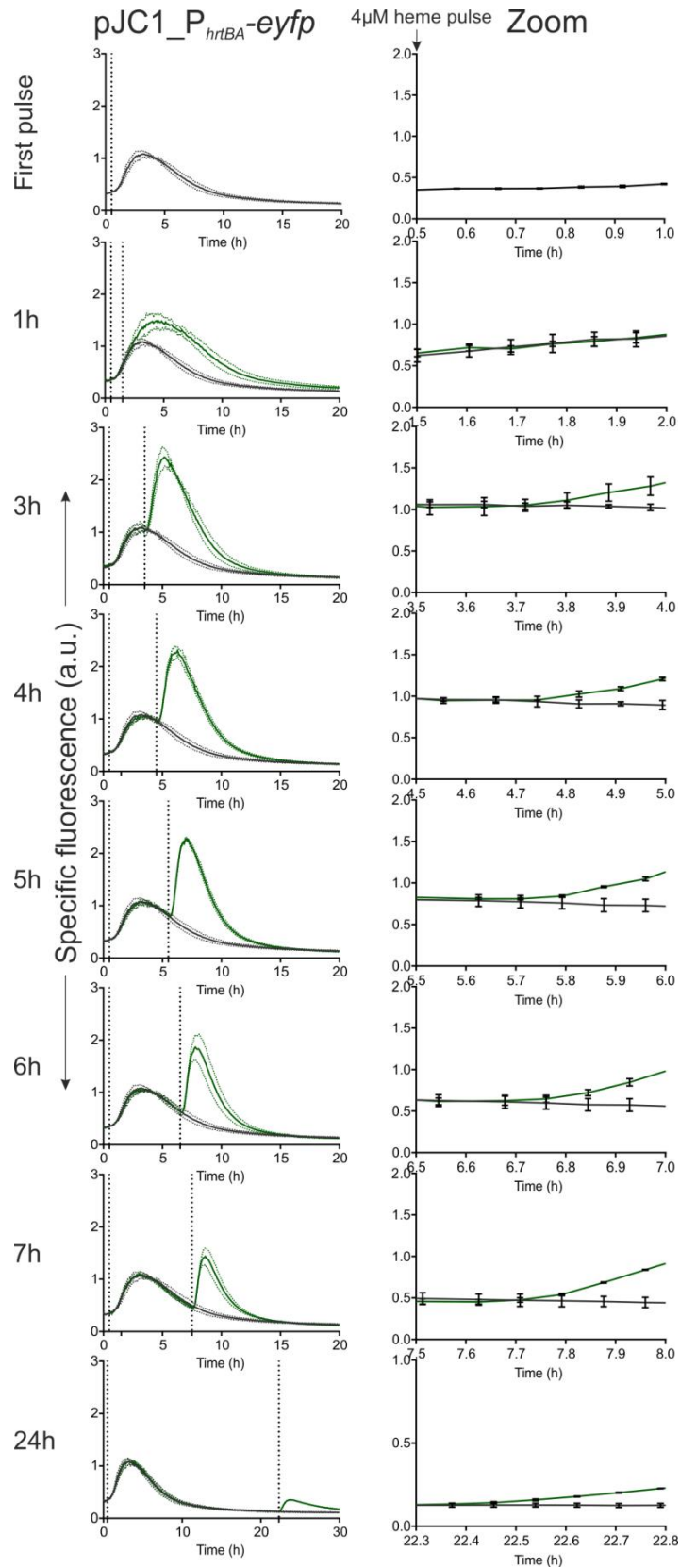


**Figure S2: Additional heme pulses do not prime *P<sub>hrtBA</sub>*.**

*C. glutamicum* cells were transformed with the target gene reporter *pJC1\_P<sub>hrtBA</sub>-eyfp* and

starved from iron overnight as described in material and methods. Subsequently, the cells were inoculated in CGXII minimal medium with 2% (w/v) glucose containing no iron source and transferred to the microbioreactor system (Biolector) where eYfp fluorescence (=reporter output) and backscatter (biomass) was measured in 5 minutes intervals. After 30 min, hemin was added to a final concentration of 4  $\mu$ M. A second pulse of 4  $\mu$ M hemin (resulting in a final hemin concentration of 8  $\mu$ M) was applied after 1h, 3h, 4h 5h, 6h, 7h or 24h, respectively.

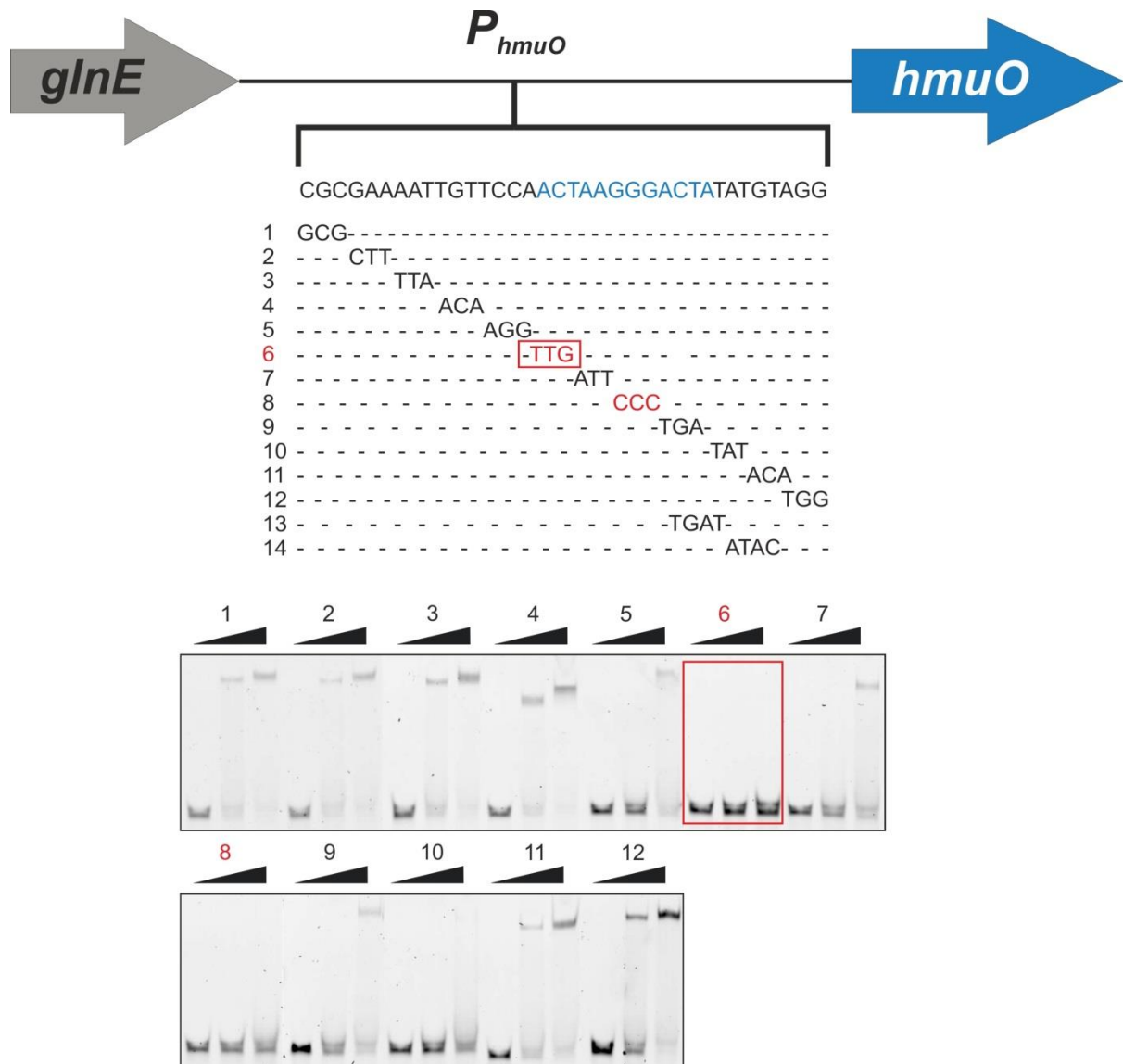


**Figure S3: Electrophoretic Mobility Shift Assays (EMSAs) reveal crucial nucleotides for HrrA binding to the operator.**

For all EMSAs, 36 Bp of mutated DNA fragments (100 ng) were used and purified HrrA-His protein was applied in 0, 10 and 30-fold molecular excess for each sample. Mutation 6 (ACT::TTG) and mutation 8 (GGG::CCC) led to strongly reduced binding of HrrA to  $P_{hmuO}$  and similar  $P_{hmuO}$ -*eyfp* output like observed in a  $\Delta hrrA$  deletion mutant (Fig. S5B).

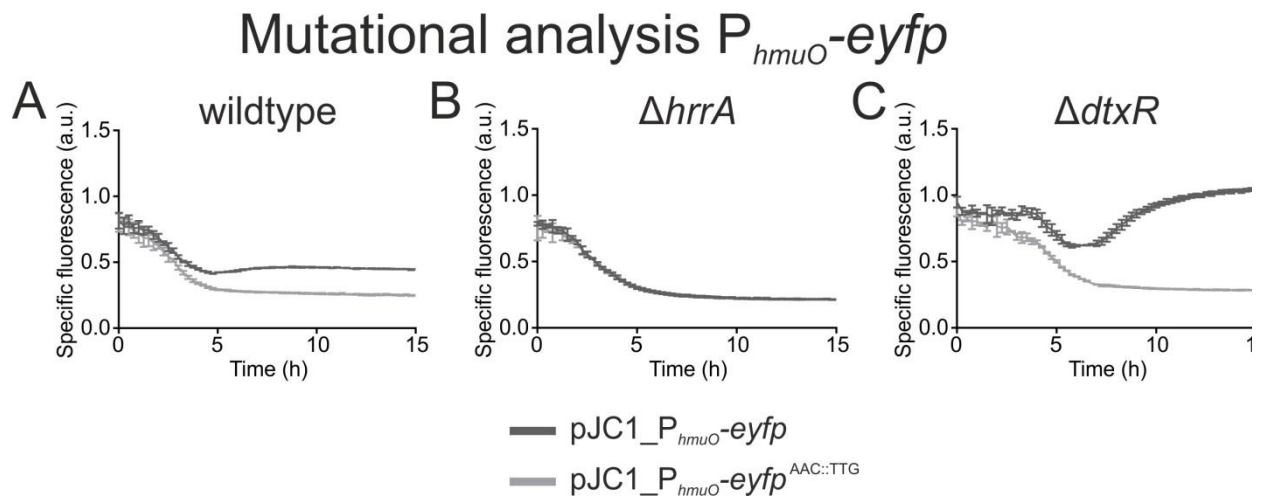


**Figure S4: Control of  $P_{hmuO}$  by HrrA and DtxR.**

HrrA binding was abolished by introducing the AAC::TTG mutation into the  $P_{hmuO}$ -*eyfp* reporter. After iron starvation overnight, the three strains (A: wildtype, B:  $\Delta hrrA$  and C:  $\Delta dtxR$ ) were inoculated in BHI complex medium supplemented with 4  $\mu$ M hemin and the specific fluorescence (eYFP-fluorescence/backscatter) was recorded in 15 minutes intervals. The strains were grown in BHI complex medium as the  $\Delta dtxR$  strain grows poorly in CGXII medium.

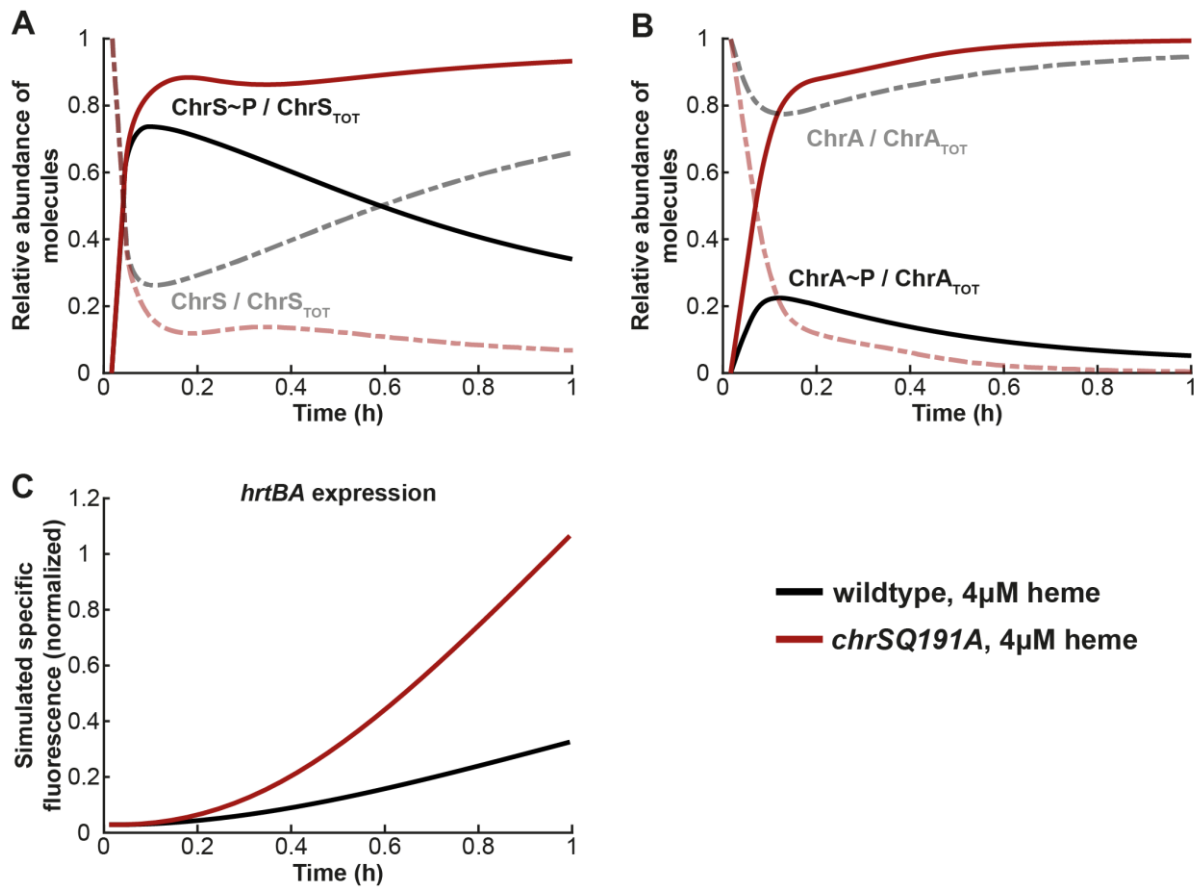


**Figure S5: Dephosphorylation of the response regulator ChrA determines the dynamics of the target gene activation in the wildtype and a *chrSQ191A* phosphatase mutant.**

The activation of the  $P_{hrtBA-eyfp}$  reporter critically hinges on the levels of phosphorylated response regulator ChrA~P in the wild type (black line) and a *chrSQ191A* phosphatase mutant (dark red line). (A) Initial high levels of external heme autophosphorylate and thereby activate the histidine kinase ChrS strongly in the wild type as well as the *chrSQ191A* phosphatase mutant, leading to a significant portion of the phosphorylated form of ChrS (ChrS~P/ChrS<sub>TOT</sub>  $\approx$  0.8, solid line). But immediately after incipient stimulus decline, the balance between ChrS~P and ChrS shifts towards the non-phosphorylated form ChrS (ChrS/ChrS<sub>TOT</sub>, dashed line) in the wild type. However, the levels of ChrS~P stay high in the *chrSQ191A* phosphatase mutant. (B) The activation of the response regulator ChrA depends

on the state of the histidine kinase ChrS. Phosphorylated and thereby activated ChrS (ChrS~P) is able to phosphorylate and activate ChrA (ChrA~P), while the non-phosphorylated form of ChrS (ChrS) naturally functions as a phosphatase for ChrA. Since the levels of non-phosphorylated ChrS are very low at the very beginning in both strains, phosphatase activity of ChrS has insignificant impact and the levels of ChrA~P are similar (ChrA~P /ChrA<sub>TOT</sub>, solid line). However, the increasing levels of ChrS after heme depletion lead to an immediate dephosphorylation of ChrA~P and in the wild type, while the ChrA~P levels stay high in the *chrSQ191A* phosphatase mutant, leading to a maximal phosphorylation level of ChrA of 25% in the wild type, compared to 100% in the phosphatase mutant. (C) As ChrA~P activates the target promoter  $P_{hrtBA}$ , the significant differences between the ChrA~P levels in the wild type and the *chrSQ191A* phosphatase mutant lead to varying reporter outputs of  $P_{hrtBA}$ -*eyfp*. While both strains show similar reporter outputs within the first minutes where ChrS~P and thereby ChrA~P levels are identical and phosphatase activity of ChrS plays no significant role, they diverge from the time point of differentiation in ChrA~P levels onwards.



### Model: *hrtBA* expression

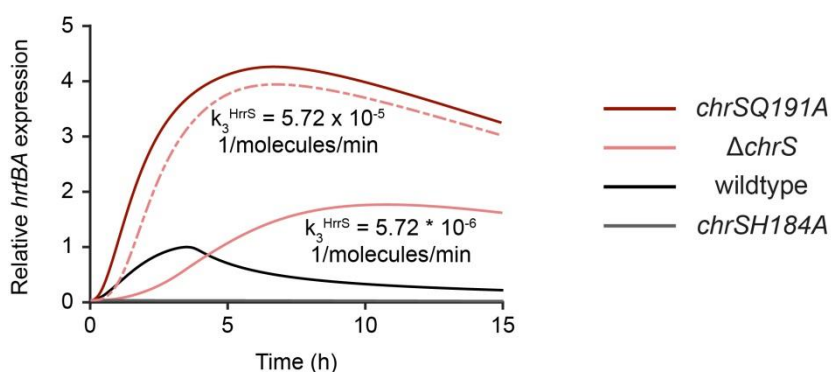


**Figure S6: The *in vitro* data suggest a cross-phosphatase activity of HrrS which did not result in a model that quantitatively fits to the behavior of the  $\Delta chrS$  mutant *in vivo* data.**

Setting  $k_3^{HrrS}$  to  $5.7 \times 10^{-5}$  1/molecules/min as expected from the *in vitro* data in (Hentschel et al., 2014) led to an excessive response of  $P_{hrtBA}$  in the  $\Delta chrS$  mutant (dashed red line). A reduced cross-phosphatase activity of HrrS by a factor of 10 reproduces the mutant behaviour quantitatively (solid red line).

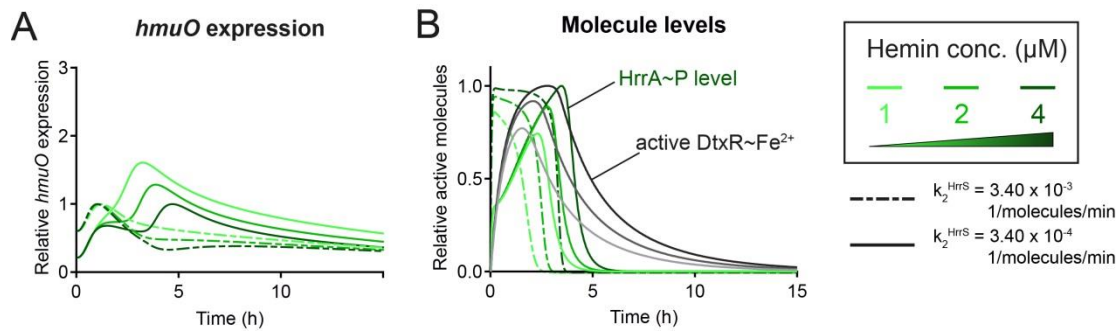


**Figure S7: An increased phosphatase activity of HrrS prevents a delayed  $P_{hmuO}$  activation by HrrA~P.**

Setting  $k_2^{HrrS}$  to  $3.40 \times 10^{-3}$  1/molecules/min as expected from the *in vitro* data in (Hentschel et al., 2014) did not result in a model that quantitatively fits to the behaviour of the *in vivo* data in wild-type. The strong phosphatase activity decreases HrrA~P levels immediately after stimulus reduction and no delayed  $P_{hmuO}$  activation is possible. Decreasing  $k_2^{HrrS}$  about a factor of 10 improved the ability to reproduce the *in vivo* behaviour.

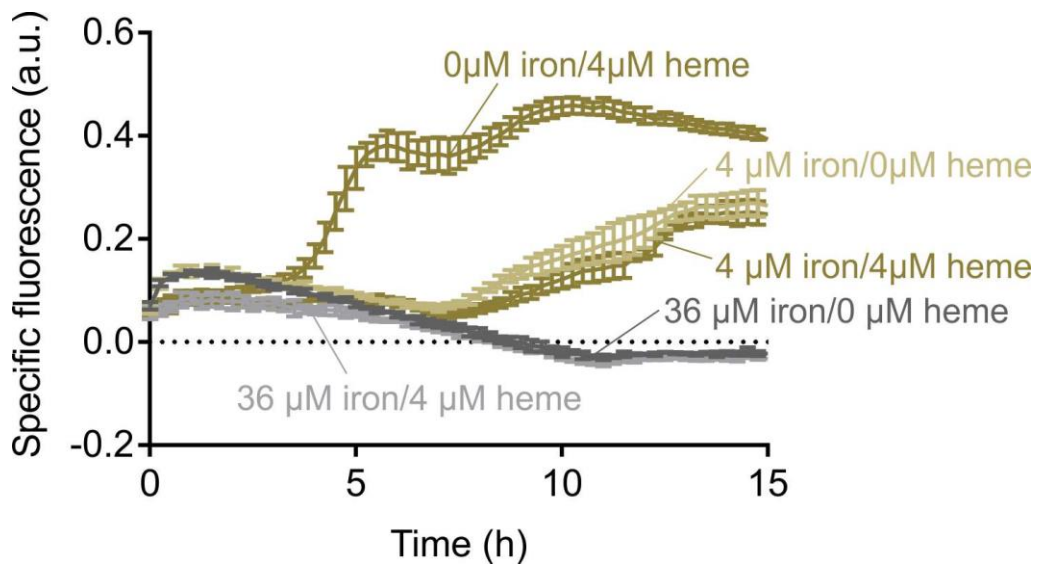


**Figure S8:  $P_{hmuO}$ -*eyfp* screening under different environmental conditions.**

*C. glutamicum* cells carrying the pJC1\_ $P_{hmuO}$ -*eyfp* reporter plasmid were iron starved overnight and inoculated in CGXII medium containing FeSO<sub>4</sub>, hemin or both as iron source in the indicated concentrations. Biomass (backscatter) and fluorescence were measured every 15 minutes and the specific fluorescence was calculated as (eYFP-fluorescence/backscatter) and normalized to an empty well.

These data demonstrate the link between the heme and iron pools in the cells. Due to the basal expression of the heme oxygenase (see Figure 1 or Figure 8, WT versus  $\Delta hrrA$ ) addition of heme will also impact the bioavailable iron pool, thereby affecting DtxR activity. According to our current model HrrA represents an essential activator of *hmuO*, which is required for a basal level of *hmuO* expression (and likely also required for the turnover of the endogenously synthesized heme). DtxR repression places an additional threshold on *hmuO* activation, which is only released when the intracellular iron pool is depleting. Then DtxR dissociates from the *hmuO* promoter allowing full activation by HrrA.

## Description of mathematical models

The heme detoxification and utilization network contains different layers of regulation that have to be considered within the mathematical model.

### Bacterial growth kinetics

Heme is used as alternative iron source for growth under iron-starvation conditions. In order to study heme depletion within the growth medium in our experiments, we described the uptake of external heme via the heme importer HmuTUV and the subsequent incorporation of the cytoplasmic heme into biomass via utilization enzymes based on Michaelis-Menten expressions. As a simplifying assumption, we expected a constant maximal velocity for the import ( $v_{max}^{IMP}$ ) as well as the heme consumption ( $v_{max}^{CON}$ ) and described the concentrations of the two extra- and intracellular heme pools ( $[H_{EX}]$  and  $[H_{IN}]$ , respectively) as follows:

$$\frac{d[H_{EX}]}{dt} = -v_{max}^{IMP} \frac{[H_{EX}]}{K_M^{IMP} + [H_{EX}]} [cells]$$
$$\frac{d[H_{IN}]}{dt} = v_{max}^{IMP} \frac{[H_{EX}]}{K_M^{IMP} + [H_{EX}]} - v_{max}^{CON} \frac{[H_{IN}]}{K_M^{CON} + [H_{IN}]} - \gamma[H_{IN}],$$

while  $K_M^{IMP}$  and  $K_M^{CON}$  represent the Michaelis constants. Thus, the bacterial growth was formulated in terms of

$$\frac{d[cells]}{dt} = \beta * \frac{[H_{IN}]}{K_M^{CON} + [H_{IN}]} * [cells]$$

with the maximal growth rate  $\beta$  that serves as an effective description of heme consumption via diverse enzymatic reactions.

Given the fact that the total content of iron in *C. glutamicum* cells is in a range of 0.3-0.5 mg<sub>FE</sub>/g<sub>CDW</sub> and 1 g<sub>CDW</sub> corresponds to approx.  $6.5 \times 10^{11}$  cells (Unthan et al., 2014), we calculate an iron demand of a single cell of  $\sim 5 \times 10^6$  Fe<sup>2+</sup> molecules per cell ( $1g_{FE} \sim 10^{22}$  molecules). Considering a generation time of  $\sim 120$  minutes in our experiments (see Fig. 2A

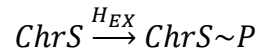
in the main text),  $\sim 4 \times 10^4$  molecules of internal heme – as alternative iron source - have to be incorporated into biomass per minute. Taking this estimation into account, our mathematical description of the bacterial growth kinetics predicted a depletion of external heme between 2.5 and 3.5 hours, dependent on the initial concentrations. The cytoplasmic pool of heme is depleted with a time delay of  $\sim 2$  hours, which then leads to cessation in cell growth (see Fig. 2B,C in the main text). Finally, the total heme pool per cell ( $[H^{cell}_{TOT}]$ , Fig. 2E), was defined as the sum of cytoplasmic heme per cell and the portion of external heme per cell

$$[H^{cell}_{TOT}] = [H_{IN}] + \frac{[H_{EX}]}{[cells]}.$$

### **Stimulus perception and signalling in the two-component systems**

The described overall flux of the stimulus heme through the network as the base for cell growth represents the first layer that was quantified within the model. In addition, the dynamics within the TCSs that sense heme as their stimulus represent a second layer of regulation within the system. According to the reporter assays, we assumed a constitutive expression and thereby production of HrrS, while the phosphorylated response regulator HrrA activates the production of HrrA and HmuO. Besides, ChrS, ChrA and HrtBA production is dependent from ChrA. We expected a production of the non-phosphorylated form exclusively, both in case of the histidine kinases as well as the response regulators. Given that no information is available about the copy number of the heme importer HmuTUV, we assumed a constant number of transporter molecules independent from time and heme levels. Both kinases, HrrS and ChrS, phosphorylate their cognate and non-cognate response regulator (Hentschel et al., 2014) in response to external heme as their stimulus (Keppel, Davoudi, Gätgens, & Frunzke, 2018). In the following, we will give the quantification of

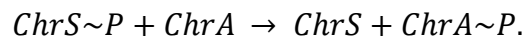
different reactions for ChrSA as an example but the description is identical for HrrSA. Following this approach of Groban and co-workers (Groban, Clarke, Salis, Miller, & Voigt, 2009), we described the transition from the non-phosphorylated form into the phosphorylated one of the histidine kinases and the response regulators but did not quantify the phosphotransfer in detail. Thus, we expected the autophosphorylation of the kinases (ChrS) in response to stimulus perception



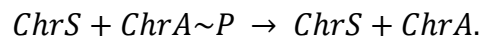
and described the reaction by

$$\frac{d[ChrS\sim P]}{dt} = I_{ChrS}(H_{EX}) [ChrS],$$

while  $I_{ChrS}(H_{EX}) = k_+^{ChrS} * \frac{[H_{EX}]}{K_{H_{EX}} + [H_{EX}]}$  describes the autophosphorylation rate, dependent on the external heme concentration. The autophosphorylation threshold is given by  $K_{H_{EX}}$ , while  $k_+^{ChrS}$  determine the speed of the autophosphorylation reaction.  $[ChrS]$  and  $[ChrS\sim P]$  describe the concentration of the phosphorylated or non-phosphorylated form of the kinase. A phosphorylated kinase (ChrS~P) can donate its phosphate to the response regulator



During the reverse process of dephosphorylation of the response regulator, the phosphate is not passed back to the kinase



The phosphorylation and dephosphorylation of ChrA was expected to follow second order kinetics, which were quantified by the rate constants  $k_i$ :

$$\frac{d[ChrA\sim P]}{dt} = k_1^{ChrS} * [ChrS\sim P] * [ChrA] - k_2^{ChrS} * [ChrS] * [ChrA\sim P]$$

The phosphotransfer from  $ChrS\sim P$  to  $ChrA$  is determined by the rate constant  $k_1^{ChrS}$ , while the reverse reaction ( $ChrS$  dephosphorylates  $ChrA\sim P$ ) occurs with a rate dependent on the

rate constant  $k_2^{ChrS}$ . Cross-phosphorylation of both kinases to their non-cognate response regulators was expected, cross-dephosphorylation could not be observed previously and was therefore not included into the model.

### Regulatory dynamics of target genes

The target gene activation of the phosphorylated response regulators represents the third layer of regulation and a mathematical description based on thermodynamic modelling quantified the observed transcriptional regulation. Following the approach of Bintu and co-workers (Bintu et al., 2005), the activation of gene expression from the  $P_{hrtBA}$  and the  $P_{chrSA}$  promoter by phosphorylated ChrA could then be formulated in terms of  $ChrA\sim P$  concentrations, such that the dynamic equation for the HrtBA protein levels,  $[HrtBA]$ , read:

$$\frac{d[HrtBA]}{dt} = \alpha * \left( \frac{1 + \omega \left( \frac{[ChrA\sim P]}{\kappa} \right)^n}{1 + \left( \frac{[ChrA\sim P]}{\kappa} \right)^n} \right) - \gamma * [HrtBA]$$

We assumed a basal protein production with an effective rate  $\alpha$  and dilution with a rate proportional to  $\gamma$  for all components within the systems according to growth. The basal production of the proteins is a combined representation of the processes of transcription and translation, justified by the fact that e.g. mRNA maturation and degradation proceed on much faster time-scales than the signalling and target gene regulation within the system and were therefore not relevant for the investigated dynamics. The ratio of maximal to basal promoter activity is defined as the fold-change  $\omega$  (Bintu et al., 2005).  $K$  in turn represents a measurement of the concentration of phosphorylated response regulator ChrA at which  $P_{hrtBA}$  is activated and the hill coefficient  $n$  reflects all forms of cooperativity in ChrA binding to the promoter. According to the fact that we based our mathematic model on the experimental data of the performed reporter assays, we discriminated within our model

between the proteins of the systems itself and the reporter output that reflects the production of detectable fluorescence proteins based on the original promoter activity. To this end, we formulated one equation for the regulated protein production and one equation for the corresponding YFP production each and integrated an effective parameter for YFP bleaching and degradation processes in the latter equation. The dynamic equations for all components can be found in M1 and M2.

### **Model parameters**

In order to calibrate the model, various parameters concerning the cell growth as well as the dynamics within the TCSs could be fixed to their physiological values based on experimental data. The remaining ones were adjusted within physiological intervals to reproduce the experimental data of promoter activity within the mathematical model (for further descriptions see Tables S4 and S5 and Fig. S5/S6).

### **Mutant simulations**

For the purpose of predicting the behaviour of several mutants within the model of the heme detoxification module, we adapted the individual parameters of the mathematic equations to the experimentally given scenarios. For the wild type, we simulated the time-dependent dynamics based on the complete set of parameters we fixed within our model. To knock out a protein in the model, we set the participating rate constants of the protein-based reactions as well as the initial concentrations to zero. In case of the  $\Delta chrS$  mutant, we set the basal concentration  $ChrS_{INI}$  as well as the rate constants for phosphorylation ( $k_1^{ChrS}$ ) and dephosphorylation ( $k_2^{ChrS}$ ) to zero. Within the phosphatase mutant  $chrSQ191A$ , the dephosphorylation step of ChrA is not possible. Thus, we exclusively chose  $k_2^{ChrS}$  to zero. In



contrast, inhibition of ChrS kinase activity (*chrSH186A*) leads to a lack in the ability of autophosphorylation of ChrS and thereby the option of phosphotransfer to the response regulator ChrA. Disrupting the autophosphorylation of ChrS could be simulated by setting  $k_+^{ChrS}$  to zero. In addition, the lack of phosphotransfer could be quantified by  $k_1^{ChrS} = 0$ .

**Model equations M1:** ODEs of the mathematical model of the *C. glutamicum* heme detoxification module

Variables within the model:

Name	Description
$H_{EX}$	External heme
$H_{IN}$	Internal heme
$cells$	Cells of <i>C. glutamicum</i>
$ChrS$	Unphosphorylated histidine kinase ChrS
$ChrS\sim P$	Autophosphorylated histidine kinase ChrS
$HrrS$	Unphosphorylated histidine kinase HrrS
$HrrS\sim P$	Autophosphorylated histidine kinase HrrS
$ChrA$	Unphosphorylated response regulator ChrA
$ChrA\sim P$	Phosphorylated response regulator ChrA
$HrtBA$	Heme exporter HrtBA
$ChrS_{TOT}\text{-YFP}$	YFP proteins corresponding to the total amount of the kinase ChrS (The production is under the control of $P_{chrSA}$ promoter)
$ChrA_{TOT}\text{-YFP}$	YFP proteins corresponding to the total amount of the response regulator ChrA (The production is under the control of $P_{chrSA}$ promoter)
$HrtBA\text{-YFP}$	YFP proteins corresponding to the total amount of the heme exporter HrtBA (The production is under the control of $P_{hrtBA}$ promoter)

ODEs:

$$\frac{d[H_{EX}]}{dt} = -v_{max}^{IMP} \frac{[H_{EX}]}{K_M^{IMP} + [H_{EX}]} [cells] + k_{cat}^{HrtBA} [HrtBA] \frac{[H_{IN}]}{K_M^{HrtBA} + [H_{IN}]} [cells] \quad (1)$$

$$\frac{d[H_{IN}]}{dt} = v_{max}^{IMP} \frac{[H_{EX}]}{K_M^{IMP} + [H_{EX}]} - v_{max}^{CON} \frac{[H_{IN}]}{K_M^{CON} + [H_{IN}]} - k_{cat}^{HrtBA} [HrtBA] \frac{[H_{IN}]}{K_M^{HrtBA} + [H_{IN}]} - \gamma [H_{IN}] \quad (2)$$

$$\frac{d[cells]}{dt} = \beta \frac{[H_{IN}]}{K_M^{CON} + [H_{IN}]} [cells] \quad (3)$$

$$\frac{d[ChrS]}{dt} = \gamma [ChrS_{INI}] \left( \frac{1 + \omega_{P_{chrSA}^{ChrA}} \left( \frac{[ChrA - P]}{\kappa_{P_{chrSA}^{ChrA}}} \right)^{n_{P_{chrSA}^{ChrA}}}}{1 + \left( \frac{[ChrA - P]}{\kappa_{P_{chrSA}^{ChrA}}} \right)^{n_{P_{chrSA}^{ChrA}}}} \right) - k_+^{ChrS} [ChrS] \frac{[H_{EX}]}{K_{H_{EX}} + [H_{EX}]} + k_1^{ChrS} [ChrS\sim P] [ChrA] - \gamma [ChrS] \quad (4)$$

$$\frac{d[ChrS\sim P]}{dt} = k_+^{ChrS} [ChrS] \frac{[H_{EX}]}{K_{H_{EX}} + [H_{EX}]} - k_1^{ChrS} [ChrS\sim P] [ChrA] - \gamma [ChrS\sim P] \quad (5)$$

$$\frac{d[HrrS]}{dt} = \gamma [HrrS_{TOT}] - k_+^{HrrS} [HrrS] \frac{[H_{EX}]}{K_{H_{EX}} + [H_{EX}]} + k_3^{HrrS} [HrrS\sim P] [ChrA] - \gamma [HrrS] \quad (6)$$

$$\frac{d[HrrS\sim P]}{dt} = k_+^{HrrS} [HrrS] \frac{[H_{EX}]}{K_{H_{EX}} + [H_{EX}]} - k_3^{HrrS} [HrrS\sim P] [ChrA] - \gamma [HrrS\sim P] \quad (7)$$

$$\begin{aligned} \frac{d[ChrA]}{dt} = & \gamma[ChrA_{INI}] \left( \frac{1 + \omega_{P_{chrSA}^{ChrA}} \left( \frac{[ChrA - P]}{\kappa_{P_{chrSA}^{ChrA}}} \right)^{n_{P_{chrSA}^{ChrA}}}}{1 + \left( \frac{[ChrA - P]}{\kappa_{P_{chrSA}^{ChrA}}} \right)^{n_{P_{chrSA}^{ChrA}}}} \right) - k_1^{ChrS}[ChrS \sim P][ChrA] + k_2^{ChrS}[ChrS][ChrA \sim P] \\ & - k_3^{HrrS}[HrrS \sim P][ChrA] - \gamma[ChrA] \end{aligned} \quad (8)$$

$$\frac{d[ChrA \sim P]}{dt} = k_1^{ChrS}[ChrS \sim P][ChrA] - k_2^{ChrS}[ChrS][ChrA \sim P] + k_3^{HrrS}[HrrS \sim P][ChrA] - \gamma[ChrA \sim P] \quad (9)$$

$$\frac{d[HrtBA]}{dt} = \gamma[HrtBA_{INI}] \left( \frac{1 + \omega_{P_{hrtBA}^{ChrA}} \left( \frac{[ChrA - P]}{\kappa_{P_{hrtBA}^{ChrA}}} \right)^{n_{P_{hrtBA}^{ChrA}}}}{1 + \left( \frac{[ChrA - P]}{\kappa_{P_{hrtBA}^{ChrA}}} \right)^{n_{P_{hrtBA}^{ChrA}}}} \right) - \gamma[HrtBA] \quad (10)$$

$$\frac{d[ChrS_{TOT} - YFP]}{dt} = \gamma[ChrS_{INI}] \left( \frac{1 + \omega_{P_{chrSA}^{ChrA}} \left( \frac{[ChrA - P]}{\kappa_{P_{chrSA}^{ChrA}}} \right)^{n_{P_{chrSA}^{ChrA}}}}{1 + \left( \frac{[ChrA - P]}{\kappa_{P_{chrSA}^{ChrA}}} \right)^{n_{P_{chrSA}^{ChrA}}}} \right) - (\gamma + k_{bl})[ChrS_{TOT} - YFP] \quad (11)$$

$$\frac{d[ChrA_{TOT} - YFP]}{dt} = \gamma[ChrA_{INI}] \left( \frac{1 + \omega_{P_{chrSA}^{ChrA}} \left( \frac{[ChrA - P]}{\kappa_{P_{chrSA}^{ChrA}}} \right)^{n_{P_{chrSA}^{ChrA}}}}{1 + \left( \frac{[ChrA - P]}{\kappa_{P_{chrSA}^{ChrA}}} \right)^{n_{P_{chrSA}^{ChrA}}}} \right) - (\gamma + k_{bl})[ChrA_{TOT} - YFP] \quad (12)$$

$$\frac{d[HrtBA - YFP]}{dt} = \gamma[HrtBA_{INI}] \left( \frac{1 + \omega_{P_{hrtBA}^{ChrA}} \left( \frac{[ChrA - P]}{\kappa_{P_{hrtBA}^{ChrA}}} \right)^{n_{P_{hrtBA}^{ChrA}}}}{1 + \left( \frac{[ChrA - P]}{\kappa_{P_{hrtBA}^{ChrA}}} \right)^{n_{P_{hrtBA}^{ChrA}}}} \right) - (\gamma + k_{bl})[HrtBA - YFP] \quad (13)$$

**Model equations M2:** ODEs of the mathematical model of the *C. glutamicum* heme utilization module

Variables within the model:

Name	Description
$H_{EX}$	External heme
$H_{IN}$	Internal heme
$cells$	Cells of <i>C. glutamicum</i>
$ChrS$	Unphosphorylated histidine kinase ChrS
$ChrS\sim P$	Autophosphorylated histidine kinase ChrS
$HrrS$	Unphosphorylated histidine kinase HrrS
$HrrS\sim P$	Autophosphorylated histidine kinase HrrS
$HrrA$	Unphosphorylated response regulator HrrA
$HrrA\sim P$	Phosphorylated response regulator HrrA
$HmuO$	Heme oxygenase HmuO
$DtxR^*$	Activated form of the iron repressor DtxR
$DtxR$	Non-activated form of the iron repressor DtxR
$HrrA_{TOT}\text{-YFP}$	YFP proteins corresponding to the total amount of the response regulator HrrA (The production is under the control of $P_{hrrA}$ promoter)
$HmuO\text{-YFP}$	YFP proteins corresponding to the total amount of heme oxygenase HmuO (The production is under the control of $P_{hmuO}$ promoter)

ODEs:

$$\frac{d[H_{EX}]}{dt} = -v_{max}^{IMP} \frac{[H_{EX}]}{K_M^{IMP} + [H_{EX}]} [cells] \quad (14)$$

$$\frac{d[H_{IN}]}{dt} = v_{max}^{IMP} \frac{[H_{EX}]}{K_M^{IMP} + [H_{EX}]} - k_{cat}^{CON} ([E^{CON}] + [HmuO]) \frac{[H_{IN}]}{K_M^{CON} + [H_{IN}]} - \gamma[H_{IN}] \quad (15)$$

$$\frac{d[cells]}{dt} = \beta' k_{cat}^{CON} ([E^{CON}] + [HmuO]) \frac{[H_{IN}]}{K_M^{CON} + [H_{IN}]} [cells] \quad (16)$$

$$\frac{d[ChrS]}{dt} = \gamma[ChrS_{TOT}] - k_+^{ChrS} [ChrS] \frac{[H_{EX}]}{K_{H_{EX}} + [H_{EX}]} + k_3^{ChrS} [ChrS\sim P][HrrA] - \gamma[ChrS] \quad (17)$$

$$\frac{d[ChrS\sim P]}{dt} = k_+^{ChrS} [ChrS] \frac{[H_{EX}]}{K_{H_{EX}} + [H_{EX}]} - k_3^{ChrS} [ChrS\sim P][HrrA] - \gamma[ChrS\sim P] \quad (18)$$

$$\frac{d[HrrS]}{dt} = \gamma[HrrS_{TOT}] - k_+^{HrrS} [HrrS] \frac{[H_{EX}]}{K_{H_{EX}} + [H_{EX}]} + k_1^{HrrS} [HrrS\sim P][HrrA] - \gamma[HrrS] \quad (19)$$

$$\frac{d[HrrS\sim P]}{dt} = k_+^{HrrS} [HrrS] \frac{[H_{EX}]}{K_{H_{EX}} + [H_{EX}]} - k_1^{HrrS} [HrrS\sim P][HrrA] - \gamma[HrrS\sim P] \quad (20)$$

$$\frac{d[HrrA]}{dt} = \gamma[HrrA_{INI}] \left( \frac{1 + \omega_{P_{hrrA}^{HrrA}} \left( \frac{[HrrA - P]}{\kappa_{P_{hrrA}^{HrrA}}} \right)^{n_{P_{hrrA}^{HrrA}}}}{1 + \left( \frac{[HrrA - P]}{\kappa_{P_{hrrA}^{HrrA}}} \right)^{n_{P_{hrrA}^{HrrA}}} + \left( \frac{DtxR_{TOT} [H_{IN}]}{\kappa_{P_{hrrA}^{DtxR}}} \right)^{n_{P_{hrrA}^{DtxR}}}} \right) \quad (21)$$

$$-k_1^{HrrS}[HrrS \sim P][HrrA] + k_2^{HrrS}[HrrS][HrrA \sim P] - k_3^{ChrS}[ChrS \sim P][HrrA] - \gamma[HrrA]$$

$$\frac{d[HrrA \sim P]}{dt} = k_1^{HrrS}[HrrS \sim P][HrrA] - k_2^{HrrS}[HrrS][HrrA \sim P] + k_3^{ChrS}[ChrS \sim P][HrrA] - \gamma[HrrA \sim P] \quad (22)$$

$$\frac{d[HmuO]}{dt} = \gamma[HmuO_{INI}] \left( \frac{1 + \omega_{P_{hmuO}^{HrrA}} \left( \frac{[HrrA - P]}{\kappa_{P_{hmuO}^{HrrA}}} \right)^{n_{P_{hmuO}^{HrrA}}}}{1 + \left( \frac{[HrrA - P]}{\kappa_{P_{hmuO}^{HrrA}}} \right)^{n_{P_{hmuO}^{HrrA}}} + \left( \frac{DtxR_{TOT} [H_{IN}]}{\kappa_{P_{hmuO}^{DtxR}}} \right)^{n_{P_{hmuO}^{DtxR}}}} \right) - \gamma[HmuO] \quad (23)$$

$$\frac{d[HrrA_{TOT} - YFP]}{dt} = \gamma[HrrA_{INI}] \left( \frac{1 + \omega_{P_{hrrA}^{HrrA}} \left( \frac{[HrrA - P]}{\kappa_{P_{hrrA}^{HrrA}}} \right)^{n_{P_{hrrA}^{HrrA}}}}{1 + \left( \frac{[HrrA - P]}{\kappa_{P_{hrrA}^{HrrA}}} \right)^{n_{P_{hrrA}^{HrrA}}} + \left( \frac{DtxR_{TOT} [H_{IN}]}{\kappa_{P_{hrrA}^{DtxR}}} \right)^{n_{P_{hrrA}^{DtxR}}}} \right) \quad (24)$$

$$-(\gamma + k_{bl})[HrrA_{TOT} - YFP]$$

$$\frac{d[HmuO - YFP]}{dt} = \gamma[HmuO_{INI}] \left( \frac{1 + \omega_{P_{hmuO}^{HrrA}} \left( \frac{[HrrA - P]}{\kappa_{P_{hmuO}^{HrrA}}} \right)^{n_{P_{hmuO}^{HrrA}}}}{1 + \left( \frac{[HrrA - P]}{\kappa_{P_{hmuO}^{HrrA}}} \right)^{n_{P_{hmuO}^{HrrA}}} + \left( \frac{DtxR_{TOT} [H_{IN}]}{\kappa_{P_{hmuO}^{DtxR}}} \right)^{n_{P_{hmuO}^{DtxR}}}} \right) \quad (25)$$

$$-(\gamma + k_{bl})[HmuO - YFP]$$

DtxR activation:

$$DtxR_{TOT} = DtxR + DtxR^* \quad (26)$$

$$DtxR^* = DtxR_{TOT} \frac{[H_{IN}]}{K_{H_{IN}} + [H_{IN}]} \quad (27)$$

$$DtxR = DtxR_{TOT} \left( 1 - \frac{[H_{IN}]}{K_{H_{IN}} + [H_{IN}]} \right) \quad (28)$$

**Supplementary Table S1.** Bacterial strains used in this study.

Strain or plasmid	Relevant characteristics	Source reference	or
<b><i>Escherichia coli</i></b>			
DH5 $\alpha$	<i>fhuA2 lac(del)U169 phoA glnV44 <math>\Phi</math>80' lacZ(del)M15 gyrA96 recA1 relA1 endA1 thi-1 hsdR17</i> ; for general cloning purposes	Invitrogen	
BL21(DE3)	B F <sup>-</sup> <i>ompT gal dcm lon hsdS<sub>B</sub>(r<sub>B</sub><sup>-</sup>m<sub>B</sub><sup>-</sup>) <math>\lambda</math>(DE3 [<i>lacI lacUV5-T7p07 ind1 sam7 nin5</i>]) [<i>malB</i><sup>+</sup>]<sub>K-12</sub>(<math>\lambda</math><sup>S</sup>); overexpression of proteins.</i>	(Studier & Moffatt, 1986)	
<b><i>Corynebacterium glutamicum</i></b>			
ATCC 13032	<i>C. glutamicum</i> wild type strain	(Kinoshita, Udaka, & Shimono, 2004)	
ATCC 13032 $\Delta$ <i>hrrS</i>	Deletion mutant of the open reading frame (orf) encoding the HK HrrS	(Hentschel et al., 2014)	
ATCC 13032 <i>hrrSQ222A</i>	Phosphatase=OFF mutant of <i>hrrS</i>	(Hentschel et al., 2014)	
ATCC 13032 $\Delta$ <i>chrS</i>	Deletion mutant of the orf encoding the HK ChrS	(Hentschel et al., 2014)	
ATCC 13032 <i>chrSQ191A</i>	Phosphatase=OFF mutant of <i>hrrS</i>	(Hentschel et al., 2014)	
ATCC 13032 <i>chrSH186A</i>	Kinase=OFF mutant of <i>chrS</i>	This study	
ATCC 13032 $\Delta$ <i>dtxR</i>	Deletion mutant of the orf encoding DtxR	(Wennerhold & Bott, 2006)	
ATCC 13032 $\Delta$ <i>hrrA</i>	Deletion mutant of the orf encoding the RR HrrA	(Frunzke, Gatgens, Brocker, & Bott, 2011)	

**Supplementary Table S2.** Oligonucleotides used in this study. Restriction sites mutations are underlined.

#	Name	Sequence	Special feature
1	<i>chrS-fw</i>	GCGCA <u>AAGCTT</u> GTGAAAAGTAGCCAAGCGAC	<i>Hind</i> III RS
2	<i>chrS-rv</i>	TATAC <u>CCGGG</u> GTCACTTATCTTGGTCCTTTTG	<i>Sma</i> I RS
3	<i>chrSH186A</i>	CCACAGTGTCA <u>AGCT</u> ATTTTCGCCGCTATGCGGGC	Mutation H186A
4	<i>chrSH186A</i>	GCCCGCATAGCGGGCGAAATAG <u>CTG</u> ACTGTGG	Mutation H186A
5	<i>P<sub>hmuO</sub></i> <sup>AAC::TTG</sup>	CACACCTACATATAGTCCCTTACA <u>AGGA</u> ACAATTTCCGCAACTTTGG	Mutation <i>P<sub>hmuO</sub></i>
6	<i>P<sub>hmuO</sub></i> <sup>AAC::TTG</sup>	CCAAAGTTGCGGAAAATTGTCC <u>TTG</u> TAAGGGACTATATGTAGGTGTG	Mutation <i>P<sub>hmuO</sub></i>

**Supplementary Table S3.** Plasmids used in this study. If plasmids were constructed in this study, primers used are indicated in Table S2.

Reporter plasmids				
#	Name	Resistance	Source	Primer used
1	pJC1_PhrtBA-eyfp	Kanamycin	(Heyer et al., 2012)	
2	pJC1_PhmuO-eyfp	Kanamycin	(Heyer et al., 2012)	
3	pJC1_PhmuO-eyfp <sup>AAC::TTG</sup>	Kanamycin	This study	#5, #6
Plasmids for genomic intergrations				
4	pK19_ΔchrS <sup>wt</sup> ::chrSH184A	Kanamycin	This study	Cloning: #1, #2 Mut.: #3, #4

**Supplementary Table S4.** Parameters used in the mathematical model of the *C. glutamicum* heme detoxification module.

Parameter	Notation	Value	Source
Maximal velocity of heme import via heme transporter HmuTUV	$v_{max}^{IMP}$	$9.83 \times 10^3 \text{ molecules/min/cell}$	Adjusted to match the average growth curve (Fig. 2)
Michaelis-Menten constant for heme import via heme transporter HmuTUV	$K_M^{IMP}$	$1.19 \times 10^{13} \text{ molecules}$	
Maximal velocity of heme consumption via diverse enzymes	$v_{max}^{CON}$	$7.86 \times 10^3 \text{ molecules/min/cell}$	
Michaelis-Menten constant for heme consumption via diverse enzymes	$K_M^{CON}$	$1.84 \times 10^6 \text{ molecules/cell}$	
Growth parameter	$\beta$	$0.04 \text{ 1/min}$	
Initial OD	$OD_{INI}$	$2.2 \sim 6.6 \times 10^7 \text{ cells}$	
Autophosphorylation threshold of ChrS/HrrS	$K_{H_{EX}}$	$1.2 \times 10^{13} \text{ molecules}$	Adjusted to guarantee approximately maximal autophosphorylation rate even for the lowest hemin concentration
Autophosphorylation rate of ChrS	$k_+^{ChrS}$	$1 \text{ 1/min}$	Adjusted to match a rate of autophosphorylation as expected in (Groban et al., 2009), taking the ChrS/HrrS levels into account.
Autophosphorylation rate of HrrS	$k_+^{HrrS}$	$1 \text{ 1/min}$	
Effective rate constants of phosphorylation reaction of the cognate kinase ChrS on ChrA	$k_1^{ChrS}$	$3.98 \times 10^{-3} \text{ 1/molecules/min}$	Correspond to the <i>in vitro</i> data in (Hentschel et al., 2014), multiplied by a factor of 10 due to the observation of (Gao & Stock, 2017; Kremling, Kremling, & Bettenbrock, 2009), that <i>in vitro</i> rates are often about $10^1$ - $10^2$ -fold lower than the actual <i>in vivo</i> ones.
Effective rate constants of dephosphorylation reaction of the cognate kinase ChrS on ChrA	$k_2^{ChrS}$	$3.76 \times 10^{-2} \text{ 1/molecules/min}$	
Effective rate constants of phosphorylation reaction of the non-cognate kinase HrrS on ChrA	$k_3^{HrrS}$	$5.72 \times 10^{-6} \text{ 1/molecules/min}$	Correspond to the <i>in vitro</i> data in (Hentschel et al., 2014), decreased by a factor of 10, suggested by Fig.S5.
Initial ChrS concentration	$ChrS_{INI}$	$100 \text{ molecules/cell}$	Correspond to reference values for total numbers in <i>E. coli</i> for several two-component systems (Cai & Inouye, 2002; Gao & Stock, 2013; Li, Burkhardt, Gross, & Weissman,
Initial ChrA concentration	$ChrA_{INI}$	$100 \text{ molecules/cell}$	
Total HrrS concentration	$HrrS_{TOT}$	$100 \text{ molecules/cell}$	

			2014): Numbers of histidine kinases are within a physiological range of $10^1$ - $10^3$ and response regulators range between $10^2$ and $10^4$ . A 1:1 stoichiometry is assumed for ChrS and ChrA due to the fact that they are within one operon.
Initial HrtBA concentration	$HrtBA_{INI}$	10 molecules/cell	Arbitrary choice
Turnover rate of heme exporter HrtBA	$k_{cat}^{HrtBA}$	20 molecules/min/transporter	Adjusted to counteract the import rate under maximal <i>hrtBA</i> expression
Michaelis-Menten constant for heme export via HrtBA	$K_M^{HrtBA}$	$8 \times 10^5$ molecules/cell	
Fold-change of $P_{chrSA}$ promoter	$\omega_{P_{chrSA}}^{ChrA}$	70	Suggested by wildtype data in Fig. S1a; within physiological range of $1$ - $10^4$ (see e.g. (Lutz & Bujard, 1997)) for promoters with high dynamic range)
Fold-change of $P_{hrtBA}$ promoter	$\omega_{P_{hrtBA}}^{ChrA}$	150	
$P_{chrSA}$ activation threshold	$\kappa_{P_{chrSA}}^{ChrA}$	75 molecules/cell	Correspond to the total levels of ChrA~P
$P_{hrtBA}$ activation threshold	$\kappa_{P_{hrtBA}}^{ChrA}$	75 molecules/cell	
Hill coefficient $P_{chrSA}$	$n_{P_{chrSA}}^{ChrA}$	1	Assuming no cooperativity in promoter binding
Hill coefficient $P_{hrtBA}$	$n_{P_{hrtBA}}^{ChrA}$	1	
Effective rate constant of YFP bleaching and protein degradation	$k_{bl}$	0.001 1/min	Arbitrary choice

**Supplementary Table S5.** Additional parameters used in the mathematical model of the *C. glutamicum* heme utilization module (all other parameters are taken from the model of *C. glutamicum* heme detoxification module, cf. Supplementary Table S4).

Parameter	Notation	Value	Source
Growth parameter	$\beta'$	$5 \times 10^{-6}$ 1/molecules	Adjusted to match the growth rate we observed in the model of <i>C. glutamicum</i> heme detoxification module
Effective rate constants of phosphorylation reaction of the cognate kinase HrrS on HrrA	$k_1^{HrrS}$	$3.76 \times 10^{-3}$ 1/molecules/min	Correspond to the <i>in vitro</i> data in (Hentschel et al., 2014), multiplied by a factor of 10 due to the observation of (Gao & Stock, 2017; Kremling et al., 2009), that <i>in vitro</i> rates are often about $10^1$ - $10^2$ -fold lower than the actual <i>in vivo</i> ones.
Effective rate constants of dephosphorylation reaction of the cognate kinase HrrS on HrrA	$k_2^{HrrS}$	$3.40 \times 10^{-4}$ 1/molecules/min	Correspond to the <i>in vitro</i> data in (Hentschel et al., 2014), decreased by a factor of 10, suggested by Fig. S5.
Effective rate constants of phosphorylation reaction of the non-cognate kinase ChrS on HrrA	$k_3^{ChrS}$	$1.40 \times 10^{-3}$ 1/molecules/min	Correspond to the <i>in vitro</i> data in (Hentschel et al., 2014), multiplied by a factor of 10 due to the observation of (Gao & Stock, 2017; Kremling et al., 2009), that <i>in vitro</i> rates are often about $10^1$ - $10^2$ -fold lower than the actual <i>in vivo</i> ones.



Total HrrS concentration	$HrrS_{TOT}$	100 molecules/cell	Reference values for total numbers in <i>E. coli</i> for several TCS: Numbers of histidine kinases are within a physiological range of $10^1$ - $10^3$ and response regulators range between $10^2$ and $10^4$ (Cai & Inouye, 2002; Gao & Stock, 2013; Li et al., 2014).
Initial HrrA concentration	$HrrA_{INI}$	100 molecules/cell	
Total ChrS concentration	$ChrS_{TOT}$	100 molecules/cell	
Initial HmuO concentration	$HmuO_{INI}$	100 molecules/cell	Arbitrary choice
Turnover rate of heme consumption via HmuO and diverse other enzymes	$k_{cat}^{CON}$	6.04 molecules/min/transporter	Adjusted to match the maximal velocity ( $v_{max}^{CON}$ ) and total reaction rate of consumption we observed in the model of <i>C. glutamicum</i> heme detoxification module
Concentration of other enzymes responsible for heme consumption next to HmuO	$E^{CON}$	1000 molecules//cell	
Michaelis-Menten constant for heme consumption via HmuO and diverse other enzymes	$K_M^{CON}$	$1.84 \times 10^6$ molecules/cell	
Total DtxR concentration	$DtxR_{TOT}$	1000 molecules/cell	Arbitrary choice
Activation threshold of DtxR	$K_{HIN}$	$8 \times 10^5$ molecules/cell	Adjusted to guarantee a sufficient activation of iron repressor DtxR for the highest hemin concentration.
Fold-change of $P_{hrrA}$ promoter	$\omega_{P_{hrrA}}^{HrrA}$	5	Suggested by wildtype data in Fig. S1a; within physiological range of $1$ - $10^4$ (see e.g. (Lutz & Bujard, 1997) for promoters with high dynamic range)
Fold-change of $P_{hmuO}$ promoter	$\omega_{P_{hmuO}}^{HrrA}$	50	
$P_{hrrA}$ activation threshold	$\kappa_{P_{hrrA}}^{HrrA}$	100 molecules/cell	Correspond to the total levels of ChrA~P and activated DtxR. Experimental Data suggest a significant higher activation via HrrA than the repression via DtxR on $P_{hrrA}$
$P_{hmuO}$ activation threshold	$\kappa_{P_{hmuO}}^{HrrA}$	300 molecules/cell	
$P_{hmuO}$ threshold of DtxR repression	$\kappa_{P_{hmuO}}^{DtxR}$	300 molecules/cell	
$P_{hrrA}$ threshold of DtxR repression	$\kappa_{P_{hrrA}}^{DtxR}$	500 molecules/cell	
Hill coefficient of HrrA binding to $P_{hrrA}$	$n_{P_{hrrA}}^{HrrA}$	1	Assuming no cooperativity in promoter binding on $P_{hrrA}$
Hill coefficient of HrrA binding to $P_{hmuO}$	$n_{P_{hmuO}}^{HrrA}$	1	
Hill coefficient of DtxR binding to $P_{hmuO}$	$n_{P_{hmuO}}^{DtxR}$	7	Adjusted to have a strong repressive effect on $P_{hmuO}/P_{hrrA}$
Hill coefficient of DtxR binding to $P_{hrrA}$	$n_{P_{hrrA}}^{DtxR}$	7	

**Supplementary Table S6.** Transformation of the units within the mathematical models

Experimental unit	Unit within the mathematical models	Source
OD = 1	$\sim 3 \times 10^8$ cells/mL	(Unthan et al., 2015)
Heme [ $\mu M$ ] in the growth medium	$\sim 6 \times 10^{13}$ molecules heme in the growth medium	Assuming a reaction volume of $\sim 100 \mu L$
Free heme [ $\mu M$ ] in the cell	$\sim 1000$ heme molecules/cell	Corresponds to a cell size of $\sim 1 \mu m^3$ [REF]

## Supporting References

- Bintu, L., Buchler, N. E., Garcia, H. G., Gerland, U., Hwa, T., Kondev, J., & Phillips, R. (2005). Transcriptional regulation by the numbers: models. *Curr Opin Genet Dev*, *15*(2), 116-124. doi: 10.1016/j.gde.2005.02.007
- Cai, S. J., & Inouye, M. (2002). EnvZ-OmpR interaction and osmoregulation in *Escherichia coli*. *J Biol Chem*, *277*(27), 24155-24161. doi: 10.1074/jbc.M110715200
- Frunzke, J., Gatgens, C., Brocker, M., & Bott, M. (2011). Control of heme homeostasis in *Corynebacterium glutamicum* by the two-component system HrrSA. *J Bacteriol*, *193*(5), 1212-1221. doi: 10.1128/jb.01130-10
- Gao, R., & Stock, A. M. (2013). Evolutionary tuning of protein expression levels of a positively autoregulated two-component system. *PLoS Genet*, *9*(10), e1003927. doi: 10.1371/journal.pgen.1003927
- Gao, R., & Stock, A. M. (2017). Quantitative Kinetic Analyses of Shutting Off a Two-Component System. *MBio*, *8*(3). doi: 10.1128/mBio.00412-17
- Groban, E. S., Clarke, E. J., Salis, H. M., Miller, S. M., & Voigt, C. A. (2009). Kinetic buffering of cross talk between bacterial two-component sensors. *J Mol Biol*, *390*(3), 380-393. doi: 10.1016/j.jmb.2009.05.007
- Hentschel, E., Mack, C., Gatgens, C., Bott, M., Brocker, M., & Frunzke, J. (2014). Phosphatase activity of the histidine kinases ensures pathway specificity of the ChrSA and HrrSA two-component systems in *Corynebacterium glutamicum*. *Mol Microbiol*, *92*(6), 1326-1342. doi: 10.1111/mmi.12633
- Heyer, A., Gatgens, C., Hentschel, E., Kalinowski, J., Bott, M., & Frunzke, J. (2012). The two-component system ChrSA is crucial for haem tolerance and interferes with HrrSA in haem-dependent gene regulation in *Corynebacterium glutamicum*. *Microbiology*, *158*(Pt 12), 3020-3031. doi: 10.1099/mic.0.062638-0
- Keppel, M., Davoudi, E., Gätgens, C., & Frunzke, J. (2018). Membrane Topology and Heme Binding of the Histidine Kinases HrrS and ChrS in *Corynebacterium glutamicum*. *Front Microbiol*, *9*(183). doi: 10.3389/fmicb.2018.00183
- Kinoshita, S., Udaka, S., & Shimono, M. (2004). Studies on the amino acid fermentation. Part 1. Production of L-glutamic acid by various microorganisms. *J Gen Appl Microbiol*, *50*(6), 331-343.
- Kremling, A., Kremling, S., & Bettenbrock, K. (2009). Catabolite repression in *Escherichia coli*- a comparison of modelling approaches. *FEBS J*, *276*(2), 594-602. doi: 10.1111/j.1742-4658.2008.06810.x
- Li, G. W., Burkhardt, D., Gross, C., & Weissman, J. S. (2014). Quantifying absolute protein synthesis rates reveals principles underlying allocation of cellular resources. *Cell*, *157*(3), 624-635. doi: 10.1016/j.cell.2014.02.033
- Lutz, R., & Bujard, H. (1997). Independent and tight regulation of transcriptional units in *Escherichia coli* via the LacR/O, the TetR/O and AraC/I1-I2 regulatory elements. *Nucleic Acids Res*, *25*(6), 1203-1210.
- Studier, F. W., & Moffatt, B. A. (1986). Use of bacteriophage T7 RNA polymerase to direct selective high-level expression of cloned genes. *J Mol Biol*, *189*(1), 113-130.
- Unthan, S., Baumgart, M., Radek, A., Herbst, M., Siebert, D., Bruhl, N., . . . Noack, S. (2015). Chassis organism from *Corynebacterium glutamicum*--a top-down approach to identify and delete irrelevant gene clusters. *Biotechnol J*, *10*(2), 290-301. doi: 10.1002/biot.201400041
- Wennerhold, J., & Bott, M. (2006). The DtxR regulon of *Corynebacterium glutamicum*. *J Bacteriol*, *188*(8), 2907-2918. doi: 10.1128/jb.188.8.2907-2918.2006

**A.2 Minimal exposure of lipid II cycle intermediates triggers cell wall antibiotic resistance.**

ARTICLE

<https://doi.org/10.1038/s41467-019-10673-4>

OPEN

# Minimal exposure of lipid II cycle intermediates triggers cell wall antibiotic resistance

Hannah Piepenbreier<sup>1</sup>, Angelika Diehl<sup>1</sup> & Georg Fritz <sup>1</sup>

Cell wall antibiotics are crucial for combatting the emerging wave of resistant bacteria. Yet, our understanding of antibiotic action is limited, as many strains devoid of all resistance determinants display far higher antibiotic tolerance in vivo than suggested by the antibiotic-target binding affinity in vitro. To resolve this conflict, here we develop a comprehensive theory for the bacterial cell wall biosynthetic pathway and study its perturbation by antibiotics. We find that the closed-loop architecture of the lipid II cycle of wall biosynthesis features a highly asymmetric distribution of pathway intermediates, and show that antibiotic tolerance scales inversely with the abundance of the targeted pathway intermediate. We formalize this principle of minimal target exposure as intrinsic resistance mechanism and predict how cooperative drug-target interactions can mitigate resistance. The theory accurately predicts the in vivo efficacy for various cell wall antibiotics in different Gram-positive bacteria and contributes to a systems-level understanding of antibiotic action.

<sup>1</sup>LOEWE Center for Synthetic Microbiology, Philipps-Universität Marburg, Hans-Meerwein-Strasse 6, 35032 Marburg, Germany. Correspondence and requests for materials should be addressed to G.F. (email: [georg.fritz@synmikro.uni-marburg.de](mailto:georg.fritz@synmikro.uni-marburg.de))

Theoretical modelling of key biological processes has advanced our understanding of how cells respond towards environmental perturbations, such as antibiotic treatment. For instance, in *Escherichia coli* mathematical modelling accurately predicted non-trivial susceptibility patterns against ribosome-targeting antibiotics at different growth rates<sup>1</sup>, showed that a positive feedback on resistance gene regulation can lead to growth bistability of an *E. coli* population under chloramphenicol treatment<sup>2</sup>, and revealed how non-optimal responses to DNA stress under ciprofloxacin treatment can lead to suppressive drug interactions when combined with ribosome-targeting antibiotics<sup>3</sup>. Jointly, these studies demonstrate that intricate interactions between well-characterised biological parts elicit emergent and sometimes counterintuitive physiological responses, which can hardly be understood without theoretical frameworks. However, to date most of the predictive models for drug-target interactions focussed on translation-inhibiting antibiotics, which is facilitated by a well-established theoretical framework describing ribosome partitioning within bacterial cells<sup>4–6</sup>. Thus, to gain a better understanding of antibiotics targeting other essential processes, such DNA synthesis, transcription, and cell envelope biogenesis, theoretical models for these essential processes are urgently needed.

Antibiotics targeting the cell wall biosynthetic pathway are amongst the most important, clinically relevant last-resort antibiotics, such as ramoplanin, vancomycin and other glycopeptides<sup>7,8</sup>. Despite decades of experimental studies of the cell wall biosynthetic pathway in various organisms, to date there remain significant gaps in our understanding of cell wall antibiotic action. Most strikingly, for many cell wall antibiotics there are vast differences between their *in vivo* efficacy compared to the *in vitro* binding affinity for their molecular target—even in strains deleted for resistance determinants that could reduce antibiotic potency *in vivo*. For instance, in mutants of *Bacillus subtilis*, *Staphylococcus aureus* and *Enterococcus faecalis* lacking all known resistance determinants against nisin, ramoplanin or vancomycin, the minimal inhibitory concentrations (MICs) against these antibiotics are 20–200-fold higher<sup>9–14</sup> than the dissociation constants ( $K_D$ ) for the respective drug-target interaction<sup>15–17</sup>, highlighting that these antibiotics are significantly less active *in vivo* than *in vitro*. This apparent *in vivo* efficacy gap led to the notion that either all of these organisms might carry additional, yet undiscovered resistance determinants, or that the antibiotics might be inactivated *in vivo*, e.g., via sequestration to auxiliary cellular structures, effectively reducing the concentration of active antibiotics<sup>10,16,18</sup>. The variety of compounds, as well as the diversity of species displaying an *in vivo* efficacy gap, raises doubts about these hypotheses and suggests that there might be another, more universal origin of this phenomenon.

A more parsimonious explanation for this gap could emerge from the complex dynamics of the cell wall biosynthetic pathway itself, which is highly conserved across the bacterial world (reviewed e.g. in <sup>8,19,20</sup>). At the core of this pathway is the lipid II cycle, which encompasses all membrane-associated reactions of cell wall biosynthesis and is responsible for shuttling peptidoglycan (PG) subunits across the cytoplasmic membrane (Fig. 1a). Briefly, MraY and MurG sequentially attach the PG precursors UDP-MurNAc-pentapeptide and UDP-GlcNAc to the lipid carrier undecaprenyl phosphate (UP), giving rise to the lipid I and lipid II intermediates, respectively. Various flippases translocate lipid II to the outer leaflet of the cytoplasmic membrane, where penicillin-binding proteins (PBPs) incorporate the subunits into the growing PG layer. The resulting pyrophosphorylated state of the lipid carrier (UPP) is dephosphorylated by UPP phosphatases (UppPs) to yield the initial substrate UP for another round of PG subunit transport. Given that these

cyclic reactions represent the rate-limiting step of cell wall biosynthesis, it is not surprising that a wide range of antibiotics act by blocking progression of the lipid II cycle. This is achieved by either targeting the activity of the involved enzymes, e.g. PBPs (inhibited by beta-lactams) and MraY (inhibited by tunicamycin), or by directly sequestering the intermediate substrates of the lipid II cycle, e.g. UP (sequestered by friulimicin), UPP (sequestered by bacitracin) or lipid II (sequestered by ramoplanin, vancomycin and nisin), see Fig. 1a for an illustration and<sup>8,20</sup> for reviews.

To gain a quantitative understanding on how cell wall antibiotics interfere with this essential pathway, we here set out to derive a detailed, computational model of the lipid II cycle. By incorporating experimentally determined parameters from the literature, our theory accounts for key biochemical knowledge of this pathway and reconciles it with the *in vivo* inhibition patterns under antibiotic treatment. In particular, by focussing on the Gram-positive model organism *Bacillus subtilis*, we provide clues on the inner working mechanisms of cell wall biosynthesis and predict the *in vivo* efficacy of different cell wall antibiotics from first principles. In particular, we focus on antibiotics targeting different intermediates of the lipid II cycle (substrate-sequestering antibiotics), i.e. bacitracin, friulimicin, ramoplanin, vancomycin and nisin (Fig. 1a), which are active against a broad range of Gram-positive bacteria. Our results reveal that the *in vivo* efficacy gap is an emergent property of the lipid II cycle, leading us to suggest a novel principle of minimal target exposure as an intrinsic resistance mechanism towards substrate-sequestering cell wall antibiotics. Strikingly, our theory predicts that this intrinsic resistance can be circumvented—at least partially—by drugs that cooperatively bind their targets, providing a quantitative explanation for the pivotal role of cooperative binding for the potency of vancomycin and other glycopeptide antibiotics<sup>21–23</sup>. Thus, the theory presented here not only provides insights into the response of a universally conserved metabolic pathway towards perturbations, but also guides the design of novel antimicrobial compounds to efficiently block this core process of cell wall biosynthesis.

## Results

**Rationale of this study.** The bacterial cell wall consists of an alternating polymer of *N*-acetylglucosamine (GlcNAc) and *N*-acetylmuramic acid (MurNAc), cross-linked by a MurNAc-attached pentapeptide (Fig. 1a)<sup>24,25</sup>. Even though Gram-negative and -positive bacteria greatly vary in cell wall thickness and some organisms show specific modifications in peptidoglycan composition (e.g. variations in the GlcNAc-MurNAc-pentapeptide known for *Staphylococci*) or cross-linking properties (e.g. in *Corynebacteria*)<sup>26</sup>, the central lipid II cycle of cell wall biosynthesis is highly conserved throughout the bacterial world (Fig. 1a). Accordingly, it seems plausible that the basic working principles of the lipid II cycle are similar between Gram-negative and Gram-positive bacteria. Most biochemical work on the enzymes and intermediates of the lipid II cycle, however, was focussed on the Gram-negative model organism *E. coli*. Therefore, in the following we will first perform some general considerations on the kinetics of cell wall synthesis in *E. coli*, which will lead us to a first quantitative model for this essential process in Gram-negatives. Given that most antibiotics targeting the intermediates of the lipid II cycle are ineffective against Gram-negatives (due to the permeability barrier posed by the outer membrane), we will adapt the model to Gram-positive-specific cell wall synthesis in a second stage. This will allow us to make testable predictions for cell wall antibiotic action in *B. subtilis* and other Gram-positive bacteria.

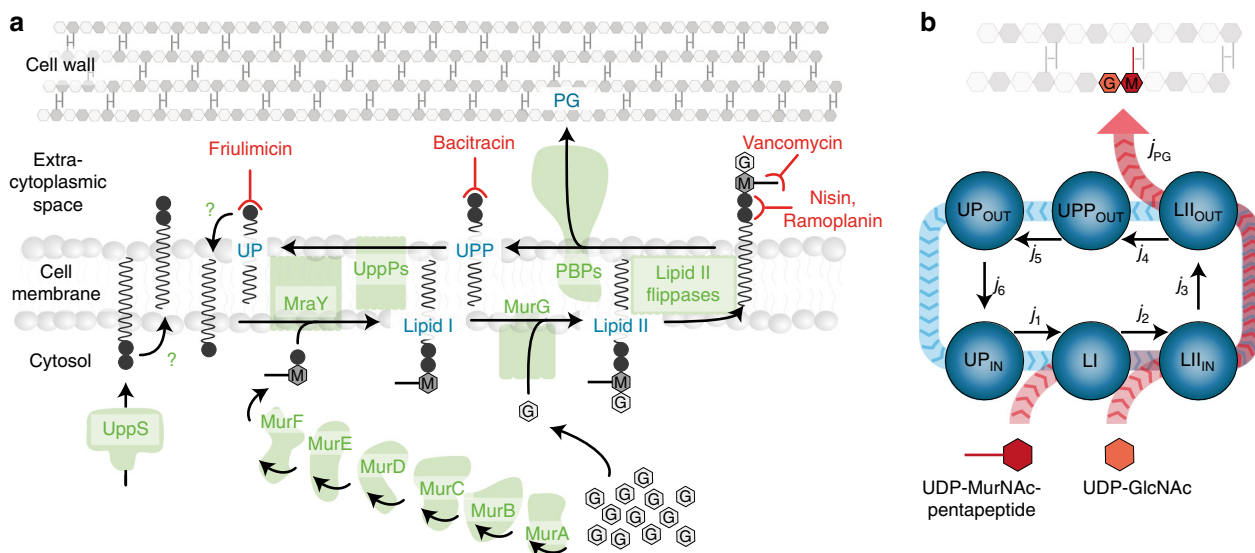


**Fig. 1** The lipid II cycle of Gram-positive bacteria is a prime target for antibiotics. **a** The lipid II cycle, as the core pathway of cell wall biosynthesis, drives the transport of PG subunits across the cytoplasmic membrane via attachment to lipid carrier molecules. The cytoplasmic production of UDP-MurNAC-pentapeptide (M) from UDP-GlcNAC (G) is catalysed by the MurA-F ligases<sup>34,75,76</sup>. Subsequently, at the internal leaflet of the cytoplasmic membrane the translocase MraY and the transferase MurG sequentially attach UDP-MurNAC-pentapeptide and UDP-GlcNAC to the lipid carrier undecaprenyl phosphate (UP), giving rise to the lipid I and lipid II intermediates, respectively. Various flippases translocate lipid II to the outer leaflet of the cytoplasmic membrane, where penicillin-binding proteins (PBPs) incorporate the subunits into the growing PG layer. This leaves the lipid carrier in its pyrophosphate form (UPP), which has to be recycled to UP by dephosphorylation to allow a new round of PG monomer transport. Given that all known UPP phosphatases (UppPs) act at the external leaflet of the cytoplasmic membrane<sup>77,78</sup>, carrier recycling requires flipping of UP to the internal leaflet by a yet unknown mechanism<sup>68,69</sup>. Finally, dilution of lipid carriers is counterbalanced by cytoplasmic synthesis of UPP by UppS, but likewise to UP flipping, the required mechanism to present UPP to the externally acting phosphatases is unknown. Several antibiotics inhibit key steps of cell wall biosynthesis by forming complexes with UP, UPP or lipid II, as indicated by the T-shaped red lines. **b** The lipid II cycle can be considered as a closed-loop system, in which all fluxes  $j_i$  from one state of the cycle into the next balance each other. Since UDP-MurNAC-pentapeptide and UDP-GlcNAC use lipid II cycle intermediates as carriers for the transport across the cytoplasmic membrane, the flux of PG precursors,  $j_{PG}$  (red arrows), is equal to the flux of the cycling reactions (blue arrows)

**Physiological constraints on PG synthesis.** In a first step we wondered about the total demand of PG synthesis of a bacterial cell, and accordingly, how fast the lipid II cycle has to shuttle PG monomers across the cytoplasmic membrane. During bacterial growth the synthesis of the wall has to precisely match the volume expansion of the cell, and any misbalance induced by antibiotic inhibition can lead to destabilization and lysis of the cell<sup>27,28</sup>. Accordingly, given that the sacculus of *E. coli* contains  $N = 3.5 \times 10^6$  PG monomers (at a doubling time  $T_D = 36$  min)<sup>29</sup> and that  $\sim \delta = 50\%$  of the produced PG is degraded by hydrolases<sup>30,31</sup>, balanced growth requires that the total rate of PG monomer translocation across the membrane,  $j_{PG}$ , has to equal  $j_{PG} = (1 + \delta)N \frac{\ln(2)}{T_D} \sim 10^5$  PG monomers per minute. This high rate of transmembrane transport is supported by attaching PG monomers to a limited number of  $1.5 \times 10^5$  lipid carrier molecules<sup>32,33</sup>. At the required synthesis rate, this implies that each lipid carrier transitions within 90 seconds through all states of the cycle (UPP > UP > lipid I > lipid II > UPP > ...) (see Supplementary Note 1 for detailed estimation). Thus, each carrier undergoes an average of  $\sim 24$  transport cycles before it gets diluted due to cell growth. This suggests that instead of synthesizing lipid carriers for one-time “use-it and lose-it” transport, lipid carrier recycling is the pace-maker of PG monomer transport across the membrane. Under these conditions the lipid II cycle can be approximated as a closed-loop system, in which the pool levels of lipid II cycle intermediates quickly equilibrate, leading to cyclic flux-balance between all of the states, i.e.  $j_1 = j_2 = \dots = j_6$  (Fig. 1b, blue arrows; Supplementary Note 1 and Supplementary Fig. 1a, b). For instance, if one reaction is limited by either the catalytic rate or the abundance of the respective enzyme, the substrate of this

reaction will accumulate and all other intermediates will deplete until all fluxes in the cycle are equal. Experiments in *E. coli* indeed revealed a highly asymmetric distribution of lipid II cycle intermediates, with a  $\sim 100$ -fold excess of UPP and UP ( $1.2 \times 10^5$  and  $0.3 \times 10^5$  molecules per cell, respectively)<sup>33</sup> over lipid I and lipid II (700 and 1000, respectively)<sup>32</sup> (Supplementary Table 1a). Also, it is noteworthy that under normal growth conditions cells homeostatically control cytoplasmic UDP-MurNAC-pentapeptide and UDP-GlcNAC at levels that saturate MraY and MurG, respectively<sup>34,35</sup> such that the rate of wall synthesis is not limited by soluble PG precursor abundance. Instead, under these conditions the total flux of PG subunits across the cytoplasmic membrane (Fig. 1b; red arrows) is only limited by the membrane-associated steps of wall synthesis and is identical to the individual, cyclic fluxes in the lipid II cycle, i.e.  $j_{PG} = j_1 = j_2 = \dots = j_6$ .

**Kinetic model of the lipid II cycle.** Are the molecular properties of the cycle compatible with the overall demand for cell wall synthesis outlined above? To test this, we developed a detailed kinetic model of the lipid II cycle, which integrates key biochemical knowledge from literature and simulates the overall rate of PG synthesis,  $j_{PG}$ . Briefly, the model takes into account the reactions depicted in Fig. 1a, by considering Michaelis-Menten kinetics for all characterised enzymes, and first order kinetics in case of the flipping reactions for UP, UPP and lipid II, since less is known about the latter. By further assuming production of UPP in the cytoplasm and dilution of all cycle intermediates due to cell growth, the model describes the dynamic changes in the concentrations of cycle intermediates in the inner and outer leaflet of the membrane (see Supplementary Fig. 1c and Methods). To

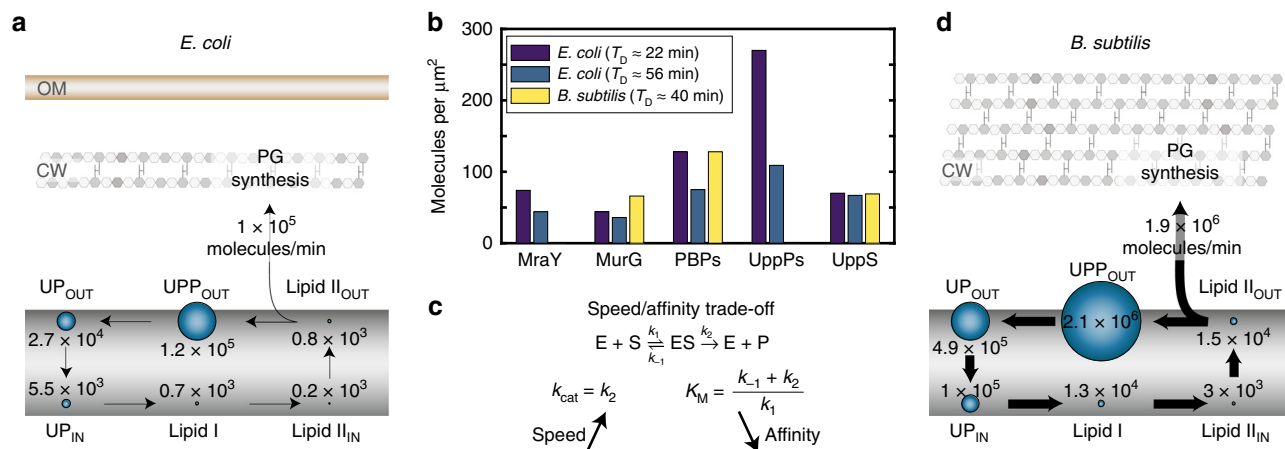


**Fig. 2** Abundance of enzymes and lipid carrier intermediates in the lipid II cycle. **a** Pool level distribution of lipid II cycle intermediates and rate of PG synthesis predicted by the theoretical model for *E. coli*. **b** The surface concentration (number of enzymes per unit surface area) of the PG synthesis machinery is similar in Gram-positive and -negative organisms. **c** Increased catalytic rates of the lipid II cycle enzymes are expected to significantly speed up the PG synthesis in Gram-positive organisms. As the catalytic rate  $k_{\text{cat}} = k_2$  also affects the Michaelis constant  $K_M$ , an increase in the speed of an enzymatic reaction can decrease the affinity of the enzyme for its substrate. **d** Pool level distribution of lipid II cycle intermediates and rate of PG synthesis predicted by the theoretical model for *B. subtilis*. The significantly thicker PG layer in *B. subtilis*, which compensates the lack of an outer membrane, demands an increase in the rate of PG synthesis, implying higher levels of lipid II intermediates shuttling faster through the cycle

calibrate the parameters in the model, we fixed all catalytic rates ( $k_{\text{cat}}$ ) and Michaelis–Menten constants ( $K_M$ ) to the values obtained from literature (Supplementary Table 1) and applied a constrained optimisation approach to estimate the remaining parameters (see Supplementary Note 1). In particular, by imposing that the overall flux within the lipid II cycle has to match the overall PG demand of the cell and by fixing the total abundances of cycle intermediates to the asymmetric distributions reported in literature (Supplementary Table 1a), we obtained precise estimates for the levels of the lipid II cycle-associated enzymes, as well as for the rates for lipid carrier flipping (Supplementary Fig. 1d). Interestingly, the theoretically predicted enzyme levels are in excellent agreement with a previous proteomics study<sup>36</sup> (Supplementary Table 2), showing that our model describes the quantitative dynamics of the lipid II cycle in a self-consistent manner—compatible with biochemical and physiological constraints.

When the flux across all reactions of the lipid II cycle is balanced, the model predicts an asymmetric distribution of cycle intermediates across the two leaflets of the cytoplasmic membrane. Especially, UPP and lipid II are predominantly found in the external leaflet, while UP displays an even distribution (Fig. 2a). Within the model, this is caused by highly efficient rates of UPP and lipid II flipping across the membrane, whereas the flipping of UP is predicted to be  $\sim 2$  orders of magnitude slower. This is consistent with the fact that lipid II is actively transported from the internal to the external leaflet via MurJ and other flippases<sup>37–39</sup> and suggests that UPP could similarly follow an active transport route. In contrast, UP may follow a passive translocation process from the outer to the inner leaflet of the membrane (see Discussion). Taken together, this initial mathematical model for the lipid II cycle provides a first holistic view on this essential metabolic pathway in the Gram-negative model organism *E. coli*, integrating key biochemical properties, enzyme concentrations and pool levels of cycle intermediates.

Even though for Gram-positive bacteria a comprehensive biochemical understanding of the PG synthetic machinery, and in particular of the PBPs, has not been laid out, we next integrated all existing quantitative knowledge from diverse species to consolidate them in a modified mathematical model for the Gram-positive cell wall synthesis. First of all, while *E. coli* features

a PG thickness of 1.5 glycan layers on average<sup>40</sup>, *B. subtilis* and many other Gram-positive bacteria have a much thicker wall of about 20 layers<sup>8</sup>. Thus, when comparing Gram-negative and Gram-positive cells of equal sizes and at similar doubling times, the lipid II cycle has to transport PG precursors at a  $\sim 13$ -fold higher rate in the latter (see Supplementary Note 1 and Supplementary Table 3a for a comparison between *E. coli* and *B. subtilis*). Theoretically, increases of the PG synthesis rate can be achieved by tuning three factors: (i) increasing the abundance of enzymes in the lipid II cycle, (ii) increasing the concentrations of lipid carriers, or (iii) increasing the catalytic rates of all associated enzymes. Interestingly, although proteomic studies in *B. subtilis* and *E. coli* revealed differences in the absolute enzyme abundances<sup>36,41</sup>, their surface concentration is almost invariant between organisms—with typically between 50 and 100 molecules per  $\mu\text{m}^2$  for each enzyme species (Fig. 2b and Supplementary Table 3b)—showing that Gram-positive bacteria do not simply increase the abundance of the PG synthetic machinery. Instead, in a range of Gram-positive bacteria the surface concentrations of the lipid carriers UP, UPP and lipid II are 10- to 20-fold higher compared to *E. coli* (Supplementary Table 3c), suggesting that these increased substrate levels are required to fully saturate the enzymes of the lipid II cycle in Gram-positives. Consistent with this, literature suggests that the  $K_M$  value of MraY is eight-fold higher in *B. subtilis* ( $K_M = 160 \mu\text{M}$ <sup>42</sup>) compared to *E. coli* ( $K_M = 20 \mu\text{M}$ <sup>43</sup>). However, if the goal is to speed up PG synthesis—why does the Gram-positive PG synthetic machinery feature lower substrate affinity while increasing substrate abundance, ultimately leading to comparable levels of enzyme saturation as in Gram-negatives? A potential origin could lie in the speed/affinity trade-off known in enzyme kinetics<sup>44,45</sup>, according to which speeding up the  $k_{\text{cat}}$  value of an enzyme can lead to a sacrifice in substrate affinity and a concomitant increase of the  $K_M$  value (Fig. 2c). For highly efficient enzymes, in particular, the  $k_{\text{cat}}$  value is larger than the substrate dissociation rate  $k_{-1}$ , leading to an inverse relationship between affinity ( $K_M^{-1}$ ) and speed, i.e.,  $K_M \approx k_{\text{cat}}/k_{-1}$ .

Taken together, the most parsimonious model for the Gram-positive lipid II cycle is that the  $\sim 13$ -fold higher demand for PG synthesis (compared to Gram-negative bacteria) is met by faster enzymes with 10–20-fold higher catalytic rates. The speed-affinity



trade-off then dictates that all substrate affinities will be 10–20-fold lower in Gram-positive enzymes, as observed for the  $K_M$  value of MraY. This model is also consistent with the experimentally observed 10–20-fold higher lipid carrier substrate pools, which would then be required to achieve similar levels of enzyme saturation as in Gram-negatives, such that enzymes can operate close to their maximal speeds. Accordingly, to establish a self-consistent generic model for the Gram-positive cell wall biosynthesis, we scaled all parameters for the lipid II cycle in *E. coli*, i.e., the  $k_{cat}$  and  $K_M$  values, as well as the rate of UPP de novo biosynthesis, by a factor of 13 (see Supplementary Note 1). Accordingly, within this rescaled model both the overall PG synthesis rate, as well as all lipid carrier concentrations increase by this factor, while the relative stoichiometries between the lipid carrier intermediates remain identical to the model for *E. coli* (Fig. 2d). Although we are well aware that this coarse-grained scaling is an approximation for the lipid II cycle in *B. subtilis*, it is the most parsimonious choice of model parameters and leads to testable predictions for the cellular response towards cell wall antibiotics, as studied in the following.

**Predicting cell wall antibiotic action from first principles.** As introduced above, many cell wall antibiotics bind to externally exposed lipid II cycle intermediates, thereby sequestering lipid carriers from the cycle. For the five antibiotics under consideration (friulimicin, bacitracin, vancomycin, nisin and ramoplanin, see Fig. 1a) both the molecular targets as well as the equilibrium dissociation constants ( $K_D$ ) for the antibiotic/target interaction have been characterised in vitro (Supplementary Table 4a). This allowed us to integrate these binding reactions into our quantitative model for the lipid II cycle (see Methods)—thereby creating a tool to generate predictions of cell wall antibiotic action without invoking further fit parameters. In the following we will first focus on the two antibiotics that bind their target non-cooperatively and later consider the effect of cooperative binding for the remaining three antibiotics.

First we studied the action of the cationic antimicrobial peptide bacitracin, which is widely used as a medicine and feed additive. Bacitracin binds to UPP by forming an amphipathic shell around its pyrophosphate group, thereby sequestering the target<sup>46</sup>. When incorporating the binding of bacitracin to UPP into our model ( $K_D^{BAC} = 1 \mu\text{M}$ <sup>47</sup>) we predict a hyperbolic decrease of the total PG synthesis rate with increasing antibiotic concentration, reaching 50% of the maximal PG synthesis rate at 1.8  $\mu\text{M}$  bacitracin ( $\text{IC}_{50}^{BAC}$ ) (Fig. 3a). To understand why the predicted  $\text{IC}_{50}$  almost coincides with the  $K_D$  value in the model, we analysed the relative abundances of lipid II cycle intermediates at different bacitracin concentrations (Fig. 3b). Here it turned out that the  $\text{IC}_{50}$  coincides with a decrease of the free external lipid II pool to approximately 50% of its untreated level, consistent with the role of lipid II as substrate for the final step of PG precursor incorporation. The reduction of free lipid II pools is correlated with an increase of the bacitracin-bound form of external UPP (commencing at the  $K_D$  value), which effectively sequesters lipid carriers from the cycle and thereby triggers a concerted decrease of all free cycle intermediates (Fig. 3b). Thus, for the binding of bacitracin to UPP, which constitutes the largest pool of lipid II cycle intermediates, our model predicts only a marginal in vivo efficacy gap, i.e., an  $\text{IC}_{50}$  very similar to the in vitro  $K_D$  value.

Next, we focussed on the commonly used food preservative nisin—a polycyclic antibacterial peptide that binds with high affinity to lipid II, the latter of which constitutes the smallest pool of externally accessible cycle intermediates. To our surprise, for nisin our model predicted an  $\text{IC}_{50}$  value ( $\text{IC}_{50}^{NIS} = 10 \mu\text{M}$ ) about 700-fold higher than the in vitro dissociation constant entering

the model simulation ( $K_D^{NIS} = 0.015 \mu\text{M}$ <sup>48</sup>) (Fig. 3c)—qualitatively similar to the in vivo efficacy gap reported in literature (see Introduction). What is the origin of this discrepancy in the model? When again considering the relative abundances of cycle intermediates at varying antibiotic concentrations, it turns out that nisin—at low levels around the  $K_D$  value—also effectively binds to its target, leading to a pool level of nisin-lipid II complexes comparable to the free form of lipid II (Fig. 3d). However, this sequestration of lipid II only corresponds to ~1% ( $10^4$  molecules) of the total number of lipid carriers in the cycle (Fig. 3d, g), thereby not reducing the overall abundance of free carriers significantly. Accordingly, the circular flux of carriers within the lipid II cycle quickly replenishes the free form of lipid II molecules and leads to a similar PG synthesis rate as in the absence of nisin (99% of max). Only when increasing the nisin concentration 700-fold over its  $K_D$  value, the amount of sequestered carriers (nisin-lipid II) rises to ~50% of the total abundance of cycle intermediates (Fig. 3d, h), thereby reducing also the free lipid II pool and hence the overall PG synthesis rate to 50% of its maximal value (Fig. 3c, d, h). Thus, within our model the small pool size of externally accessible lipid II (~1/100 of total lipid carriers) leads to inefficient sequestration of lipid carriers, thereby reducing the susceptibility of cell wall biosynthesis towards lipid II-binding antibiotics. In contrast, the binding of bacitracin to external UPP, constituting the largest pool of cycle intermediates (~2/3 of total lipid carriers), leads to efficient sequestration of lipid carriers already at concentrations around the  $K_D$  value (Fig. 3e, f). In summary, these results indicate that the in vivo efficacy gap results from asymmetric distributions of externally accessible targets, and that the discrepancy between  $K_D$  and  $\text{IC}_{50}$  increases for decreasing target pool sizes.

To assess the predictive power of our model, we next compared the theoretical  $\text{IC}_{50}$  values with experimentally determined MICs for the given antibiotics (Fig. 3a and Supplementary Table 4b). On first sight, the in vivo MIC of wildtype *B. subtilis* strain W168 ( $\text{MIC}^{BAC} = 180 \mu\text{M}$  bacitracin<sup>49</sup>) was ~100-fold higher than the predicted  $\text{IC}_{50}$  value ( $\text{IC}_{50}^{BAC} = 1.8 \mu\text{M}$ ). However, the model did not factor in the action of the BceAB resistance pump, which confers high levels of bacitracin resistance to wildtype *B. subtilis* cells<sup>49</sup>. The MIC of a strain deleted for *bceAB* (W168  $\Delta bceAB$ ;  $\text{MIC}^{BAC} = 1.7 \mu\text{M}$  bacitracin<sup>49</sup>); instead closely matches the model-predicted  $\text{IC}_{50}$ , confirming that the in vivo efficacy gap is only ~two-fold for the UPP-binding antibiotic bacitracin (Fig. 3a). Similarly, the model prediction for nisin ( $\text{IC}_{50}^{NIS} = 10 \mu\text{M}$ ) is only a factor of two higher than the experimental MIC of a strain deleted for the primary nisin resistance determinant (W168  $\Delta psdAB$ ;  $\text{MIC}^{NIS} = 4.8 \mu\text{M}$ <sup>11</sup>), revealing a 330-fold higher in vivo MIC compared to the in vitro  $K_D$  (Fig. 3c). Here, the slightly lower experimental  $\text{MIC}^{NIS}$  compared to the predicted  $\text{IC}_{50}^{NIS}$  might be caused by membrane pore formation triggered by high nisin levels<sup>16,50,51</sup>, which will increase the potency of nisin but is not reflected in the model. These results indicate that our model provides an accurate description of the lipid II cycle under antibiotic treatment, and allows for precise predictions of the in vivo antibiotic susceptibility from first principles.

**Analytical expression of the in vivo efficacy gap.** Next, we wanted to derive an intuitive mathematical formula describing how antibiotic susceptibility depends on the pool size of the targeted lipid carrier, thereby rationalizing the origin of the in vivo efficacy gap. To obtain a closed analytical expression for the PG synthesis rate as a function of the antibiotic concentration, we considered a simplified model of the lipid II cycle (see Methods and Fig. 4a): This model takes into account first order reactions between the antibiotic, A, and its unbound lipid carrier



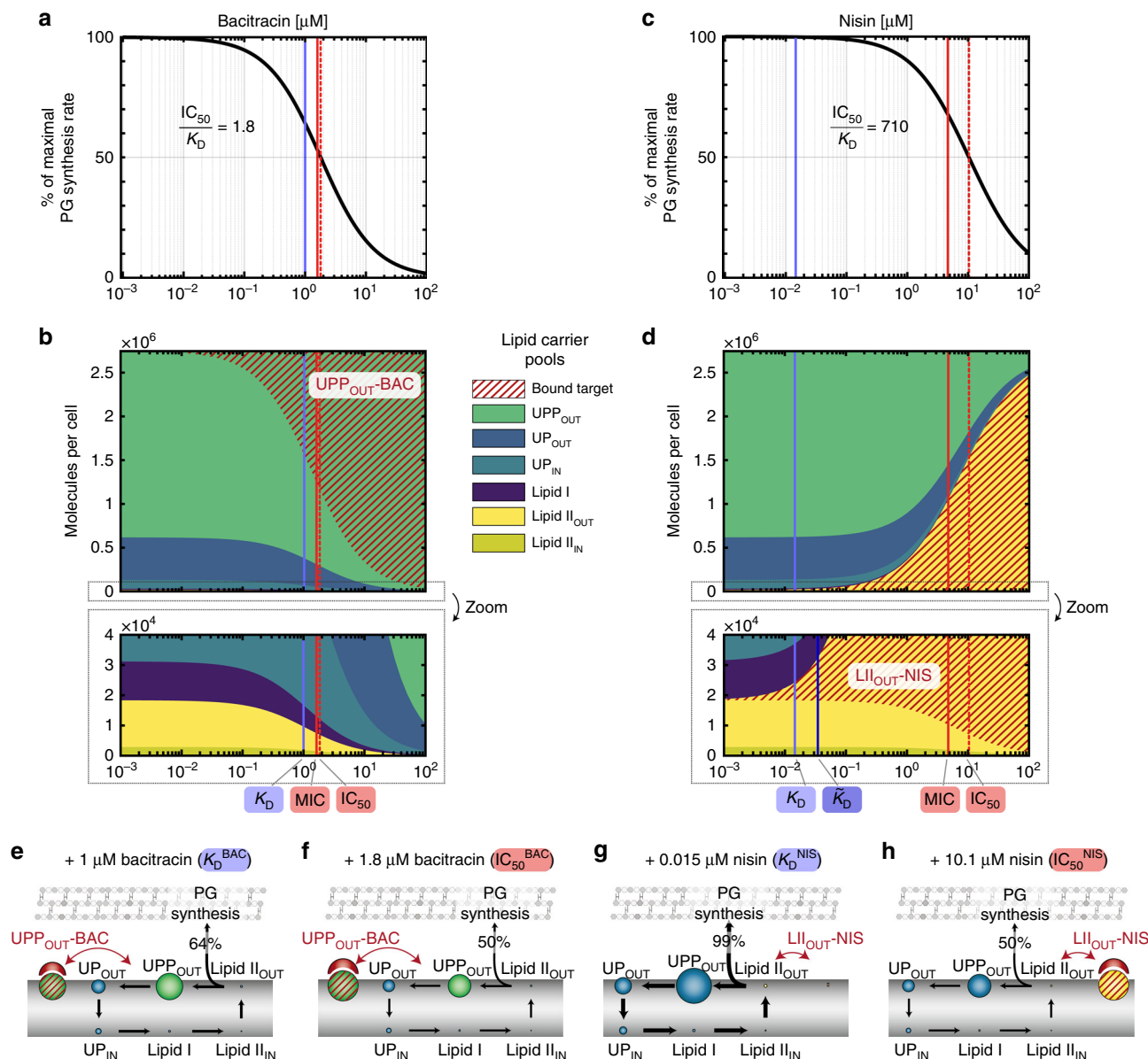


**Fig. 3** The asymmetric distribution of lipid II cycle intermediates can generate a massive in vivo efficacy gap in *B. subtilis*. **a, c** Model prediction of the PG synthesis rate (black lines) for varying bacitracin (**a**) and nisin (**c**) concentrations. Blue lines indicate the in vitro dissociation constants  $K_D$  and red solid lines the experimental MICs derived from literature (see Supplementary Table 4 for parameter values and references). The red dashed line indicates  $IC_{50}$  value predicted by the model, i.e. the concentration at which the PG synthesis reaches 50% of the maximal rate. **b, d** Model prediction of the pool levels of lipid II cycle intermediates at different bacitracin (**b**) and nisin (**d**) concentrations. **e-h** Schematic illustrations of pool level distributions at bacitracin and nisin concentrations corresponding to the respective  $K_D$  and  $IC_{50}$  values. **e** At a bacitracin concentration equal to the  $K_D$  value, the external UPP pool is significantly reduced, implying efficient sequestration of high levels of lipid II cycle intermediates from the cycle, thereby decreasing all free cycle intermediates, especially lipid II. While this already reduces the rate of PG synthesis to a level of 64% of its maximum, only slightly higher bacitracin concentrations (**f**) are required to reduce the rate of PG synthesis to 50%. **g** In contrast, although nisin—at a concentration around the  $K_D$ —binds 50% of the free lipid II pool, this only sequesters ~1% of all lipid intermediates from the cycle. As the remaining lipid carriers quickly replenish the free form of lipid II molecules by on-going cycling, the rate of PG synthesis is not reduced significantly (99% of maximum). **h** Eventually, high concentrations of nisin are required at the  $IC_{50}$  value to sequester ~50% of the total lipid II cycle intermediates into nisin-lipid II complexes, in order to decrease the pool of free lipid II pool and the PG synthesis rate to 50%. For an analysis of the remaining three antibiotics please refer to Supplementary Fig. 3

target,  $S_{unbound}$ , with association- and dissociation rates  $k_{ass}$  and  $k_{diss}$ , respectively. Moreover, all other (non-target) lipid carrier intermediates of the cycle are summarised as a bactoprenol reservoir,  $S_{reservoir}$ , which can be interconverted into the unbound lipid carrier with first order rate constants  $k_1$  and  $k_{-1}$ , leading to PG synthesis at a rate  $j_{PG} = k_{-1}[S_{unbound}]$  (and in equilibrium also  $j_{PG} = k_1[S_{reservoir}]$ ). Under the assumption that the lipid II cycle runs much faster than the doubling rate ( $k_1, k_{-1} \gg \gamma$ ) the PG

synthesis rate decreases with the antibiotic concentration  $[A]$  according to

$$j_{PG} \sim \frac{\tilde{K}_D(1 + \tilde{K}_G)}{[A] + \tilde{K}_D(1 + \tilde{K}_G)}, \tag{1}$$

highly reminiscent of the hyperbolic decrease observed in the full model above (cf. Fig. 3a, c). Interestingly, the half-maximal rate of PG synthesis is reached at an antibiotic concentration of

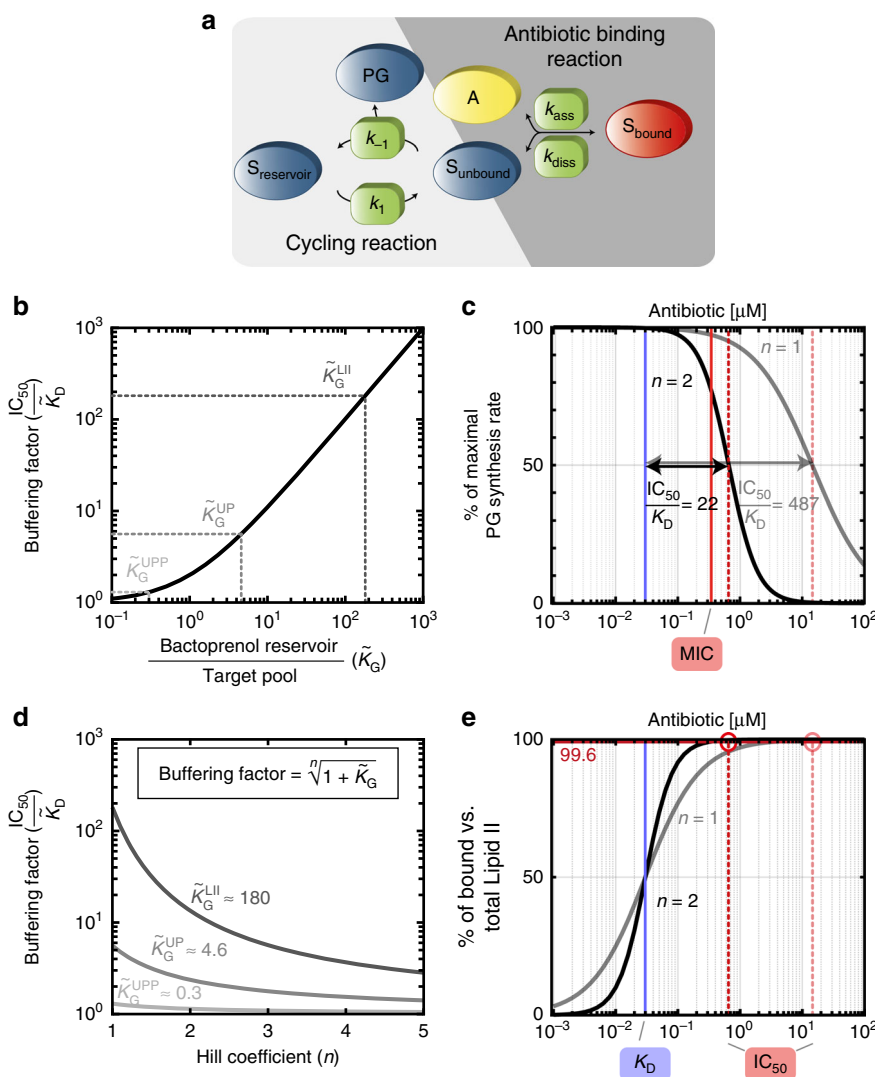


**Fig. 4** A reduced model for the lipid II cycle rationalises the in vivo efficacy gap and elucidates the boost of antibiotic potency by cooperative drug-target interactions. **a** The reduced model for the lipid II cycle considers antibiotic (A) binding to its lipid carrier target ( $S_{unbound}$ ) via first order reactions with association- and dissociation rates  $k_{ass}$  and  $k_{diss}$ , respectively, leading to the antibiotic-bound form of the target ( $S_{bound}$ ). The model summarises all non-target lipid II cycle intermediates as a bactoprenol reservoir ( $S_{reservoir}$ ), which can be converted into the unbound lipid target intermediate and vice versa via first order kinetics at rate constants  $k_1$  and  $k_{-1}$ , respectively. **b** The buffering factor ( $\frac{IC_{50}}{K_D} = 1 + \tilde{K}_G$ ), which is the major determinant of the in vivo efficacy gap, increases for increasing bactoprenol reservoir size relative to the unbound target pool in the absence of the antibiotic ( $S_{target}$ ) according to  $\tilde{K}_G = \frac{S_{reservoir}}{S_{target}}$ . Buffering factors are indicated for antibiotics binding to external lipid II ( $\tilde{K}_G^{LII}$ ), external UP ( $\tilde{K}_G^{UP}$ ), or UPP ( $\tilde{K}_G^{UPP}$ ). **c** Influence of cooperative drug-target interaction on the  $IC_{50}$  value predicted for lipid II-binding antibiotics. Assuming identical in vitro  $K_D$  values (corresponding to the in vitro value of vancomycin; blue line) the model predicts that for an antibiotic variant binding in a cooperative manner (Hill coefficient  $n = 2$ ; black and red dashed lines), the  $IC_{50}$  is approximately 22 times lower than for a non-cooperative antibiotic binding ( $n = 1$ ; grey and pale red lines). The experimentally measured MIC for vancomycin (red solid line<sup>9</sup>), is close to the predicted  $IC_{50}$  for the cooperative variant. **d** Scaling of the in vivo efficacy gap with the Hill coefficient  $n$  within the reduced model (see Supplementary Fig. 2 for further details). **e** For the simulated vancomycin variants (binding to lipid II), the reduction of the PG synthesis rate to 50% requires that the equilibrium is strongly shifted towards the bound form of lipid II (99.6% bound vs. total lipid II). As increasing Hill coefficients  $n$  generally lead to steeper binding curves, the required level of target binding is achieved at a 22-fold lower antibiotic concentration by cooperative antibiotic binding (black) compared to the non-cooperative variant (grey)

$IC_{50} \equiv \tilde{K}_D(1 + \tilde{K}_G)$ , which is strikingly different from the naïve in vitro expectation for the antibiotic-target interaction ( $IC_{50} = K_D$ ). Indeed, the  $IC_{50}$  in vivo is not only governed by the biochemical properties of antibiotic binding, but strongly influenced by two factors governing the lipid II cycling reactions: First, the dissociation constant for the antibiotic-target interaction is substituted by the in vivo dissociation constant,  $\tilde{K}_D = \frac{k_{diss} + \gamma}{k_{ass}}$ , which can deviate up to approximately three-fold from the in vitro value ( $K_D = \frac{k_{diss}}{k_{ass}}$ ), depending on the growth rate  $\gamma$ , as

well as the kinetics of antibiotic binding and unbinding from its target (see Supplementary Note 1, Supplementary Table 4c and Supplementary Fig. 4c, e). Second, the in vivo dissociation constant is scaled by a buffering factor, which we define as  $(1 + \tilde{K}_G)$ . Here  $\tilde{K}_G = \frac{[R]}{[T]} \approx \frac{k_{-1}}{k_1}$  describes the ratio between the size of the bactoprenol reservoir (serving as a buffer) and the size of the carrier target in the absence of antibiotic (Fig. 4b). For example, if the buffering reservoir is small compared to the target pool ( $\tilde{K}_G \ll 1$ ), the model predicts only a marginal shift in the

$IC_{50}$  ( $IC_{50} \approx \tilde{K}_D$ ), indicating that in this case 50% of the total bactoprenol carriers are easily sequestered by an antibiotic concentration equal to the in vivo  $\tilde{K}_D$  value. In contrast, if the buffering reservoir is large compared to the target pool ( $\tilde{K}_G \gg 1$ ), an antibiotic concentration equal to the in vivo  $\tilde{K}_D$  value only sequesters a small amount of the overall bactoprenol carrier level, leading to substantial shifts in the  $IC_{50}$  ( $IC_{50} \gg \tilde{K}_D$ ). Specifically, when considering that the external lipid II pool in *B. subtilis* (15  $\mu\text{M}$ ) is expected to be much smaller than the sum of all other carrier intermediates (2700  $\mu\text{M}$ ), the model predicts a buffering factor for the lipid II binding nisn of  $(1 + \tilde{K}_G) \approx 180$ -fold (Fig. 4b). In contrast, for the UPP pool (2100  $\mu\text{M}$ ) the other lipid carriers constitute a much smaller reservoir (600  $\mu\text{M}$ ), which leads only to a marginal buffering factor for bacitracin of  $(1 + \tilde{K}_G) \approx 1.3$ -fold (Fig. 4b). These results demonstrate that the asymmetric distributions of lipid carrier intermediates lead to a buffering effect against antibiotic attacks, which is particularly pronounced for lipid II binding antibiotics, displaying a several 100-fold in vivo efficacy gap. Thus, although other factors, such as the difference between the in vitro and in vivo dissociation constant and enzyme saturation (see Supplementary Note 1 and Supplementary Fig. 3g) have additional impact on antibiotic susceptibility in the full model, the buffering effect is the major cause for the in vivo efficacy gap for antibiotics targeting small lipid carrier pools.

### Cooperative drug-target interaction boosts antibiotic efficacy.

Next, we focussed on another long-standing debate in the field of antibiotic resistance research, which is related to the effect of cooperative drug-target interaction on antibiotic susceptibility. Here, it is well documented that antibiotics binding in a cooperative manner to lipid II cycle intermediates, e.g., via multimeric complex formation with the target, have a higher potency than antibiotic variants unable to multimerise<sup>23,52–54</sup>. For instance, dimer formation plays a key role in the efficient action of the clinically important antimicrobial peptide vancomycin, as well as in many other glycopeptides<sup>52–54</sup>, and has been recognised to enhance the potency of engineered antimicrobial peptides<sup>23</sup>. However, until now the mechanism behind the cooperativity-induced activity boost remained elusive.

We therefore studied the quantitative impact of cooperative drug-target interactions on antibiotic efficacy within our mathematical model. To this end we considered the case of vancomycin, which has a dissociation constant of  $K_D^{\text{VAN}} = 0.03 \mu\text{M}$ <sup>15</sup> and interacts with lipid II molecules<sup>55</sup> via vancomycin dimerization<sup>56</sup>. In vitro, cooperative antibiotic-target interactions typically lead to sigmoidal binding curves of the form  $[A]^n / (K_D^n + [A]^n)$ , with a Hill coefficient  $n$  ranging between 1–2 for dimeric binding. For instance, if drug dimerization occurs at a concentration around the dissociation constant to the target, the Hill coefficient will be close to 2, while both strong and weak dimerization relative to target binding will generally lead to  $n < 2$  (see Methods and Supplementary Fig. 2c). When analysing the effect of two hypothetical vancomycin variants with identical  $K_D$ , but different Hill coefficients within our model (Fig. 4c), we find that for a non-cooperatively binding variant ( $n = 1$ ) the model predicts an in vivo efficacy gap similar to nisn ( $\frac{K_D}{\text{MIC}} = 470$ ), while this is significantly reduced for a cooperatively binding vancomycin variant ( $n = 2$ ), for which the model predicts a 20-fold lower efficacy gap ( $\frac{K_D}{\text{MIC}} = 22$ ). Interestingly, the experimentally measured MIC for vancomycin in *B. subtilis* ( $\text{MIC}^{\text{VAN}} = 0.35 \mu\text{M}$ <sup>9</sup>) is remarkably similar to the value predicted for the cooperatively binding variant ( $IC_{50}^{\text{VAN}} = 0.65 \mu\text{M}$ ) (Fig. 5),

consistent with the observation that dimerization of vancomycin is key for blocking the lipid II pool. Strikingly, also for the dimeric glycolipodepsipeptide ramoplanin, our model predicts almost the same in vivo efficacy gap as for vancomycin ( $IC_{50}^{\text{RAM}} = 0.41 \mu\text{M}$ ), which we find in excellent quantitative agreement with experimental data ( $\text{MIC}^{\text{RAM}} = 0.49 \mu\text{M}$ <sup>10</sup>) (Fig. 5).

Why does dimerisation have such a drastic influence on the  $IC_{50}$  in our model? To rationalise this behaviour, we extended the simplified model (Fig. 4a) by accommodating cooperative drug-target interactions (see Methods). Under similar assumptions as in the previous section ( $k_1, k_{-1} \gg \gamma$ ) the PG synthesis rate now takes the form

$$j_{\text{PG}} \sim \frac{\tilde{K}_D^n (1 + \tilde{K}_G)}{[A]^n + \tilde{K}_D^n (1 + \tilde{K}_G)}. \quad (2)$$

Following a similar rationale as before, the half-maximal rate of PG synthesis is now reached at an antibiotic concentration of  $IC_{50} = \tilde{K}_D \sqrt[n]{1 + \tilde{K}_G}$ , where the generalised buffering factor  $\sqrt[n]{1 + \tilde{K}_G}$  gets attenuated by the Hill coefficient via the  $n$ -th root. Thus, the higher the cooperativity  $n$ , the lower the buffering factor and the smaller the gap between MIC and  $K_D$  value. This attenuation of the buffering effect is particularly pronounced if the buffering factor is large, e.g. for antibiotics targeting the lipid II pool ( $\tilde{K}_G \approx 180$ ) (Fig. 4d). Intuitively, the mitigating role of cooperativity can be understood as follows: Since the buffering factor is large, the cycle is slowed down only if the antibiotic-target complexes vastly exceed the free target, such that the  $IC_{50}$  for lipid II-binding antibiotics is only achieved if the ratio between bound and unbound lipid II molecules is 99.6% (Fig. 4e). Clearly, if the drug-target interaction follows a sigmoidal binding kinetics (as incurred by a Hill coefficient  $n = 2$ ), a similar level of target binding is achieved at a 22-fold lower antibiotic concentration compared to hyperbolic binding kinetics ( $n = 1$ ) (Fig. 4e). This explains why in vivo vancomycin ( $n = 2$ ) is drastically more active than nisn ( $n = 1$ ), although both antibiotics have almost identical in vitro dissociation constants to lipid II. Thus, cooperativity in drug-target interactions can greatly boost the vivo efficacy of the drug by more efficiently sequestering the target as soon as the  $K_D$  value is exceeded.

However, we also noted that cooperative drug-target interactions do not always confer such drastic effects. For antibiotics targeting the largest pools of cycle intermediates, UPP and UP, the respective buffering factors are already low ( $1 + \tilde{K}_G \approx 1.3$  and  $1 + \tilde{K}_G \approx 5.6$ , respectively) such that increasing cooperativity only leads to a mild reduction of the buffering effects in our model, with virtually no change for UPP-binding antibiotics (Fig. 4d). Only for UP-binding antibiotics the model predicts that changing cooperativity from monomeric ( $n = 1$ ) to dimeric target binding ( $n = 2$ ) will increase antibiotic potency by a factor  $\sqrt{5.6} \approx 2.4$ . Interestingly, while it has been controversial whether the UP-targeting lipopeptide antibiotic frulimicin binds its target as monomer or dimer<sup>57</sup>, our model predictions for monomeric binding ( $IC_{50}^{\text{FRI}} = 1.46 \mu\text{M}$ ) are in excellent agreement with the experimental susceptibility in *B. subtilis* ( $\text{MIC}^{\text{FRI}} = 1.15 \mu\text{M}$ <sup>58</sup>) (Fig. 5), suggesting that frulimicin inhibits its target in a non-cooperative manner.

### Discussion

Over the last decade quantitative experimentation and theoretical modelling has fostered significant progress in our understanding of antibiotic action against bacteria<sup>3,59–61</sup>. While previous theory uncovered a range of non-trivial effects in the action of ribosome-targeting antibiotics<sup>1</sup>, our work rationalises similarly

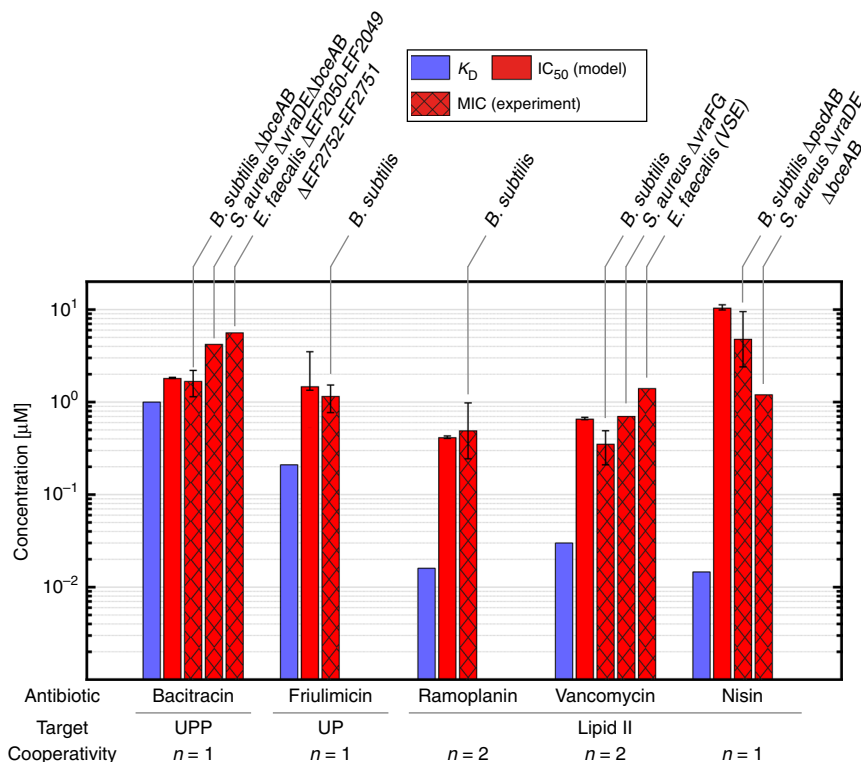


**Fig. 5** Prediction of in vivo efficacy for various cell wall antibiotics in diverse Gram-positive organisms. The mathematical model predicts the in vivo efficacy ( $IC_{50}$ , red solid bars) exclusively from the antibiotics in vitro dissociation constants ( $K_D$ , blue bars) and available information about the cooperativity in antibiotic-target-interaction. The model predictions are in good agreement with experimental data published for *B. subtilis*<sup>9–11,49,58</sup>, *S. aureus*<sup>12,13</sup> and *E. faecalis*<sup>14,79</sup> strains deleted for the known resistance determinants against the different antibiotics ( $MIC$ , red hashed bars), highlighting the universality of the theoretical model for various Gram-positive organisms. Error bars of literature  $MIC$  values either represent standard deviations from multiple measurements, when available in the original publications, or were derived from the increments of the serial dilution steps in the published  $MIC$  assays. Error bars for the model predictions of  $IC_{50}$  values represent confidence intervals propagated from uncertainties in model parameters (see Supplementary Fig. 4 and<sup>80</sup>)

counterintuitive effects for cell wall antibiotics. In particular, our theory predicts an inverse correlation between the tolerance towards substrate-sequestering cell wall antibiotics and the abundance of their cellular target, suggesting the principle of minimal target exposure as an intrinsic resistance mechanism against cell wall antibiotics. We show that resistance emerges from the cyclic nature of the cell wall biosynthetic pathway, in which high-abundance intermediates provide a buffer against sequestration of low-abundance intermediates. In this light it seems plausible that bacteria may have evolved to minimise the abundance of externally exposed lipid II molecules, e.g. by speeding up the rate of PG monomer insertion into the cell wall, in order to evade blocking by lipid II-binding antibiotics, which are ubiquitously produced by competing species, such as *Lactobacillus lactis* (nisin), *Amycolatopsis orientalis* (vancomycin) or *Actinomycetes* species (ramoplanin)<sup>62–65</sup>.

Our theory further resolves a longstanding conundrum dating back to the 1990s, where it was first observed that cooperative drug-target interactions play a crucial role in the in vivo efficacy of glycopeptide antibiotics<sup>18,22</sup>. Although molecular studies have revealed how cooperativity can emerge from glycopeptide–lipid II interactions<sup>66</sup>, it remained enigmatic why it has such a drastic effect on antibiotic efficacy in vivo. Our work reveals that cooperativity alleviates the buffering effect within the lipid II cycle, such that much less antibiotic is required to achieve a similar level of target-inhibition compared to a non-cooperatively binding drug (Fig. 4e). Interestingly, our results indicate that the most pronounced advantage of cooperative drug-target binding arises when the buffering effect is large (Fig. 4d), and to our knowledge,

all cooperatively acting antibiotics bind to lipid II, for which this is the case.

Taken together, our theory correctly predicts the in vivo action of five different antibiotics against the Gram-positive model organism *B. subtilis* (Fig. 5). Since our theory is based on cumulative information about lipid II cycle properties in diverse bacterial species, we wondered whether the derived principles also apply to other organisms, including clinically relevant bacteria. Indeed, *S. aureus* strains deprived of all known resistance determinants also display pronounced in vivo efficacy gaps for nisin ( $MIC^{NIS}/K_D^{NIS} = 82$ <sup>13</sup>) and for vancomycin ( $MIC^{VAN}/K_D^{VAN} = 24$ <sup>12</sup>), and also the  $MIC$  of *E. faecalis* against vancomycin exceeds the in vitro dissociation constant 47-fold<sup>14</sup>—all very similar to the values in *B. subtilis* (Fig. 5 and Supplementary Table 4b). Thus, both the in vivo efficacy gap as well as its molecular origin—namely the asymmetric distribution of lipid II cycle intermediates—seem to be conserved between diverse Gram-positive organisms, highlighting the universality of our model.

Besides the prediction of antibiotic susceptibility in vivo, our theory provides clues about physiological features of the lipid II cycle, which have not been experimentally accessible to date. For instance, our quantitative considerations of lipid II cycling put constraints on the enzyme copy numbers, their reaction kinetics and, most notably, on the so far unknown processes of UP and UPP flipping. Here, our analysis indicates that the flipping of UPP from the inner to the outer leaflet of the cytoplasmic membrane is about as fast as lipid II flipping, both of which are >100-fold faster than the flipping of UP from the outer to the



inner leaflet (Supplementary Table 2). Given that the dual negative charge of the UPP headgroup energetically strongly disfavours spontaneous flip-flop between bilayers<sup>67</sup>, such rapid flipping can only be achieved by active UPP transport across the membrane, but a specific UPP flippase has yet to be discovered<sup>68,69</sup>. The 500-fold slower UP flipping suggests that it might follow a passive flip-flop mechanism driven by concentration- and/or charge-gradients, but further experiments are needed to shed light on this.

Another intriguing insight from literature mining was that Gram-negative and -positive bacteria feature similar levels of lipid II cycle-associated enzymes per surface area (Fig. 2b), despite their vastly different demand for peptidoglycan synthesis (Supplementary Table 3a, b). As a consequence, our analysis suggests that the Gram-positive lipid II cycle is driven by faster enzymes, which sacrificed some of their substrate recognition in a speed-affinity trade-off (Fig. 2c). This is consistent with the idea that the increased levels of lipid carrier intermediates found in Gram-positive bacteria are required to saturate these faster enzymes. But why do Gram-positive bacteria not simply produce higher levels of lipid II cycle-associated enzymes to meet this demand? One reason could be that these enzymes are either integral membrane or membrane-associated proteins, such that raising the abundance of the PG synthetic machinery could exceed the carrying capacity of the membrane. Indeed, in *E. coli* the cytoplasmic membrane bears a total of ~33,000 proteins per  $\mu\text{m}^2$ <sup>70,71</sup>, and the sum of all enzymes in the lipid II cycle constitutes ~1–3% of the membrane proteome. Thus, raising the PG synthetic machinery by a factor of 13 to meet the PG demand of Gram-positive bacteria could clearly lead to fitness trade-offs with other essential transport- and biosynthetic processes. Comparative experimental studies of the PG synthetic machinery in Gram-positive and -negative organisms will help to further elucidate the quantitative differences in this rate-limiting step of bacterial cell wall synthesis.

The insights gained here can help guiding the design of new drugs—by suggesting that novel cell wall antibiotics will perturb the lipid II cycle most effectively by (i) binding low-abundant cycle intermediates in a highly cooperative manner or by (ii) targeting the high-abundant intermediate pools. In addition, our model of the lipid II cycle provides the basis for broader analyses of various further classes of cell wall antibiotics, such as drugs inhibiting the enzymes in the lipid II cycle (e.g. beta-lactams inhibiting PBPs) or drugs targeting the substrates of PG precursor production (e.g. fosfomycin). To this end, the model will need to be expanded, e.g., to explicitly incorporate the biochemical characteristics and copy numbers of all redundant PBPs (as opposed to treating them as one effective reaction, as in the present model), highlighting the importance of further biochemical studies of PBPs and other lipid II cycle-associated enzymes for developing a complete systems-level description of this essential cellular pathway. Likewise, the seamless biochemical characterization of enzymes involved in PG precursor synthesis and cell wall recycling will enable quantitative modelling of drugs interfering with these important aspects of cell wall synthesis. Hence, the presented model serves as an excellent starting point to develop a whole-cell model of antibiotic action. One important aspect will be the development of theoretical models describing the regulation and action of known resistance mechanisms (which are deleted in the strains considered in this work), to provide a systems-level description of antibiotic action in wild-type cells. First steps in developing such models have been made, e.g., for the bacitracin resistance determinant BceAB in *B. subtilis*<sup>72</sup> and for beta-lactamases in *S. aureus*<sup>73</sup>. Coupling our theory of wall synthesis with the bacterial growth laws<sup>1,4–6</sup> will lead to new insights into the growth-rate dependency of antibiotic action

and may advance our understanding of antibiotic tolerance of slow- and non-growing cells<sup>74</sup>. Beyond this, a comprehensive model will contribute to a quantitative understanding of whole-cell physiology, which is the starting point to predict drug–drug interactions between antibiotics targeting different physiological pathways. Finally, we believe that such rational approaches to understand the physiological targets of antibiotics are urgently needed to develop novel strategies in our fight against antimicrobial resistance.

## Methods

**Mathematical model of the lipid II cycle.** Our computational model of cell wall synthesis focuses on the core reactions of the lipid II cycle and describes peptidoglycan synthesis for each individual cell (Supplementary Fig. 1c). Time-dependent changes of the pool levels of lipid II cycle intermediates are described by deterministic differential equations to monitor the dynamics of cell wall synthesis. Diverse model assumptions, based on the current state of knowledge about the lipid II cycle, determine the frame of the kinetic model:

- (i) The individual states of lipid carrier are included as time-dependent variables in the model, distinguishing between lipid carriers localised in the inner (IN) and outer (OUT) leaflet of the cytoplasmic membrane:
  - UPP<sub>IN</sub> = internal pool of undecaprenyl pyrophosphate (UPP)
  - UPP<sub>OUT</sub> = external pool of undecaprenyl pyrophosphate
  - UP<sub>IN</sub> = internal pool of undecaprenyl phosphate (UP)
  - UP<sub>OUT</sub> = external pool of undecaprenyl phosphate
  - LI = pool of lipid I
  - LI<sub>IN</sub> = internal pool of lipid II
  - LI<sub>OUT</sub> = external pool of lipid II
- (ii) The cytoplasmic production of soluble PG precursors (UDP-MurNAc-pentapeptide and UDP-GlcNAc) is not described in detail in the model. Since the precursor pool levels are homeostatically controlled<sup>34,35</sup> at sufficiently high levels to saturate the enzymes of the corresponding reactions (Supplementary Table 1), the rate of cell wall synthesis is normally not limited by PG precursor abundance. Although we are well aware that this assumption does not accurately reflect the situation when PG precursor synthesis itself is targeted, e.g. by fosfomycin, it is plausible to assume constant pools of PG precursors when considering antibiotics targeting the membrane-anchored steps of PG synthesis only.
- (iii) The de novo synthesis of UPP in the cytoplasm has to balance the overall growth-driven dilution of all lipid II cycle intermediates. To this end, we assume a constant UPP production rate  $\alpha = \frac{\ln(2)}{T_D} \sum [S_i]$  in the cytoplasm, balancing dilution within one generation time  $T_D$ . Likewise, the growth-dependent dilution of all individual lipid intermediate pools occurs at a rate  $\gamma = \frac{\ln(2)}{T_D}$ .
- (iv) The individual enzymatic reactions are modelled by Michaelis-Menten kinetics, for which substrate levels ( $S_i$ ), enzyme levels ( $E$ ), catalytic constants of the enzymes ( $k_{\text{cat}}$ ) as well as the Michaelis-Menten constants ( $K_M$ ) parameterise the reaction dynamics.
- (v) Since the biochemical properties of the enzymes catalysing the flipping reaction of lipid II (LI<sub>IN</sub> to LI<sub>OUT</sub>) are largely unknown, and the flipping of UPP (UPP<sub>IN</sub> to UPP<sub>OUT</sub>) and UP (UP<sub>OUT</sub> to UP<sub>IN</sub>) was only hypothesised, for parsimony reasons we assumed first order kinetics for these reactions, as quantified by an effective rate constant  $k_i$  ( $i = \text{UP, UPP, LI}$ ).

Under these assumptions the following set of ordinary differential equations describes the time-dependent changes of the lipid II cycle intermediate pools and the concomitant effect on the rate of PG synthesis,  $j_{\text{PG}}$

$$\frac{d[\text{UPP}_{\text{IN}}]}{dt} = \alpha - k_{\text{UPP}}[\text{UPP}_{\text{IN}}] - \gamma[\text{UPP}_{\text{IN}}] \quad (3)$$

$$\begin{aligned} \frac{d[\text{UPP}_{\text{OUT}}]}{dt} = & k_{\text{UPP}}[\text{UPP}_{\text{IN}}] - v_{\text{max}}^{\text{UPP}} \frac{[\text{UPP}_{\text{OUT}}]}{K_M^{\text{UPP}} + [\text{UPP}_{\text{OUT}}]} \\ & + v_{\text{max}}^{\text{PBP}} \frac{[\text{LI}_{\text{OUT}}]}{K_M^{\text{PBP}} + [\text{LI}_{\text{OUT}}]} - \gamma[\text{UPP}_{\text{OUT}}] \end{aligned} \quad (4)$$

$$\frac{d[\text{UP}_{\text{OUT}}]}{dt} = v_{\text{max}}^{\text{UPP}} \frac{[\text{UPP}_{\text{OUT}}]}{K_M^{\text{UPP}} + [\text{UPP}_{\text{OUT}}]} - k_{\text{UP}}[\text{UP}_{\text{OUT}}] - \gamma[\text{UP}_{\text{OUT}}] \quad (5)$$

$$\frac{d[\text{UP}_{\text{IN}}]}{dt} = k_{\text{UP}}[\text{UP}_{\text{OUT}}] - v_{\text{max}}^{\text{MraY}} \frac{[\text{UP}_{\text{IN}}]}{K_M^{\text{MraY}} + [\text{UP}_{\text{IN}}]} - \gamma[\text{UP}_{\text{IN}}] \quad (6)$$

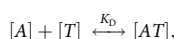
$$\frac{d[\text{LI}]}{dt} = v_{\text{max}}^{\text{MraY}} \frac{[\text{UP}_{\text{IN}}]}{K_M^{\text{MraY}} + [\text{UP}_{\text{IN}}]} - v_{\text{max}}^{\text{MurG}} \frac{[\text{LI}]}{K_M^{\text{MurG}} + [\text{LI}]} - \gamma[\text{LI}] \quad (7)$$

$$\frac{d[\text{LII}_{\text{IN}}]}{dt} = v_{\text{MurG}}^{\text{MurG}} \frac{[\text{LI}]}{K_{\text{M}}^{\text{MurG}} + [\text{LI}]} - k_{\text{LII}}[\text{LII}_{\text{IN}}] - \gamma[\text{LII}_{\text{IN}}] \quad (8)$$

$$\frac{d[\text{LII}_{\text{OUT}}]}{dt} = k_{\text{LII}}[\text{LII}_{\text{IN}}] - v_{\text{max}}^{\text{PBPs}} \frac{[\text{LII}_{\text{OUT}}]}{K_{\text{M}}^{\text{PBPs}} + [\text{LII}_{\text{OUT}}]} - \gamma[\text{LII}_{\text{OUT}}] \quad (9)$$

$$j_{\text{PG}} = v_{\text{max}}^{\text{PBPs}} \frac{[\text{LII}_{\text{OUT}}]}{K_{\text{M}}^{\text{PBPs}} + [\text{LII}_{\text{OUT}}]} \quad (10)$$

**Simulations of antibiotic treatment.** In order to accommodate cell wall antibiotic treatment in the theoretical model of the lipid II cycle, we considered ligand-binding between the antibiotic (*A*) and its target (*T*) (where *T* can be any of the dynamic variables in Eqs. (3–9))

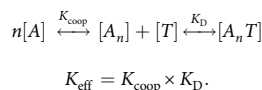


with the in vitro equilibrium dissociation constant  $K_{\text{D}} = \frac{k_{\text{diss}}}{k_{\text{ass}}}$ , defined as the ratio between dissociation and association rate, respectively. Consequently, the model for the lipid II cycle defined in Eqs. (3–10) was extended by one differential equation describing the dynamics of the antibiotic-bound lipid intermediate pool (*AT*),

$$\frac{d[\text{AT}]}{dt} = k_{\text{ass}}[\text{A}][\text{T}] - k_{\text{diss}}[\text{AT}] - \gamma[\text{AT}]. \quad (11)$$

Since the individual dissociation and association rates were rarely studied in vitro, we set the association rate to the fixed value of  $k_{\text{ass}} = 0.75 \mu\text{M}^{-1} \times \text{min}^{-1}$  (as measured for the binding of bacitracin to its target UPP<sup>72</sup>) and calculated the dissociation rates from experimentally determined in vitro dissociation constants  $K_{\text{D}} = \frac{k_{\text{diss}}}{k_{\text{ass}}}$  (Supplementary Table 4a). As we are well aware that association rates can be different for different antibiotics, we subsequently investigated the robustness of our model predictions against variations in the association rates (see Supplementary Note 1; Influence of binding dynamics on the IC<sub>50</sub>).

Given that the five antibiotics analysed here vary in both the binding dynamics (quantified by the  $K_{\text{D}}$  values) as well as the cooperativity of antibiotic-target-interactions (defined by the Hill coefficient *n*) (Supplementary Table 4a), we integrated an effective quantitative description of the multimer formation as well as the antibiotic binding reaction into our model:



Since it was not always clear (e.g. in case of vancomycin) whether the antibiotic multimerisation occurs before or after target-binding, and also the stoichiometry within the antibiotic-target-complex was not always known precisely, we asked if all differential binding scenarios generate cooperativity, i.e. a Hill coefficient  $n > 1$ . To this end, we deduced the Hill expression describing the probability of bound and thereby inactivated target  $P_{\text{bound}}$  from analysing all possible states of antibiotic-target-interaction (Supplementary Fig. 2a, b) and estimated the Hill coefficient *n* arising from this (Supplementary Fig. 2c). Here, the Hill coefficient *n* and thereby the cooperativity reaches its maximum if the dissociation constants of multimer formation and antibiotic binding are comparable, i.e.  $K_{\text{coop}} \approx K_{\text{D}}$ . Obviously, if one of the two reactions dominates the other, that is dimerization is significantly weaker than target binding or vice versa, the effect of cooperativity disappears. Hence, in order to study cooperativity in our model, we took a coarse-grained approach assuming an effective Hill coefficient and binding threshold  $K_{\text{eff}}^n = \frac{k_{\text{diss}}}{k_{\text{ass}}}$ , leading to the following kinetic equation

$$\frac{d[\text{A}_n\text{T}]}{dt} = k_{\text{ass}}[\text{A}]^n[\text{T}] - k_{\text{diss}}[\text{A}_n\text{T}] - \gamma[\text{A}_n\text{T}] \quad (12)$$

Within this expanded model including the quantitative description of antibiotic-target-interaction, we studied the effect of antibiotic action on the lipid II cycle for the five different cell wall antibiotics. In particular, we determined the antibiotic concentration necessary to decrease the PG synthesis rate to its half-maximal level to quantify the antibiotic efficacy and defined this concentration as the IC<sub>50</sub> (Fig. 3a, c and Supplementary Fig. 3a, c, e). Additionally, we analysed the changes in the pool sizes of the different lipid II cycle intermediates *S<sub>i</sub>* under varying antibiotic concentrations (Fig. 3b, d and Supplementary Fig. 3b, d, f).

**Reduced model of the lipid II cycle.** To arrive at an analytical expression for the PG synthesis rate in dependence on the antibiotic concentration, we developed a reduced model of the lipid II cycle (Fig. 4a). Similar to the full model in Eqs. (3–12), the antibiotic (*A*) can bind to its free target (*S<sub>unbound</sub>*) within the lipid II cycle with in vitro dissociation constant  $K_{\text{D}} = \frac{k_{\text{diss}}}{k_{\text{ass}}}$ , leading to a pool of bound target (*S<sub>bound</sub>*), but now the sum of all other, non-target lipid II cycle intermediates are represented as ‘bactoprenol reservoir’ (*S<sub>reservoir</sub>*). For simplifying reasons, the inter-conversion of one species into the other follows first order kinetics, determined by

the equilibrium constant  $K_{\text{G}} = \frac{k_{-1}}{k_1}$ . As in the full model, production of new lipid carriers at rate  $\alpha$  balances the overall growth-driven dilution of all reaction species with rate  $\gamma$ :

$$\frac{d[\text{S}_{\text{reservoir}}]}{dt} = \alpha - k_1[\text{S}_{\text{reservoir}}] + k_{-1}[\text{S}_{\text{unbound}}] - \gamma[\text{S}_{\text{reservoir}}] \quad (13)$$

$$\frac{d[\text{S}_{\text{unbound}}]}{dt} = k_1[\text{S}_{\text{reservoir}}] - k_{-1}[\text{S}_{\text{unbound}}] - k_{\text{ass}}[\text{S}_{\text{unbound}}][\text{A}] + k_{\text{diss}}[\text{S}_{\text{bound}}] - \gamma[\text{S}_{\text{unbound}}] \quad (14)$$

$$\frac{d[\text{S}_{\text{bound}}]}{dt} = k_{\text{ass}}[\text{S}_{\text{unbound}}][\text{A}] - k_{\text{diss}}[\text{S}_{\text{bound}}] - \gamma[\text{S}_{\text{bound}}] \quad (15)$$

Here, we assume that the production of new lipid carriers enriches the bactoprenol reservoir (*S<sub>reservoir</sub>*), and later consider the scenario in which new lipid carriers feed the free target pool (*S<sub>unbound</sub>*), the latter of which is the case for UPP-binding antibiotics. In flux-balance ( $\frac{d}{dt} = 0$ ) the fraction of antibiotic-bound target relative to the total abundance of cycle intermediates ( $S_{\text{TOT}} = S_{\text{reservoir}} + S_{\text{unbound}} + S_{\text{bound}}$ ) is given by

$$\frac{[\text{S}_{\text{bound}}]}{S_{\text{TOT}}} = \frac{[\text{A}]}{[\text{A}] + \frac{\gamma}{k_1} + \tilde{K}_{\text{D}}(1 + \tilde{K}_{\text{G}})},$$

where  $\tilde{K}_{\text{D}} = \frac{k_{\text{diss}} + \gamma}{k_{\text{ass}}}$  and  $\tilde{K}_{\text{G}} = \frac{k_{-1} + \gamma}{k_1}$  are the respective in vivo equilibrium constants. Moreover, when new lipid carriers feed the free target pool, arrive at an analytical solution of a similar form

$$\frac{[\text{S}_{\text{bound}}]}{S_{\text{TOT}}} = \frac{[\text{A}]}{[\text{A}] + \tilde{K}_{\text{D}}(1 + \tilde{K}_{\text{G}})},$$

where  $\tilde{K}_{\text{G}} = \frac{k_{-1}}{k_1 + \gamma}$ . However, as the cycling reactions dominate the de novo synthesis, i.e.  $k_{-1}, k_1 \gg \gamma$  (see Supplementary Note 1; Quantitative considerations of the peptidoglycan synthesis in *E. coli*), both solutions can be approximated by

$$\frac{[\text{S}_{\text{bound}}]}{S_{\text{TOT}}} \approx \frac{[\text{A}]}{[\text{A}] + \tilde{K}_{\text{D}}(1 + \tilde{K}_{\text{G}})},$$

with  $\tilde{K}_{\text{D}} = \frac{k_{\text{diss}} + \gamma}{k_{\text{ass}}}$  and  $\tilde{K}_{\text{G}} \approx \frac{k_{-1}}{k_1}$ . Likewise, the unbound form of the target takes the form

$$\frac{[\text{S}_{\text{unbound}}]}{S_{\text{TOT}}} \approx \frac{\tilde{K}_{\text{D}}}{[\text{A}] + \tilde{K}_{\text{D}}(1 + \tilde{K}_{\text{G}})},$$

such that the relative reduction of the PG synthesis rate in presence of the antibiotic (concentration *[A]*) compared to the unperturbed synthesis rate is

$$\frac{j_{\text{PG}}([\text{A}])}{j_{\text{PG}}([\text{A}] = 0)} = \frac{k_{-1}[\text{S}_{\text{unbound}}]_{[\text{A}]}}{k_{-1}[\text{S}_{\text{unbound}}]_{[\text{A}] = 0}} = \frac{\tilde{K}_{\text{D}}(1 + \tilde{K}_{\text{G}})}{[\text{A}] + \tilde{K}_{\text{D}}(1 + \tilde{K}_{\text{G}})}.$$

When incorporating cooperative drug-target binding as in Eq. (12), we analogously obtain

$$\frac{j_{\text{PG}}([\text{A}])}{j_{\text{PG}}([\text{A}] = 0)} = \frac{\tilde{K}_{\text{D}}^n(1 + \tilde{K}_{\text{G}})}{[\text{A}]^n + \tilde{K}_{\text{D}}^n(1 + \tilde{K}_{\text{G}})},$$

representing the key result for in vivo antibiotic action in the main text. Thus, the half-maximal rate  $j_{\text{PG}}$  is reached at an antibiotic concentration

$$[\text{A}] = \text{IC}_{50} = \tilde{K}_{\text{D}} \sqrt[n]{1 + \tilde{K}_{\text{G}}}. \text{ Given that in the absence of the antibiotic}$$

$\tilde{K}_{\text{G}} \approx \frac{k_{-1}}{k_1} \approx \frac{[\text{S}_{\text{reservoir}}]}{[\text{S}_{\text{target}}]}$ , the IC<sub>50</sub> clearly scales with the *n*-th root of the ratio between bactoprenol reservoir and target pool in the absence of antibiotic (*S<sub>target</sub>*).

Finally, taking cycling rates and pool level distributions equal to the full model into account, we show that the reduced model reproduces the model predictions of the full model (Supplementary Fig. 3g). The only subtle differences arise from the fact that the reduced model considers first order kinetics, leading to a linear dependency between the lipid pool sizes and the individual fluxes from one intermediate to the next. Consequently, a reduction of the pool sizes to 50% of their maxima by antibiotic binding directly leads to a half-maximal rate of PG synthesis. In contrast, the Michaelis-Menten kinetics implemented in the full model features saturation effects. Since the pool levels of lipid carrier are on the same order as the  $K_{\text{M}}$  values of the respective enzymes (Supplementary Table 1), most enzymes are on the brink of saturation, indicating that there is not necessarily linear dependency between the flux from substrate to product pool and substrate levels. Indeed, the substrate pools have to be reduced by slightly more than 50% to concomitantly reach a halved PG synthesis rate, requiring slightly higher antibiotic concentrations as predicted from the simplified scenario (Supplementary Fig. 3g).

**Model simulations and parameter fitting.** The numerical solution of the differential equations and all simulations were performed with custom scripts developed in MATLAB<sup>TM</sup> R2017b software (The MathWorks, Inc.). To constrain the model to a physiological parameter regime we followed the rationale detailed in the Supplementary Note 1. These constraints lead to eleven objective functions

with seven unknown parameters. To solve this over-determined non-linear data-fitting problem, we used the function *lsqnonlin* imbedded in the MATLAB<sup>TM</sup> software, solving nonlinear least-squares curve fitting problems of the form

$$\min \|f(x)\|_2^2 = \min (f_1(x)^2 + f_2(x)^2 + \dots + f_n(x)^2).$$

by using a trust-region-reflective Newton algorithm. As outputs, it returns the optimum  $\bar{x}$  of the problem as well as the squared 2-norm  $\chi^2$  of the residual at  $\bar{x}$  ( $\chi^2 = \sum f(\bar{x})^2$ ). To account for the presence of local optima, 100 independent fits were performed with randomly chosen initial parameter sets. Eventually, the best-fit result (minimal  $\chi^2$ ) was defined as the final parameter set (Supplementary Table 2).

**Reporting summary.** Further information on research design is available in the Nature Research Reporting Summary linked to this article.

## Data availability

The authors declare that the data supporting the findings of this study are available within the paper and its supplementary information files.

## Code availability

Matlab code used in this project for data analysis is available from the corresponding author upon reasonable request.

Received: 16 January 2019 Accepted: 23 May 2019

Published online: 21 June 2019

## References

- Greulich, P., Scott, M., Evans, M. R. & Allen, R. J. Growth-dependent bacterial susceptibility to ribosome-targeting antibiotics. *Mol. Syst. Biol.* **11**, 796 (2015).
- Deris, J. B. et al. The innate growth bistability and fitness landscapes of antibiotic-resistant bacteria. *Science* **342**, 1237435 (2013).
- Bollenbach, T., Quan, S., Chait, R. & Kishony, R. Nonoptimal microbial response to antibiotics underlies suppressive drug interactions. *Cell* **139**, 707–718 (2009).
- Klumpp, S., Zhang, Z. & Hwa, T. Growth rate-dependent global effects on gene expression in bacteria. *Cell* **139**, 1366–1375 (2009).
- Klumpp, S. & Hwa, T. Bacterial growth: global effects on gene expression, growth feedback and proteome partition. *Curr. Opin. Biotechnol.* **28**, 96–102 (2014).
- Scott, M., Klumpp, S., Mateescu, E. M. & Hwa, T. Emergence of robust growth laws from optimal regulation of ribosome synthesis. *Mol. Syst. Biol.* **10**, 747–747 (2014).
- Kahne, D., Leimkuhler, C., Lu, W. & Walsh, C. Glycopeptide and lipoglycopeptide antibiotics. *Chem. Rev.* **105**, 425–448 (2005).
- Breukink, E. & de Kruijff, B. Lipid II as a target for antibiotics. *Nat. Rev. Drug. Discov.* **5**, 321–332 (2006).
- Mota-Meira, M., LaPointe, G., Lacroix, C. & Lavoie, M. C. MICs of mutacin B-Ny266, nisin A, vancomycin, and oxacillin against bacterial pathogens. *Antimicrob. Agents Chemother. (Bethesda)* **44**, 24–29 (2000).
- Tiyanont, K. et al. Imaging peptidoglycan biosynthesis in *Bacillus subtilis* with fluorescent antibiotics. *Proc. Natl Acad. Sci. USA* **103**, 11033–11038 (2006).
- Staroń, A., Finkeisen, D. E. & Mascher, T. Peptide antibiotic sensing and detoxification modules of *Bacillus subtilis*. *Antimicrob. Agents Chemother. (Bethesda)* **55**, 515–525 (2011).
- Yoshida, Y. et al. Bacitracin sensing and resistance in *Staphylococcus aureus*. *FEMS Microbiol. Lett.* **320**, 33–39 (2011).
- Hiron, A., Falord, M., Valle, J., Débarbouillé, M. & Msadek, T. Bacitracin and nisin resistance in *Staphylococcus aureus*: a novel pathway involving the BraS/BraR two-component system (SA2417/SA2418) and both the BraD/BraE and VraD/VraE ABC transporters. *Mol. Microbiol.* **81**, 602–622 (2011).
- Shaaly, A., Kalamorz, F., Gebhard, S. & Cook, G. M. Undecaprenyl pyrophosphate phosphatase confers low-level resistance to bacitracin in *Enterococcus faecalis*. *J. Antimicrob. Chemother.* **68**, 1583–1593 (2013).
- Beauregard, D. A., Maguire, A. J., Williams, D. H. & Reynolds, P. E. Semiquantitation of cooperativity in binding of vancomycin-group antibiotics to vancomycin-susceptible and -resistant organisms. *Antimicrob. Agents Chemother. (Bethesda)* **41**, 2418–2423 (1997).
- Wiedemann, I. et al. Specific binding of nisin to the peptidoglycan precursor lipid II combines pore formation and inhibition of cell wall biosynthesis for potent antibiotic activity. *J. Biol. Chem.* **276**, 1772–1779 (2001).
- Hu, Y., Helm, J. S., Chen, L., Ye, X.-Y. & Walker, S. Ramoplanin inhibits bacterial transglycosylases by binding as a dimer to lipid II. *J. Am. Chem. Soc.* **125**, 8736–8737 (2003).
- Good, V. M., Gwynn, M. N. & Knowles, D. MM 45289, a potent glycopeptide antibiotic which interacts weakly with diacetyl-L-lysyl-D-alanyl-D-alanine. *J. Antibiot.* **43**, 550–555 (1990).
- van Heijenoort, J. Murein synthesis. In *Escherichia coli and Salmonella*. (eds Neidhardt, F. C., et al.) 1025–1034 (ASM Press, Washington, DC, 1996)
- Schneider, T. & Sahl, H.-G. An oldie but a goodie—cell wall biosynthesis as antibiotic target pathway. *Int. J. Med. Microbiol.* **300**, 161–169 (2010).
- Groves, P., Searle, M. S., Mackay, J. P. & Williams, D. H. The structure of an asymmetric dimer relevant to the mode of action of the glycopeptide antibiotics. *Structure* **2**, 747–754 (1994).
- Beauregard, D. A., Williams, D. H., Gwynn, M. N. & Knowles, D. Dimerization and membrane anchors in extracellular targeting of vancomycin group antibiotics. *Antimicrob. Agents Chemother. (Bethesda)* **39**, 781–785 (1995).
- Thamri, A. et al. Peptide modification results in the formation of a dimer with a 10-fold enhanced antimicrobial activity. *PLoS. One.* **12**, e0173783 (2017).
- Schleifer, K. H. & Kandler, O. Peptidoglycan types of bacterial cell walls and their taxonomic implications. *Bacteriol. Rev.* **36**, 407–477 (1972).
- Harz, H., Burgdorf, K. & Hölte, J.-V. Isolation and separation of the glycan strands from murein of *Escherichia coli* by reversed-phase high-performance liquid chromatography. *Anal. Biochem.* **190**, 120–128 (1990).
- Müñch, D. & Sahl, H.-G. Structural variations of the cell wall precursor lipid II in Gram-positive bacteria—Impact on binding and efficacy of antimicrobial peptides. *Biochim. Biophys. Acta* **1848**, 3062–3071 (2015).
- Tomasz, A. The mechanism of the irreversible antimicrobial effects of penicillins: how the beta-lactam antibiotics kill and lyse bacteria. *Annu. Rev. Microbiol.* **33**, 113–137 (1979).
- Kohanski, M. A., Dwyer, D. J. & Collins, J. J. How antibiotics kill bacteria: from targets to networks. *Nat. Publ. Group* **8**, 423–435 (2010).
- Mengin-Lecreulx, D. & van Heijenoort, J. Effect of growth conditions on peptidoglycan content and cytoplasmic steps of its biosynthesis in *Escherichia coli*. *J. Bacteriol.* **163**, 208–212 (1985).
- Goodell, E. W. & Schwarz, U. Release of cell wall peptides into culture medium by exponentially growing *Escherichia coli*. *J. Bacteriol.* **162**, 391–397 (1985).
- Goodell, E. W. Recycling of murein by *Escherichia coli*. *J. Bacteriol.* **163**, 305–310 (1985).
- van Heijenoort, Y., Gómez, M., Derrien, M., Ayala, J. & van Heijenoort, J. Membrane intermediates in the peptidoglycan metabolism of *Escherichia coli*: possible roles of PBP 1b and PBP 3. *J. Bacteriol.* **174**, 3549–3557 (1992).
- Barreteau, H. et al. Quantitative high-performance liquid chromatography analysis of the pool levels of undecaprenyl phosphate and its derivatives in bacterial membranes. *J. Chromatogr. B. Anal. Technol. Biomed. Life. Sci.* **877**, 213–220 (2009).
- Mengin-Lecreulx, D., Flouret, B. & van Heijenoort, J. Cytoplasmic steps of peptidoglycan synthesis in *Escherichia coli*. *J. Bacteriol.* **151**, 1109–1117 (1982).
- Mengin-Lecreulx, D., Flouret, B. & van Heijenoort, J. Pool levels of UDP N-acetylglucosamine and UDP N-acetylglucosamine-enolpyruvate in *Escherichia coli* and correlation with peptidoglycan synthesis. *J. Bacteriol.* **154**, 1284–1290 (1983).
- Li, G.-W., Burkhardt, D., Gross, C. A. & Weissman, J. S. Quantifying absolute protein synthesis rates reveals principles underlying allocation of cellular resources. *Cell* **157**, 624–635 (2014).
- Mohammadi, T. et al. Identification of FtsW as a transporter of lipid-linked cell wall precursors across the membrane. *EMBO J.* **30**, 1425–1432 (2011).
- Sham, L.-T. et al. MurJ is the flippase of lipid-linked precursors for peptidoglycan biogenesis. *Science* **345**, 220–222 (2014).
- Meeske, A. J. et al. MurJ and a novel lipid II flippase are required for cell wall biogenesis in *Bacillus subtilis*. *Proc Natl Acad. Sci. USA* **112**, 6437–6442 (2015).
- Labischinski, H., Goodell, E. W., Goodell, A. & Hochberg, M. L. Direct proof of a more-than-single-layered peptidoglycan architecture of *Escherichia coli* W7: a neutron small-angle scattering study. *J. Bacteriol.* **173**, 751–756 (1991).
- Muntel, J. et al. Comprehensive absolute quantification of the cytosolic proteome of *Bacillus subtilis* by data independent, parallel fragmentation in liquid chromatography/mass spectrometry (LC/MS(E)). *Mol. Cell. Proteom.* **13**, 1008–1019 (2014).
- Bouhss, A., Crouvoisier, M., Blanot, D. & Mengin-Lecreulx, D. Purification and characterization of the bacterial MraY translocase catalyzing the first membrane step of peptidoglycan biosynthesis. *J. Biol. Chem.* **279**, 29974–29980 (2004).
- Brandish, P. E. et al. Slow binding inhibition of phospho-N-acetylmuramyl-pentapeptide-translocase (*Escherichia coli*) by mureidomycin A. *J. Biol. Chem.* **271**, 7609–7614 (1996).
- Meyer, J. R., Gudelj, I. & Beardmore, R. Biophysical mechanisms that maintain biodiversity through trade-offs. *Nat. Commun.* **6**, 6278 (2015).



45. Bosdriesz, E. et al. Low affinity uniporter carrier proteins can increase net substrate uptake rate by reducing efflux. *Sci. Rep.* **8**, 5576 (2018).
46. Economou, N. J., Cocklin, S. & Loll, P. J. High-resolution crystal structure reveals molecular details of target recognition by bacitracin. *Proc. Natl Acad. Sci. USA* **110**, 14207–14212 (2013).
47. Storm, D. R. & Strominger, J. L. Complex formation between bacitracin peptides and isoprenyl pyrophosphates. The specificity of lipid-peptide interactions. *J. Biol. Chem.* **248**, 3940–3945 (1973).
48. 't Hart, P., Oppedijk, S. F., Breukink, E. & Martin, N. I. New insights into nisin's antibacterial mechanism revealed by binding studies with synthetic lipid II analogues. *Biochemistry* **55**, 232–237 (2016).
49. Radeck, J. et al. Anatomy of the bacitracin resistance network in *Bacillus subtilis*. *Mol. Microbiol.* **100**, 607–620 (2016).
50. Wiedemann, I., Benz, R. & Sahl, H.-G. Lipid II-mediated pore formation by the peptide antibiotic nisin: a black lipid membrane study. *J. Bacteriol.* **186**, 3259–3261 (2004).
51. Oppedijk, S. F., Martin, N. I. & Breukink, E. Hit 'em where it hurts: The growing and structurally diverse family of peptides that target lipid-II. *Biochim. Biophys. Acta* **1858**, 947–957 (2016).
52. Loll, P. J., Miller, R., Weeks, C. M. & Axelsen, P. H. A ligand-mediated dimerization mode for vancomycin. *Chem. Biol.* **5**, 293–298 (1998).
53. Jia, Z., O'Mara, M. L., Zuegg, J., Cooper, M. A. & Mark, A. E. Vancomycin: ligand recognition, dimerization and super-complex formation. *Febs. J.* **280**, 1294–1307 (2013).
54. Wang, F., Zhou, H., Olademehin, O. P., Kim, S. J. & Tao, P. Insights into key interactions between vancomycin and bacterial cell wall structures. *ACS Omega* **3**, 37–45 (2018).
55. Perkins, H. R. Specificity of combination between mucopeptide precursors and vancomycin or ristocetin. *Biochem. J.* **111**, 195–205 (1969).
56. Schäfer, M., Schneider, T. & Sheldrick, G. M. Crystal structure of vancomycin. *Structure* **4**, 1509–1515 (1996).
57. Schneider, T. et al. The lipopeptide antibiotic Friulimicin B inhibits cell wall biosynthesis through complex formation with bactoprenol phosphate. *Antimicrob. Agents Chemother. (Bethesda)* **53**, 1610–1618 (2009).
58. Wecke, T. et al. Daptomycin versus Friulimicin B: in-depth profiling of *Bacillus subtilis* cell envelope stress responses. *Antimicrob. Agents Chemother. (Bethesda)* **53**, 1619–1623 (2009).
59. Michel, J.-B., Yeh, P. J., Chait, R., Moellering, R. C. & Kishony, R. Drug interactions modulate the potential for evolution of resistance. *Proc Natl Acad. Sci. USA* **105**, 14918–14923 (2008).
60. Chevereau, G. & Bollenbach, T. Systematic discovery of drug interaction mechanisms. *Mol. Syst. Biol.* **11**, 807 (2015).
61. Brochado, A. R. et al. Species-specific activity of antibacterial drug combinations. *Nature* **559**, 259–263 (2018).
62. Rogers, L. A. The inhibiting effect of *Streptococcus lactis* on *Lactobacillus bulgaricus*. *J. Bacteriol.* **16**, 321–325 (1928).
63. Levine, D. P. Vancomycin: a history. *Clin. Infect. Dis.* **42**(Suppl 1), S5–S12 (2006).
64. Millette, M., Dupont, C., Archambault, D. & Lacroix, M. Partial characterization of bacteriocins produced by human *Lactococcus lactis* and *Pediococcus acidilactici* isolates. *J. Appl. Microbiol.* **102**, 274–282 (2007).
65. de la Cruz, M. et al. Production of ramoplanin and ramoplanin analogs by Actinomycetes. *Front. Microbiol.* **8**, 343 (2017).
66. Williams, D. H., Maguire, A. J., Tsuzuki, W. & Westwell, M. S. An analysis of the origins of a cooperative binding energy of dimerization. *Science* **280**, 711–714 (1998).
67. Kol, M. A. et al. Phospholipid flop induced by transmembrane peptides in model membranes is modulated by lipid composition. *Biochemistry* **42**, 231–237 (2003).
68. Touzé, T., Blanot, D. & Mengin-Lecreux, D. Substrate specificity and membrane topology of *Escherichia coli* PgpB, an undecaprenyl pyrophosphate phosphatase. *J. Biol. Chem.* **283**, 16573–16583 (2008).
69. Manat, G. et al. Membrane topology and biochemical characterization of the *Escherichia coli* BacA undecaprenyl-pyrophosphate phosphatase. *PLoS ONE* **10**, e0142870 (2015).
70. Kadner, R. J. Cytoplasmic membrane. In *Escherichia coli and Salmonella*. (eds Neidhardt, F. C., et al.) 58–87 (ASM Press, Washington, DC, 1996).
71. Neidhardt, F. C. & Umbarger, H. E. Chemical composition of *Escherichia coli*. In *Escherichia coli and Salmonella*. (eds Neidhardt, F. C., Curtiss, R., Ingraham, J. L., Lin, E. C. C., Brooks Low, K., Magasanik, B., et al.) 13–16 (ASM Press, Washington, DC, 1996).
72. Fritz, G. et al. A new way of sensing: need-based activation of antibiotic resistance by a flux-sensing mechanism. *mBio* **6**, e00975–15 (2015).
73. Murphy, J. T., Walshe, R. & Devocelle, M. A computational model of antibiotic-resistance mechanisms in methicillin-resistant *Staphylococcus aureus* (MRSA). *J. Theor. Biol.* **254**, 284–293 (2008).
74. Brauner, A., Fridman, O., Gefen, O. & Balaban, N. Q. Distinguishing between resistance, tolerance and persistence to antibiotic treatment. *Nat. Publ. Group* **14**, 320–330 (2016).
75. van Heijenoort, J. Lipid intermediates in the biosynthesis of bacterial peptidoglycan. *Microbiol. Mol. Biol. Rev.* **71**, 620–635 (2007).
76. Barreteau, H. et al. Cytoplasmic steps of peptidoglycan biosynthesis. *FEMS Microbiol. Rev.* **32**, 168–207 (2008).
77. Tatar, L. D., Marolda, C. L., Polischuk, A. N., van Leeuwen, D. & Valvano, M. A. An *Escherichia coli* undecaprenyl-pyrophosphate phosphatase implicated in undecaprenyl phosphate recycling. *Microbiology* **153**, 2518–2529 (2007).
78. Chang, H.-Y., Chou, C.-C., Hsu, M.-F. & Wang, A. H. J. Proposed carrier lipid-binding site of undecaprenyl pyrophosphate phosphatase from *Escherichia coli*. *J. Biol. Chem.* **289**, 18719–18735 (2014).
79. Gebhard, S. et al. Identification and characterization of a bacitracin resistance network in *Enterococcus faecalis*. *Antimicrob. Agents Chemother. (Bethesda)* **58**, 1425–1433 (2014).
80. Fritz, G. et al. Induction kinetics of a conditional pH stress response system in *Escherichia coli*. *J. Mol. Biol.* **393**, 272–286 (2009).

## Acknowledgements

We thank Susanne Gebhard and Peter Graumann for discussion and suggestions. The research was supported via the Cusanuswerk scholarship programme (Germany), a grant from the Deutsche Forschungsgemeinschaft (DFG, Germany; grant FR3673/1-2) and the LOEWE programme of the State of Hesse (Germany).

## Author contributions

H.P. and G.F. designed research. H.P. performed research and analysed data with input from A.D. and G.F. All authors wrote the manuscript.

## Additional information

**Supplementary Information** accompanies this paper at <https://doi.org/10.1038/s41467-019-10673-4>.

**Competing interests:** The authors declare no competing interests.

**Reprints and permission** information is available online at <http://npg.nature.com/reprintsandpermissions/>

**Peer review information:** *Nature Communications* thanks the anonymous reviewers for their contribution to the peer review of this work. Peer reviewer reports are available.

**Publisher's note:** Springer Nature remains neutral with regard to jurisdictional claims in published maps and institutional affiliations.



**Open Access** This article is licensed under a Creative Commons Attribution 4.0 International License, which permits use, sharing, adaptation, distribution and reproduction in any medium or format, as long as you give appropriate credit to the original author(s) and the source, provide a link to the Creative Commons license, and indicate if changes were made. The images or other third party material in this article are included in the article's Creative Commons license, unless indicated otherwise in a credit line to the material. If material is not included in the article's Creative Commons license and your intended use is not permitted by statutory regulation or exceeds the permitted use, you will need to obtain permission directly from the copyright holder. To view a copy of this license, visit <http://creativecommons.org/licenses/by/4.0/>.

© The Author(s) 2019



## Supplementary Information

### Minimal exposure of lipid II cycle intermediates triggers cell wall antibiotic resistance

Piepenbreier *et al.*

#### Content

##### Supplementary Note 1

**Supplementary Figure 1:** Calibration of the theoretical model of the lipid II cycle in *E. coli*.

**Supplementary Figure 2:** Different multimeric binding scenarios lead to cooperative antibiotic-target-interaction.

**Supplementary Figure 3:** Theory predicts a moderate *in vivo* efficacy gap for friulimicin and a more pronounced difference between  $IC_{50}$  and  $K_D$  for vancomycin and ramoplanin.

**Supplementary Figure 4:** Model predictions of the *in vivo* efficacy gap are robust against variations in the model parameters.

**Supplementary Figure 5.** Sensitivity of predicted  $IC_{50}$  values on changes of experimentally determined model parameters.

**Supplementary Table 1:** Model calibration.

**Supplementary Table 2:** Parameter fitting and validation.

**Supplementary Table 3:** Comparison between *E. coli* and *B. subtilis*.

**Supplementary Table 4:** Antibiotic activity in *B. subtilis*.

##### Supplementary References

## Supplementary Note 1

### Quantitative considerations on peptidoglycan synthesis in *E. coli*

The rate of peptidoglycan (PG) production in the studied organisms was estimated based on experimentally determined total number of peptidoglycan monomers per cell. The cell wall of *E. coli* comprises of ~1.5 layers of PG (1), containing  $3.5 \times 10^6$  PG monomers (GlcNAc-MurNAc-pentapeptides) in total (2). However, a significant portion  $\delta$  of PG is degraded by hydrolases during cell growth. Accordingly, since a cell wall turnover of ~50% was observed (3, 4), within one doubling time a total number of  $5.25 \times 10^6$  monomers of PG has to be translocated across the cytoplasmic membrane in order to satisfy the demand of PG of one *E. coli* cell. Hence, for a doubling time  $T_D$  of 36 min (corresponding to the measured amount of PG monomers (2)), the rate of PG synthesis is given by:

$$\begin{aligned} j_{PG} &= (1 + \delta) \times (\text{PG monomers per cell}) \times \frac{\ln(2)}{T_D} \\ &= 3.5 \times 10^6 \text{ PG monomers cell}^{-1} \times 1.5 \times \frac{\ln(2)}{36 \text{ min}} = 1.01 \times 10^5 \text{ PG monomers cell}^{-1} \text{ min}^{-1} \end{aligned}$$

Given that the lipid II cycle (Fig. 1a) is the major pathway of PG synthesis, the transition time of individual carriers through all states of the cycle determines the rate of PG monomer transport across the cytoplasmic membrane. We derived this transition time from assuming a closed-loop system of cyclic reactions – showing subsequently the validity of this assumption by assessing the relevance of *de novo* synthesis of individual carriers (Supplementary Fig. 1a). In such a closed-loop system, all substrate pools of the individual reactions equilibrate such that the individual fluxes - defined as the actual number of reactions occurring per time interval - are identical and, in particular, equal to the PG synthesis rate. Accordingly, by transitioning through the different states of the cycle, the dwell time of individual intermediates in every state differs, based on the speed of the subsequent enzymatic reaction (Supplementary Fig. 1b). More precisely, in highly efficient enzymatic reactions, catalyzed by enzymes with elevated catalytic rates or with high enzyme abundances, a substrate is converted into the product state much faster and, consequently, dwells much shorter in the substrate state, than in less efficient reactions. This governs the distribution of the pool levels within the cycle and leads to small substrate pools for fast enzymatic reactions and an accumulation of substrates for reactions catalyzed by slower or less enzymes (compare Supplementary Table 1a). Hence, the time one carrier molecule needs to complete a full round in the lipid II cycle was calculated from the dwell times within every intermediate state (Supplementary Fig. 1b). Considering the simplest scenario, the flux from one state into the next one,  $j_i$ , depends on the substrate levels ( $S_i$ ) and the speed of the reactions ( $k_i$ ) and is equal to the PG synthesis rate  $j_{PG}$ , as mentioned before

$$j_i = j_{PG} \sim k_i [S_i]$$

This assumption of a proportional dependency of the flux from the substrate pools is valid in the case of first order kinetics or sub-saturated enzyme reactions. For highly saturated enzyme reactions, the flux is unaffected from the substrate pools but directly dependent on maximal velocity of the enzyme. As shown in Supplementary Table 1 and discussed later in detail (see section *Simplified model of the lipid II cycle* in Methods), the enzymes in the lipid II cycle operate on the brink of saturation, where the actual substrate pools still have a significant impact on the fluxes. Hence, the rate ( $k_i$ ) at which a single molecule reacts from substrate state to product state is

$$k_i = \frac{j_{PG}}{[S_i]}$$

and the dwell time ( $t_i$ ) within the substrate state is given by

$$t_i = \frac{1}{k_i}$$

Finally, the total time ( $t_{\text{tot}}$ ) one carrier molecule needs to complete a full round of the cycle is the sum of all dwell times in the individual states

$$t_{\text{tot}} = \sum t_i = \sum \frac{1}{k_i} = \sum \frac{[S_i]}{j_{\text{PG}}} = \frac{\sum [S_i]}{j_{\text{PG}}}.$$

Considering the PG synthesis rate of  $1.01 \times 10^5$  molecules per minute and the sum of all lipid II carrier molecules in the individual states ( $\sum [S_i] \sim 1.5 \times 10^5$  molecules; Supplementary Table 1a), a full transport cycle requires  $\sim 90$  seconds (Supplementary Fig. 1b).

In the full *in vivo* scenario, the *de novo* production of UPP in the cytoplasm and the dilution of all lipid II cycle intermediates create a non-trivial system of PG synthesis different from the considered closed-loop assumption (Supplementary Fig. 1a). In order to assess the validity of the principles derived from the closed-loop system for the *in vivo* scenario, we evaluated the impact of carrier (re-)cycling and *de novo* synthesis on PG synthesis. As detailed in the section below, the *de novo* synthesis of UPP balances the increasing demand of lipid carrier during bacterial growth. In particular, total amount of lipid II cycle intermediates has to be reproduced during one doubling time to satisfy the PG demand of both daughter cells. Accordingly, each individual lipid carrier molecule has to be produced once during one doubling time, that is within 36 min in *E. coli*. However, since a complete round takes approximately 1.5 minutes, each individual lipid carrier molecule can undergo 24 transport cycles within this time frame. Consequently, each lipid carrier is replenished by *de novo* synthesis due to cell growth not until 24 rounds of cycling, highlighting carrier recycling as the dominant process driving PG monomer transport across the cytoplasmic membrane. Thus, the assumption of a closed-loop system is a good approximation of the *in vivo* scenario, and can therefore help to rationalize the quantitative behavior of our full theoretical model of peptidoglycan biosynthesis.

### Calibration of the mathematical model for *E. coli*

To identify physiologically relevant parameter values for the model in Eqs. (1-8) given in the Methods, we mined the literature for biochemical characterizations of the involved enzymes (Supplementary Table 1b). Since part of the reactions in the lipid II cycle are catalyzed by a single enzyme (e.g. MraY or MurG), the corresponding  $K_M$  values were directly used in the mathematical model. For all reactions catalyzed by several enzymes we found  $K_M$  values for at least one of the redundant enzymes, and, for parsimony reasons, fixed the parameters of our model to these values. In doing so, we assume that all PBPs and UppPs operate at similar, effective substrate levels determined by these  $K_M$  values. However, given that the enzyme catalytic rates,  $k_{\text{cat}}$ , as well as the precise enzyme abundances,  $[E]$ , were only partially characterized (Supplementary Table 2), and that the effective flipping rates  $k_i$  were unknown altogether, we determined these missing parameters via a constrained optimization approach. To this end we optimized the maximal velocities ( $v_{\text{max}} = k_{\text{cat}} \times [E]$ ) and  $k_i$ 's for each reaction in Eqs. (1-8) given in the Methods, while matching 3 physiological constraints, as detailed in below, and later performing plausibility tests for the resulting parameter values. The physiological constraints are:

- (i) While the precise distribution lipid II cycle intermediates in the outer and inner leaflet of the cytoplasmic membrane was unknown, the total pool levels (sum of outer and inner sub-pool) of all individual lipid carriers were determined experimentally during balanced growth (Supplementary Table 1a). This imposes constraints on the equilibrium values of the total lipid carrier pool levels in Model-Eqs. (1-8):

$$\begin{aligned} \text{UPP}_{\text{IN}} + \text{UPP}_{\text{OUT}} &= \text{UPP}_{\text{TOT}} = 1.2 \times 10^5 \text{ molecules per cell} \\ \text{UP}_{\text{IN}} + \text{UP}_{\text{OUT}} &= \text{UP}_{\text{TOT}} = 3.2 \times 10^4 \text{ molecules per cell} \\ \text{LII}_{\text{IN}} + \text{LII}_{\text{OUT}} &= \text{LII}_{\text{TOT}} = 1000 \text{ molecules per cell} \\ \text{LI} &= \text{LI}_{\text{TOT}} = 700 \text{ molecules per cell} \end{aligned}$$

- (ii) During balanced growth, all fluxes  $j_i$  from one state of the cycle to the next have to be identical and need to equal the PG synthesis rate,  $j_{PG}$ . Consequently, flux balance requires that individual fluxes match the physiological estimate for the overall PG demand, i.e.

$$j_i = v_{\max} \frac{[S_i]}{K_M + [S_i]} = j_{PG} = 1.01 \times 10^5 \text{ molecules per minute}$$

for the enzymatic reactions and

$$j_i = k_i[S_i] = j_{PG} = 1.01 \times 10^5 \text{ molecules per minute}$$

for the flipping reactions for UP and lipid II.

- (iii) Given that UPP is synthesized in the cytoplasm and then fed into the cycle by flipping from the inner to the outer leaflet of the membrane, this flipping rate is not constrained by the rate of PG synthesis itself. However, if flipping of UPP to the external leaflet would be too slow, UPP carriers would be diluted by cell growth before entering the cycle. Therefore, it seemed plausible that cells flip UPP to the external leaflet at a rate comparable to *de novo* UPP synthesis in the cytoplasm. Under this constraint of 'efficient carrier usage', we demanded the rate of UPP flipping is equal to the rate of *de novo* synthesis required to keep the total lipid carrier pool  $\sum[S_i]$  at a constant level, i.e.

$$k_{\text{UPP}}[\text{UPP}_{\text{IN}}] = \alpha = \frac{\ln(2)}{T_D} \sum [S_i].$$

Ultimately, the parameters of the resulting set of equations and constraints were determined with a non-linear optimization approach (for further details of the algorithm see section *Parameter fitting algorithm*), providing an optimal set of parameters (Supplementary Table 2, Supplementary Fig. 1d), as well as an estimate for the variances and co-variances of individual parameters (Supplementary Fig. 1d). Furthermore, as the fitted parameters set the speed of the cycle reactions, they determine the distribution of the different lipid II cycle intermediates in the external and internal leaflet of the cytoplasmic membrane shown in the main text (Fig. 2a). The uncertainties in optimal parameters have only a moderate influence on the predicted distribution of individual lipid II cycle intermediate pool levels (Supplementary Fig. 4b), which in turn does not significantly affect our key results concerning the model predictions of the  $IC_{50}$  for different antibiotics (Supplementary Fig. 4a).

### Quantitative considerations on peptidoglycan synthesis in *B. subtilis*

The PG demand of a single cell is determined by the size of the cell, in particular the cell surface area, and the number of PG layers that make up the cell wall. While the cell wall of *E. coli* comprises  $\sim 1.5$  PG layers on average (1), *B. subtilis* features a PG thickness of about 20 layers (7), clearly leading to a raised demand of PG per unit of cell surface area in the latter. When further considering that at similar doubling times ( $T_D^{B.subtilis} = 40$  min vs.  $T_D^{E.coli} = 36$  min) the cell size and thereby cell surface area of *B. subtilis* is slightly higher compared to *E. coli* (Supplementary Table 3a), the theoretical demand of PG in *B. subtilis* is

$$PG_{\text{TOT}}^{B.subtilis} = PG_{\text{TOT}}^{E.coli} \times R_T \times R_A,$$

with  $R_T = \frac{\text{cell wall thickness}^{B.subtilis}}{\text{cell wall thickness}^{E.coli}}$  defining the ratio between the thickness of the cell wall in Gram-positive and Gram-negative organisms and  $R_A = \frac{\text{surface area}^{B.subtilis}}{\text{surface area}^{E.coli}}$  taking the ratios of cell surface areas between both organisms into account. To further factor in the slight differences in generation times (Supplementary Table 3a), the PG synthesis rate in *B. subtilis* is

$$\begin{aligned}
j_{PG}^{B.subtilis} &= PG_{TOT}^{B.subtilis} \times \frac{\ln(2)}{T_D^{B.subtilis}} \\
&= PG_{TOT}^{E.coli} \times R_T \times R_A \times \frac{\ln(2)}{T_D^{B.subtilis}} \\
&= j_{PG}^{E.coli} \times R_T \times R_A \times \frac{1}{R_G}
\end{aligned}$$

with  $R_G = \frac{T_D^{B.subtilis}}{T_D^{E.coli}}$ . Ultimately, for *B. subtilis* this leads to a PG production rate of  $\sim 1.85 \times 10^6$  molecules  $\text{min}^{-1}$  (Supplementary Table 3a). To meet this higher PG demand we thus adapted all individual fluxes within the cycle,  $j_i^{B.subtilis}$ , by the same factor, i.e.

$$j_i^{B.subtilis} = j_{PG}^{B.subtilis}.$$

As explained in the section *Kinetic model of the lipid II cycle* of the main text, the most parsimonious model consistent with all experimental observations assumes enzymes with higher catalytic rates and lower affinities to their substrates, as well as higher lipid II cycle intermediate pools to sufficiently saturate the enzymes. Hence, for the model in *B. subtilis* we increased the maximal velocities ( $v_{\max}$ ) of the individual enzymatic reactions proportional to the overall PG synthesis rate, to meet the increase of individual fluxes

$$E^{B.subtilis} \times k_{\text{cat}}^{B.subtilis} = v_{\max}^{B.subtilis} = v_{\max}^{E.coli} \times R_T \times R_A \times \frac{1}{R_G}.$$

Since at similar surface concentrations of enzymes, the slightly larger surface area of *B. subtilis* compared to *E. coli* (compare Fig. 2b, Supplementary Table 3b) suggests that the enzyme abundance scales according to

$$E^{B.subtilis} \sim E^{E.coli} \times R_A,$$

we demanded that the catalytic constants ( $k_{\text{cat}}$ ) to increase in proportion to the remaining factors

$$k_{\text{cat}}^{B.subtilis} = k_{\text{cat}}^{E.coli} \times R_T \times \frac{1}{R_G}.$$

Following the assumption of the speed/affinity tradeoff (see section *Kinetic model of the lipid II cycle*), the Michaelis constants  $K_M$  were raised by the same factor

$$K_M^{B.subtilis} = K_M^{E.coli} \times R_T \times \frac{1}{R_G}.$$

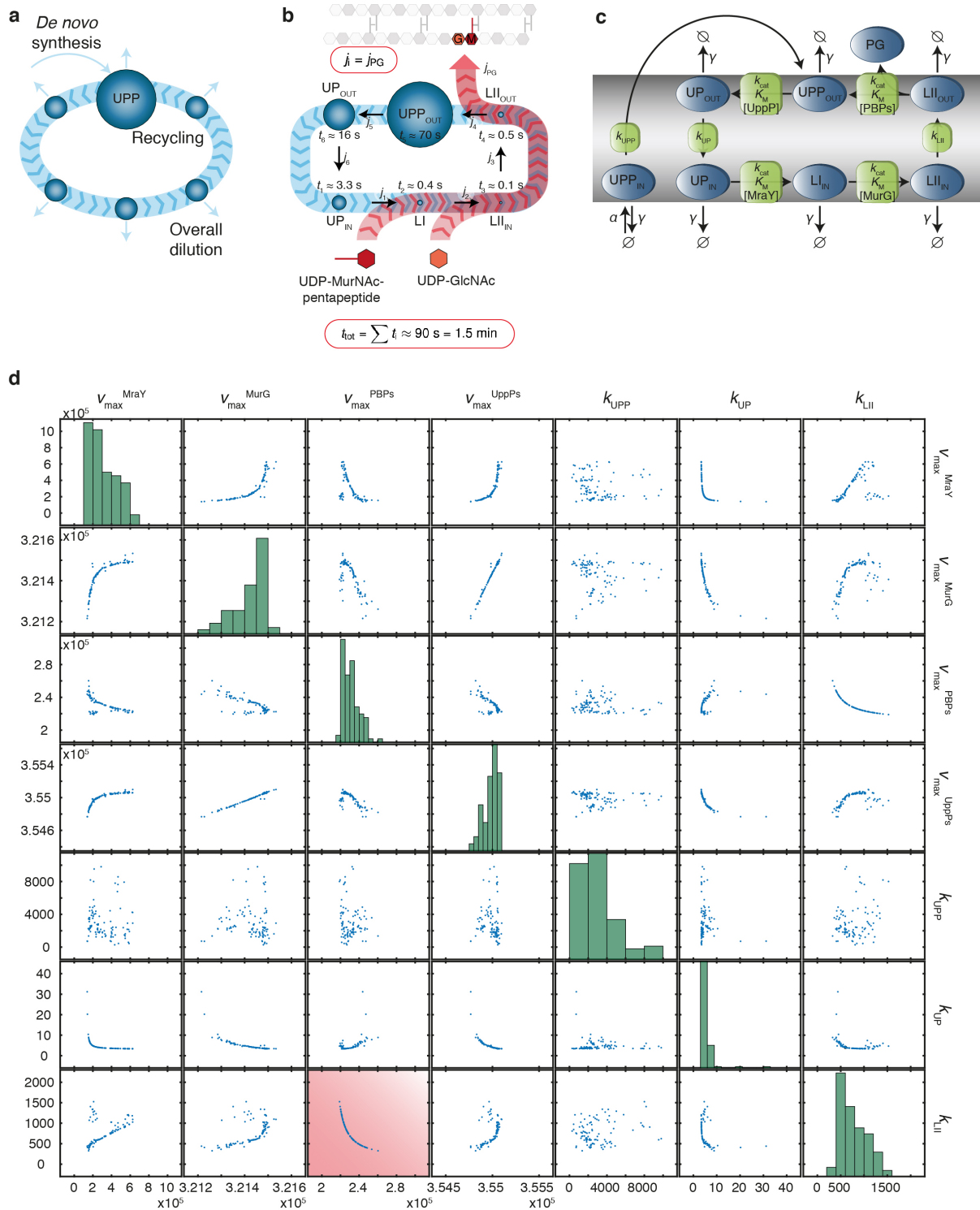
Finally, the need of higher lipid carrier concentrations in order to saturate the lower-affinity enzymes in *B. subtilis* demanded an increase in the UPP production rate  $\alpha$  by a factor ( $R_T \times R_A \times \frac{1}{R_G}$ ). The resulting elevated lipid carrier concentrations proportionally raise the fluxes of the first order flipping reactions of UP, UPP and lipid II, such that the rate constants  $k_i$  had to remain unchanged.

### Influence of antibiotic binding kinetics on the IC<sub>50</sub>

While we extensively discussed the effect of the buffering factor ( $1 + \tilde{K}_G$ ) as the major contribution to the *in vivo* efficacy gap, there is a second factor arising from the difference between *in vivo* dissociation constant ( $\tilde{K}_D = \frac{k_{\text{diss}} + \gamma}{k_{\text{ass}}}$ ) for the antibiotic-target interaction (Supplementary Table 4c). Compared to the *in vitro* dissociation constant ( $K_D = \frac{k_{\text{diss}}}{k_{\text{ass}}}$ ) this altered expression reflects a competition between the antibiotic binding reaction and the dilution of bound and unbound form target. If the antibiotic-bound

target is diluted before spontaneous dissociation (i.e.  $k_{\text{diss}} \ll \gamma$ ), antibiotic action is less effective and the *in vivo* dissociation constant increases compared to the *in vitro* value. In contrast, if antibiotic-target interactions occur on much faster time scales than cell growth (i.e.  $k_{\text{diss}}, k_{\text{ass}} \gg \gamma$ ), the dilution of the pools of bound and unbound lipid intermediates has negligible impact on the efficacy of antibiotic action. This is indeed the case for the on-/off-kinetics ( $k_{\text{diss}}$  and  $k_{\text{ass}}$ ) measured for the bacitracin/UPP interaction (Supplementary Table 4c, Supplementary Fig. 4c). Although there are no experimental data available for the binding kinetics of the other antibiotic-target interactions, simultaneously scaling  $k_{\text{diss}}$  and  $k_{\text{ass}}$  up and down by a factor  $\beta$  in our full model (while keeping their ratio  $K_D = \frac{k_{\text{diss}}}{k_{\text{ass}}}$  constant) reveals that the impact on the  $\text{IC}_{50}$  predictions is moderate (Supplementary Fig. 4d) and that the kinetic parameters chosen in our simulations (for  $\beta = 1$ ) represent a conservative estimate for the *in vivo* shift of the  $\text{IC}_{50}$  (Supplementary Fig. 4d).

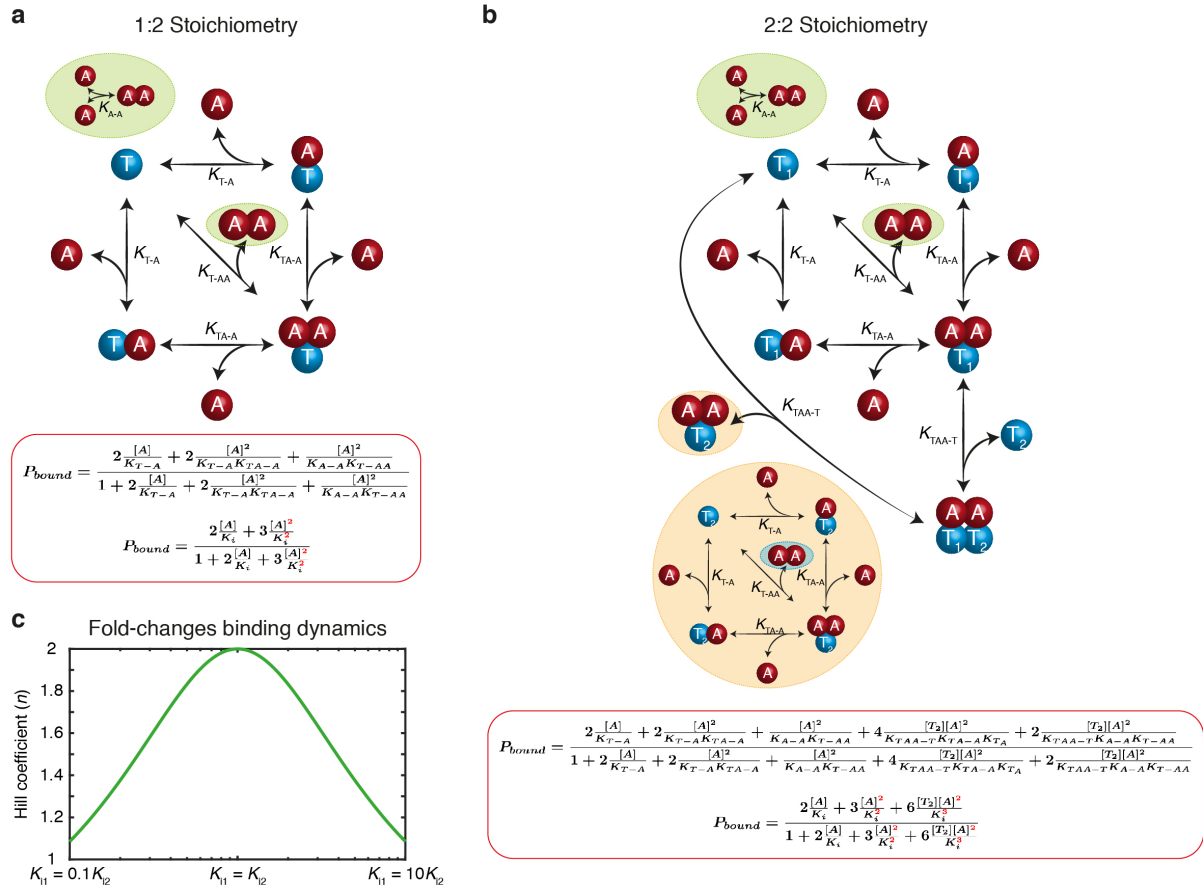
## Supplementary Figures



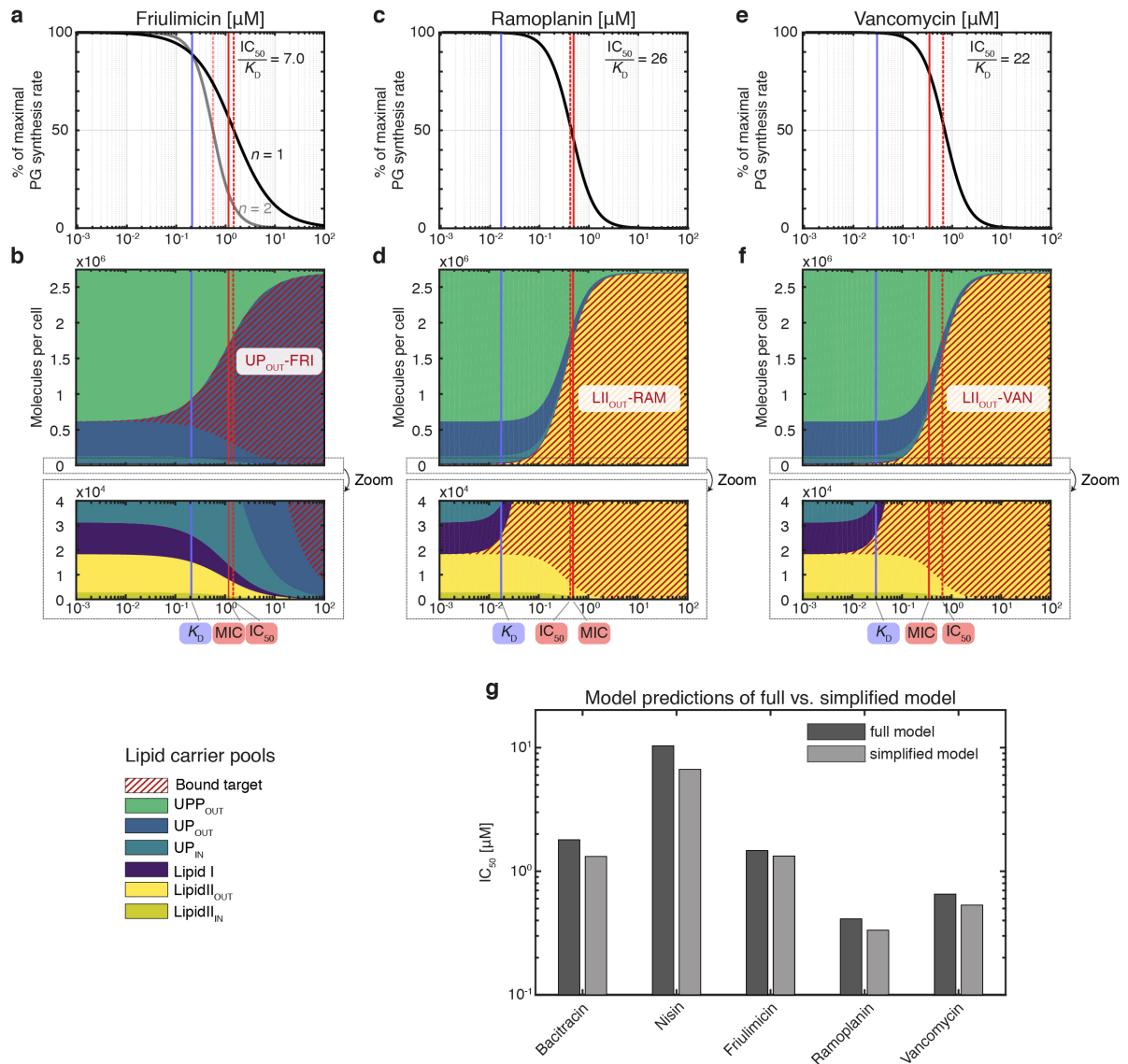
**Supplementary Figure 1. Calibration of the theoretical model of the lipid II cycle in *E. coli*** (a) The *de novo* synthesis of UPP balances the overall dilution of all lipid II cycle intermediates due to cell growth. However, as each individual lipid carrier molecule undergoes 24 rounds within the lipid II cycle before it is replenished by *de novo* synthesis, the (re-) cycling of lipid carrier is the dominant process that drives the synthesis of PG, as indicated by the thickness of the arrows. (b) Accordingly, the lipid II cycle can be considered as a closed-loop system with equilibrated fluxes  $j_1, \dots, j_6$  between the individual states of the system. In fact, all these fluxes equal the rate of PG synthesis,  $j_{PG}$ . Consequently, the dwell time of the individual molecules within one of the cycle states, which is dependent on the speed of the

reaction converting this molecule into the next state, can be calculated from the known overall rate of PG synthesis (see Supplementary Text for a detailed description). **(c)** The theoretical model quantifies the individual reactions of the lipid II cycle. The well-studied enzymatic reactions are parameterized by Michaelis-Menten kinetics, determined by the enzyme abundances ( $[E]$ ), the catalytic rates of the enzymes ( $k_{cat}$ ) as well as the substrate affinities to the enzymes ( $K_M$ ). However, the less-studied flipping reactions are assumed to follow first order kinetics, defined by rate constants  $k_{UPP}$ ,  $k_{UP}$  and  $k_{LII}$ , respectively. The production of UPP at rate  $\alpha$  counterbalances the dilution of all lipid intermediates with rate  $\gamma$ , while  $\frac{\alpha}{\gamma} = \sum[S_i]$  with  $S_i$  representing the intermediate substrate  $i$  in the cycle. **(d)** Since the rate constants of the flipping reactions, as well as the  $v_{max}$  values of the enzymatic reaction ( $v_{max} = k_{cat} * [E]$ ), are largely unknown, we apply a constrained optimization approach based on the previous quantitative considerations to estimate the remaining parameters (see Supplementary Text for further details). The parameter sets of 100 independent parameter fits show variations in some of the parameter values. In fact, the most significant variations appear in the rate constants of the flipping reactions. In particular, a relation between the parameters of the flipping reactions and the upstream or downstream reactions exists – the product of both reaction rates is constant, that is a slower flipping reaction is predicted if the up- or downstream reaction is faster and *vice versa*. For instance, if the flipping of lipid II is fast, the lipid II pool accumulates at the outer leaflet of the membrane and the maximal velocity of the subsequent PBP-catalysed reaction is assumed to be slightly lower compared to a slower flipping because the higher substrate levels of lipid II also contribute partially to a higher flux (*red box*). This relation reflects the fact that the pool levels equilibrate in a way that all fluxes are identical. Consequently faster reactions immediately convert the substrate, leading to an accumulation of the product pool, which again displays the substrate pool for the subsequent reaction and thereby demands a reduced maximal velocity of this reaction for a balanced flux.

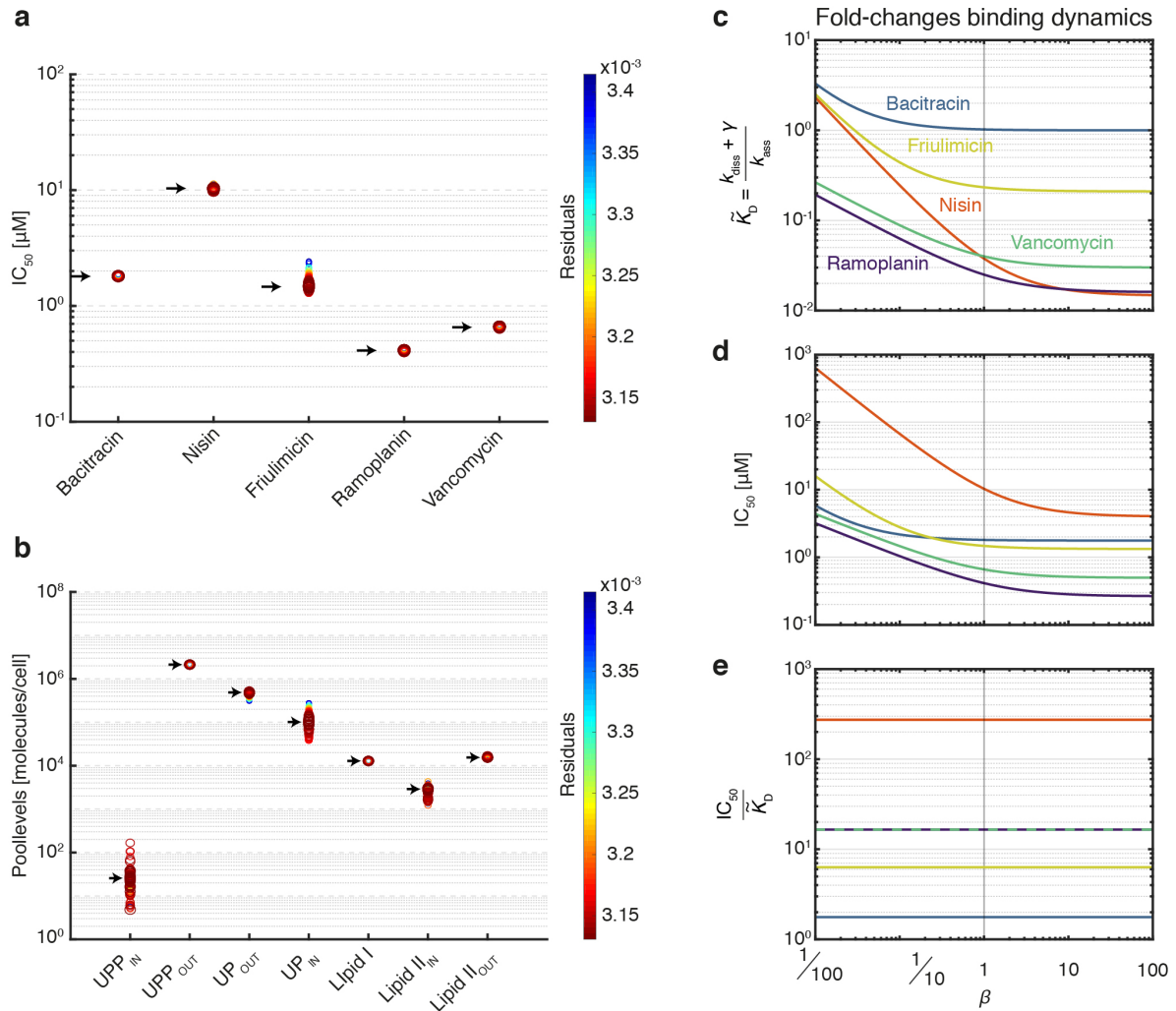




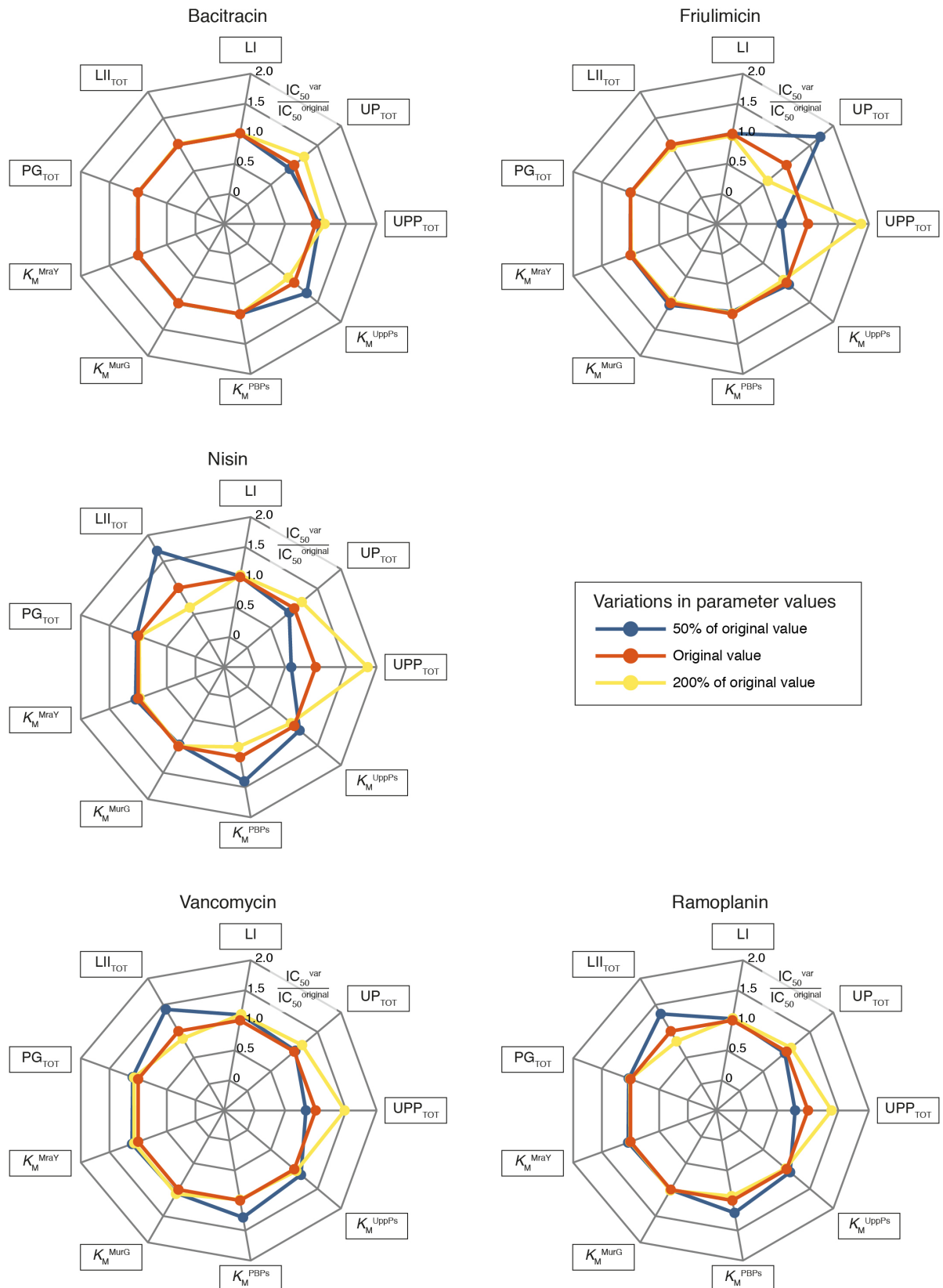
**Supplementary Figure 2. Different multimeric binding scenarios lead to cooperative antibiotic-target-interaction.** (a) In case of a two identical antibiotic molecules (A) interacting with one target molecule (T), the following binding events are conceivable: (i) The monomeric antibiotic binds to the target, determined by the dissociation constant  $K_{T-A}$ ; (ii) the second antibiotic binds to the formed antibiotic-target-complex, determined by the dissociation constant  $K_{TA-A}$  and (iii) the dimeric form of the antibiotic (dimer formation is determined by the dissociation constant  $K_{A-A}$ ) directly interacts with target, determined by the dissociation constant  $K_{T-AA}$ . By evaluating all binding probabilities, we end up with a closed expression that describes the cumulative probability of a bound target  $P_{\text{bound}}$ , summarizing all possible forms of antibiotic-target-complexes (red box, top) (see Supplementary Text for calculation details). When assuming similar dissociation constants  $K_i$  for the individual interactions, the equation can be simplified and appears as the second one in the red box. Obviously, As Hill coefficients  $n > 1$  appear in the equation, the different binding scenarios can generate cooperativity in antibiotic-binding-interactions. (b) In the more complex scenario of two antibiotics interacting with two targets ( $T_1$  and  $T_2$ ), one further possible binding reaction arises, namely the binding of the second target to the complex formed by two antibiotic molecules and the other target molecule, which is determined by the dissociation constant  $K_{TAA-T}$ . Again, a closed expression describes the cumulative probability of a bound target  $P_{\text{bound}}$  (red box, top) and a simplified equation can be found, assuming similar  $K_i$  values for all binding reactions (red box, bottom). (c) Ultimately, evaluating the expression for the probability of a bound target, we also show that the Hill coefficient  $n$  takes the highest value if the dissociation constants of all binding reactions ( $K_{i1}$ ,  $K_{i2}$ ) are identical.



**Supplementary Figure 3. Theory predicts a moderate *in vivo* efficacy gap for friulimycin and a more pronounced difference between  $IC_{50}$  and  $K_D$  for vancomycin and ramoplanin. (a, c, e)** The mathematical model predicts the  $IC_{50}$  values (*red dashed lines*) for the non-cooperative (*grey*) and cooperative (*black*) binding of friulimycin to UP and the cooperative binding of ramoplanin and vancomycin to lipid II. The model predictions match the experimentally determined MICs (*red solid lines*) for all three antibiotics highly precise. In case of friulimycin, the comparison between the model predictions and the experimentally determined MIC supports the hypothesis of a non-cooperative binding to UP. **(b, d, f)** Lipid II cycle intermediate pools under different antibiotic concentrations as predicted by the theoretical model. While an efficient binding of the antibiotics to their target is always observable for antibiotic concentrations around the  $K_D$  values (*blue lines*), the reduction of the external levels of lipid II to 50% of its maximum - to achieve a halved PG synthesis rate - demands higher antibiotic concentrations ( $IC_{50}$ ). However, as illustrated in the results section, this *in vivo* efficacy gap increases with smaller pool levels ( $LII < UP$ ) and decreases with higher cooperativity ( $n = 2$  for vancomycin and ramoplanin). **(g)** Taking similar pool levels distributions as well as comparable reactions rates as in the full model into account, the reduced model reproduces the predictions of the full model. The remaining differences arise from the different reaction kinetics in the two models, as elucidated in detail in the Supplementary Text.



**Supplementary Figure 4. Model predictions of the *in vivo* efficacy gap are robust against variations in the model parameters. (a, b)** The repeatedly performed fitting procedure generates several close-to-optimal sets of model parameters, as characterized by the residuals  $\chi^2$ . However, all parameter sets with  $\chi^2 \leq 1.1 \times \min(\chi^2)$  displayed here only lead to minor variations in the model predictions of the  $IC_{50}$  as well as the distribution of the individual pool levels. The most pronounced variation of the  $IC_{50}$  is observable for friulimicin, correlating with the shift between external and internal levels of UP. **(c, d, e)** Since the specific association- and dissociation rates of the different antibiotic-binding reactions ( $k_{diss}$  and  $k_{ass}$ , respectively) are unknown, we study the impact of faster and slower binding dynamics on the predictions of the  $IC_{50}$  by scaling  $k_{diss}$  and  $k_{ass}$  up and down by a factor  $\beta$ . The vertical grey lines identify the default model value  $\beta = 1$ . As the  $IC_{50}$  is a function of the *in vivo* dissociation constant ( $IC_{50} = \widetilde{K}_D(1 + \widetilde{K}_G)$ ), variations in the *in vivo* dissociation constant ( $\widetilde{K}_D$ ) caused by an acceleration of the antibiotic binding reaction directly lead to variations in the  $IC_{50}$ . However, the *in vivo* dissociation constant ( $\widetilde{K}_D$ ) and thereby the model-predicted  $IC_{50}$  is robust against faster binding dynamics for most of the antibiotics, with nisin as an exception that features a slightly decreased *in vivo* dissociation constant ( $\widetilde{K}_D$ ) and consequently a reduced  $IC_{50}$  for an accelerated antibiotic binding and unbinding. Ultimately, the predicted buffering factor ( $\frac{IC_{50}}{\widetilde{K}_D} = 1 + \widetilde{K}_G$ ) is unaffected by fold-changes in the binding dynamics.



**Supplementary Figure 5. Sensitivity of predicted  $IC_{50}$  values on changes of experimentally determined model parameters.** The model includes experimentally measured  $K_M$  values as well as measurements of intermediate pools levels. Since the actual *in vivo* values of these parameters can differ from their *in vitro* measured quantities and can vary between different experimental setups, a sensitivity analysis of the model predictions against errors in the experimentally determined model parameters was performed. Here, the  $IC_{50}$  predictions for all 5 studied antibiotics were investigated upon

perturbation of each experimental parameter by a factor of two, i.e., for parameters taking 200% and 50% of the original parameter values given in Supplementary Table 1, respectively. For each parameter value, the relative deviation of the  $IC_{50}$  under parameter variation ( $IC_{50}^{var}$ ) compared to the original model prediction ( $IC_{50}^{original}$ ) is displayed on the respective axis of the spider's web. *Blue lines* indicate the deviations of the  $IC_{50}$  when the respective parameter value is reduced by a factor of two from the original value and *yellow lines* represent the results for two-fold increased parameter values compared to the original quantities. *Red lines* serve as references, as they illustrate the results based on the original parameter values. In general, the predictions of the  $IC_{50}$  for the 5 different antibiotics vary only sub-linearly under parameter variations. More precisely, two patterns are observable: (I) Changes in  $K_M$  values only affect the  $IC_{50}$  prediction for antibiotics that target the substrate of the corresponding reaction. For example, variations in  $K_M^{UPP^s}$  lead to changes in bacitracin sensitivity and variations in  $K_M^{PBPs}$  cause variation in the  $IC_{50}$  of the lipid II-binding antibiotics (nisin, vancomycin and ramoplanin), respectively. These variations of the  $IC_{50}$  result from differences in the enzyme saturation according to the different  $K_M$  values, which has been shown to affect the  $IC_{50}$  as explained in the section *Reduced model of the lipid II cycle* in the Methods. (II) Variations in the pool size of UPP and the size of the target pool of each antibiotic affect the  $IC_{50}$  prediction of the respective antibiotic. In particular, a raised UPP pool ( $UPP_{TOT}$ ) leads to higher  $IC_{50}$  predictions for friulimicin and the lipid II binding antibiotics and *vice versa*. Furthermore, an increase in the target pool levels of these antibiotics reduces the  $IC_{50}$  and lower target pools raise the  $IC_{50}$  respectively. These results once again highlight the influence of the buffering effect on the efficacy of the antibiotics that target the less-abundant intermediates in the cycle, such as friulimicin and especially the lipid II-binding antibiotics. While an increase of the UPP pool, which functions as the biggest reservoir in the lipid II cycle, supports the buffering effect and raises the  $IC_{50}$  consequently, an increase in the target pool size shifts the ratio between the reservoir and the target pool towards the target pool and reduces the buffering effect accordingly. Overall, all  $IC_{50}$ 's vary at maximum 2-fold under the analysed parameter variations and only deviations of orders of magnitudes from the experimentally determined quantities would lead to significant changes in the model predictions. Thus, the general conclusions of this study stay unaffected from moderate uncertainties in the experimentally determined model parameters.

## Supplementary Tables

### Supplementary Table 1: Model calibration

a) Pool levels of lipid II cycle intermediates in *E. coli*

Lipid intermediate	Pool level [molecules cell <sup>-1</sup> ]	Literature
undecaprenyl phosphate (UP)	3.21 x 10 <sup>4</sup>	(8)
undecaprenyl pyrophosphate (UPP)	1.16 x 10 <sup>5</sup>	(8)
Lipid I	700	(9)
Lipid II	1000	(9)
UDP-MurNAc-pentapeptide	1.75 x 10 <sup>5</sup>	(5)
UDP-GlcNAc	1.25 x 10 <sup>5</sup>	(6)
total amount of PG in the sacculus	3.5 x 10 <sup>6</sup>	(2)

b) Michaelis constants of lipid II cycle enzymes in *E. coli*

Enzyme	Substrate	K <sub>M</sub> [μM]	Literature
MraY	UP	20	(10)
	UDP-MurNAc-pentapeptide	87	(11)
MurG	Lipid I	2.8	(12)
	UDP-GlcNAc	45	
PBPs	Lipid II	2	(13)
UppPs	UPP	530	(14)

**Supplementary Table 2: Parameter fitting and validation**

Reaction	Optimized parameter value	$k_{\text{cat}}$ [ $\text{min}^{-1}$ ] (literature)	Enzyme levels [molecules $\text{cell}^{-1}$ ] (calculated)	Enzyme levels [molecules $\text{cell}^{-1}$ ] (literature) <sup>(d)</sup>
MraY	$v_{\text{max}} = 3.01 \times 10^5 \text{ molecules min}^{-1}$			210-885
MurG	$v_{\text{max}} = 3.21 \times 10^5 \text{ molecules min}^{-1}$	560* <sup>(a)</sup>	573	168-518
PBPs (PBP1A+ PBP1B+ RodA)	$v_{\text{max}} = 2.32 \times 10^5 \text{ molecules min}^{-1}$	188 <sup>(b)</sup>	1234	358-1510 <sup>(e)</sup>
UppPs	$v_{\text{max}} = 3.55 \times 10^5 \text{ molecules min}^{-1}$	540 <sup>(c)</sup>	657	519-3215 <sup>(f)</sup>
flipping UPP	$k_{\text{UPP}} = 1.84 \times 10^3 \text{ min}^{-1}$			
flipping UP	$k_{\text{UP}} = 3.81 \text{ min}^{-1}$			
flipping lipid II	$k_{\text{LII}} = 642.23 \text{ min}^{-1}$			

(a) Ref: (15), \*based on the importance of an intact membrane for the activity of MurG (16), we assumed a value 10-fold higher than measured *in vitro* for purified protein without membrane

(b)  $k_{\text{cat}}$  for the bifunctional transglycosylase PBP1b (17)

(c)  $k_{\text{cat}}$  measured for the undecaprenyl pyrophosphate phosphatase PgpB (14)

(d) Range of enzyme levels measured in (18) for *E. coli* doubling times of  $T_D = 56.3 \text{ min}$  (lower enzyme levels) and  $T_D = 21.5 \text{ min}$  (higher enzyme levels)

(e) Sum of PBP1A, PBP1B and RodA as the major penicillin-binding proteins with transglycosylase activity (19)

(f) Sum of all known undecaprenyl pyrophosphate phosphatases BacA, PgpB, YbjG and YeiU



### Supplementary Table 3: Comparison between *E. coli* and *B. subtilis*

#### a) Cell size

Parameter	<i>E. coli</i>	Literature	<i>B. subtilis</i>	Literature
average cell length	3.27 $\mu\text{m}$	(20)	3.6 $\mu\text{m}$	(21)
average cell width	0.61 $\mu\text{m}$	(20)	0.86 $\mu\text{m}$	(21)
average cell area	6.26 $\mu\text{m}^2$ (a)		9.57 $\mu\text{m}^2$ (b)	
average cell volume	0.91 $\mu\text{m}^3$ (a)		1.89 $\mu\text{m}^3$ (b)	
PG thickness	1.5- fold layer	(1)	20-fold layer	(7)
PG	3.5 x 10 <sup>6</sup> monomers cell <sup>-1</sup>	(2)	7.13 x 10 <sup>7</sup> monomers cell <sup>-1</sup> (d)	
generation time	36 min (LB)	(2)	40 min (CH medium)	(21)
PG turnover rate	0.5 (50%)	(3, 4)	0.5 (50%)	(22, 23)
PG synthesis rate	1.01 x 10 <sup>5</sup> monomers cell <sup>-1</sup> (c)		1.85 x 10 <sup>6</sup> monomers cell <sup>-1</sup> (c)	

(a) Calculated according to volume and area formula

$$V_{\text{rod}} = V_{\text{cyl}} + V_{\text{ball}} = \pi * \left(\frac{w}{2}\right)^2 * (l - w) + \frac{4}{3} * \pi * \left(\frac{w}{2}\right)^3$$

$$O_{\text{rod}} = M_{\text{cyl}} + O_{\text{ball}} = 2 * \pi * \left(\frac{w}{2}\right) * (l - w) + 4 * \pi * \left(\frac{w}{2}\right)^2$$

(b) Fit of cell size data from (21)

$$(c) \frac{\text{PG monomers}}{\text{cell}} * (1 + \text{PG turnover rate}) * \frac{\ln(2)}{\text{generation time}}$$

(d) Calculated according to scaling assumptions

$$\text{PG monomers per cell}^{B.\text{subtilis}} = \text{PG monomers per cell}^{E.\text{coli}} * \frac{\text{thickness PG}^{B.\text{subtilis}}}{\text{thickness PG}^{E.\text{coli}}} * \frac{\text{surface area}^{B.\text{subtilis}}}{\text{surface area}^{E.\text{coli}}}$$

#### b) Enzyme levels

Enzyme	Level in <i>E. coli</i> [molecules cell <sup>-1</sup> ] (20) (a)	Surface concentration [molecules $\mu\text{m}^{-2}$ ] (d)	Level in <i>B. subtilis</i> [molecules cell <sup>-1</sup> ] (26) (e)	Surface concentration [molecules $\mu\text{m}^{-2}$ ] (g)
MraY	210-885	44-74		
MurG	168-518	36-44	627	66
PBPs	358-1510 (b)	75-128	1227 (f)	128
UppPs	519-3215 (c)	109-270		
UppS/IspU	318-830	67-70	661	69

(a) Enzyme levels measured for two different growth rates ( $T_{D1} = 56.3$  min and  $T_{D2} = 21.5$  min)

(b) Sum of PBP1A, PBP1B and RodA as the major penicillin-binding proteins (19)

(c) Sum of all known undecaprenyl pyrophosphate phosphatases BacA, PgpB, YbjG and YeiU

(d) Considering a surface area of *E. coli* corresponding to the doubling times of enzyme measurements:

$$A = 4.37 \mu\text{m}^2 \text{ for a doubling time of } T_{D1} = 56.3 \text{ min; } A = 11.88 \mu\text{m}^2 \text{ for a doubling time of } T_{D2} = 21.5 \text{ min (20)}$$

(e) Enzyme levels measured in CH medium ( $T_D = 40$  min)

(f) Sum of PBP1 and PBP 4 (only available data)

(g) Considering a surface area of *B. subtilis* of  $A = 9.57 \mu\text{m}^2$  for a doubling time of  $T_D = 40$  min (21)



c) Pool levels of lipid II cycle intermediates

Intermediates	Surface concentration Gram-positives [molecules $\mu\text{m}^{-2}$ ]	Surface concentration Gram-negatives [molecules $\mu\text{m}^{-2}$ ]	Ratio	Literature
UP	9.2 ( $\pm$ 3.1) $\times 10^4$ ( <i>M. flavus</i> ) 11.5 ( $\pm$ 3.8) $\times 10^4$ ( <i>L. monocytogenes</i> )	5.1 $\times 10^3$ ( <i>E. coli</i> )	18-22	(8, 25)
UPP + UP	3.3 $\times 10^5$ ( <i>S. aureus</i> )	2.4 $\times 10^4$ ( <i>E. coli</i> )	14	(8)
Lipid II	2.0 $\times 10^3$ ( <i>B. megaterium</i> )	160 ( <i>E. coli</i> )	12	(9, 26)

#### Supplementary Table 4: Antibiotic activity in *B. subtilis*

a)  $K_D$  values and cooperativity of antibiotic-target-interaction

Antibiotic	Target	$K_D$ [ $\mu$ M]	Cooperativity ( $n$ )	Literature
bacitracin	UPP	1	1	(27)
frulimicin	UP	0.21		(28)
ramoplanin	Lipid II	0.016	2	(29)
vancomycin	Lipid II	0.03	2	(30, 31)
nisin	Lipid II	0.015	1	(32, 33)

b) MIC values of antibiotic-target-interaction

Antibiotic	Strain	MIC [ $\mu$ M]	Method	Medium	Literature
bacitracin	<i>B. subtilis</i> (W168 $\Delta$ bceAB)	1.67	E-test	Müller-Hinton (MH)	(34)
	<i>S. aureus</i> (NCTC 8325 rsbU <sup>+</sup> $\Delta$ vraDE $\Delta$ bceAB)	4.2	killing curve assay	Trypticase Soy Broth (TSB)	(35)
	<i>E. faecalis</i> (JH2-2 $\Delta$ EF2050-EF2049 $\Delta$ EF2752-EF2751)	5.6	broth dilution assay	MH	(36)
frulimicin	<i>B. subtilis</i> (W168)	1.15	killing curve assay	Luria-Bertani (LB)	(37)
ramoplanin	<i>B. subtilis</i> (PY79)	0.49	broth dilution assay	LB	(38)
vancomycin	<i>B. subtilis</i> (ATCC 6633)	0.35	broth dilution assay	TSB	(39)
	<i>S. aureus</i> (RN4220 $\Delta$ vraFG)	0.7	broth dilution assay	TSB	(40)
	<i>E. faecalis</i> (VSE)	1.4	broth dilution assay and E-test	MH	(41)
nisin	<i>B. subtilis</i> (W168 $\Delta$ psdAB)	4.77	killing curve assay	MH	(42)
	<i>S. aureus</i> (NCTC 8325 rsbU <sup>+</sup> $\Delta$ vraDE $\Delta$ bceAB)	1.2	killing curve assay	TSB	(35)

c) *In vivo*  $K_D$  values of antibiotic-target-interaction

Antibiotic	Target	$\widetilde{K}_D$ [ $\mu$ M]
bacitracin	UPP	1.02
frulimicin	UP	0.23
ramoplanin	Lipid II	0.025
vancomycin	Lipid II	0.04
nisin	Lipid II	0.038

## Supplementary References

- (1) Labischinski, H., Goodell, E.W., Goodell, A. & Hochberg, M.L. Direct proof of a more-than-single-layered peptidoglycan architecture of *Escherichia coli* W7: a neutron small-angle scattering study. *Journal of Bacteriology* **173**, 751–756 (1991).
- (2) Mengin-Lecreulx, D. & van Heijenoort, J. Effect of growth conditions on peptidoglycan content and cytoplasmic steps of its biosynthesis in *Escherichia coli*. *Journal of Bacteriology* **163**, 208–212 (1985).
- (3) Goodell, E.W. & Schwarz, U. Release of cell wall peptides into culture medium by exponentially growing *Escherichia coli*. *Journal of Bacteriology* **162**, 391–397 (1985).
- (4) Goodell, E.W. Recycling of murein by *Escherichia coli*. *Journal of Bacteriology* **163**, 305–310 (1985).
- (5) Mengin-Lecreulx, D., Flouret, B. & van Heijenoort, J. Cytoplasmic steps of peptidoglycan synthesis in *Escherichia coli*. *Journal of Bacteriology* **151**, 1109–1117 (1982).
- (6) Mengin-Lecreulx, D., Flouret, B. & van Heijenoort, J. Pool levels of UDP N-acetylglucosamine and UDP N-acetylglucosamine-enolpyruvate in *Escherichia coli* and correlation with peptidoglycan synthesis. *Journal of Bacteriology* **154**, 1284–1290 (1983).
- (7) Breukink, E. & de Kruijff, B. Lipid II as a target for antibiotics. *Nat Rev Drug Discov* **5**, 321–332 (2006).
- (8) Barreteau, H. *et al.* Quantitative high-performance liquid chromatography analysis of the pool levels of undecaprenyl phosphate and its derivatives in bacterial membranes. *J Chromatogr B Analyt Technol Biomed Life Sci* **877**, 213–220 (2009).
- (9) van Heijenoort, Y., Gómez, M., Derrien, M., Ayala, J. & van Heijenoort, J. Membrane intermediates in the peptidoglycan metabolism of *Escherichia coli*: possible roles of PBP 1b and PBP 3. *Journal of Bacteriology* **174**, 3549–3557 (1992).
- (10) Brandish, P.E. *et al.* Slow binding inhibition of phospho-N-acetylmuramyl-pentapeptide-translocase (*Escherichia coli*) by mureidomycin A. *Journal of Biological Chemistry* **271**, 7609–7614 (1996).
- (11) Geis, A. & Plapp, R. Phospho-N-acetylmuramoyl-pentapeptide-transferase of *Escherichia coli* K12. Properties of the membrane-bound and the extracted and partially purified enzyme. *Biochimica et Biophysica Acta (BBA) - Biomembranes* **527**, 414–424 (1978).
- (12) Crouvoisier, M., Auger, G., Blanot, D. & Mengin-Lecreulx, D. Role of the amino acid invariants in the active site of MurG as evaluated by site-directed mutagenesis. *Biochimie* **89**, 1498–1508 (2007).
- (13) Schwartz, B., Markwalder, J.A., Seitz, S.P., Wang, Y. & Stein, R.L. A kinetic characterization of the glycosyltransferase activity of *Escherichia coli* PBP1b and development of a continuous fluorescence assay. *Biochemistry* **41**, 12552–12561 (2002).
- (14) Touzé, T., Blanot, D. & Mengin-Lecreulx, D. Substrate specificity and membrane topology of *Escherichia coli* PgpB, an undecaprenyl pyrophosphate phosphatase. *Journal of Biological Chemistry* **283**, 16573–16583 (2008).
- (15) Auger, G., van Heijenoort, J., Mengin-Lecreulx, D. & Blanot, D. A MurG assay which utilises a synthetic analogue of lipid I. *FEMS Microbiology Letters* **219**, 115–119 (2003).
- (16) Müller, A. *et al.* Daptomycin inhibits cell envelope synthesis by interfering with fluid membrane microdomains. *P Natl Acad Sci Usa* **113**, E7077–E7086 (2016).
- (17) Sung, M.-T. *et al.* Crystal structure of the membrane-bound bifunctional transglycosylase PBP1b from *Escherichia coli*. *P Natl Acad Sci Usa* **106**, 8824–8829 (2009).

- (18) Li, G.-W., Burkhardt, D., Gross, C.A. & Weissman, J.S. Quantifying absolute protein synthesis rates reveals principles underlying allocation of cellular resources. *Cell* **157**, 624–635 (2014).
- (19) Typas, A., Banzhaf, M., Gross, C.A. & Vollmer, W. From the regulation of peptidoglycan synthesis to bacterial growth and morphology. *Nat Rev Micro* **10**, 123–136 (2012).
- (20) Taheri-Araghi, S. *et al.* Cell-size control and homeostasis in bacteria. *Curr Biol* **25**, 385–391 (2015).
- (21) Sharpe, M.E., Hauser, P.M., Sharpe, R.G. & Errington, J. *Bacillus subtilis* cell cycle as studied by fluorescence microscopy: constancy of cell length at initiation of DNA replication and evidence for active nucleoid partitioning. *Journal of Bacteriology* **180**, 547–555 (1998).
- (22) Mauck, J. & Glaser, L. Turnover of the cell wall of *Bacillus subtilis* W-23 during logarithmic growth. *Biochemical and Biophysical Research Communications* **39**, 699–706 (1970).
- (23) Mauck, J., Chan, L. & Glaser, L. Turnover of the cell wall of Gram-positive bacteria. *Journal of Biological Chemistry* **246**, 1820–1827 (1971).
- (24) Muntel, J. *et al.* Comprehensive absolute quantification of the cytosolic proteome of *Bacillus subtilis* by data independent, parallel fragmentation in liquid chromatography/mass spectrometry (LC/MS(E)). *Mol Cell Proteomics* **13**, 1008–1019 (2014).
- (25) Kramer, N.E. *et al.* Resistance of Gram-positive bacteria to nisin is not determined by lipid II levels. *FEMS Microbiology Letters* **239**, 157–161 (2004).
- (26) Fuchs-Cleveland, E. & Gilvarg, C. Oligomeric intermediate in peptidoglycan biosynthesis in *Bacillus megaterium*. *Proc Natl Acad Sci USA* **73**, 4200–4204 (1976).
- (27) Storm, D.R. & Strominger, J.L. Complex formation between bacitracin peptides and isoprenyl pyrophosphates. The specificity of lipid-peptide interactions. *Journal of Biological Chemistry* **248**, 3940–3945 (1973).
- (28) Reder-Christ, K. *et al.* Model membrane approaches to determine the role of calcium for the antimicrobial activity of friulimicin. *Int J Antimicrob Agents* **37**, 256–260 (2011).
- (29) Hu, Y., Helm, J.S., Chen, L., Ye, X.-Y. & Walker, S. Ramoplanin inhibits bacterial transglycosylases by binding as a dimer to lipid II. *J Am Chem Soc* **125**, 8736–8737 (2003).
- (30) Beauregard, D.A., Maguire, A.J., Williams, D.H. & Reynolds, P.E. Semiquantitation of cooperativity in binding of vancomycin-group antibiotics to vancomycin-susceptible and -resistant organisms. *Antimicrobial Agents and Chemotherapy* **41**, 2418–2423 (1997).
- (31) Schäfer, M., Schneider, T. & Sheldrick, G.M. Crystal structure of vancomycin. *Structure* **4**, 1509–1515 (1996).
- (32) Wiedemann, I. *et al.* Specific binding of nisin to the peptidoglycan precursor lipid II combines pore formation and inhibition of cell wall biosynthesis for potent antibiotic activity. *Journal of Biological Chemistry* **276**, 1772–1779 (2001).
- (33) 't Hart, P., Oppedijk, S.F., Breukink, E. & Martin, N.I. New insights into nisin's antibacterial mechanism revealed by binding studies with synthetic lipid II analogues. *Biochemistry* **55**, 232–237 (2016).
- (34) Radeck, J. *et al.* Anatomy of the bacitracin resistance network in *Bacillus subtilis*. *Molecular Microbiology* **100**, 607–620 (2016).
- (35) Hiron, A., Falord, M., Valle, J., Débarbouillé, M. & Msadek, T. Bacitracin and nisin resistance in *Staphylococcus aureus*: a novel pathway involving the BraS/BraR two-component system

- (SA2417/SA2418) and both the BraD/BraE and VraD/VraE ABC transporters. *Molecular Microbiology* **81**, 602–622 (2011).
- (36) Gebhard, S. *et al.* Identification and characterization of a bacitracin resistance network in *Enterococcus faecalis*. *Antimicrobial Agents and Chemotherapy* **58**, 1425–1433 (2014).
- (37) Wecke, T. *et al.* Daptomycin versus Friulimicin B: in-depth profiling of *Bacillus subtilis* cell envelope stress responses. *Antimicrobial Agents and Chemotherapy* **53**, 1619–1623 (2009).
- (38) Tiyanont, K. *et al.* Imaging peptidoglycan biosynthesis in *Bacillus subtilis* with fluorescent antibiotics. *Proc Natl Acad Sci USA* **103**, 11033–11038 (2006).
- (39) Mota-Meira, M., LaPointe, G., Lacroix, C. & Lavoie, M.C. MICs of mutacin B-Ny266, nisin A, vancomycin, and oxacillin against bacterial pathogens. *Antimicrobial Agents and Chemotherapy* **44**, 24–29 (2000).
- (40) Yoshida, Y. *et al.* Bacitracin sensing and resistance in *Staphylococcus aureus*. *FEMS Microbiology Letters* **320**, 33–39 (2011).
- (41) Shaaly, A., Kalamorz, F., Gebhard, S. & Cook, G.M. Undecaprenyl pyrophosphate phosphatase confers low-level resistance to bacitracin in *Enterococcus faecalis*. *J Antimicrob Chemother* **68**, 1583–1593 (2013).
- (42) Staroń, A., Finkeisen, D.E. & Mascher, T. Peptide antibiotic sensing and detoxification modules of *Bacillus subtilis*. *Antimicrobial Agents and Chemotherapy* **55**, 515–525 (2011).

### **A.3 From modules to networks: A systems-level analysis of the bacitracin stress response in *Bacillus subtilis***

## Manuscript in preparation

### From modules to networks:

#### A systems-level analysis of the bacitracin stress response in *Bacillus subtilis*

Hannah Piepenbreier<sup>1</sup>, Andre Sim<sup>1</sup>, Carolin M. Kobras<sup>2</sup>, Jara Radeck<sup>3</sup>, Thorsten Mascher<sup>3</sup>,  
Susanne Gebhard<sup>2</sup> and Georg Fritz<sup>1,\*</sup>

<sup>1</sup>LOEWE Center for Synthetic Microbiology and Department of Physics, Philipps-Universität Marburg, Germany; <sup>2</sup>Department of Biology & Biochemistry, Milner Centre for Evolution, University of Bath, United Kingdom; <sup>3</sup>Institute of Microbiology, Technische Universität (TU) Dresden, 01062 Dresden, Germany

\*For correspondence: Email: [georg.fritz@synmikro.uni-marburg.de](mailto:georg.fritz@synmikro.uni-marburg.de);

Tel: +49 6422 28 22582; Fax: + 49 6411 28 24430

### Abstract

Bacterial resistance against antibiotics often involves multiple mechanisms that are interconnected to ensure robust protection. So far, the knowledge about underlying regulatory features of those resistance networks is sparse, since they can hardly be determined by experimentation alone. Here, we present the first computational approach to elucidate the interplay between multiple resistance modules against a single antibiotic, and how regulatory network structure allows the cell to respond to and compensate for perturbations of resistance. Based on the response of *B. subtilis* towards the cell wall synthesis-inhibiting antibiotic bacitracin, we developed a mathematical model that comprehensively describes the protective effect of two well-studied resistance modules (BceAB and BcrC) on the progression of the lipid II cycle. By integrating experimental measurements of expression levels, the model accurately predicts the efficacy of bacitracin against the *B. subtilis* wild-type as well as mutant strains lacking one or both of the resistance modules. Our study reveals that bacitracin-induced changes in the properties of the lipid II cycle itself control the interplay between the two resistance modules. In particular, variations in the concentrations of UPP, the lipid II cycle intermediate that is targeted by bacitracin, connect the effect of the BceAB transporter and the homeostatic response via BcrC to an overall resistance response. We propose that monitoring changes in pathway properties caused by a stressor allows the cell to fine-tune deployment of multiple resistance systems and may serve as a cost-beneficial strategy to control the overall response towards this stressor.

### Keywords:

cell wall antibiotic, antimicrobial peptide, bacitracin, peptidoglycan, resistance network, regulatory network, computational model

## Introduction

Computational approaches significantly improved our understanding of bacterial responses to environmental conditions, which often comprise multiple interconnected modules orchestrated in complex regulatory networks. For instance, mathematical modelling elucidated differences in signalling and signal processing in bacterial chemotaxis in *Bacillus subtilis* and *Escherichia coli* (Rao *et al.*, 2004; Rao *et al.*, 2005); contributed to our understanding of how environmental and cellular conditions shape the complex phosphorelay-system controlling sporulation and competence in *B. subtilis* (Bischofs *et al.*, 2009; Schultz *et al.*, 2009; Jabbari *et al.*, 2011), and helped to uncover the regulatory mechanisms of  $\sigma^F$ -dependent sporulation control in *Bacillus subtilis* (Iber *et al.*, 2006; Igoshin *et al.*, 2006). In all of these studies, the overall cellular response towards environmental changes involves an intricate interplay between different regulatory modules, which can hardly be understood without theoretical frameworks.

The cell envelope stress response (CESR) is another example for a particularly important, multi-layered regulatory network in bacteria, as it provides effective protection against crucial cell wall-targeting antibiotics, including the antimicrobial peptides (AMPs) bacitracin, ramoplanin and vancomycin. In many bacteria, the CESR involves orchestrated expression of various resistance determinants that protect against these AMPs via an array of mechanisms (Jordan *et al.*, 2008). These include, for instance, changes in cell envelope composition to shield cellular targets from AMPs (Revilla-Guarinos *et al.*, 2014), production of resistance pumps to remove AMPs from their site of action (Gebhard, 2012), enzymatic or genetic modifications of target structures to prevent AMP binding (Cetinkaya *et al.*, 2000), or the synthesis of immunity proteins to degrade AMPs altogether (Sun *et al.*, 2009). Although many of the resistance mechanisms are well-described and we have a good understanding of the gene regulatory control of individual resistance modules, the complex interplay and cross-regulation between individual resistance modules remains poorly understood. Given that eight out of the twelve bacterial pathogens on the WHO's priority list have acquired resistance towards cell wall-targeting antibiotics (<https://www.who.int/news-room/detail/27-02-2017-who-publishes-list-of-bacteria-for-which-new-antibiotics-are-urgently-needed>), theoretical models rationalizing the cellular response towards such drugs are urgently needed.

To address this knowledge gap, we here focussed on the resistance network of *B. subtilis* towards bacitracin (BAC), an AMP that interferes with the lipid II cycle of cell wall biosynthesis (Fig. 1) (Schneider and Sahl, 2010). Briefly, within this essential pathway the peptidoglycan (PG) precursors N-Acetylglucosamine (GlcNAc) and N-Acetylmuramic acid (MurNAc)-pentapeptide are sequentially attached to the lipid carrier molecule undecaprenyl phosphate (UP), thereby forming lipid II (Fig. 1). Subsequently, lipid II is flipped across the cytoplasmic membrane, where the PG monomer (GlcNAc-MurNAc-pentapeptide) is



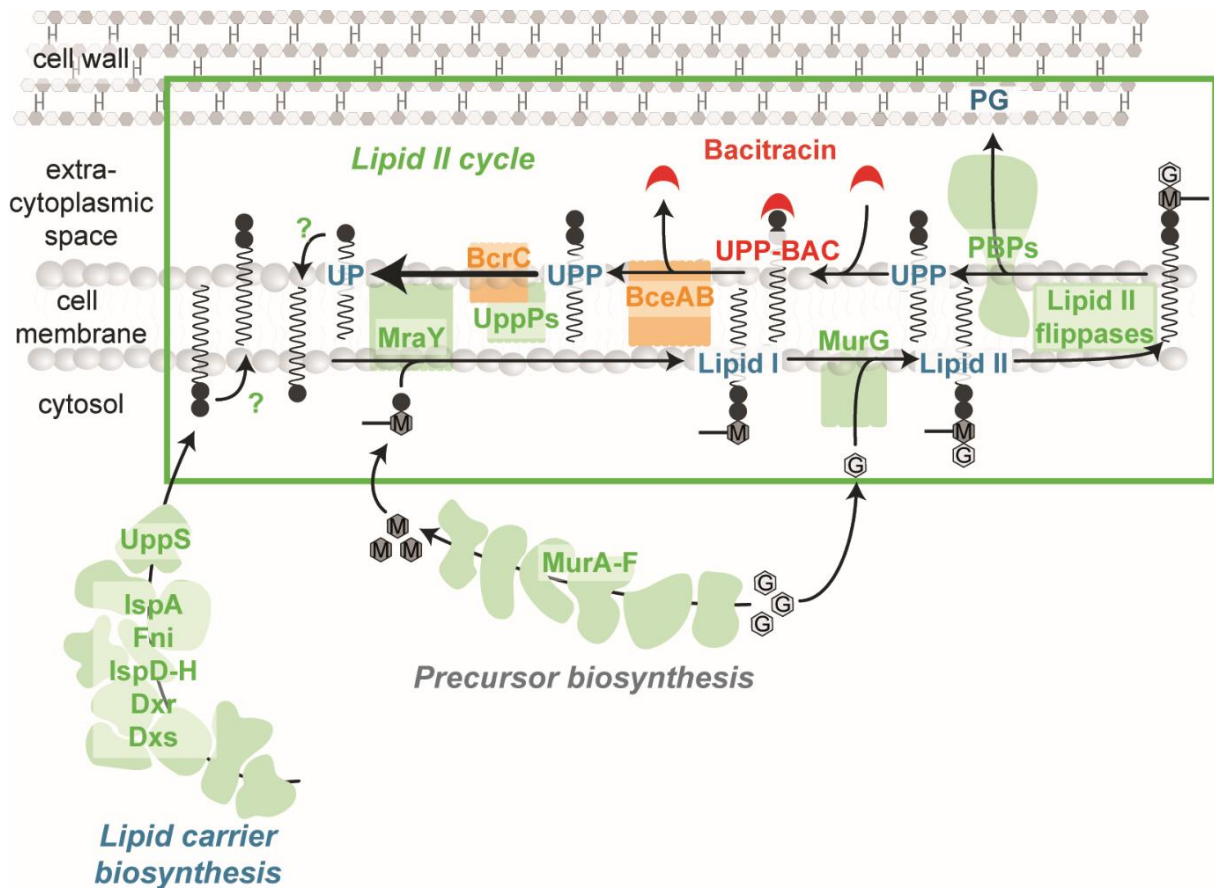


**Figure 1. Scheme of the cell wall biosynthetic pathway and its inhibition by bacitracin.** The lipid II cycle of cell wall biosynthesis is responsible for the translocation of PG precursors across the cytoplasmic membrane and represents the rate-limiting step in this process. The cytoplasmic production of UDP-MurNAc-pentapeptide (M) from UDP-GlcNAc (G) is catalysed by the MurA-F ligases. Subsequently, at the internal leaflet of the cytoplasmic membrane the translocase MraY and the transferase MurG sequentially attach UDP-MurNAc-pentapeptide and UDP-GlcNAc to the lipid carrier undecaprenyl phosphate (UP), giving rise to the lipid I and lipid II intermediates, respectively. Various flippases translocate lipid II to the outer leaflet of the cytoplasmic membrane, where penicillin-binding proteins (PBPs) incorporate the subunits into the growing PG layer. In order to recycle the resulting pyrophosphorylated state of the lipid carrier (UPP), dephosphorylation by UPP phosphatases (UppPs), including BcrC, yield the initial substrate UP for another round of PG subunit transport. Lipid carrier recycling requires flipping of UP to the internal leaflet by a yet unknown mechanism. Finally, dilution of lipid carriers is counterbalanced by cytoplasmic synthesis of UPP, which involves the isoprenoid biosynthesis pathway with the undecaprenyl pyrophosphate synthetase UppS catalyzing the last committed step. Likewise to UP flipping, the required mechanism to present UPP to the externally acting phosphatases is unknown. Bacitracin inhibits the lipid II cycle by binding to UPP, thereby preventing UPP dephosphorylation and progression of the cycle.

incorporated into the growing cell wall. This leaves the lipid carrier in its pyrophosphate form (UPP), which has to be recycled to UP by dephosphorylation to allow a new round of PG monomer transport. Bacitracin blocks the cycle by forming a tight complex with UPP (UPP-BAC), which efficiently prevents recycling of the lipid carrier and ultimately leads to lysis of cells (Storm and Strominger, 1973; Economou *et al.*, 2013). Like in many Gram-positive bacteria, bacitracin resistance in *B. subtilis* is mediated by multiple resistance determinants, which are transcriptionally up-regulated in response to bacitracin treatment (reviewed in (Radeck *et al.*, 2017a). The most effective (primary) resistance determinant is the ABC transporter BceAB (Rietkötter *et al.*, 2008), which protects UPP from the inhibitory grip of bacitracin (Fig. 2A) – presumably by breaking UPP-BAC complexes and thereby shifting the

binding equilibrium towards the free form of UPP (Fritz *et al.*, 2015). The second line of defence is mediated by the UPP phosphatase BcrC, which increases the rate of UPP dephosphorylation and thereby promotes progression of the lipid II cycle (Cao and Helmann, 2002; Ohki *et al.*, 2003; Mascher *et al.*, 2003; Bernard *et al.*, 2005) (Fig. 2A). Simultaneously, *B. subtilis* induces production of the phage shock-like proteins Lial and LiaH (Mascher *et al.*, 2003; Jordan *et al.*, 2006), which only play a minor role in bacitracin resistance and seem to be involved in stabilization of membrane integrity by a mechanism that is yet to be determined (Domínguez-Escobar *et al.*, 2014, Radeck *et al.*, 2016).

Expression of *bceAB* is activated by a two-component system comprising the histidine kinase BceS and the response regulator BceR (Mascher *et al.*, 2003, Ohki *et al.*, 2003; Bernard *et al.*, 2007; Rietkötter *et al.*, 2008). BceS forms a sensory complex with BceAB in the membrane (Dintner *et al.*, 2011; Dintner *et al.*, 2014), which acts as a “flux-sensor” reporting on the antibiotic load experienced by each individual transporter – thereby activating further transporter expression only if their detoxification capacity approaches saturation (Fritz *et al.*, 2015). Expression of BcrC is primarily controlled by the extracytoplasmic function sigma factor  $\sigma^M$  (Cao and Helmann, 2002; Eiamphungporn and Helmann, 2008). While the physiological input triggering activation of  $\sigma^M$  still remains elusive (Asai, 2018; Zhao *et al.*, 2019), the broad range of inducing conditions, including cell wall antibiotics, salt, ethanol and others, suggests that it is not a specific chemical compound but rather a cellular cue upon cell envelope damage that activates the  $\sigma^M$  response (Helmann, 2016). Interestingly, despite the seemingly unrelated input stimuli for the BceAB and the BcrC resistance modules – with BceAB being activated by a “drug-sensing” mechanism (=antibiotic flux) and BcrC by a “damage-sensing” mechanism – previous work revealed that there is a high level of inter-dependency between the modules (Radeck *et al.*, 2016). In particular, in mutants lacking the ABC transporter BceAB, the secondary layers of resistance are induced more strongly and *vice versa*, suggesting that this compensatory regulation is the origin of robust cell wall homeostasis in *B. subtilis*.

In this study, we set out to decipher the regulatory interplay between these two resistance determinants by considering the dynamics of the lipid II cycle as a pivotal connection between drug- and damage-sensing resistance modules. To this end, we took advantage of a recently established computational model for the lipid II cycle, which describes the dynamics of PG synthesis based on biochemical parameters of the involved enzymes and cycle intermediates (Piepenbreier *et al.*, 2019). By integrating the existing mathematical description of the lipid II cycle with a previously established model for BceAB resistance module (Fritz *et al.*, 2015) and a novel theoretical description of the BcrC module (Fig. 2A), we developed a systems-level description of the bacitracin stress response that captures the MIC of a wild-type *B. subtilis* strain, as well as several mutants deleted for resistance systems individually or in combination. Additionally, our theoretical and experimental analyses reveal that an increased

total number of lipid carriers as well as an accumulation of the lipid carrier UPP in a  $\Delta bcrC$  mutant are the origin of the significantly higher impact of the BceAB resistance module on bacitracin resistance when BcrC is lacking. As our model does not include any additional layers of regulation, our results show that the properties of the lipid II cycle itself contribute to the homeostatic control of the overall resistance response towards bacitracin. Thus, the theory presented here not only provides a comprehensive quantitative description of the bacitracin resistance network in *B. subtilis*, but also uncovers regulatory mechanisms of the multi-layered response towards this antibiotic.

## Material and Methods

### Bacterial strains and growth conditions

*Bacillus subtilis* and *Escherichia coli* were routinely grown in lysogeny broth (LB medium) at 37°C with agitation (200 rpm). Transformations of *B. subtilis* were carried out as described previously (Harwood and Cutting, 1990). All strains used in this study are derivatives of the wild-type strain W168 and are listed in Supplementary Table 1. Kanamycin (10 mg ml<sup>-1</sup>), chloramphenicol (5 mg ml<sup>-1</sup>), tetracycline (10 mg ml<sup>-1</sup>) and erythromycin (1 mg ml<sup>-1</sup>) plus lincomycin (25 mg ml<sup>-1</sup>) for macrolide-lincosamide-streptogramin B (“MLS”) resistance were used for the selection of the *B. subtilis* mutants used in this study. Solid media contained 1.5% (w/v) agar.

### Luciferase assays

Luciferase activities of *B. subtilis* strains harboring pAH328-derivates were assayed using a Synergy2 multi-mode microplate reader from BioTek® (Winooski, VT, USA), essentially as described in (Radeck *et al.*, 2016). Briefly, the reader was controlled using the software Gen5™ (version 2.06). Cells were inoculated 1:1000 from fresh overnight cultures and grown to OD<sub>600</sub> = 0.1–0.5. Subsequently, cultures were diluted to OD<sub>600</sub> = 0.01 and split into 100 µl per well in 96-well plates (black walls, clear bottom; Greiner Bio-One, Frickenhausen, Germany). Cultures were incubated at 37°C with linear agitation (medium intensity) and the OD<sub>600</sub> as well as luminescence were monitored every 5 min. After one hour, freshly diluted Zn<sup>2+</sup>-bacitracin was added to the indicated final concentrations and incubation and monitoring every 5 min was resumed for 8h. Specific luminescence activity is given by the raw luminescence output (relative luminescence units, RLU) normalized by cell density (RLU/OD<sub>600</sub>).

### Minimal inhibitory concentration assays

For concentration-dependent growth experiments, cells were grown as described for the luciferase assays and OD<sub>600</sub> was measured analogously. The growth rate within the first hour after bacitracin addition was determined to monitor the concentration-dependent effects of

bacitracin on cell growth (Fig. 2B(i)). The MIC was defined as the concentration of antibiotic that fully inhibited growth, i.e. for which the growth rate equals zero.

### **Relative quantitative RT-PCR**

*Bacillus subtilis* W168 and  $\Delta bcrC$  cells were collected at OD<sub>600</sub> between 0.3-0.5 and suspended in Trizol (Ambion). The cells were lysed through bead beating with 0.1mm zirconia beads. RNA was extracted from exponentially growing cells with Trizol Reagent. DNA was removed with DNase (Thermo Scientific) and the DNase was then heat-deactivated in the presence of EDTA. RT-qPCR was performed with the Luna Universal One-Step RT-qPCR Kit (New England Biolabs). 1  $\mu$ l of 10-fold diluted RNA was added to 4  $\mu$ l of rtPCR mix and subjected to a reverse transcription step at 55°C and 45 cycles of PCR (10 seconds at 95°C and 30 seconds at 60°C). The average CT value of three technical replicates of three biological replicates for each sample was used in  $\Delta\Delta C_t$  relative expression analysis (Livak and Schmittgen, 2001). The reference genes were the constitutively expressed genes *recA* (BSU16940) and *gyrB* (BSU00060).

### **Computational model and simulations**

A detailed description of the model assumptions and equations for the bacitracin resistance network, as well as additional analyses of the model are given in the Supplementary Information. The numerical calculations of the differential equations of the model as well as the individual simulations were performed with custom scripts developed in MATLAB™ software (The MathWorks, Inc.).

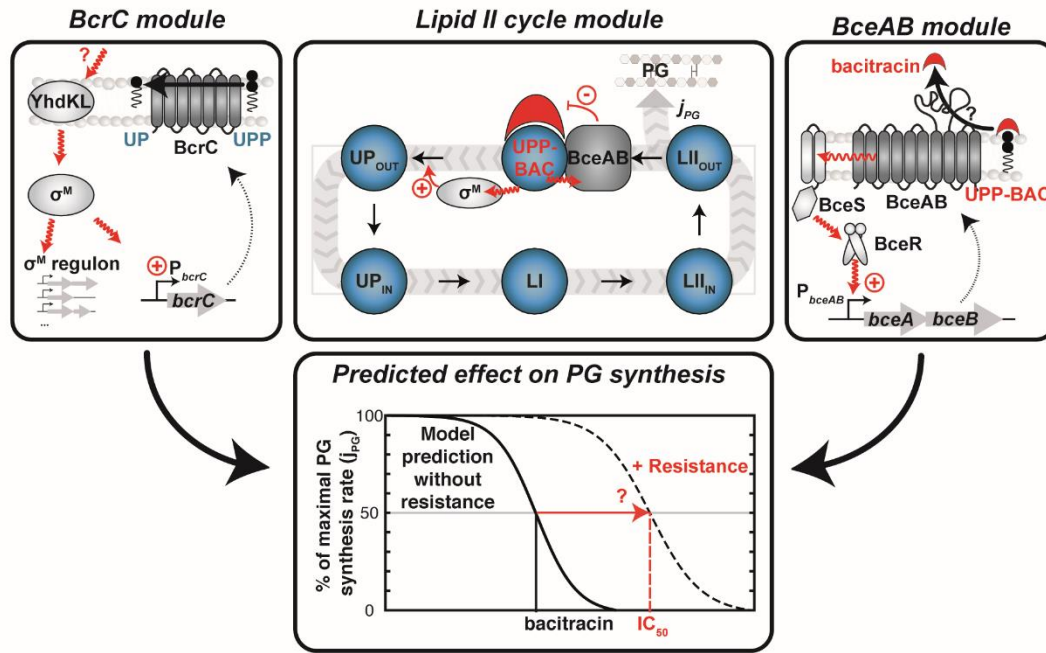
## **Results**

The common purpose of the UPP phosphatase BcrC and the ABC transporter BceAB is to ensure progression of the lipid II cycle under bacitracin treatment, since bacitracin inhibits an important step of this cycle. Consequently, to study the impact of the two resistance modules on lipid II cycle homeostasis, we successively integrated the resistance modules into a detailed computational description of the lipid II cycle (Piepenbreier *et al.*, 2019), which served as the basis of our mathematical model of the overall bacitracin resistance network. In a first step, we included the BcrC module and studied its protective effect on the lipid II cycle. In a second step, we investigated the interaction of the two resistance modules by integrating the pre-existing theory of the BceAB module (Fritz *et al.*, 2015) into the model.

### **Impact of the UPP phosphatase BcrC on bacitracin resistance**

In our previous computational description of the lipid II cycle (Piepenbreier *et al.*, 2019) we made the simplifying assumption that the enzymes involved in lipid II cycle progression feature

**A Theoretical model**



**B Experimental analysis**

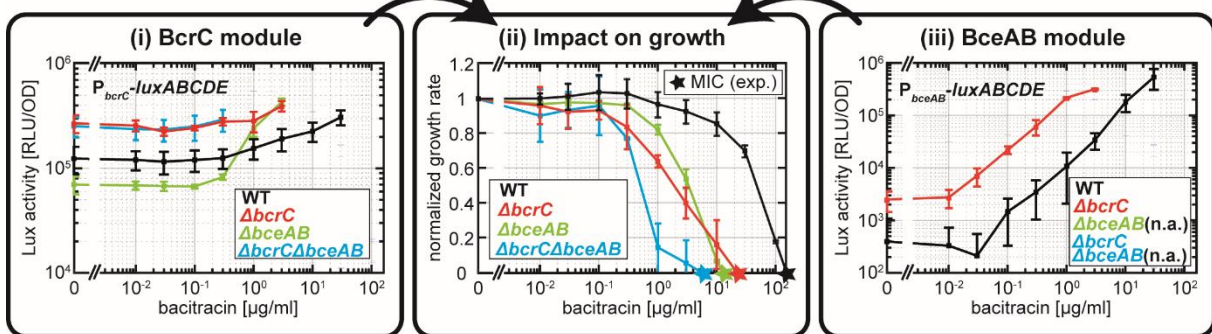


**Figure 2. Modular composition of the bacitracin stress response network and its experimental analysis in *B. subtilis*.** (A) Our theoretical model of the bacitracin stress response network is based on three interconnected modules. At the core of the model is a previously established theoretical description of the lipid II cycle module (*center panel*), which predicts the PG synthesis rate ( $j_{PG}$ ) of a *B. subtilis* strain devoid of any inducible resistance determinants under antibiotic perturbation (Piepenbreier *et al.*, 2019). The dynamic variables within the model are the concentrations of the lipid II cycle intermediates (*blue bubbles*) in the inner and outer leaflet of the cytoplasmic membrane, as indicated by the subscripts IN and OUT. To arrive at a model for wildtype cells, we first incorporated the action of the  $\sigma^M$  module (*left panel*), in which an unknown cue activates the anti- $\sigma$  factors YdhL and YdhK in response to cell envelope stress, triggering the release of  $\sigma^M$  and the concomitant up-regulation of BcrC and an array of further  $\sigma^M$ -dependent genes. As a second module we incorporated the action of the ABC transporter BceAB (*right panel*), in which a complex of the histidine kinase BceS and the BceAB transporter jointly act as a sensor for bacitracin flux, triggering phosphorylation of the response regulator BceR and concomitant up-regulation of *bceAB* expression. Both resistance modules are qualitatively expected to increase resistance (*lower panel*) by shifting the bacitracin concentration at which the PG synthesis rate reaches its half-maximal level ( $IC_{50}$ ) to higher values. (B) Experimental analysis of resistance module gene expression and their impact on the growth rate. Target promoter activities of  $P_{bcrC}$ -*luxABCDE* (*panel i*) and  $P_{bceAB}$ -*luxABCDE* (*panel iii*) in *B. subtilis* strains carrying indicated deletions of resistance modules, as given by specific luciferase activity (RLU/OD<sub>600</sub>) one hour after addition of indicated amounts of bacitracin. Panel (*ii*) shows the corresponding normalized growth rates of the same strains. Measurements were performed during exponential growth phase in LB medium at 37°C in a microtiter plate reader. Data are shown for strains TMB1619, TMB1620 (wild-type strain W168); TMB1623, TMB1624 ( $\Delta bceAB$ ); TMB1627, TMB1628 ( $\Delta bcrC$ ) and TMB1632 ( $\Delta bceAB\Delta bcrC$ ) containing  $P_{bceA}$ -*luxABCDE* or  $P_{bcrC}$ -*luxABCDE*, respectively, see Table S1. Note that we did not test  $P_{bceA}$ -*luxABCDE* activity in strains carrying a  $\Delta bceAB$  deletion, because the flux-sensing mechanism activating  $P_{bceA}$  strictly relies the presence of BceAB (Fritz *et al.*, 2015). Data points and error bars indicate means and standard deviations derived from at least three biological replicates.

constant expression levels under antibiotic treatment, but it is known that the UPP phosphatase BcrC is upregulated in response to bacitracin treatment. Also, the model did not include the activity of the BceAB transporter and, as such, was only able to predict the approximate MIC for bacitracin in a  $\Delta bceAB$  mutant strain of *B. subtilis* (Piepenbreier *et al.*, 2019). Thus, the first step in arriving at a more realistic description of lipid II cycle homeostasis was to include the bacitracin-dependent up-regulation of *bcrC* expression into our computational model for the  $\Delta bceAB$  mutant strain. To experimentally assess *bcrC* expression in response to bacitracin treatment under our experimental conditions, we integrated a  $P_{bcrC}$ -*luxABCDE* reporter construct into the chromosome of a  $\Delta bceAB$  mutant and measured luciferase activity 1 hour after addition of various bacitracin levels (Fig. 2B(i), *green*). The  $P_{bcrC}$  promoter activity clearly correlated with increasing levels of bacitracin, leading to a maximal ~6-fold induction at 3  $\mu\text{g/ml}$  bacitracin treatment compared to the untreated condition. In contrast, wild-type cells only displayed a ~3-fold  $P_{bcrC}$  induction reached at 10-fold higher bacitracin levels (30  $\mu\text{g/ml}$ ) (Fig. 2B(i), *black*), suggesting that the additional expression of *bceAB* in the wild-type mitigates the demand for *bcrC* expression, as discussed further below. Furthermore, we investigated the impact of the BcrC resistance module on bacitracin resistance, by comparing the growth of a  $\Delta bceAB$  mutant and a  $\Delta bceAB\Delta bcrC$  double mutant. In doing so, we were able to study the resistance contribution of BcrC alone, and avoided any compensatory upregulation of *bceAB* expression that may complicate the interpretation of a comparison between wild-type and a  $\Delta bcrC$  mutant strain. By defining the minimal inhibitory concentration (MIC) as the lowest antibiotic concentration leading to zero growth rate after bacitracin addition, we observed a 2.3-fold lower MIC value for the  $\Delta bceAB\Delta bcrC$  mutant (Fig. 2B(ii); *light blue star*,  $\text{MIC}^{\Delta bceAB\Delta bcrC} \sim 6.3 \mu\text{g/ml}$ ) compared to the  $\Delta bceAB$  mutant (Fig. 2B(ii); *green star*,  $\text{MIC}^{\Delta bceAB} \sim 14.5 \mu\text{g/ml}$ ), consistent with earlier results (Radeck *et al.*, 2016). This clearly confirmed that the BcrC resistance module by itself contributes significantly to the growth of *B. subtilis* under bacitracin treatment.

Next, we incorporated the observed up-regulation of *bcrC* into our existing model of the lipid II cycle, with the goal of accurately predicting the antibiotic susceptibility towards bacitracin in the  $\Delta bceAB$  mutant strain. Briefly, the previous model of the lipid II cycle (Piepenbreier *et al.*, 2019) considered Michaelis-Menten kinetics for all characterized enzymes, while the mostly unknown flipping reactions of the intermediates UPP, UP and lipid II were described by first order kinetics (see Supplementary Text for a detailed description of the model). To integrate the different levels of *bcrC* expression in response to bacitracin into our model, we modified the mathematical description of the dephosphorylation reaction of UPP. Since the speed of every single enzymatic reaction within the lipid II cycle is proportional to the concentration of the enzymes that catalyses the reaction - according to the Michaelis-Menten theory - the bacitracin-induced increase in BcrC levels implies an increase in the speed of UPP



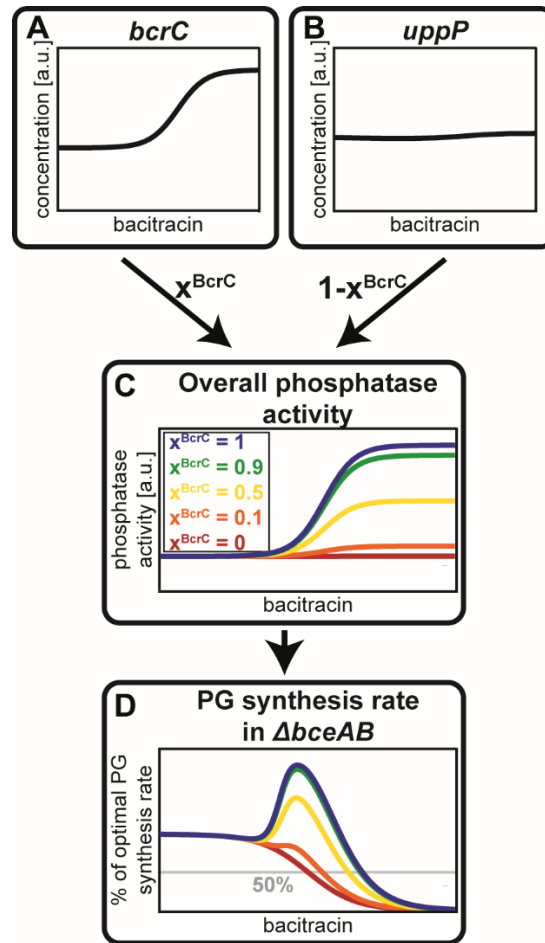


**Figure 3. Different contributions of BcrC and UppP to the overall UPP phosphatase activity lead to variable levels of protection against bacitracin.** To capture the influence of the BcrC module to lipid II cycle homeostasis, the bacitracin-dependent induction profiles of the two phosphatases *bcrC* (A) and *uppP* (B) are used as proxies for their contributions to the total UPP phosphatase activity. Given that no biochemical characterization regarding the relative phosphatase activities of the two proteins exists, we introduce the parameter  $x^{BcrC}$  describing the relative contribution of BcrC (and  $(1 - x^{BcrC})$  the contribution of UppP) to the overall phosphatase activity in panel (C). Integrating the bacitracin-dependent UPP phosphatase activity in (C) in the model for the lipid II cycle (Piepenbreier et al., 2019) leads to predictions for the PG synthesis rate in (D). This shows that the stronger the contribution by  $x^{BcrC}$ , the higher the bacitracin concentration at which the PG synthesis rate reaches its half-maximal value, which we define as the  $IC_{50}$ . Previous work showed that this  $IC_{50}$  serves as a good proxy for the experimental MIC for various cell wall antibiotics (Piepenbreier et al., 2019).

dephosphorylation (Fig. 3A,C). However, the dephosphorylation of UPP is additionally catalysed by a second phosphatase UppP in *B. subtilis*, the expression of which is independent of bacitracin (Cao and Helmann, 2002; Zhao et al., 2016; Radeck et al., 2017b) (Fig. 3B). Thus, the total speed of the UPP desphosphorylation reaction is given by the weighted sum of the bacitracin-dependent contribution from BcrC and the bacitracin-independent contribution from UppP (Fig. 3C), with  $x^{BcrC}$  quantifying the relative contribution of BcrC, and  $1 - x^{BcrC}$  the relative contribution of UppP. The stronger the contribution of BcrC towards the overall phosphatase activity (higher  $x^{BcrC}$ ), the more pronounced the acceleration of the UPP dephosphorylation reaction in response to bacitracin (Fig. 3C). To determine the unknown parameter  $x^{BcrC}$ , we first assumed that the BcrC protein level is proportional to the detected luminescence output from the  $P_{bcrC}$ -*luxABCDE* reporter in the *bceAB* mutant (Fig. 2B(i)). We then simulated the

model of the lipid II cycle for different values of  $x^{BcrC}$  and monitored how the up-regulation of BcrC in response to bacitracin affects the overall rate of PG synthesis (Fig. 3D). Here, it turned out that in the absence of BcrC upregulation ( $x^{BcrC} = 0$ ) the PG synthesis rate decreased hyperbolically with increasing bacitracin concentration, as seen before (Piepenbreier *et al.*, 2019). In contrast, for high values of  $x^{BcrC}$ , the up-regulation of BcrC led to a peak of the PG synthesis rate at intermediate bacitracin levels, and to a shift of the IC<sub>50</sub> value – the antibiotic concentration reducing the PG synthesis rate to 50% of its unperturbed rate – to higher values. Studying the dependence of the predicted IC<sub>50</sub> values on different values of  $x^{BcrC}$  showed that the IC<sub>50</sub> matched the experimentally measured MIC of the  $\Delta bceAB$  mutant when UppP and BcrC have approximately equal contributions to the overall phosphatase activity (Fig. 4A).

### **The total amount of lipid carrier is increased under *bcrC* deletion to ensure close-to-optimal PG synthesis rate**

If the two phosphatases make approximately equal contributions to the overall phosphatase activity, one would predict that the deletion of one of the phosphatases should have significant impact on cellular physiology even in the absence of cell wall antibiotics. In fact, within our model the deletion of *bcrC* significantly reduces the speed of the dephosphorylation reaction of the lipid II cycle – leading to an accumulation of UPP (Supplementary Fig. S2B). Given that the lipid II cycle can be approximated as a closed-loop system in which the total amount of lipid intermediates running through the cycle stays constant (Piepenbreier *et al.*, 2019), the accumulation of UPP simultaneously reduces the concentrations of all other lipid II cycle carriers (Supplementary Fig. S2B). In addition, especially the shortage of lipid II directly leads to a distinct reduction of the overall rate of PG synthesis of the lipid II cycle, since lipid II ultimately releases the PG monomers for incorporation into the cell wall (see theoretical description of the PG synthesis rate in the Supplementary files). Hence, within the simulated range of BcrC and UppP contributions to the overall phosphatase activity, the lack of BcrC was predicted to reduce the rate of PG synthesis below its half-maximum for some of the parameters tested (Supplementary Fig. S2B). Furthermore, the model predicted relatively low IC<sub>50</sub> values since the overall PG synthesis rate was already reduced and very small amounts of bacitracin should be sufficient to further decrease it to the assumed critical rate of 50% of its optimal level.

However, such a reduction in the overall rate of PG synthesis even without bacitracin treatment would cause clear defects in cell growth, which was neither observable in the absence of bacitracin nor under low bacitracin concentrations when monitoring the growth of  $\Delta bceAB\Delta bcrC$  mutant strain. Instead, the growth rate of the double mutant was only slightly affected without bacitracin (Supplementary Fig. S1) and the experimentally determined MIC (Fig. 2B(ii), *light blue*) was significantly higher than the IC<sub>50</sub> values predicted by the model.



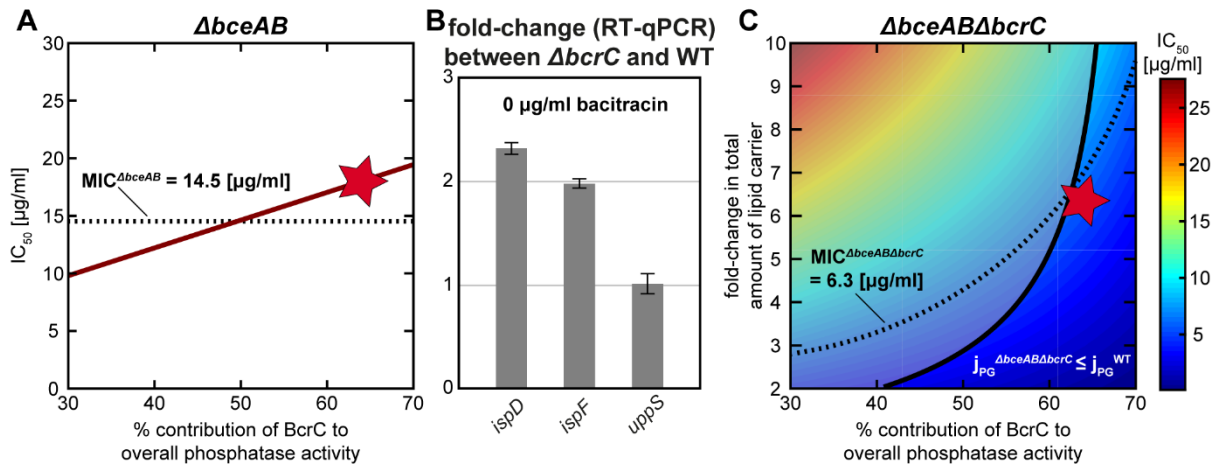


**Figure 4. Calibration of a model integrating the lipid II cycle with the BcrC resistance module.** (A) Combining the lipid II cycle module with the BcrC module (cf. Fig. 2A) leads to a model describing a  $\Delta bceAB$  mutant strain. Predictions of this model for the IC<sub>50</sub> value (the bacitracin concentration at which the PG synthesis rate declines to 50% of the unperturbed value) are shown under various contributions of BcrC ( $x^{BcrC}$ ) to the overall UPP phosphatase activity (red line). The linear increase of the IC<sub>50</sub> value with  $x^{BcrC}$  is the result of the stronger overall phosphatase activity incurred by BcrC up-regulation (cf. Fig. 3C, D). The dashed line shows the experimental MIC of bacitracin in a  $\Delta bceAB$  mutant and the red star indicates the optimal parameter obtained by in our constrained optimization approach (see Supplementary Text). (B) In the absence of bacitracin, expression of *ispD* and *ispF* is up-regulated in a  $\Delta bcrC$  mutant relative to the *B. subtilis* wild-type, as quantified by RT-qPCR described in Materials and Methods. Given that *ispD* and *ispF* are involved in early steps of UPP *de novo* synthesis, this suggests that the deletion of *bcrC* triggers elevated levels of lipid II cycle intermediates, which may in turn compensate for the reduced UPP dephosphorylation rate in this mutant. (C) Predictions of the bacitracin IC<sub>50</sub> in a model for the  $\Delta bceAB\Delta bcrC$  double mutant (color code) as a function of various contributions of BcrC to the overall UPP phosphatase activity ( $x$ -axis) and the fold-change of total lipid II cycle intermediates as induced by the *bcrC* deletion ( $y$ -axis). Within this model, the higher  $x^{BcrC}$  in the model in the  $\Delta bceAB$  mutant, the stronger the *bcrC* deletion in the double mutant reduces the IC<sub>50</sub> value. Accordingly, in order to achieve a similar IC<sub>50</sub> value (=same color in the background), higher  $x^{BcrC}$  fractions require higher up-regulation of the total abundance of lipid II cycle intermediates in this model. The dashed line indicates the experimental MIC of bacitracin in a  $\Delta bceAB\Delta bcrC$  double mutant. The parameters below the solid black line represent physiologically plausible combinations, in which the PG synthesis rate in the mutant ( $j_{PG}^{\Delta bceAB\Delta bcrC}$ ) does not exceed the rate in the wild-type ( $j_{PG}^{WT}$ ). The red star indicates the optimal parameter set obtained by in our constrained optimization approach (see Supplementary Text).

These results led us speculate that *B. subtilis* uses additional routes to respond to the deletion of *bcrC* – thereby ensuring a close-to-optimal rate of PG synthesis – probably by increasing the concentrations of lipid II. How does the cell implement this homeostatic control? As previous studies revealed,  $\sigma^M$  not only regulates the expression of *bcrC* in response to bacitracin, but also induces individual steps of the methylerythritol phosphate (MEP) pathway (e.g. *ispD-F*), which is responsible for early steps of lipid carrier (UPP) synthesis (Julsing *et al.*, 2007; Eiamphungporn and Helmann, 2008). Indeed, it was shown that the expression of  $\sigma^M$  itself is significantly increased in a mutant strain lacking BcrC (Zhao *et al.*, 2016). Hence, we hypothesized that the lipid II concentrations might be homeostatically regulated by  $\sigma^M$ -dependent control of the production of new lipid carrier. To test this hypothesis, we used RT-qPCR to quantify transcript levels of  $\sigma^M$ -regulated genes involved in the production of UPP synthesis. As illustrated in Fig. 4B, we found that during exponential growth in LB medium (without bacitracin) expression of both *ispD* and *ispF* was 2-fold higher in the *bcrC* deletion strain compared to the wild-type strain. Furthermore, the UPP synthetase encoded by *uppS*,

which is not part of the  $\sigma^M$ -regulon, did not show differential expression between both strains (Fig. 4B). These results suggest that the upregulation of early steps of UPP synthesis in a *bcrC* deletion mutant may increase the overall abundance of lipid carriers in the lipid II cycle, thereby counteracting the bottleneck induced by UPP phosphatase deletion.

Hence, we asked how a higher total concentration of the lipid II cycle intermediates (in the following referred to as “LII intermediates”) would affect the model prediction for a *bcrC* deletion mutant (see Supplementary Text for a detailed description). As we did not know the precise change in LII intermediates in the *bcrC* deletion strain, we simulated the model for different fold-changes in LII intermediates and predicted the  $IC_{50}$  under bacitracin treatment. Here it turned out that an increase in LII intermediates raises both the lipid II concentrations and the overall PG synthesis rate (Supplementary Fig. S2C) and thus, ensures progression of the lipid II cycle without bacitracin treatment – as suggested by the experimental growth data (Supplementary Fig. S1). Accordingly, the model predicts that higher levels of LII intermediates in the  $\Delta bceAB\Delta bcrC$  mutant lead to higher  $IC_{50}$  values under bacitracin treatment (Fig. 4C; *dependence along vertical axis*). The model also predicts that the higher the contribution of BcrC to the overall phosphatase activity, the higher the required fold-change in LII intermediates to reach the same  $IC_{50}$  values in the  $\Delta bceAB\Delta bcrC$  mutant (Fig. 4C; *dependence along horizontal axis*). This underlines the idea that upregulation of LII intermediates can compensate for the lack of UPP phosphatase activity. However, we also noted that some of the tested parameter combinations led to predictions in which the PG synthesis rate in the mutant ( $j_{PG}^{\Delta bceAB\Delta bcrC}$ ) was higher than the rate in the WT ( $j_{PG}^{WT}$ ), which is physiologically implausible (Fig. 4C; *shaded area*). Thus, to arrive at a physiologically plausible parameter set we performed parameter optimization to simultaneously fit the experimental MIC values of the  $\Delta bceAB$  and  $\Delta bceAB\Delta bcrC$  mutant strains while meeting the constraint  $j_{PG}^{\Delta bceAB\Delta bcrC} \leq j_{PG}^{WT}$ . This resulted in a set of parameters in which BcrC was the dominant phosphatase ( $x^{BcrC} = 63(\pm 9.5)\%$ ) and in which the LII intermediate level was upregulated  $6.2(\pm 0.7)$ -fold, resulting in a close-to-optimal PG synthesis rate and  $IC_{50}$  predictions ranging closely around the measured MICs for both mutant strains (Fig. 4A,C; *red stars*). These results are in line with previous experimental studies in *B. subtilis* (Radeck *et al.*, 2017b), showing that a *bcrC* deletion lead to a stronger reduction in resistance against bacitracin than a deletion of *uppP*. Hence, by integrating the homeostatic control of the overall LII intermediate level in response to a lack of BcrC, we arrived at a theoretical model that quantifies the impact of BcrC as secondary resistance module on the progression of the lipid II cycle – both in the absence and in the presence of bacitracin.

### Interaction between the BcrC and BceAB resistance modules

Next, we focussed on the interplay between the primary and secondary resistance modules BceAB and BcrC, respectively. As noted above, it turned out that the presence of BceAB in the wild-type mitigates the demand for *bcrC* expression, as reflected in a ~2-fold lower fold-induction in  $P_{bcrC}$  activity upon bacitracin treatment in the wild-type compared to the  $\Delta bceAB$  mutant (Fig. 2B(i); *black vs. green line*). *Vice versa*, we found that the  $P_{bceAB}$  promoter displays a ~10-fold lower activity in wild-type compared to a  $\Delta bcrC$  mutant, suggesting that also the presence of BcrC reduces the demand for *bceAB* expression in wild-type cells. These results clearly indicate a high level of cross-regulation between the resistance modules, which we wanted to rationalize via our computational model.

In order to complete the computational model of the bacitracin resistance network in *B. subtilis* wild-type, we next integrated the BceAB transporter into our theory of the lipid II cycle. To this end, we took advantage of a previously developed theoretical description of the BceAB resistance module in *B. subtilis* (Fritz *et al.*, 2015). Briefly, this model is based on differential equations describing the binding of bacitracin (BAC) to UPP (yielding UPP-BAC complexes), the up-regulation of *bceAB* expression in response to increasing UPP-BAC complexes and ultimately the release of bacitracin from UPP catalysed by increasing BceAB transporters levels. Here, the relative bacitracin flux ( $J_{BAC}$ ) experienced by each BceAB transporter is described by Michaelis-Menten kinetics,

$$J_{BAC} = \frac{[UPP - BAC]}{K_M + [UPP - BAC]}, \quad (1)$$

where  $K_M$  is the UPP-BAC concentration at which the catalytic rate of BceAB reaches its half-maximal value. Importantly, within this model  $J_{BAC}$  not only sets the rate at which UPP is released from the inhibitory grip of bacitracin, but also regulates expression of *bceAB* expression via the flux-sensing mechanism depicted in Fig. 2A and as detailed in the Supplementary Text. Combining this model for the BceAB module with the equations for the lipid II cycle – including the bacitracin-dependent up-regulation of the BcrC module – ultimately led us to a comprehensive computational model for both resistance modules in the *B. subtilis* wild-type strain (see Supplementary Text for a detailed model description).

We then asked whether this full model is in quantitative agreement with the data describing the bacitracin response of the BceAB module in wild-type cells. To this end, we fixed all parameters for the lipid II cycle to the optimal values derived above and imposed that the regulation of BcrC protein levels is proportional to the  $P_{bcrC}$  promoter activity measured in the wild-type strain (Fig. 2B(i); *black data*). Then we estimated the additional parameters describing the induction of the BceAB resistance module by a fit to the experimental  $P_{bceAB}$  promoter activity (Fig. 2B(iii), *black data*); see Materials and Methods for details of the fitting procedure and Supplementary Table 3 for parameter values. This led us to a parameter combination for which the model output closely resembles the observed response of  $P_{bceAB}$

towards bacitracin (Fig. 5A), suggesting that the model accurately captures the cross-regulation between the two resistance modules. Importantly, when studying the PG synthesis rate within this model (Fig. 5C; *black line*), it turned out that with increasing bacitracin concentration the increasing production of BcrC and BceAB stabilized the PG synthesis rate even in the presence of bacitracin, and increased the  $IC_{50}$  to a value close to the MIC experimentally measured in the wild-type strain (Fig. 5C; *black star*  $MIC^{WT} \sim 125 \mu\text{g/ml}$ ). These results show that the computational model of the bacitracin resistance network now precisely rebuilds the interplay of the two resistance modules and suggests that the simultaneous induction of the two resistance modules jointly mediate lipid II cycle homeostasis under bacitracin treatment.

To further test the validity of our model, we demanded that it should be able to correctly predict the behaviour of a  $\Delta bcrC$  strain, in which BceAB is the sole genuine resistance determinant under bacitracin treatment (Fig. 5A; *red data points*). Due to the lack of BcrC in this strain, our model predicts that these cells produce higher levels of LII intermediates (similar to the  $\Delta bcrC\Delta bceAB$  double mutant), which also leads to a higher abundance of UPP in the cell. This increased exposure of UPP then leads to higher levels of the bacitracin-bound form UPP-BAC in the presence of the antibiotic, which in turn serves as the stimulus for the activation of the  $P_{bceA}$  promoter via the previously described flux-sensing mechanism. Accordingly, our model predicts that the accumulation of UPP-BAC in the  $\Delta bcrC$  strain triggers a  $\sim 10$ -fold higher  $P_{bceA}$  promoter activity compared to the wild-type strain (Fig. 5A; *red dashed line*), in qualitative agreement with the increased  $P_{bceA}$  activity in the  $\Delta bcrC$  strain determined experimentally (Fig. 5A; *red data points*). Also, without invoking any further parameter fitting, for a strain lacking BcrC the model-predicted  $IC_{50}^{\Delta bcrC} = 22 \mu\text{g/ml}$  closely matches the experimentally determined MIC of a  $\Delta bcrC$  mutant (Fig. 5C;  $MIC^{\Delta bcrC} \sim 25 \mu\text{g/ml}$ ). This suggests that the simulated response of the BceAB resistance module – in conjunction with the elevated pool of LII intermediates – accurately capture the physiology of the system under bacitracin treatment.

One striking discrepancy between our model and the experimental data, however, was visible in the absence of bacitracin, where our experiments showed that the promoter activity of  $P_{bceAB}$  was also  $\sim 10$ -fold higher than in the wild-type (Fig. 5A). This result is not compatible with the idea that UPP-BAC is the sole substrate for the flux-sensing mechanism via the BceAB transporter (triggering the activation of  $P_{bceA}$ ), because UPP-BAC cannot be formed in the absence of bacitracin and thus the signalling mechanism should be inactive. However, it was previously hypothesized that UPP itself somehow triggers (futile?) ATP hydrolysis by BceAB and that high levels of UPP may contribute to the activation of  $P_{bceAB}$  (Kingston *et al.*, 2014; Radeck *et al.*, 2016). Such an interaction seems plausible, given that the recognition of the UPP-BAC complex by BceAB likely involves interactions with both the UPP as well as the BAC

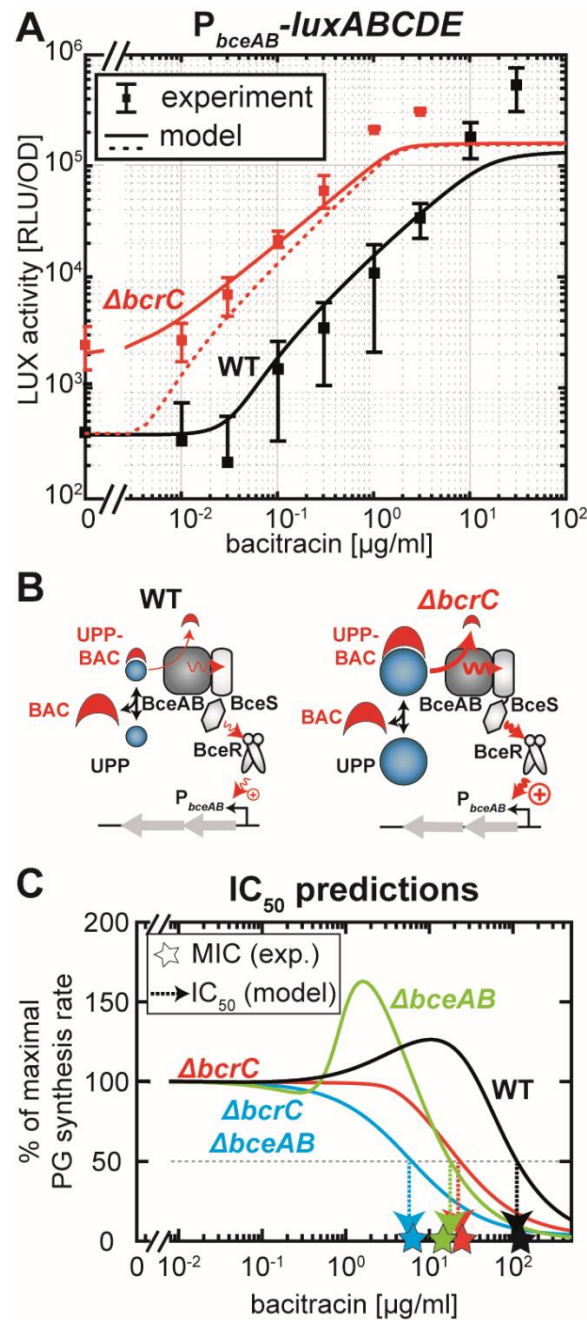


**Figure 5. Model calibration of the BceAB resistance module and MIC predictions in *B. subtilis* wild-type and mutant strains.** (A) Fit of the full model for the bacitracin resistance network (including the BceAB module) to the experimental dose-response characteristic of the  $P_{bceAB}$ -*luxABCDE* reporter in *B. subtilis* wild-type (WT) cells (black line). The red dashed line shows the model prediction for the  $\Delta bcrC$  mutant without invoking further fit parameters, revealing that although the model captures the overall increase in  $P_{bceAB}$  activity under bacitracin treatment, it does not describe the elevated basal promoter activity in the absence of bacitracin (see Supplementary Text for details). The red solid line shows the prediction of the model when the BceAB/BceS flux-sensing complex recognizes unbound UPP as a secondary substrate, which leads to a futile flux and triggers signaling in the BceRS two-component system. (B) Schematic model behavior in wild-type and  $\Delta bcrC$  mutant at identical bacitracin concentrations, illustrating that the higher UPP pool in the  $\Delta bcrC$  mutant leads to higher UPP-BAC levels and thus to stronger activation of the BceRS signaling cascade when compared to the wild-type. (C) The model behavior of the PG synthesis rate under bacitracin treatment for *B. subtilis* wild-type and mutant cells, generates predictions for the respective  $IC_{50}$  values (arrows), which are close to the experimental MIC values of the corresponding strains.

moieties, raising the possibility that BceAB has some residual affinity for UPP. Interestingly, as noted above, the model predicts a significantly higher concentration of UPP in the  $\Delta bcrC$  mutant compared to the wild-type (Supplementary Figure 3B) – mainly caused by the expected increase of the overall concentration lipid II cycle intermediates as well as the reduced overall phosphatase activity in the absence of BcrC. To test if futile activation of  $P_{bceAB}$  by these elevated UPP levels can explain the higher basal promoter activity observed in the  $\Delta bcrC$  mutant, we modified the theoretical description of the total load per BceAB transporter,  $J_{load}$ , which is proportional to the rate of ATP hydrolysis and in turn regulates the promoter activity of  $P_{bceAB}$ , as follows:

$$J_{load} = J'_{BAC} + J_{futile} , \quad (2)$$

where

$$J'_{BAC} = \frac{[UPP-BAC]}{K_M} / \left( 1 + \frac{[UPP-BAC]}{K_M} + \frac{[UPP]}{\tilde{K}_M} \right) \quad (3)$$

describes the flux of bacitracin released from UPP-BAC complexes and

$$J_{futile} = \frac{[UPP]}{\tilde{K}_M} / \left( 1 + \frac{[UPP-BAC]}{K_M} + \frac{[UPP]}{\tilde{K}_M} \right) \quad (4)$$

describes the rate of futile ATP hydrolysis triggered by UPP alone – with Michaelis constants  $\tilde{K}_M$  and  $K_M$  describing the binding constants of the transporter for UPP and UPP-BAC, respectively. Within these equations an increasing level of UPP increases the overall load per transporter,  $J_{load}$ , which then triggers signalling and activation of  $P_{bceAB}$ , while the same increase in UPP leads to a reduction of the flux of bacitracin release,  $J'_{BAC}$ , induced by competitive binding to the transporter. Strikingly, by modifying the model as depicted, the predictions of  $P_{bceAB}$  promoter activation differed significantly between the simulated scenarios (Fig. 5A; *red solid line*). While the model output for the wild-type equalled the prediction of the former model, the modified model predicted a significant elevation of  $P_{bceAB}$  promoter activities in a strain lacking BcrC, which closely resembles the experimental data for the  $\Delta bcrC$  strain (Fig. 5A). Thus, our results of the modified model support the hypothesis of futile activation of  $P_{bceAB}$  by UPP under BcrC deletion (Fig. 5B). However, since the model modifications did not affect the  $IC_{50}$  predictions of the various mutants (see Supplementary Text), the effect of UPP on  $P_{bceAB}$  activation is likely negligible under bacitracin treatment and solely affects the level of basal promoter activity.



## Discussion

Building on the experimental characterization of the bacitracin resistance network in *B. subtilis* (Radeck *et al.*, 2016), we here present the first theoretical description of this regulatory network. The mathematical model developed here not only accurately predicts the efficacy of bacitracin in the wild-type and various mutant strains lacking one or both of the resistance modules (Fig. 5C), but also uncovers important regulatory features of the resistance network. By successively incorporating mathematical descriptions of the individual resistance modules into a pre-existing theory of the lipid II cycle, we showed that the interplay between the two major resistance determinants (BceAB and BcrC) is strictly linked to the properties of the lipid II cycle, which change in response to bacitracin.

One important insight of our analysis is that BcrC is the more dominant UPP phosphatase compared to UppP - dictating the bulk of the overall UPP recycling rate in the lipid II cycle of *B. subtilis*. This is also reflected by the fact that *bcrC* expression is significantly elevated under bacitracin stress (Fig. 2B(i)), while *uppP* is constitutively expressed (Cao and Helmann, 2002; Zhao *et al.*, 2016; Radeck *et al.*, 2017b), implying even more pronounced changes in the total phosphatase activity in response to bacitracin than previously appreciated. These results are in accordance with experiments showing that a *bcrC* deletion significantly reduced the resistance towards bacitracin in *B. subtilis*, while a deletion of *uppP* only had moderate effects (Cao and Helmann, 2002; Radeck *et al.*, 2017b). In fact, to ensure a strong protective effect in response to cell envelope stress, it seems physiologically plausible for the cell to activate expression of the phosphatase contributing strongest to the progression of the lipid II cycle.

Another finding arising from the combination of theory and experiment was the homeostatic control of lipid II cycle intermediate levels in a  $\Delta bcrC$  mutant – ensuring the close-to-optimal progression of the cycle despite the lack of the important phosphatase BcrC. To counteract the depletion of the lipid II pool caused by a shortage of UPP phosphatase activity, we found two  $\sigma^M$ -controlled genes, *ispD* and *ispF*, involved in the *de novo* synthesis of UPP to be significantly up-regulated. While we did not directly prove that this leads to an increase in the overall abundance of lipid II cycle intermediates, our experimental and theoretical results indirectly support this hypothesis in three ways: (1) The  $\Delta bcrC\Delta bceAB$  double mutant is significantly more resistant to bacitracin than naively predicted by a model with constant total lipid II cycle intermediate pools, suggesting that a compensatory up-regulation of these pools contributes to bacitracin resistance in this mutant. (2) Under bacitracin treatment the  $P_{bceA}$  promoter is ~10-fold more active in a  $\Delta bcrC$  mutant compared to the wild-type, suggesting that the major substrate, UPP-BAC, of the BceAB transporter is more abundant in the mutant, which in turn triggers stronger activation of  $P_{bceA}$  via the flux-sensing mechanism. (3) Even in the absence of bacitracin the  $\Delta bcrC$  mutant displays a ~10-fold higher  $P_{bceA}$  activity than the

wild-type, suggesting that the elevated UPP pool in this mutant is sufficient to trigger some futile ATP hydrolysis by the BceAB transporter, which then activates  $P_{bceA}$  via the flux-sensing mechanism.

From a systems-level perspective, the up-regulation of lipid carrier production seems to be a particularly elegant way to maintain cycle homeostasis under antibiotic treatment, because it naturally preserves the relative balance between the different lipid II cycle intermediates. In fact, in a closed-loop system like the lipid II cycle, the stoichiometry between the intermediate pools is only determined by the catalytic rates and abundances of the enzymes catalysing cycle progression and not the overall abundance of all intermediates (Piepenbreier *et al.*, 2019). Thus, the sequestration of one cycle intermediate by an antibiotic (such as bacitracin, vancomycin or nisin) will lead to the stoichiometric reduction of all other intermediates. One possible way to accelerate lipid II cycle progression would be the simultaneous up-regulation of all lipid II cycle-associated enzymes. In contrast to such a fine-tuned, orchestrated regulation, our results suggest that the cell compensates this shortage by *de novo* synthesis of cycle intermediates, which rapidly equilibrates among the different stages of the lipid II cycle intermediates and naturally replenishes intermediate levels in the correct stoichiometry. We suggest that this strategy implements a robust way of ensuring lipid II cycle homeostasis.

Although we did not decipher the exact stimulus for activation of the BcrC resistance module, our theory revealed that the regulation of *bcrC* and *bceAB* expression are tightly interconnected via the properties of the lipid II cycle itself. Since the activation of the resistance determinants in response to bacitracin go along with significant changes in the concentrations of the different lipid II cycle intermediates, it is plausible that not only BceAB but also the BcrC resistance module somehow responds to these changes. Indeed, it seems advantageous to regulate the overall resistance against bacitracin by responding to changes in the properties of the lipid II cycle, since this does not demand additional regulatory structures for each resistance module, which might be costly to produce and would further complicate the resistance network. More generally, monitoring the physiological state of the pathway itself may serve as a cost-effective strategy to regulate the interplay between the different resistance determinants protecting the cell against cell envelope stress.

Ultimately, this study clearly highlights how mathematical modelling provides a better understanding of sophisticated cellular responses towards environmental conditions, in particular antibiotic treatment. By combining existing theoretical descriptions of the various modules of the cellular response, a comprehensive model of the complex network structure evolved. Successive integration of additional modules of the cellular response into the growing model enabled us to study both the basal regulatory features of every individual layer as well as the factors determining the interplay between them within the whole network. We showed



that a simple existing model can be expanded to develop a more and more complex picture, and eventually the model itself could even become a building block when describing a network on a broader scale. This approach can act as a blueprint for acquiring true systems-level understanding of complex regulatory structures, not only describing the organisation of resistance system against other antibiotics, but also more generally multi-tiered response networks that can be expected across many bacterial species and a range of environmental stressors.

## **Acknowledgements**

This work was supported by the LOEWE Program of the State of Hesse (SYNMIKRO support to G.F.), the Deutsche Forschungsgemeinschaft (DFG grants FR3673/1-2 to G.F. and MA2837/2-2 to T.M. in the framework of the DFG priority program SPP1617) and the Biotechnology and Biological Sciences Research Council (BBSRC grant BB/M029255/1 to S.G.). HP was supported by the Cusanuswerk scholarship programme (Germany) and CMK was supported by a University of Bath Research Studentship Award.

## References

- Asai, K. (2018) Anti-sigma factor-mediated cell surface stress responses in *Bacillus subtilis*. *Genes Genet Syst* **92**: 223–234.
- Bernard, R., Ghachi, El, M., Mengin-Lecreulx, D., Chippaux, M., and Denizot, F. (2005) BcrC from *Bacillus subtilis* acts as an undecaprenyl pyrophosphate phosphatase in bacitracin resistance. *Journal of Biological Chemistry* **280**: 28852–28857.
- Bernard, R., Guiseppi, A., Chippaux, M., Foglino, M., and Denizot, F. (2007) Resistance to bacitracin in *Bacillus subtilis*: unexpected requirement of the BceAB ABC transporter in the control of expression of its own structural genes. *Journal of Bacteriology* **189**: 8636–8642.
- Bischofs, I.B., Hug, J.A., Liu, A.W., Wolf, D.M., and Arkin, A.P. (2009) Complexity in bacterial cell-cell communication: Quorum signal integration and subpopulation signaling in the *Bacillus subtilis* phosphorelay. *Proc Natl Acad Sci USA* **106**: 6459–6464.
- Cao, M., and Helmann, J.D. (2002) Regulation of the *Bacillus subtilis* *bcrC* bacitracin resistance gene by two extracytoplasmic function sigma factors. *Journal of Bacteriology* **184**: 6123–6129.
- Cetinkaya, Y., Falk, P., and Mayhall, C.G. (2000) Vancomycin-resistant enterococci. *Clin Microbiol Rev* **13**: 686–.
- Dintner, S., Heermann, R., Fang, C., Jung, K., and Gebhard, S. (2014) A sensory complex consisting of an ATP-binding cassette transporter and a two-component regulatory system controls bacitracin resistance in *Bacillus subtilis*. *Journal of Biological Chemistry* **289**: 27899–27910.
- Dintner, S., Staroń, A., Berchtold, E., Petri, T., Mascher, T., and Gebhard, S. (2011) Coevolution of ABC transporters and two-component regulatory systems as resistance modules against antimicrobial peptides in *Firmicutes* Bacteria. *Journal of Bacteriology* **193**: 3851–3862.
- Domínguez-Escobar, J., Wolf, D., Fritz, G., Höfler, C., Wedlich-Söldner, R., and Mascher, T. (2014) Subcellular localization, interactions and dynamics of the phage-shock protein-like Lia response in *Bacillus subtilis*. *Molecular Microbiology* **92**: 716–732.
- Economou, N.J., Cocklin, S., and Loll, P.J. (2013) High-resolution crystal structure reveals molecular details of target recognition by bacitracin. *Proc Natl Acad Sci USA* **110**: 14207–14212.
- Eiamphungporn, W., and Helmann, J.D. (2008) The *Bacillus subtilis*  $\sigma^M$  regulon and its contribution to cell envelope stress responses. *Molecular Microbiology* **67**: 830–848.
- Fritz, G., Dintner, S., Treichel, N.S., Radeck, J., Gerland, U., Mascher, T., and Gebhard, S. (2015) A new way of sensing: Need-based activation of antibiotic resistance by a flux-sensing mechanism. *mBio* **6**: e00975.
- Gebhard, S. (2012) ABC transporters of antimicrobial peptides in Firmicutes bacteria - phylogeny, function and regulation. *Molecular Microbiology* **86**: 1295–1317.

Helmann, J.D. (2016) *Bacillus subtilis* extracytoplasmic function (ECF) sigma factors and defense of the cell envelope. *Current Opinion in Microbiology* **30**: 122–132.

Iber, D., Clarkson, J., Yudkin, M.D., and Campbell, I.D. (2006) The mechanism of cell differentiation in *Bacillus subtilis*. *Nature* **441**: 371–374.

Igoshin, O.A., Price, C.W., and Savageau, M.A. (2006) Signalling network with a bistable hysteretic switch controls developmental activation of the sigma transcription factor in *Bacillus subtilis*. *Molecular Microbiology* **61**: 165–184.

Jabbari, S., Heap, J.T., and King, J.R. (2011) Mathematical modelling of the sporulation-initiation network in *Bacillus subtilis* revealing the dual role of the putative quorum-sensing signal molecule PhrA. *Bull Math Biol* **73**: 181–211.

Jordan, S., Hutchings, M.I., and Mascher, T. (2008) Cell envelope stress response in Gram-positive bacteria. *FEMS Microbiol Rev* **32**: 107–146.

Jordan, S., Junker, A., Helmann, J.D., and Mascher, T. (2006) Regulation of LiaRS-dependent gene expression in *Bacillus subtilis*: Identification of inhibitor proteins, regulator binding sites, and target genes of a conserved cell envelope stress-sensing two-component system. *Journal of Bacteriology* **188**: 5153–5166.

Julsing, M.K., Rijpkema, M., Woerdenbag, H.J., Quax, W.J., and Kayser, O. (2007) Functional analysis of genes involved in the biosynthesis of isoprene in *Bacillus subtilis*. *Applied Microbiology and Biotechnology* **75**: 1377–1384.

Kingston, A.W., Zhao, H., Cook, G.M., and Helmann, J.D. (2014) Accumulation of heptaprenyl diphosphate sensitizes *Bacillus subtilis* to bacitracin: implications for the mechanism of resistance mediated by the BceAB transporter. *Molecular Microbiology* **93**: 37–49.

Livak, K.J., and Schmittgen, T.D. (2001) Analysis of relative gene expression data using real-time quantitative PCR and the  $2^{-\Delta\Delta CT}$  Method. *Methods* **25**: 402–408.

Mascher, T., Margulis, N.G., Wang, T., Ye, R.W., and Helmann, J.D. (2003) Cell wall stress responses in *Bacillus subtilis*: the regulatory network of the bacitracin stimulon. *Molecular Microbiology* **50**: 1591–1604.

Ohki, R., Giyanto, Tateno, K., Masuyama, W., Moriya, S., Kobayashi, K., and Ogasawara, N. (2003) The BceRS two-component regulatory system induces expression of the bacitracin transporter, BceAB, in *Bacillus subtilis*. *Molecular Microbiology* **49**: 1135–1144.

Piepenbreier, H., Diehl, A., and Fritz, G. (2019) Blocking of peptidoglycan synthesis by cell wall antibiotics. *Submitted*.

Radeck, J., Fritz, G., and Mascher, T. (2017a) The cell envelope stress response of *Bacillus subtilis*: from static signaling devices to dynamic regulatory network. *Current Genetics* **63**: 79–90.

Radeck, J., Gebhard, S., Orchard, P.S., Kirchner, M., Bauer, S., Mascher, T., and Fritz, G. (2016) Anatomy of the bacitracin resistance network in *Bacillus subtilis*. *Molecular Microbiology* **100**: 607–620.

Radeck, J., Lautenschläger, N., and Mascher, T. (2017b) The essential UPP phosphatase pair BcrC and UppP connects cell wall homeostasis during growth and sporulation with cell envelope stress response in *Bacillus subtilis*. *Front Microbiol* **8**: 2403.

Rao, C.V., Kirby, J.R., and Arkin, A.P. (2004) Design and diversity in bacterial chemotaxis: a comparative study in *Escherichia coli* and *Bacillus subtilis*. *PLoS Biol* **2**: E49.

Rao, C.V., Kirby, J.R., and Arkin, A.P. (2005) Phosphatase localization in bacterial chemotaxis: divergent mechanisms, convergent principles. *Phys Biol* **2**: 148–158.

Revilla-Guarinos, A., Gebhard, S., Mascher, T., and Zúñiga, M. (2014) Defence against antimicrobial peptides: different strategies in *Firmicutes*. *Environmental Microbiology* **16**: 1225–1237.

Rietkötter, E., Hoyer, D., and Mascher, T. (2008) Bacitracin sensing in *Bacillus subtilis*. *Molecular Microbiology* **68**: 768–785.

Schneider, T., and Sahl, H.-G. (2010) An oldie but a goodie - cell wall biosynthesis as antibiotic target pathway. *Int J Med Microbiol* **300**: 161–169.

Schultz, D., Wolynes, P.G., Ben Jacob, E., and Onuchic, J.N. (2009) Deciding fate in adverse times: sporulation and competence in *Bacillus subtilis*. *P Natl Acad Sci Usa* **106**: 21027–21034.

Storm, D.R., and Strominger, J.L. (1973) Complex formation between bacitracin peptides and isoprenyl pyrophosphates. The specificity of lipid-peptide interactions. *Journal of Biological Chemistry* **248**: 3940–3945.

Sun, Z., Zhong, J., Liang, X., Liu, J., Chen, X., and Huan, L. (2009) Novel mechanism for nisin resistance via proteolytic degradation of nisin by the nisin resistance protein NSR. *Antimicrobial Agents and Chemotherapy* **53**: 1964–1973.

Zhao, H., Roistacher, D.M., and Helmann, J.D. (2019) Deciphering the essentiality and function of the anti- $\sigma^M$  factors in *Bacillus subtilis*. *Molecular Microbiology*.

Zhao, H., Sun, Y., Peters, J.M., Gross, C.A., Garner, E.C., and Helmann, J.D. (2016) Depletion of undecaprenyl pyrophosphate phosphatases disrupts cell envelope biogenesis in *Bacillus subtilis*. *Journal of Bacteriology* **198**: 2925–2935.

## Supplementary Information

### From modules to networks: A systems-level analysis of the bacitracin stress response in *Bacillus subtilis*

Hannah Piepenbreier<sup>1</sup>, Andre Sim<sup>1</sup>, Carolin M. Kobras<sup>2</sup>, Jara Radeck<sup>3</sup>, Thorsten Mascher<sup>3</sup>,  
Susanne Gebhard<sup>2</sup> and Georg Fritz<sup>1,\*</sup>

<sup>1</sup>LOEWE Center for Synthetic Microbiology and Department of Physics, Philipps-Universität Marburg, Germany; <sup>2</sup>Department of Biology & Biochemistry, Milner Centre for Evolution, University of Bath, United Kingdom; <sup>3</sup>Institute of Microbiology, Technische Universität (TU) Dresden, 01062 Dresden, Germany

\*For correspondence: georg.fritz@synmikro.uni-marburg.de

## Content

### Supplementary Text

**Supplementary Figure 1:** Growth curves of *B. subtilis* W168 wild-type and  $\Delta bcrC$ ,  $\Delta bceAB$  and  $\Delta bceAB\Delta bcrC$  mutant strains.

**Supplementary Figure 2:** Model-predicted distribution of lipid II cycle intermediates in the  $\Delta bceAB$  and  $\Delta bceAB\Delta bcrC$  mutant strains.

**Supplementary Figure 3:** Best-fit results of the model parameters  $x^{BcrC}$  and  $s^{UPP}$  and their corresponding confidence intervals

**Supplementary Table 1:** Bacterial strains used in this study

**Supplementary Table 2:** Plasmids used in this study

**Supplementary Table 3:** Model parameters

**Supplementary References**

## Supplementary Text

### **Computational model of the bacitracin stress response network**

To build the computational model of the bacitracin stress response network, we combined the pre-existing mathematical description of the lipid II cycle (Piepenbreier *et al.*, 2019) and the previously developed theory of the BceAB transporter production in response to bacitracin (Fritz *et al.*, 2015) and included a description of the BcrC module in addition.

The kinetic model of the lipid II cycle (Piepenbreier *et al.*, 2019) describes the time-dependent changes of the concentrations of the different lipid II cycle intermediates (as illustrated in Fig. 1 in the main text) by deterministic differential equations to monitor the dynamics of cell wall biosynthesis per individual cell. The well-studied enzymatic reactions of MraY, MurG, the diverse penicillin-binding protein (PBPs) and the two undecaprenyl pyrophosphate phosphatases (UppPs) were modelled by Michaelis-Menten kinetics, for which substrate levels ( $S_i$ ), enzyme levels ( $E$ ), catalytic constants of the enzymes ( $k_{cat}$ ) as well as the Michaelis-Menten constants ( $K_M$ ) parameterize the reaction dynamics. Since the biochemical properties of the enzymes catalysing the flipping reaction of lipid II were largely unknown and the flipping of UPP and UP were only hypothesized, the model describes these reactions by first order kinetics, as quantified by an effective rate constant  $k_i$  ( $i = UP, UPP, LII$ ). Furthermore, growth-driven dilution of all lipid II cycle intermediates occurring at a constant rate  $\gamma$  was integrated in the model of the lipid II cycle. This dilution was assumed to be counterbalanced by the constant *de novo* synthesis of UPP in the cytoplasm by rate  $\alpha$ . Additionally, the previous model comprised a theoretical description of cell wall antibiotic treatment. In particular, the interaction between an antibiotic and its target within the lipid II cycle was described as a ligand-binding reaction determined by the *in vitro* dissociation constant ( $K_D$ ), which is defined as the ratio between the dissociation ( $k_{diss}$ ) and association rate ( $k_{ass}$ ), respectively. Thus, the following time-dependent model variables result from this described scope of the pre-existing model of the lipid II cycle:

- UPP<sub>IN</sub> = internal pool of undecaprenyl pyrophosphate (UPP)
- UPP<sub>OUT</sub> = external pool of undecaprenyl pyrophosphate
- UP<sub>IN</sub> = internal pool of undecaprenyl phosphate (UP)
- UP<sub>OUT</sub> = external pool of undecaprenyl phosphate
- LI = pool of lipid I
- LII<sub>IN</sub> = internal pool of lipid II
- LII<sub>OUT</sub> = external pool of lipid II
- UPP-BAC = pool of bacitracin-bound UPP

The existing theory of the BceAB resistance module (Fritz *et al.*, 2015) describes the regulatory dynamics of the Bce system in response to bacitracin in detail. Here, the BceAB transporter was assumed to catalyse the release of bacitracin from UPP with Michaelis-Menten enzyme kinetics. Furthermore, the model comprised a detailed description of the production of new BceAB transporter in response to bacitracin, which is governed by a special flux-sensing mechanism. In particular, it was proposed that the production of new BceAB transporter is adapted to the capacity of the cell to deal with the present amount of bacitracin – monitored via the load of UPP-BAC per existing BceAB transporter. Accordingly, the load of UPP-BAC per transporter - called  $J_{BAC}$  – was assumed to dictate the BceAB synthesis. While the sensing and signalling process via the TCS BceRS was not modelled in detail, the activation of transporter production was assumed to be directly proportional to  $J_{BAC}$ . To describe the

synthesis process of BceAB based on the flux sensing mechanism in detail, both the processes of transcription and translation were taken into account. Hence, the transcriptional synthesis of *bceAB* mRNA was described as a function of  $J_{BAC}$  by following a thermodynamic model for translational regulation. Here, the concentration of *bceAB* mRNA is dependent on a basal transcription rate ( $\alpha$ ), the ratio of maximal to basal promoter activity ( $\omega$ ), the relative load per transporter at which  $P_{bceA}$  is activated ( $\kappa$ ) and the mRNA degradation rate ( $\lambda$ ). Finally, the concentration of the BceAB transporter depends on the translation rate per mRNA ( $\beta$ ) and the protein dilution due to cell growth. However, the model aimed to quantitatively describe the results of measurements of the  $P_{bceA}$ -*luxABCDE* reporter, which illustrates the activation of BceAB production in response to bacitracin. Thus, the dynamic equations quantifying the Lux protein production were formulated analogously to the described assumptions above and a multiplicative scaling factor was introduced to relate the Lux protein levels to the experimentally measured luminescence output ( $\delta$ ). Hence, from this comprehensive description of the BceAB resistance module additional model variables arise:

- $m_{BceAB}$  = *bceAB* mRNA
- BceAB = pool of BceAB transporter
- $m_{LUX}$  = *luxABCDE* mRNA
- Lux = pool of Lux proteins
- lumi = levels of luminescence (Lux activity)

Finally, to describe the BcrC resistance module, we introduced a scaling factor ( $s^{BcrC}$ ) for the reaction rate of UPP dephosphorylation, which reflects the increase in BcrC levels in response to bacitracin (as described in detail in the main text). Considering the contribution of BcrC and UppP to the overall phosphatase activity, the scaling factor was calculated as follows:

$$s^{BcrC} = x^{BcrC} * f^{BcrC} + (1 - x^{BcrC}) * 1$$

Here,  $x^{BcrC} \in [0; 1]$  describes the contribution of BcrC to the overall phosphatase activity and  $(1 - x^{BcrC})$  the contribution of UppP, respectively. Furthermore,  $f^{BcrC}$  displays the fold-change in BcrC levels between no bacitracin treatment and a certain bacitracin concentration (derived from the  $P_{bcrC}$  activity, as explained in the main text). In addition, we aimed to integrate the observation that the total concentration of lipid intermediates increases when BcrC is lacking. To this end, we introduced another scaling factor ( $s^{UPP}$ ) for the *de novo* synthesis of lipid intermediates in the form of UPP, which was set to 1 in the wild-type scenario.

In the end, when taking all the individual parts of the bacitracin stress response network into account, the model equations that quantify the time-dependent changes of the concentrations of lipid II cycle intermediates and BceAB were formulated as follows:

$$\frac{d[UPP_{IN}]}{dt} = s^{UPP} * \alpha^{UPP} - k_{UPP}[UPP_{IN}] - \gamma[UPP_{IN}] \quad (I)$$

$$\begin{aligned} \frac{d[UPP_{OUT}]}{dt} = & k_{UPP}[UPP_{IN}] - s^{BcrC} * v_{max}^{UppPs} \frac{[UPP_{OUT}]}{K_M^{UppPs} + [UPP_{OUT}]} + v_{max}^{PBPs} \frac{[LII_{OUT}]}{K_M^{PBPs} + [LII_{OUT}]} \\ & - k_{ass}^{BAC;UPP}[UPP_{OUT}][BAC] + k_{diss}^{BAC;UPP}[UPP - BAC] + k_{cat}^{BceAB}[BceAB] J_{BAC} \\ & - \gamma[UPP_{OUT}] \end{aligned} \quad (II)$$

$$\frac{d[UP_{OUT}]}{dt} = s^{BcrC} * v_{max}^{UppPs} \frac{[UPP_{OUT}]}{K_M^{UppPs} + [UPP_{OUT}]} - k_{UP}[UP_{OUT}] - \gamma[UP_{OUT}] \quad (III)$$

From modules to networks: A systems-level analysis of the bacitracin stress response in *Bacillus subtilis*

$$\frac{d[UP_{IN}]}{dt} = k_{UP}[UP_{OUT}] - v_{max}^{MraY} \frac{[UP_{IN}]}{K_M^{MraY} + [UP_{IN}]} - \gamma[UP_{IN}] \quad (IV)$$

$$\frac{d[LI]}{dt} = v_{max}^{MraY} \frac{[UP_{IN}]}{K_M^{MraY} + [UP_{IN}]} - v_{max}^{MurG} \frac{[LI]}{K_M^{MurG} + [LI]} - \gamma[LI] \quad (V)$$

$$\frac{d[LII_{IN}]}{dt} = v_{max}^{MurG} \frac{[LI]}{K_M^{MurG} + [LI]} - k_{LII}[LII_{IN}] - \gamma[LII_{IN}] \quad (VI)$$

$$\frac{d[LII_{OUT}]}{dt} = k_{LII}[LII_{IN}] - v_{max}^{PBPs} \frac{[LII_{OUT}]}{K_M^{PBPs} + [LII_{OUT}]} - \gamma[LII_{OUT}] \quad (VII)$$

$$\begin{aligned} \frac{d[UPP - BAC]}{dt} = & k_{ass}^{BAC;UPP}[UPP_{OUT}][BAC] - k_{diss}^{BAC;UPP}[UPP - BAC] - k_{cat}^{BceAB}[BceAB] J_{BAC} \\ & - \gamma[UPP - BAC] \end{aligned} \quad (VIII)$$

$$\frac{d[m_{BceAB}]}{dt} = \alpha^{BceAB} \left( \frac{1 + \omega \left( \frac{J_{BAC}}{\kappa} \right)^n}{1 + \left( \frac{J_{BAC}}{\kappa} \right)^n} \right) - \lambda^{BceAB} [m_{BceAB}] \quad (IX)$$

$$\frac{d[BceAB]}{dt} = \beta [m_{BceAB}] - \gamma[BceAB] \quad (X)$$

$$\frac{d[m_{Lux}]}{dt} = \alpha^{BceAB} \left( \frac{1 + \omega \left( \frac{J_{BAC}}{\kappa} \right)^n}{1 + \left( \frac{J_{BAC}}{\kappa} \right)^n} \right) - \lambda^{Lux} [m_{Lux}] \quad (XI)$$

$$\frac{d[Lux]}{dt} = \beta [m_{Lux}] - \gamma^{Lux}[Lux] \quad (XII)$$

$$lumi = \delta[Lux] \quad (XIII)$$

$$\text{with } J_{BAC} = \frac{\frac{[UPP - BAC]}{K_M^{BceAB}}}{1 + \frac{[UPP - BAC]}{K_M^{BceAB}}}$$

To study the effect of bacitracin on the progression of the lipid II cycle, we monitored the effect of bacitracin on the rate of PG synthesis,  $j_{PG}$ , which was formulated as follows

$$j_{PG} = v_{max}^{PBPs} \frac{[LII_{OUT}]}{K_M^{PBPs} + [LII_{OUT}]} \quad (XIV)$$

### **Model adaptations to describe the mutant strains**

The full model described above reproduces the scenario of a wild-type strain where both resistance determinants (BceAB and BcrC) are fully intact. However, adaptations were necessary to simulate a lack of one or both of the two resistance modules. In order to describe the scenario of a  $\Delta bceAB$  mutant, we set the basal production rate of BceAB to zero ( $\alpha^{BceAB} = 0$ ) to avoid BceAB and Lux production. Furthermore, we adapted the fold-change  $f^{BcrC}$  to the reporter output of  $P_{bcrC-luxABCDE}$  in a  $\Delta bceAB$  mutant. Secondly, we simulated a lack of BcrC, as in a  $\Delta bcrC$  mutant, by setting the contribution of BcrC to the overall phosphatase activity to zero ( $x^{BcrC} = 0$ ). In addition, the scaling factor for the production rate of UPP was adapted



( $s^{UPP} > 1$ ), since lipid carrier production was assumed to be up-regulated in response to *bcrC* deletion (see qPCR data in the main text). The deviation of the precise value for this parameter is explained in the section below. Finally, to study a lack of both resistance modules ( $\Delta bceAB\Delta bcrC$  mutant), we combined the two adaptations for the single mutants ( $\alpha^{BceAB} = 0$ ,  $x^{BcrC} = 0$  and  $s^{UPP} > 1$ ).

### Calibration of the mathematical model

In order to calibrate the model, we aimed to identify physiologically relevant values for the parameters in Eqs. (I-XIV). At first, we set all known parameters from the model of the lipid II cycle to its previously defined values (see Supplementary Table 3).

Subsequently, we determined the new parameters arising from the mathematical description of the BcrC resistance module, namely  $x^{BcrC}$ , which defined  $s^{BcrC}$ , and  $s^{UPP}$ , respectively. For this purpose, we compared the scenarios of a strain lacking both resistance modules ( $\Delta bceAB\Delta bcrC$  mutant) or featuring the BcrC resistance module solely ( $\Delta bceAB$  mutant). Each of the two parameters affects both, the progression of the lipid II cycle without bacitracin and the effect of bacitracin treatment on the lipid II cycle. While a higher impact of BcrC on the overall phosphatase activity supports the progression of the cycle more efficiently when BcrC is present, the rate of PG synthesis is reduced more strongly in this case when BcrC is lacking. This demands a more pronounced upregulation of the production of lipid II cycle intermediates in response to *bcrC* deletion to recover a close-to-optimal PG synthesis rate. However, the model also predicted a PG synthesis rate above the optimal one when assuming an excessive upregulation of lipid carrier production, which is not valid in a physiological sense. Furthermore, variations in the PG synthesis rate without bacitracin treatment clearly imply significant differences in the amount of bacitracin cells can stand. Obviously, in the scenario where BcrC is present as a resistance module ( $\Delta bceAB$  mutant), a stronger contribution of BcrC to the overall phosphatase activity confers higher resistance and coincides with a raised  $IC_{50}$ . However, when lacking BcrC ( $\Delta bceAB\Delta bcrC$  mutant), the PG synthesis rate without bacitracin treatment dictates the susceptibility towards bacitracin. If the PG synthesis rate is still distinctly affected in the untreated scenario, little amounts of bacitracin are sufficient to reduce the PG synthesis rate to half of its optimum. In contrast, much higher bacitracin concentrations are required to reach 50% of the optimal PG synthesis rate when the rate is nearly unaffected without antibiotic. Thus, as the PG synthesis rate without bacitracin treatment is governed by the contribution of BcrC on the overall phosphatase activity ( $x^{BcrC}$ ) and lipid carrier upregulation in response to BcrC shortage ( $s^{UPP}$ ) – as explained above – the  $IC_{50}$  prediction of the model for the  $\Delta bceAB\Delta bcrC$  mutant strongly depends on these two parameters. We ultimately aimed to find a theoretical model that simultaneously describe the progression of the lipid II cycle with ( $\Delta bceAB$ ) and without BcrC ( $\Delta bcrC\Delta bceAB$ ) precisely and matches physiological conditions as well. Therefore, we simulated the  $IC_{50}$  model predictions for 50x50 combinations of the two parameters  $x^{BcrC}$  and  $s^{UPP}$  and determined the weighted squared 2-norm  $\chi^2$  for all possible combinations as follows:

$$\chi^2(x^{BcrC}, s^{UPP}) = \frac{(IC_{50}^{\Delta bceAB}(x^{BcrC}, s^{UPP}) - MIC^{\Delta bceAB})^2}{(\sigma_{MIC^{\Delta bceAB}})^2} + \frac{(IC_{50}^{\Delta bceAB\Delta bcrC}(x^{BcrC}, s^{UPP}) - MIC^{\Delta bceAB\Delta bcrC})^2}{(\sigma_{MIC^{\Delta bceAB\Delta bcrC}})^2}$$

Here,  $MIC^{\Delta bceAB}$  and  $MIC^{\Delta bceAB\Delta bcrC}$  represent the experimentally determined MICs in the different strains and  $\sigma_{MIC^{\Delta bceAB}}$  and  $\sigma_{MIC^{\Delta bceAB\Delta bcrC}}$  the respective errors in the experimental MICs, calculated by the error propagation formula (errors are given in the main text).

From modules to networks: A systems-level analysis of the bacitracin stress response in *Bacillus subtilis*

Furthermore,  $IC_{50}^{\Delta bceAB}$  and  $IC_{50}^{\Delta bceAB\Delta bcrC}$  describe the model-predicted  $IC_{50}$ 's, dependent on the parameters  $x^{BcrC}$  and  $s^{UPP}$ .

To find the optimal parameter combination, we demanded the following two constraints:

$$i. \quad \chi^2(x^{BcrC}, s^{UPP}) \rightarrow \min$$

and

$$ii. \quad j_{PG}^{\Delta bceAB\Delta bcrC}(x^{BcrC}, s^{UPP}) \leq j_{PG}^{WT}$$

$j_{PG}^{WT}$  and  $j_{PG}^{\Delta bceAB\Delta bcrC}$  display the rates of PG synthesis without bacitracin treatment in the wild-type scenario and a scenario where both resistance modules are lacking, respectively. The second constraint accounts for the physiological plausible limitation of the PG synthesis rate by its wild-type level. In Supplementary Figure S3, the  $\chi^2$  values are plotted against the parameter combinations. Standard deviations on the two parameters were determined from the 68.3 % confidence intervals as described (Press *et al.*, 1992) and also illustrated in Supplementary Figure S3. The final parameter values of  $x^{BcrC}$  and  $s^{UPP}$  as well as their standard deviation  $\sigma$  are given in Supplementary Table 3).

Finally, we determined the parameters originating from the previous model of the BceAB resistance module. Since the setup of the experiments, which we now aimed to quantitatively describe by the new model, was quite different from the previous experimental study that determined the pre-existing model, we were not able to transfer the existing parameters to our new model. Rather, significant variations in the growth conditions between both experimental approaches demanded adaptations in the model parameters that describe the dynamics of the Bce system. Therefore, we fixed the parameters that are independent from the growth conditions (e.g. mRNA degradation rates, translation rate) to their physiological values and determined the remaining ones by a constrained optimization approach. The experimental data of the  $P_{bceAB-luxABCDE}$  reporter output provide nine objectives to the seven unknown parameters. To solve this over-determined non-linear data-fitting problem, we used the solving function *lsqnonlin*, embedded in the MATLAB™ software. This function solves nonlinear least-square curve fitting problems of the form

$$\min \|f(x)\|_2^2 = \min (f_1(x)^2 + f_2(x)^2 + \dots + f_n(x)^2)$$

by using a trust-region reflective Newton algorithm. As outputs, it returns the optimal parameter set  $\bar{x}$  of the problem as well as the squared-2 norm  $\chi^2$  of the residual at  $\bar{x}$  ( $\chi^2 = \sum f(\bar{x})^2$ ). To account for the presence of local optima, 50 independent fits were performed with randomly chosen initial parameter sets and the best-fit result was given at minimal  $\chi^2$ . The optimal parameters are shown in Supplementary Table S3. We followed (Wall *et al.*, 2009) to compute the asymmetric errors  $\sigma_+$  and  $\sigma_-$  with respect to the optimal parameter values  $\bar{x}$ , listed in Supplementary Table S3. The squared errors for the parameter  $x_k$  were calculated using the following equations:

$$\sigma_{k,+}^2 = \frac{\sum_{i:x_{k,i} > \bar{x}_k} (x_{k,i} - \bar{x}_k)^2 e^{-\chi_i^2/2}}{\sum_{i:x_{k,i} > \bar{x}_k} e^{-\chi_i^2/2}}$$

and

$$\sigma_{k,-}^2 = \frac{\sum_{i:x_{k,i} < \bar{x}_k} (x_{k,i} - \bar{x}_k)^2 e^{-\chi_i^2/2}}{\sum_{i:x_{k,i} < \bar{x}_k} e^{-\chi_i^2/2}}$$

Where  $x_{k,i}$  is the value of the parameter  $x_k$  in the  $i^{\text{th}}$  fit,  $\bar{x}_k$  is the value of  $x_k$  in the fit with the lowest value of  $\chi^2$ , and  $\chi_i^2$  is the value of  $\chi^2$  for the  $i^{\text{th}}$  fit. In using the likelihood function  $e^{-\chi_i^2/2}$ , we assumed that the errors in the measurements are independent and normally distributed with widths equal to the standard error of the mean.

### Model modification

In order to study the futile activation of BceAB production by UPP (as explained in detail in the main text), we slightly modified the model description of the BceAB resistance module. According to the assumption that UPP affects the transporter state by futile binding, we expected the load per transporter dependent from both UPP and UPP-BAC, which were assumed to bind in a competitive manner. Thus, we adapted the description of the load per transporter, which affects the activation of BceAB production, and introduced a modified description of transporter load  $J_{load}$ :

$$J_{load} = J'_{BAC} + J_{futile}$$

with

$$J'_{BAC} = \frac{\frac{[UPP - BAC]}{K_M^{BceAB}}}{1 + \frac{[UPP - BAC]}{K_M^{BceAB}} + \frac{[UPP]}{\tilde{K}_M^{BceAB}}}$$

and

$$J_{futile} = \frac{\frac{[UPP]}{\tilde{K}_M^{BceAB}}}{1 + \frac{[UPP - BAC]}{K_M^{BceAB}} + \frac{[UPP]}{\tilde{K}_M^{BceAB}}},$$

leading to

$$J_{load} = \frac{\frac{[UPP - BAC]}{K_M^{BceAB}} + \frac{[UPP]}{\tilde{K}_M^{BceAB}}}{1 + \frac{[UPP - BAC]}{K_M^{BceAB}} + \frac{[UPP]}{\tilde{K}_M^{BceAB}}},$$

Here, the Michaelis constants  $\tilde{K}_M^{BceAB}$  and  $K_M^{BceAB}$  describe the binding affinities of UPP and UPP-Bac to the transporter, respectively. Since the load per transporter affects the activation of BceAB and Lux protein production, the respective two model Eqs. (IX) and (XI) were changed as follows:

$$\frac{d[m_{BceAB}]}{dt} = \alpha^{BceAB} \left( \frac{1 + \omega \left( \frac{J_{load}}{\kappa} \right)^n}{1 + \left( \frac{J_{load}}{\kappa} \right)^n} \right) - \lambda^{BceAB} [m_{BceAB}] \quad (\text{XV})$$

$$\frac{d[m_{Lux}]}{dt} = \alpha^{BceAB} \left( \frac{1 + \omega \left( \frac{J_{load}}{\kappa} \right)^n}{1 + \left( \frac{J_{load}}{\kappa} \right)^n} \right) - \lambda^{Lux} [m_{Lux}] \quad (\text{XVI})$$

From modules to networks: A systems-level analysis of the bacitracin stress response in *Bacillus subtilis*

However, we expected that futile binding of UPP inactivates the transporter but does not provoke any reaction. Therefore, the rate of release of bacitracin from UPP is solely dependent on  $J'_{BAC}$ :

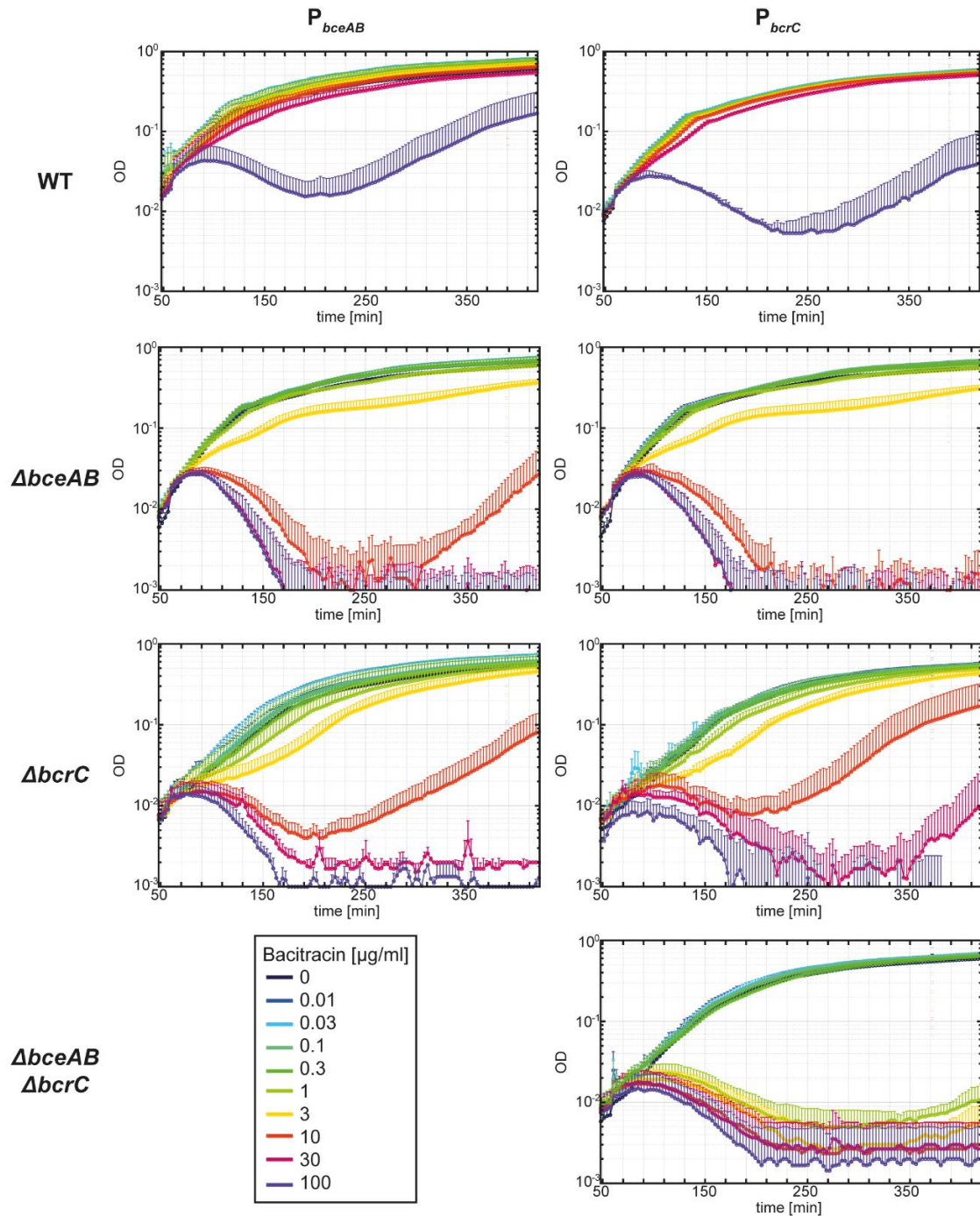
$$\begin{aligned} \frac{d[UPP_{OUT}]}{dt} = & k_{UPP}[UPP_{IN}] - s^{BcrC} * v_{max}^{UPP} \frac{[UPP_{OUT}]}{K_M^{UPP} + [UPP_{OUT}]} + v_{max}^{PBP} \frac{[LII_{OUT}]}{K_M^{PBP} + [LII_{OUT}]} \\ & - k_{ass}^{BAC;UPP} [UPP_{OUT}][BAC] + k_{diss}^{BAC;UPP} [UPP - BAC] + k_{cat}^{BceAB} [BceAB] J'_{BAC} \\ & - \gamma [UPP_{OUT}] \end{aligned} \quad (XVII)$$

$$\begin{aligned} \frac{d[UPP - BAC]}{dt} = & k_{ass}^{BAC;UPP} [UPP_{OUT}][BAC] - k_{diss}^{BAC;UPP} [UPP - BAC] \\ & - k_{cat}^{BceAB} [BceAB] J'_{BAC} - \gamma [UPP - BAC] \end{aligned} \quad (XVIII)$$

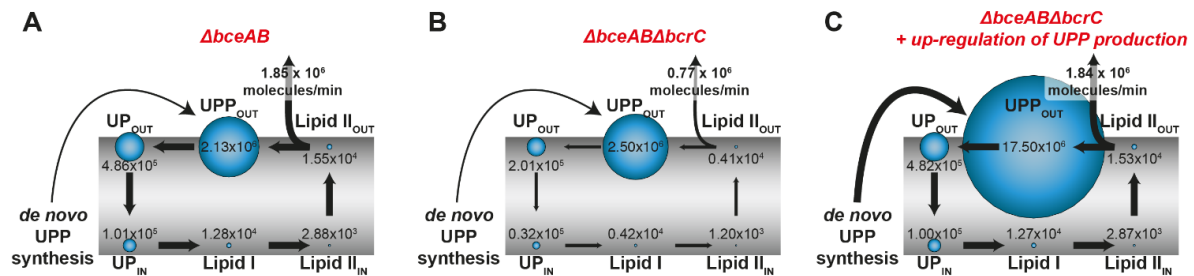
After model modification, we proved that the predictions the  $IC_{50}$ s remain unaffected from the modifications.

## Supplementary Figures

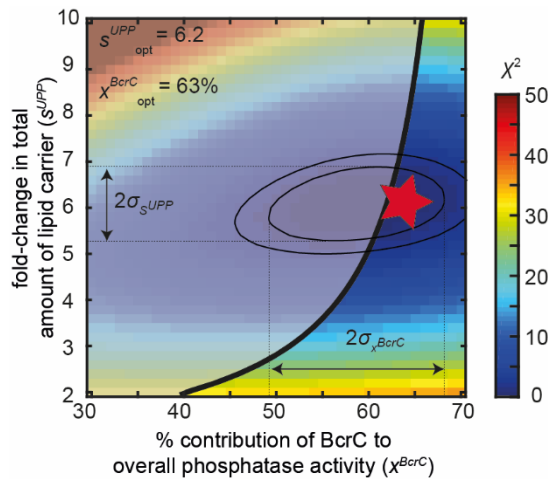
## Supplementary Figure 1



**Growth curves of *B. subtilis* W168 wild-type and  $\Delta bcrC$ ,  $\Delta bceAB$  and  $\Delta bceAB\Delta bcrC$  mutant strains.** Growth dynamics in strains carrying indicated deletions of bacitracin resistance modules and the reporter constructs  $P_{bceAB}$ -*luxABCDE* and  $P_{bcrC}$ -*luxABCDE*. Indicated amounts of bacitracin were added at  $t = 60$  min. The respective growth rates, as displayed in the dose-response curve in Figure 2B, were determined within the first hour after bacitracin induction (60-120 min). Measurements were performed during exponential growth phase in LB medium at 37°C in a microtiter plate reader. Data points and error bars indicate mean and standard deviation from at least three biological replicates. Strains used here are listed in Supplementary Table 1.

**Supplementary Figure 2**

**Model-predicted distribution of lipid II cycle intermediates in the  $\Delta bceAB$  and  $\Delta bceAB\Delta bcrC$  mutant strains.** The distribution of the different lipid II cycle intermediates without bacitracin treatment is highly asymmetric. The lipid II cycle is located around the cell membrane, which is indicated in grey. Lipid II cycle intermediates are illustrated with blue circles, while the size of the circles correlates with the concentration of the respective intermediate.  $UPP_{OUT}$ ,  $UP_{OUT}$  and  $LII_{OUT}$  represent the fraction the intermediates UPP, UP and Lipid II, respectively, which is located at the outer leaflet of the cell membrane. Accordingly, the fraction of intermediates located at the inner leaflet of the cell membrane is described by  $UP_{IN}$  and  $LII_{IN}$ .  $UPP_{IN}$  is not displayed, as this lipid intermediate is not directly involved in the lipid II cycle. Lipid I (LI) is solely present on the inner leaflet of the cell membrane. The *de novo* synthesis of new lipid carrier in the form of UPP is indicated. The thickness of the arrows correlates with the fluxes from one intermediate state into the next one within the lipid II cycle. In addition, the rate of PG synthesis is displayed (**A**) When BceAB is lacking ( $\Delta bceAB$ ), the concentrations of the various lipid II cycle intermediates equal the concentrations predicted in the basic model without bacitracin stress response determinants (Piepenbreier *et al.*, 2019). While  $UPP_{OUT}$  is most abundant, the concentrations of LI and  $LII_{IN}$  and  $LII_{OUT}$  are two orders of magnitude lower.  $UP_{IN}$  and  $UP_{OUT}$  are present in intermediate concentrations. (**B**) When additionally deleting *bcrC* ( $\Delta bceAB\Delta bcrC$ ), the rate of UPP dephosphorylation is significantly reduced and lipid intermediates accumulate in the form of  $UPP_{OUT}$ , as this is the substrate of the respective reaction. Since the lipid II cycle is a close-loop-system (Piepenbreier *et al.*, 2019), all other concentrations are depleted concomitantly. However, as  $UPP_{OUT}$  is still the most abundant intermediate in the lipid II cycle, its concentration is not raised significantly. The distinct reduction (>50%) of the concentrations of  $UP_{OUT}$ ,  $UP_{IN}$ , LI,  $LII_{IN}$  and  $LII_{OUT}$  leads to significantly reduced fluxes within the lipid II cycle. In particular, the reduction of the concentration of  $LII_{OUT}$  of ~75% leads to a decreased rate of PG synthesis, far below the half-maximal level. (**C**) However, the model predicts a nearly unaffected rate of PG synthesis when a 6.6-fold increase in total lipid intermediates (caused by a higher rate of UPP *de novo* synthesis) in response to *bcrC* deletion is expected. While the concentration of  $UPP_{OUT}$  is massively increased, all other lipid II cycle intermediates are as abundant as in the  $\Delta bceAB$  scenario. Consequently, the similar concentrations of  $LII_{OUT}$  imply similar rates of PG synthesis in both the mutant lacking BceAB exclusively ( $\Delta bceAB$ ) and the mutant lacking both resistance modules ( $\Delta bceAB\Delta bcrC$ ).

**Supplementary Figure 3**

**Best-fit results of the model parameters  $x^{BcrC}$  and  $s^{UPP}$  and their corresponding confidence intervals.** The colour codes for the  $\chi^2(x^{BcrC}, s^{UPP})$  values of the different parameter combinations, where a low  $\chi^2$  indicates high quality of the fit for a given combination. The shaded area represents the physiologically non-plausible regime for  $j_{PG}^{\Delta bceAB\Delta bcrC}(x^{BcrC}, s^{UPP}) > j_{PG}^{WT}$ . The standard deviations  $\sigma_{x^{BcrC}}$  and  $\sigma_{s^{UPP}}$  were determined from the 68.3% confidence interval corresponding to  $\Delta\chi^2 = (\chi^2 - \chi_{opt}^2) = 1$ , which is represented by the inner ellipse (see Supplementary Table S3). The outer ellipse marks the 95.4% confidence interval ( $\Delta\chi^2 = 2$ ). The red star marks the optimal parameter set compatible with the physiological constraints.

**Supplementary Tables****Supplementary Table 1: Bacterial strains used in this study**

Name	Description <sup>a</sup>	Source
<b>TMB1619</b>	W168 <i>sacA::pCHlux103 (P<sub>bceA</sub>-lux)</i>	Höfler <i>et al.</i> , 2016
<b>TMB1620</b>	W168 <i>sacA::pCHlux104 (P<sub>bcrC</sub>-lux)</i>	Höfler <i>et al.</i> , 2016
<b>TMB1623</b>	W168 <i>bceAB::kan sacA::pCHlux103 (P<sub>bceA</sub>-lux)</i>	Radeck <i>et al.</i> , 2016
<b>TMB1624</b>	W168 <i>bceAB::kan sacA::pCHlux104 (P<sub>bcrC</sub>-lux)</i>	Radeck <i>et al.</i> , 2016
<b>TMB1627</b>	W168 <i>bcrC::tet sacA::pCHlux103 (P<sub>bceA</sub>-lux)</i>	Radeck <i>et al.</i> , 2016
<b>TMB1628</b>	W168 <i>bcrC::tet sacA::pCHlux104 (P<sub>bcrC</sub>-lux)</i>	Radeck <i>et al.</i> , 2016
<b>TMB1632</b>	W168 <i>bceAB::kan bcrC::tet sacA::pCHlux104 (P<sub>bcrC</sub>-lux)</i>	This study

<sup>a</sup> kan, kanamycin resistance; tet, tetracycline resistance.

**Supplementary Table 2: Plasmids used in this study**

Name	Description	Resistance in <i>E. coli</i> / <i>B. subtilis</i> <sup>a</sup>	Source
<b>pCHlux103</b>	pAH328-derivative, <i>sacA::P<sub>bceA</sub>-lux, cat, bla</i>	Amp <sup>r</sup> / cm <sup>r</sup>	Höfler <i>et al.</i> , 2016
<b>pCHlux104</b>	pAH328-derivative, <i>sacA::P<sub>bcrC</sub>-lux, cat, bla</i>	Amp <sup>r</sup> / cm <sup>r</sup>	Höfler <i>et al.</i> , 2016

<sup>a</sup> Amp<sup>r</sup>, ampicillin resistance; cm<sup>r</sup>, chloramphenicol resistance.



**Supplementary Table 3: Model parameters**

Parameter	Notation	Value	Source
<b>LII module</b>			
Michaelis-Menten constant for Lipid I synthesis via <i>MraY</i>	$K_M^{MraY}$	177 $\mu\text{M}$	Piepenbreier <i>et al.</i> , 2019
Michaelis-Menten constant for Lipid II synthesis via <i>MurG</i>	$K_M^{MurG}$	25 $\mu\text{M}$	Piepenbreier <i>et al.</i> , 2019
Michaelis-Menten constant for PG synthesis via PBPs	$K_M^{PBPs}$	18 $\mu\text{M}$	Piepenbreier <i>et al.</i> , 2019
Michaelis-Menten constant for UPP dephosphorylation via UppPs	$K_M^{UppPs}$	$4.69 \times 10^3 \mu\text{M}$	Piepenbreier <i>et al.</i> , 2019
Maximal Lipid I synthesis rate via <i>MraY</i>	$v_{max}^{MraY}$	$3.01 \times 10^5 \frac{\text{molecules}}{\text{min}}$	Piepenbreier <i>et al.</i> , 2019
Maximal Lipid II synthesis rate via <i>MurG</i>	$v_{max}^{MurG}$	$3.21 \times 10^5 \frac{\text{molecules}}{\text{min}}$	Piepenbreier <i>et al.</i> , 2019
Maximal PG synthesis rate via PBPs	$v_{max}^{PBPs}$	$2.32 \times 10^5 \frac{\text{molecules}}{\text{min}}$	Piepenbreier <i>et al.</i> , 2019
Maximal UPP dephosphorylation rate via UppPs	$v_{max}^{UppPs}$	$3.55 \times 10^5 \frac{\text{molecules}}{\text{min}}$	Piepenbreier <i>et al.</i> , 2019
Reaction rate of UPP flipping	$k_{UPP}$	$1.84 \times 10^3 \frac{1}{\text{min}}$	Piepenbreier <i>et al.</i> , 2019
Reaction rate of UP flipping	$k_{UP}$	$3.81 \frac{1}{\text{min}}$	Piepenbreier <i>et al.</i> , 2019
Reaction rate of LII flipping	$k_{LII}$	$642.23 \frac{1}{\text{min}}$	Piepenbreier <i>et al.</i> , 2019
Production rate of UPP	$\alpha^{UPP}$	$4.76 \times 10^4 \frac{\text{molecules}}{\text{min}}$	Piepenbreier <i>et al.</i> , 2019
Dilution rate of all proteins	$\gamma$	$0.017 \frac{1}{\text{min}}$	Adapted to cell's doubling time, $\gamma = \frac{\ln 2}{T_D}$
<b>Antibiotic action</b>			
Binding constant for bacitracin – UPP interaction	$K_D^{BAC;UPP}$	1 $\mu\text{M}$	Storm and Strominger, 1973
Dissociation rate for bacitracin – UPP interaction	$k_{diss}^{BAC;UPP}$	$0.75 \frac{1}{\text{min}}$	Estimated from Fig. 2B in (Economou <i>et al.</i> , 2013)
Association rate for bacitracin – UPP interaction	$k_{ass}^{BAC;UPP}$	$0.75 \frac{1}{\mu\text{M min}}$	Adjusted to match $K_D^{BAC;UPP}$
<b>BceAB module</b>			
Michaelis-Menten constant for bacitracin transport via BceAB	$K_M^{BceAB}$	129 (+137/-59) <sup>a</sup> $\mu\text{M}$	Estimated parameter
Catalytic efficiency of every BceAB transporter	$k_{cat}^{BceAB}$	$1.51 (+1.4/-0.2)^a \times 10^3 \frac{\text{molecules}}{\text{transporter} \cdot \text{min}}$	Estimated parameter
Basal transcription rate of $P_{bceAB}$ promoter	$\alpha^{BceAB}$	$2.62 (+1.0/-0.8)^a \times 10^{-2} \frac{\text{mRNA}}{\text{min}}$	Estimated parameter
Fold-change of $P_{bceAB}$ promoter	$\omega$	$2.776 (+0.7/-0.7)^a \times 10^3$	Estimated parameter (Suggested by data in Fig. 2C in the main text)
$P_{bceAB}$ activation threshold	$\kappa$	1.3 (+3.0/-0.2) <sup>a</sup>	Estimated parameter
Hill coefficient (reflects all forms of cooperativity in stimulus perception and signal transduction)	$n$	4.7 (+4.0/-1.1) <sup>a</sup>	Estimated parameter
<i>bceAB</i> mRNA degradation rate	$\lambda^{BceAB}$	$0.462 \frac{1}{\text{min}}$	Corresponds to a <i>bceAB</i> mRNA half-life of 1.5 min (Fritz <i>et al.</i> , 2015)
<i>luxABCDE</i> mRNA degradation rate	$\lambda^{Lux}$	$0.138 \frac{1}{\text{min}}$	Corresponds to a <i>lux</i> mRNA half-life of 5 min; upper limit

			for mRNA half-life inferred in (Radeck <i>et al.</i> , 2013)
LuxABCDE protein decay rate	$\gamma^{Lux}$	$0.023 \frac{1}{\text{min}}$	Corresponds to a protein half-life of 30 min (Fritz <i>et al.</i> , 2015)
Translation rate	$\beta$	$10 \frac{\text{proteins}}{\text{mRNA} \cdot \text{min}}$	(Fritz <i>et al.</i> , 2015)
Scaling factor between protein level and luminescence	$\delta$	$4.56 (+3.1/-1.6)^a$	Estimated parameter
<b>BcrC module</b>			
Relative contribution of BcrC to overall phosphatase activity	$x^{BcrC}$	$0.63 (+/- 0.095)^b$	Estimated parameter
Scaling factor for lipid carrier concentrations in $\Delta bcrC$	$s^{UPP}$	$6.2 (+/- 0.7)^b$	Estimated parameter
<b>Modified model</b>			
Michaelis-Menten constant for futile binding of UPP to BceAB	$K_M^{UPP}$	$3.38 \times 10^4 \mu\text{M}$	Arbitrary choice, expecting an affinity of UPP to BceAB two orders of magnitude lower than the for the native substrate (UPP-BAC)

<sup>a</sup> Asymmetric errors  $\sigma_+$  and  $\sigma_-$  of the parameter values are given in brackets ( $+\sigma_+/-\sigma_-$ ).

<sup>b</sup> Standard deviations  $\sigma$  of the parameter values, determined from the 68.3 % confidence intervals, are given in brackets ( $+/- \sigma$ ).


## Supplementary References

- Economou, N.J., Cocklin, S., and Loll, P.J. (2013) High-resolution crystal structure reveals molecular details of target recognition by bacitracin. *Proc Natl Acad Sci USA* **110**: 14207–14212.
- Fritz, G., Dintner, S., Treichel, N.S., Radeck, J., Gerland, U., Mascher, T., and Gebhard, S. (2015) A new way of sensing: Need-based activation of antibiotic resistance by a flux-sensing mechanism. *mBio* **6**: e00975.
- Höfler, C., Heckmann, J., Fritsch, A., Popp, P., Gebhard, S., Fritz, G., and Mascher, T. (2016) Cannibalism stress response in *Bacillus subtilis*. *Microbiology (Reading, Engl)* **162**: 164–176.
- Piepenbreier, H., Diehl, A., and Fritz, G. (2019) Blocking of peptidoglycan synthesis by cell wall antibiotics. *Submitted*.
- Press, W.H., Teukolsky, S.A., Vetterling, W.T., and Flannerty, B.P. (1992) *Numerical Recipes in C: The Art of Scientific Computing*. New York: Cambridge University Press.
- Radeck, J., Gebhard, S., Orchard, P.S., Kirchner, M., Bauer, S., Mascher, T., and Fritz, G. (2016) Anatomy of the bacitracin resistance network in *Bacillus subtilis*. *Molecular Microbiology* **100**: 607–620.
- Radeck, J., Kraft, K., Bartels, J., Cikovic, T., Duerr, F., Emenegger, J., *et al.* (2013) The Bacillus BioBrick Box: generation and evaluation of essential genetic building blocks for standardized work with *Bacillus subtilis*. *J Biol Eng* **7**.
- Storm, D.R., and Strominger, J.L. (1973) Complex formation between bacitracin peptides and isoprenyl pyrophosphates. The specificity of lipid-peptide interactions. *Journal of Biological Chemistry* **248**: 3940–3945.
- Wall, M.E., Markowitz, D.A., Rosner, J.L., and Martin, R.G. (2009) Model of transcriptional activation by MarA in *Escherichia coli*. arXiv:0902.0959v1.

## **A.4 Transporters as information processors in bacterial signalling pathways**

## MicroReview

## Transporters as information processors in bacterial signalling pathways

Hannah Piepenbreier,<sup>1</sup> Georg Fritz <sup>1\*\*</sup> and Susanne Gebhard <sup>2\*</sup>

<sup>1</sup>LOEWE Center for Synthetic Microbiology, Philipps-University Marburg, Germany.

<sup>2</sup>Milner Centre for Evolution, Department of Biology and Biochemistry, University of Bath, UK.

## Summary

**Transporters are essential players in bacterial growth and survival, since they are key for uptake of nutrients on the one hand, and for defence against endogenous and environmental stresses on the other hand. Remarkably, in addition to their primary role in substrate translocation, it has become clear that some transporters have acquired a secondary function as sensors and information processors in signalling pathways. In this review, we describe recent advances in our understanding of the role of transporters in such signalling cascades, and discuss some of the emergent dynamic behaviour found in hallmark examples. A particular focus is placed on new insights into mechanistic details of information transfer between transporters and regulatory proteins. Quantitative considerations reveal that these signalling complexes can implement a remarkable diversity of regulatory logic functions, where the transporter can act as activity switch, as positive or negative reporter of transport flux, or as a signalling hub for the integration of multiple inputs. Such a dual use of transport proteins not only enables efficient substrate translocation but is also an elegant strategy to integrate important information about the cell's external conditions with its current physiological state.**

Accepted 24 January, 2017. For correspondence. \*E-mail s.gebhard@bath.ac.uk; Tel. +44 1225 386421; Fax +44 1225 386779 or \*\*E-mail georg.fritz@synmikro.uni-marburg.de; Tel. +49 6421 28 22582; Fax +49 6421 2824430.

## Introduction

Active transporters are essential players in bacterial growth and survival, since they are key for uptake of essential nutrient on the one hand, and for defence against endogenous and environmental stresses, for example, by export of toxic compounds, on the other hand (Fig. 1). This is reflected by the vast functional and mechanistic diversity in bacterial transport systems, which can be energised by ATP hydrolysis or the proton motif force, can act as importers or exporters, and can have broad substrate ranges or be highly specific (Padan, 2009; Wang *et al.*, 2009).

In addition to their primary role in substrate translocation, transporters can also possess a secondary function and serve as accessory components of sensory and signalling systems. In this role, they contribute to decision-making processes that enable the bacterial cell to adapt to changes in the prevailing environmental or intracellular conditions. For instance, transporters play a pivotal role in nutrient sensing, because many substrates first need to be actively translocated to the cytoplasm before a cytoplasmic sensor protein may detect the cue (Fig. 1). This is frequently the case in inducible carbohydrate utilization systems, such as the arabinose and lactose systems of *Escherichia coli* (Müller-Hill, 1996; Schleif, 2000). The importers for these carbon sources are constitutively produced at a low level to allow a basal rate of uptake. Only when this results in accumulation of elevated intracellular substrate concentrations can these be detected by cytoplasmic regulators, which in turn activate expression of genes required for increased rates of import and metabolism of the available carbon source (Megerle *et al.*, 2008; Fritz *et al.*, 2014). In cells lacking the transporter, the substrate cannot enter the cytoplasm, preventing detection and the resulting cellular response (Daruwalla *et al.*, 1981).

While this example may be viewed as an indirect role of transporters in substrate perception, it is becoming increasingly recognized that some transporters have acquired *bona fide* signalling functions. These so-called

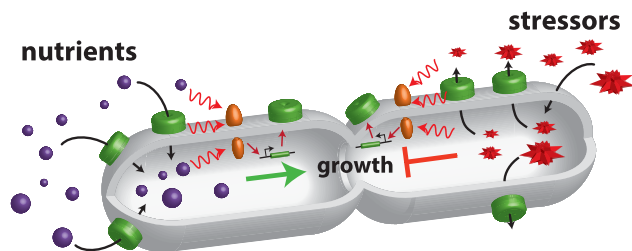


**Fig. 1.** Transporters as information processors in bacterial cells. The optimization of bacterial growth and survival critically relies on active transporters (green) responsible for uptake of essential nutrients (purple) and export of endogenous and environmental stressors (red). In order to adapt their transport capacity to changes in prevailing conditions, transporters frequently play pivotal roles in signalling (red wavy arrows) to regulatory systems (orange) that control the expression of transporter genes (straight red arrows). These roles range from transporters as sensors of external substrate level, to transporters as indirect mediators for internal substrate detection, to transporters serving as *bona fide* flux sensors that report on their transport activity *per se*.

'trigger transporters' can directly bind to and communicate with bacterial signalling pathways, such as one-component (1CS) and two-component (2CS) regulatory systems (Tetsch and Jung, 2009; Unden *et al.*, 2016). In this way, the cell elegantly combines the exquisitely sensitive ability of transporters to bind and report on substrate availability with the regulatory power of 1CS and 2CS to translate this information into an appropriate cellular response. The information relayed from transporter to regulatory system may be the external or internal concentration of a ligand, or it may be the transport activity itself (Fig. 1). Interestingly, in some cases the transporters have even lost their primary substrate-translocating function and only retained their role as ligand binding 'scaffolds' reporting on extracellular substrate concentrations. In the Uhp system of *E. coli*, for instance, the UhpC transporter displays only marginal transport activity for its substrate, glucose 6-phosphate (G6P), but faithfully detects and signals the presence of G6P to the UhpB/UhpA 2CS, which in turn activates the production of the hexose phosphate transporter UhpT (Island and Kadner, 1993; Schwöppe *et al.*, 2003).

In this MicroReview, we will discuss the role of active transporters as accessory or sensory components of signalling pathways. We will address systems in which the transporter functions as activity switch, as positive or negative reporter of transport flux as well as systems in which transporters mediate the integration of multiple signals. Based on recent advances in our molecular and quantitative understanding of such signalling pathways, we provide a descriptive theoretical framework for their classification according to system behaviour, which will aid researchers in the characterisation of newly identified sensory transporters.

## Transporters as activity switches

Uptake and metabolism of  $C_4$ -dicarboxylates, such as fumarate or malate, in many bacteria is regulated by a 2CS that is under negative control of secondary  $C_4$ -dicarboxylate transporters (Unden *et al.*, 2016). In *E. coli*, this 2CS is comprised of the histidine kinase DcuS and the response regulator DcuR. Under aerobic conditions, fumarate and other  $C_4$ -dicarboxylates are taken up by the secondary transporter DctA, and expression of the *dctA* gene and fumarate metabolic genes is controlled by DcuS-DcuR. Under anaerobic conditions, fumarate can be used as electron acceptor for fumarate respiration, leading to production of succinate. Here, uptake occurs via the fumarate/succinate antiporter DcuB, and expression of *dctB* and genes required for fumarate respiration is again controlled by DcuS-DcuR. These processes have been recently reviewed in detail (Unden *et al.*, 2016). Interestingly, DcuS itself is fully capable of binding suitable substrates (Kneuper *et al.*, 2005; Monzel and Unden, 2015), but is only able to respond to such binding events in the presence of either DctA or DcuB. In the absence of transporters, the kinase adopts a constitutive 'ON' state and fails to respond to stimuli (Kleefeld *et al.*, 2009; Witan *et al.*, 2012; Unden *et al.*, 2016). The role of the transporters in  $C_4$ -dicarboxylate sensing appears to be that of an activity switch, transferring the kinase from the constitutively active state to a substrate-responsive state (Fig. 2A).

DcuS possesses an extracellular PAS domain flanked by two transmembrane helices, which serves as the ligand binding site for  $C_4$ -dicarboxylates or citrate (Kneuper *et al.*, 2005; Unden *et al.*, 2016). The cytoplasmic part of DcuS is composed of a second PAS domain, followed by the kinase domains. Activation of DcuS occurs by a piston-like movement of transmembrane helix 2 by four amino acids towards the periplasmic side, most likely caused by conformational changes in the periplasmic PAS domain upon ligand binding (Monzel and Unden, 2015). Under aerobic conditions, the transporter DctA forms a complex with DcuS, mediated by direct protein-protein interactions between an amphipathic cytoplasmic helix near the C-terminus of DctA and the cytoplasmic PAS domain of DcuS (Witan *et al.*, 2012). Several lines of evidence suggest that formation of this complex is sufficient to bring DcuS into its substrate-responsive state, and that neither transport nor substrate binding by DctA (or DcuB) play any direct role in the signalling process. First, mutations in the  $C_4$ -dicarboxylate binding site of DctA abolish transport, but do not affect signalling by DcuS (Steinmetz *et al.*, 2014). Similarly, transport-defective DcuB variants have been constructed that maintain their ability to switch DcuS to the responsive state (Kleefeld *et al.*, 2009).

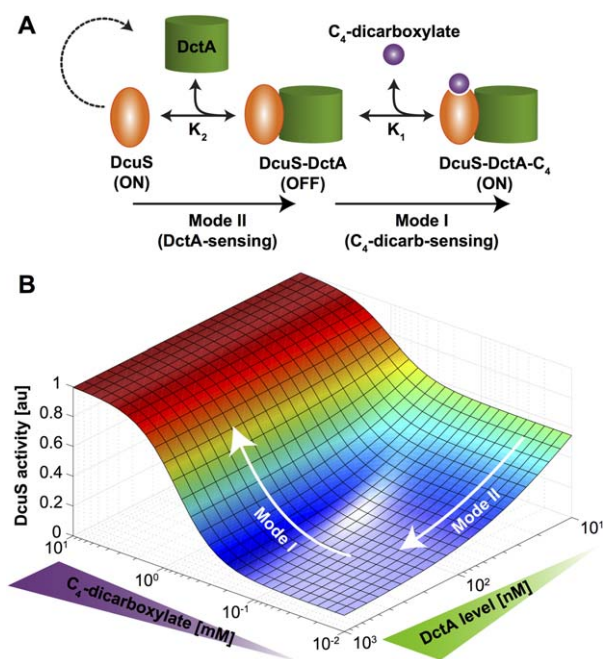


**Fig. 2.** The transporter DctA acts as activity switch on the histidine kinase DcuS during regulation of  $C_4$ -dicarboxylate utilization in *E. coli*.

A. The  $C_4$ -dicarboxylate transporter DctA (green) is not only responsible for high-affinity uptake of  $C_4$ -dicarboxylates (purple), but also involved in regulating its own production. In the absence of DctA, the kinase DcuS is constitutively active (left) and up-regulates transporter production (dashed arrow). Binding of DctA to DcuS sequesters DcuS to an 'OFF'-state (centre), leading to a negative feedback of DctA on its own production. This is referred to as Mode II and serves as sensor of DctA levels. In complex with DctA, DcuS is switched to a substrate-sensitive state, in which the histidine kinase is activated by binding of  $C_4$ -dicarboxylates (right; referred to as Mode I). B. A simple mathematical model derived from the reaction scheme in panel A illustrates the dual modes of sensing and is compatible with quantitative experimental data published previously (Steinmetz *et al.*, 2014). Within the model, DcuS activity is proportional to the probability of finding DcuS in an 'ON' conformation, that is, either unbound or in a DcuS-DctA- $C_4$ -dicarboxylate complex, as given by Eq. (1) in the main text. The graph was generated using the following parameters:  $K_1 = 0.5$  mM,  $K_2 = 10$  nM and  $n = 2$ .

Second, DcuS can be activated by citrate, which is not a substrate for DctA (Steinmetz *et al.*, 2014). And third, the substrate concentrations required for transport and signalling differ by several orders of magnitude. Uptake of fumarate by *E. coli*, presumably catalysed by DctA, occurs with an apparent  $K_m$  of 30  $\mu$ M (Kay and Kornberg, 1971), compared to an apparent  $K_m$  of 2–3 mM for activation of DcuS-dependent promoters (Kneuper *et al.*, 2005). Thus, maximal rates of transport are already supported by substrate concentrations that are insufficient to fully induce DcuS (Uندن *et al.*, 2016). DctA therefore clearly acts as an activity switch for DcuS and does not contribute any additional sensory functions to the signalling process. It was recently

shown that a functionally equivalent complex is formed between DcuS and DcuB under anaerobic conditions (Wörner *et al.*, 2016).

At a first glance, it does not appear clear what advantages such a regulatory strategy imparts to the cell. Why employ a transporter in a signalling pathway when neither substrate binding nor transport are factored into the regulatory decision taken by the cell? The citrate-responsive kinase CitA of *E. coli*, which is closely related to DcuS, does not require a transporter to respond to its substrate, showing that these kinases can function on their own (Scheu *et al.*, 2012). Intriguingly, the dual use of DctA as both a signalling modulator of DcuS and high-affinity uptake system for  $C_4$ -dicarboxylates causes the DcuS-DcuR system to respond in a two-mode fashion (Uندن *et al.*, 2016) (Fig. 2A). When no or only micromolar concentrations of  $C_4$ -dicarboxylates are present, DcuS will be present in the ligand-free state. Its activity under these conditions will only depend on the presence of DctA. If insufficient amounts of DctA are present to occupy all DcuS proteins, any free kinase molecules will be constitutively active, leading to increased production of DctA. This response is switched off as soon as DcuS is saturated with DctA (Steinmetz *et al.*, 2014). In this mode, termed Mode II (Uندن *et al.*, 2016), the input information is 'concentration of DctA', thereby leading to a negative autoregulation of transporter levels (Fig. 2B). The physiological role of keeping DctA at such an equilibrium may be to ensure homeostatic control of the transport capacity for  $C_4$ -dicarboxylates. The high affinity of the transporter allows uptake even at low substrate concentrations, enabling the cell to utilise these in anabolic or catabolic metabolism (Uندن *et al.*, 2016). In Mode I, DcuS is saturated with DctA and therefore fully switched to its substrate-responsive state (Uندن *et al.*, 2016) (Fig. 2A). The sole input information here is 'concentration of substrate' (Steinmetz *et al.*, 2014), but high (millimolar) concentrations of the substrate are required to elicit a strong response (Kneuper *et al.*, 2005) (Fig. 2B). The low substrate affinity of DcuS may ensure that the cell does not commit to a costly induction of  $C_4$ -dicarboxylate utilization systems unless sufficiently high concentrations are available to support growth on these substrates as primary carbon sources. Hence, the qualitative model of signal integration by the DcuS-DcuR system (Fig. 2A) seems to implement the regulatory logic of an OR gate, which either becomes activated by high external  $C_4$ -dicarboxylate levels or by a shortage of transporters within the cell. This OR-gate logic can be nicely illustrated with the aid of a mathematical model for the DcuS/DctA/ $C_4$ -dicarboxylate interaction scheme depicted in Fig. 2A: If one assumes binding of DctA to DcuS (Mode II binding with binding constant  $K_2$ ) and



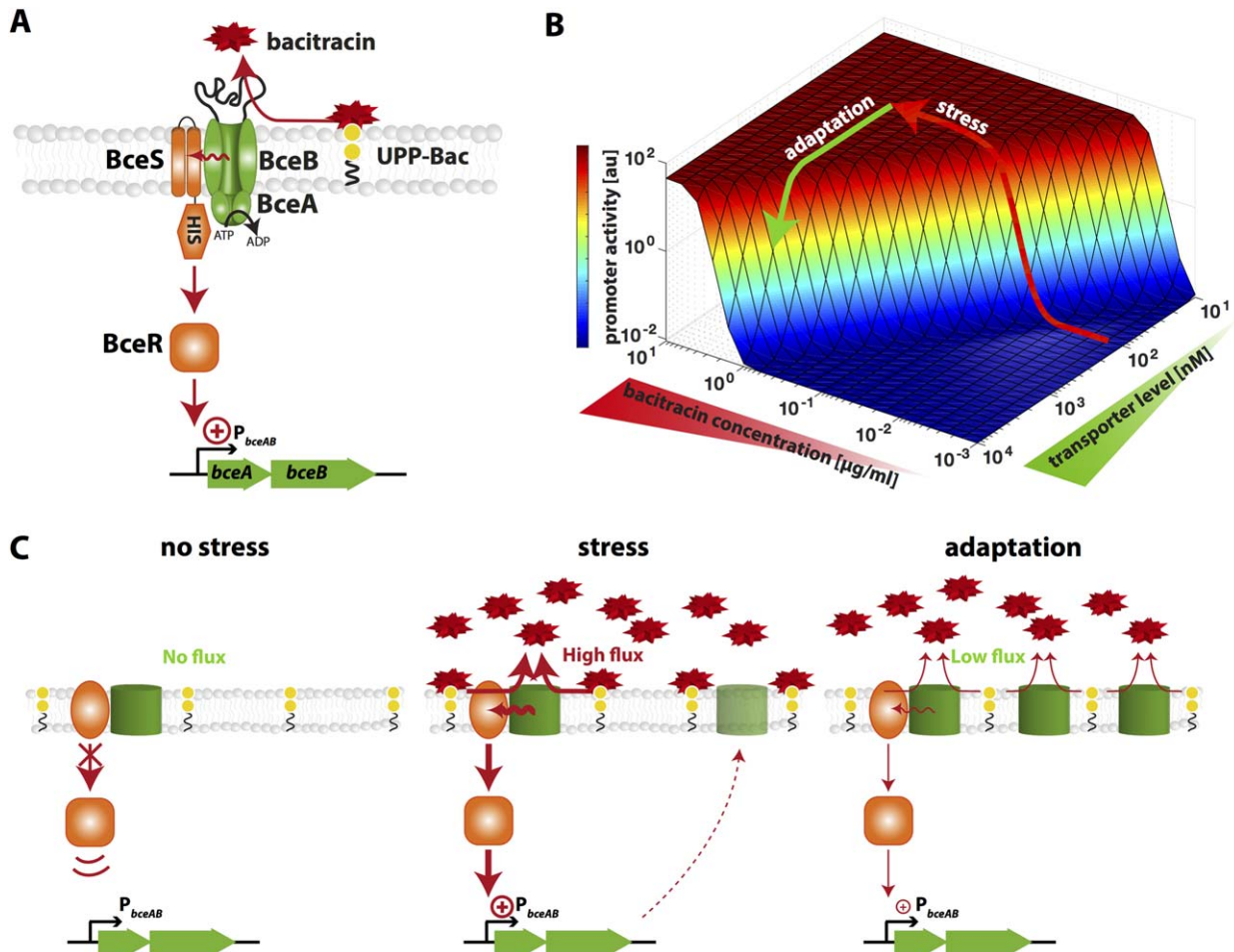


**Fig. 3.** In *B. subtilis*, a sensory complex of the histidine kinase BceS and the ABC transporter BceAB serves as a positive flux sensor. **A.** The ATP-binding cassette transporter BceAB (green) confers resistance against the antimicrobial peptide bacitracin (Bac, red) by removing the latter from its cellular target undecaprenyl pyrophosphate (UPP, yellow). A complex between the 2CS BceRS (orange) and BceAB serves as a sensor of transport activity ('flux-sensing'), which stimulates expression of the *bceAB* operon in response to bacitracin stress. For simplicity, BceS is represented as a monomer instead of the biologically active dimer. **B.** Mathematical simulations of a previously published model for the Bce system (Fritz *et al.*, 2015) show the long-term activity of the  $P_{bceAB}$  promoter in response to different levels of bacitracin and BceAB transporter. **C.** Illustration of the *B. subtilis* response to sudden bacitracin exposure. In the absence of bacitracin (left panel), BceAB is inactive and BceRS remains in its default OFF state. Upon bacitracin exposure (middle panel) high amounts of UPP-Bac complexes are formed and transport activity of BceAB is high, triggering signalling via BceRS to induce *bceAB* expression (see also red arrow in panel B). As a response, BceAB transporters accumulate in the cytoplasmic membrane and remove bacitracin from UPP. This in turn reduces the flux experienced by individual transporters, which ultimately reduces *bceAB* expression to an adapted steady-state level (right panel and green arrow in panel B).

cooperative binding of  $C_4$ -dicarboxylates to the DctA-DcuS complex (Mode I binding with binding constant  $K_1$  and Hill coefficient  $n$ ), then the active fraction of the histidine kinase,  $f_{ON}$ , (i.e., the sum of the unbound DcuS fraction and DcuS-DctA- $C_4$ -dicarboxylate complex) reads

$$f_{ON} = \frac{1 + \frac{[A][C]^n}{K_2 K_1^n}}{1 + \frac{[A]}{K_2} + \frac{[A][C]^n}{K_2 K_1^n}}, \quad (1)$$

where  $[A]$  and  $[C]$  are the concentrations of DctA and  $C_4$ -dicarboxylates, respectively. Note that this mathematical

model not only resembles the regulatory logic of an OR gate (Fig. 2B), as expected qualitatively, but is also in good quantitative agreement with the experimental data by (Steinmetz *et al.*, 2014). This underlines that the simple reaction scheme depicted in Fig. 2A is indeed sufficient to describe this elegant way of signal integration.

### Sensors of transport flux

Although in the previous example the DctA transporter is a fully functional importer for  $C_4$ -dicarboxylates, transport activity *per se* is dispensable for signalling. There



are, however, an increasing number of systems in which substrate translocation by the transporter is essential for stimulus perception via the signalling system. Based on this strict dependence on transport flux, we will in the following refer to such tandems of transporters and signalling systems as 'flux sensors'. Moreover, we will distinguish between two classes of flux sensors: On the one hand, we define positive flux sensors as those in which a high transport activity acts as cue for the activation of signalling, while on the other hand, in negative flux sensors signalling is activated at a low transport activity. Accordingly, mutants deleted for the respective transporters also show opposing behaviour of the signalling systems: In positive flux sensors the signalling system turns to its default 'OFF' state in the absence of the transporter, while in negative flux sensors the signalling system remains locked in the default 'ON' state.

#### Positive flux sensors

The paradigm example for a positive flux sensor is the Bce system of *Bacillus subtilis*, which provides resistance against the peptide antibiotic bacitracin and a few other antimicrobial peptides (Fig. 3A). The system consists of the ABC-transporter BceAB that mediates the actual resistance, and the 2CS BceRS that controls expression of the transporter operon (*bceAB*) (Ohki *et al.*, 2003). The most striking characteristic of this system is that the BceS kinase lacks any obvious sensory domains. Instead BceS completely depends on the transporter for detection of substrate peptides, and deletion of the transporter abolishes any induction of the target promoter,  $P_{bceA}$  (Rietkötter *et al.*, 2008), highlighting that the default state of the 2CS is 'OFF'. BceAB therefore not only acts as resistance determinant but also as primary sensor of the antibiotic. Interestingly, resistance and signalling can be genetically separated by single amino acid substitutions in the transport permease BceB, showing that BceAB truly is a dual-function transporter (Kallenberg *et al.*, 2013). Biochemical analysis of the proteins involved showed that the kinase and transporter form a sensory complex in the cytoplasmic membrane of the cell, and that the transporter can directly influence kinase activity (Dintner *et al.*, 2014). The mechanistic basis of signal transmission between BceB and BceS, however, remains unknown. Mutagenesis of the ATPase component, BceA, further demonstrated that ATP hydrolysis is required for activation of BceS, suggesting that transport *activity* is essential for the signalling process, rather than mere ligand binding (Rietkötter *et al.*, 2008). Mathematical modelling of the quantitative response dynamics of the Bce system provided evidence that it directly responds to transport

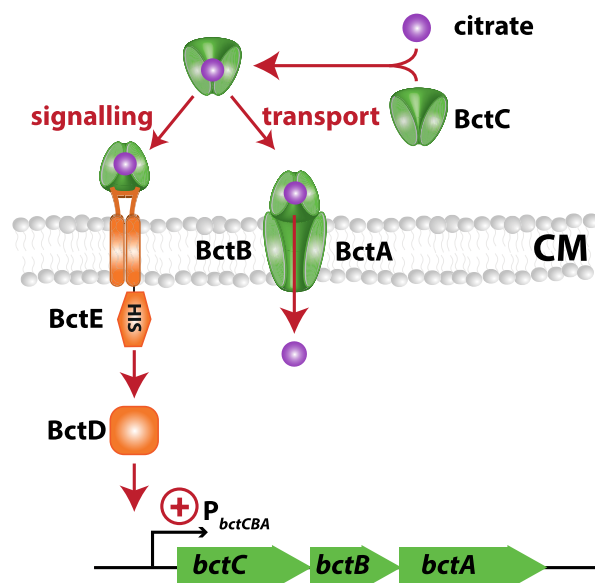


**Fig. 4.** The periplasmic binding protein of the BctCAB transporter mediates transport as well as signalling in *Bordetella pertussis*. The citrate uptake system (green) of *B. pertussis* consists of the permease domains BctA and BctB, as well as the periplasmic binding protein BctC, which binds citrate (purple) and thus mediates citrate import via BctAB. In addition, BctC-citrate binds to and activates the histidine kinase BctE (orange), which in response stimulates expression of the *bctCAB* operon via the response regulator BctD. Hence, citrate binding to BctC increases the rate of transport and the magnitude of signal transduction in proportional ways, suggesting that the system might function akin to a positive flux sensor.

activity of BceAB, with each BceS kinase measuring the antibiotic flux experienced by the transporter with which it forms a sensory complex (Fritz *et al.*, 2015) (Fig. 3B).

Our current understanding of the Bce system has led to the following model of its biological function (Fig. 3B and C). In un-challenged cells, basal promoter activity of the *bceAB* operon produces a small number of transporters that can form sensory complexes with BceS, which itself is produced from a constitutive promoter. Bacitracin and other antimicrobial peptides bind to intermediates of the lipid II cycle of cell wall biosynthesis (Breukink and de Kruijff, 2006; Economou *et al.*, 2013). How transport can mediate resistance against an antibiotic targeting a surface structure of the cell is currently unknown, but presumably involves removal of the antibiotic from the target, freeing the latter for access by cell wall biosynthetic enzymes. Such a mechanism would be similar to that observed for self-resistance in some producer organisms of antimicrobial peptides (Stein *et al.*, 2003; Okuda *et al.*, 2008). In this case, the complexes between the antibiotic and its target molecule form the substrate for the BceAB transporter. The higher the concentration of the antibiotic, the more antibiotic-target complexes are formed, and the higher is the transport

activity of BceAB. This increased activity is directly detected by the BceS kinase, presumably through physical contact to the transporter, and leads to activation of signalling and increased production of the transporter (cf. Fig. 3B; *red arrow*). The resulting additional capacity for transport will keep the cellular target free of antibiotic, thereby reducing the concentration of substrates for individual transporters. The decreased transport activity experienced by individual BceAB molecules then in turn swiftly turns off signalling via BceS (cf. Fig. 3B; *green arrow*). This flux-sensing mechanism thus implements a negative feedback on regulation, allowing the cell to quickly establish a new steady-state level of transporter numbers. Experimentally observed response times were indeed very fast with equilibrium reached after approximately one third to one half of the generation time (Fritz *et al.*, 2015). Importantly, using the transporter as both activator of signalling and remover of its own substrate, the cell precisely adapts the new steady-state level of transporters depending directly on the cell's capacity for detoxification, not merely the present concentration of the antibiotic. The adaptive power of this regulatory strategy is highlighted by a very large input-dynamic range, allowing a gradual response over nearly three orders of magnitude of antibiotic concentrations, which is considered to be more cost-effective than a simple dose-dependent response to antibiotic concentrations (Fritz *et al.*, 2015).

Phylogenetic analyses of Bce-like systems revealed that they are found throughout the low G + C content Gram-positive bacteria, but not outside of this group (Joseph *et al.*, 2002; Dintner *et al.*, 2011). BceAB-like transporters are almost always found together with BceRS-like 2CS, and their transport permeases and histidine kinases have coevolved, suggesting a general functional interdependence between them (Dintner *et al.*, 2011). All systems that have been studied experimentally to date are involved in resistance against antimicrobial peptides, so not only the regulatory principle but also their physiological role seems to be conserved (Dintner *et al.*, 2011; Gebhard and Mascher, 2011; Gebhard, 2012; Revilla-Guarinos *et al.*, 2014). In some bacteria, variations on the theme described above for the Bce-system in *B. subtilis* exist. Whereas in the Bce-system the same transporter fulfils the roles of resistance determinant and antibiotic sensor, these functions are divided between two separate transporters in *Staphylococcus aureus* (Hiron *et al.*, 2011) and *Enterococcus faecalis* (Gebhard *et al.*, 2014). Whether this is an evolutionary intermediate, for example, following loss of the 2CS for one of the transporters, or gain of an additional orphan transporter, or whether such a regulatory strategy gives the cell a particular advantage remains unclear. Interestingly, two systems have been described where the 2CS is activated by a sensory BceAB-like transporter, but the actual resistance is then mediated by

induction of entirely unrelated genes, such as the *dltABCD* operon (coding for D-alanylation of teichoic acids) and *mprF* (for L-lysinylation of phospholipids). One example for this is the nisin resistance system 'module 12' of *Lactobacillus casei* (Revilla-Guarinos *et al.*, 2013). The second example is comprised of the 2CS GraSR and transporter VraFG of *S. aureus*, where communication between transporter and kinase appears to involve a fifth protein, GraX (Falord *et al.*, 2012). The VraFG transporter does not have the ability to confer resistance against antimicrobial peptides on its own (Falord *et al.*, 2012). In this case, the negative feedback that governs the response dynamics of the *B. subtilis* Bce-system appears to be missing. It would be interesting to investigate the effects of this on gene regulation, or if induction of *dltABCD* and *mprF*, which together reduce access of the antibiotics to their targets (Revilla-Guarinos *et al.*, 2014), could have an effect equivalent to active removal of the antibiotic.

While in the Bce system discussed above the transporter interacts via its permease domain with the 2CS to implement a flux sensor, also other components of multipartite transporters were described to interact with signalling systems. For instance, in *E. coli* the periplasmic maltose binding protein MalE interacts with the Tar chemoreceptors in the presence of maltose and thereby modulates chemotactic behaviour (Hazelbauer, 1975; Zhang *et al.*, 1999). Similarly, in *Agrobacterium tumefaciens* the chromosomal virulence gene E (*chvE*) encodes a periplasmic binding protein that binds several neutral sugars and sugar acids, and subsequently interacts with the VirAG 2CS to stimulate virulence gene expression (Hu *et al.*, 2013).

Another well-studied example is the citrate uptake system of *Bordetella pertussis*, in which the tripartite tricarboxylate transporter (TTT) BctCAB interacts via its periplasmic binding protein BctC with the histidine kinase BctE (Antoine *et al.*, 2003) (Fig. 4). Here, citrate binding to BctC not only enables citrate uptake through BctAB, but also activates the 2CS BctDE, which in turn triggers expression of the *bctCAB* transporter operon (Antoine *et al.*, 2005). Intriguingly, disruption of *bctA* was shown to abolish citrate uptake by *B. pertussis* (Antoine *et al.*, 2003), while signalling through BctDE was highly elevated in this mutant (Antoine *et al.*, 2005). This clearly shows that not active citrate transport by BctCAB, but rather accumulating levels of citrate-bound BctC molecules are the cue detected by the 2CS BctDE. It is nevertheless conceivable that the fully functional (wild-type) Bct system may function akin to a positive flux sensor: qualitatively, one would expect that the rate of citrate uptake is directly proportional to the level of citrate-bound BctC molecules. Because these citrate-BctC complexes at the same time serve as the input to the signalling system, citrate influx

should be proportional to signalling. To understand the quantitative implications of this signalling strategy, it will be important to consider the relative affinities of substrate-bound BctC to the histidine kinase, BctE on the one hand, and the transport permease components BctAB on the other hand. Preferential binding of BctC to one of its partners could have drastic effects on the relationship between transport flux and signalling. Therefore, more quantitative experiments and mathematical modelling are needed to fully understand the regulatory implications of linking transport to signalling in this way.

The Bct system of *B. pertussis* is homologous to the paradigm TTT transporter TctCAB of *Salmonella typhimurium*, which is likewise controlled by a 2CS, TctE-TctD (Widenhorn *et al.*, 1989). It is, however, not known whether TctC plays a similar role in signalling as in the *B. pertussis* system. Intriguingly, *B. subtilis* possesses an orphan homologue to BctC, named YfiP, which is genetically associated with a 2CS, YfiR-YfiQ. Although it remains to be proven experimentally, it has been proposed, based on gene arrangement and the absence of the transmembrane components of the transporter, that YfiP may have a sensory role in this system (Winnen *et al.*, 2003). This suggestion raises the question as to the original function of BctC-like binding proteins, substrate binding for transport or as an accessory component of signalling systems. A phylogenetic analysis of TTT systems revealed that the larger transmembrane component, the TctA-like proteins, are often found alone and are most widely distributed, even including Archaea (Winnen *et al.*, 2003). They are only occasionally found together with TctB- and TctC-homologues, and the full set of proteins only occurs in bacteria. This has been interpreted as TctA being the actual transporter in its ancestral form that later acquired the smaller accessory membrane protein TctB and the periplasmic binding protein TctC, for example, to modify function or increase substrate affinity (Winnen *et al.*, 2003). It is therefore conceivable that TctC-like proteins originated as signalling proteins and were later co-opted into transport systems. It would be highly interesting to test if the regulatory principle so far only shown for the *B. pertussis* Bct system holds true for its homologues and if orphan TctC-like proteins truly possess signalling activities.

#### Negative flux sensors

One of the best-understood examples for a negative flux sensor is the regulation of the phosphate starvation response of *E. coli*. Here, the 2CS PhoR-PhoB forms a sensory complex with the ATP-binding cassette (ABC) transporter PstSCAB<sub>2</sub>, mediated by the chaperone-like

protein PhoU [reviewed in (Hsieh and Wanner, 2010)]. Phosphate-limitation activates signalling by PhoR-PhoB and leads to the induction of the entire Pho-regulon, which includes genes encoding the PhoR-PhoB 2CS, the PstSCAB<sub>2</sub> transporter, PhoU and several transporters and enzymes involved in exploiting alternative phosphorus sources (Wanner, 1993; van Veen, 1997). Through the resulting changes, the cell increases both its capacity for phosphate uptake and the availability of free phosphate. In the absence of PstSCAB<sub>2</sub> or PhoU, the kinase PhoR is in a constitutively activated state, leading to full induction of the Pho-regulon, irrespective of phosphate availability. Thus, the default state of the 2CS is 'ON', and the transporter acts as repressor of signalling under phosphate-replete conditions. This functional interdependence of 2CS, PstSCAB<sub>2</sub> and PhoU has not only been found in *E. coli*, but also in *Sinorhizobium meliloti* (Yuan *et al.*, 2006) and *Mycobacterium smegmatis* (Gebhard and Cook, 2008). Interestingly, in *Bacillus subtilis* the transporter does not appear to be involved in phosphate-signalling (Qi *et al.*, 1997), showing that the regulatory principle is wide-spread but not universal.

The PhoR histidine kinase is devoid of any apparent extracellular sensory domains, but contains a cytoplasmic PAS (Per-ARNT-Sim) domain harbouring the interaction interface with PhoU (Gardner *et al.*, 2014; Gardner *et al.*, 2015). PhoU also interacts with the ATPase component of the transporter, PstB, and therefore appears to be the hub of the seven-protein signalling complex (Gardner *et al.*, 2014) (Fig. 5). Signalling is thought to occur by the following mechanism. Under high phosphate conditions, the PstSCAB<sub>2</sub> transporter is fully occupied and all transporters are switched to the 'transport active' state. In this state, the transporter is also 'signalling active' and represses the kinase activity of PhoR-PhoB while the phosphatase activity dominates (Hsieh and Wanner, 2010) (Fig. 5A). When phosphate becomes limiting, not all transporters are active at all times, and those that temporarily become inactive lose their repressive function, leading to the activation of signalling (Fig. 5B). According to this model, a cell experiencing phosphate-limitation possesses a mixture of transport-active and inactive copies of PstSCAB<sub>2</sub>. At any given time, the currently inactive copies promote signalling and cause activation of the Pho-regulon, while the active copies import phosphate and allow the cell to continue growing (Hsieh and Wanner, 2010). In this way, the cell responds not simply to the external concentration of phosphate, but rather to its ability to scavenge this essential nutrient, which ultimately is the more relevant parameter for survival.

In addition to increasing the number of transporters as a response to phosphate-limitation, the cell also

produces enzymes such as alkaline phosphatases to liberate phosphate from other sources (Wanner, 1993; van Veen, 1997). This will increase the external concentration of free phosphate, raise the intake flux per PstSCAB<sub>2</sub> transporter and ultimately shut down the response (Fig. 5C).

Notably, on phosphate starvation the cell not only responds by increasing the copy number of PstSCAB<sub>2</sub> transporters, but also up-regulates the production of the PhoR-PhoB 2CS in an autoactivating positive feedback loop (Hoffer *et al.*, 2001) (Fig. 5C)1. In principle, positive feedback can lead to switch-like or even hysteretic

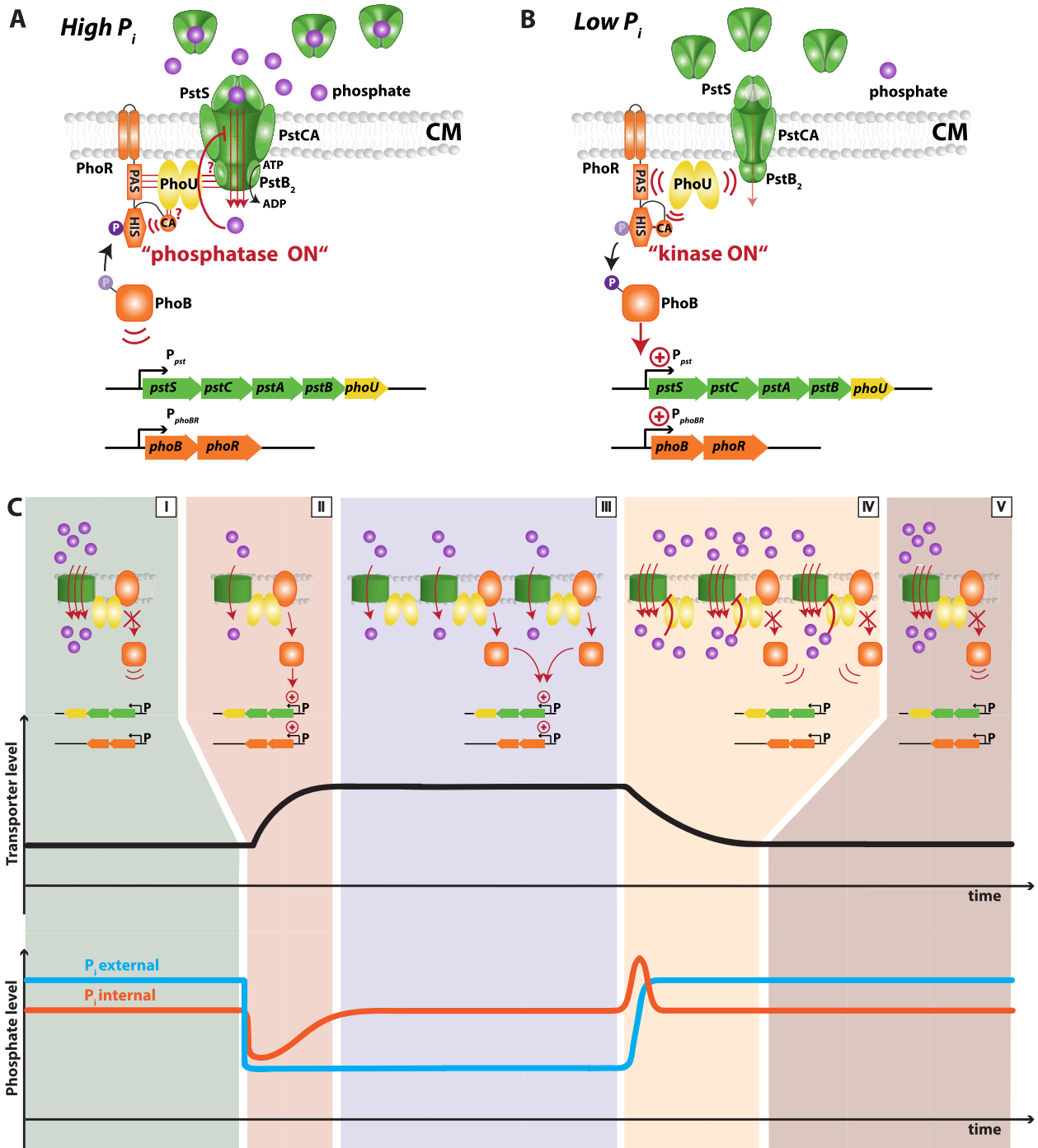


Fig. 5..



**Fig. 5.** In the phosphate starvation response of *E. coli*, the 2CS PhoR-PhoB in conjunction with the PstSCAB<sub>2</sub> transporter functions as a negative flux sensor. Regulation of phosphate (purple) uptake in *E. coli* is controlled by a seven-protein signalling complex consisting of the phosphate transporter PstSCAB<sub>2</sub> (green), the 2CS PhoR-PhoB (orange) and the accessory membrane protein PhoU (yellow).

A. Under phosphate-replete conditions the PstSCAB<sub>2</sub> transporter is fully active and imports phosphate at high rate. In this state the transporter is believed to bring PhoU into a conformation that turns the bifunctional histidine kinase PhoR into a 'phosphatase ON' state. This leads to inactivation of the response regulator PhoB and thereby keeps transcription of the Pho regulon at a basal level. The functional domains of PhoR are shown as CA, catalytic domain; PAS, Per-Arnt-Sim domain; HIS, histidine-transfer and dimerization domain (please refer to text for details of information transfer and transport-repressing functions of PhoU).

B. Under phosphate-limiting conditions, PstSCAB<sub>2</sub> transporter activity decreases, leading to a weakening or loss in PstSCAB<sub>2</sub>-PhoU-PhoR interaction. As a result, the kinase is derepressed, causing activation of signalling ('kinase on') and induction of *pstSCAB*, *phoU* and *phoBR* expression.

C. Schematic illustration of the phosphate starvation response in *E. coli*. During phosphate starvation, the drop in external and internal inorganic phosphate (P<sub>i</sub>) leads to reduced P<sub>i</sub> influx via PstSCAB<sub>2</sub>, which in turn triggers the production of further transporters (*phase II*). The increasing number of transporters recovers the internal P<sub>i</sub> to its initial level and guarantees an adequate supply (*phase III*). Once external P<sub>i</sub> levels return to high levels, internal phosphate might transiently accumulate to high intracellular levels, because of the high number of transporters still present (*phase IV*). Excessive phosphate uptake is prevented by PhoU. Additionally, PstSCAB<sub>2</sub> restore repression of signalling and transporter levels drop to pre-starvation levels by dilution during cell growth (*phases I and V*).

behaviour, where the response to a current stimulus depends on the previous history of stimuli (Fritz *et al.*, 2007; Lambert *et al.*, 2014). Indeed autoamplification of the PhoR-PhoB 2CS has been attributed with 'learning' behaviour, because phosphate-starved cells displayed a significantly faster induction of the Pho response than nonstarved cells – even after 2 h of growth in phosphate-containing medium (Hoffer *et al.*, 2001). While the physiological role of such priming behaviour is still elusive, clear selective advantages may arise if fluctuations in environmental phosphate availability are correlated. For instance, if one period of phosphate starvation is indicative of subsequent starvation periods, it might be beneficial to keep memory on previous starvation responses.

Not much is known about the molecular mechanism by which the transporter and PhoU repress PhoR activation. One hypothesis is that PhoU somehow transmits conformational changes as part of the transport cycle of PstSCAB<sub>2</sub> to the kinase (Gardner *et al.*, 2014). Importantly, transport and signalling are genetically separable functions of PstSCAB<sub>2</sub>, as amino acid substitutions have been identified in the permease component PstC that abolish transport but still allow repression of PhoR (Cox *et al.*, 1989). In contrast, mutations that prevent ATP-hydrolysis by the ATPase PstB caused defects in both transport and signalling (Cox *et al.*, 1989). Considering that PhoU interacts with the PstB subunit of the transporter (Gardner *et al.*, 2014; Gardner *et al.*, 2015), it therefore appears likely that the information transmitted to the kinase is derived from the ATPase activity of the transporter, that is, as long as the ATPase hydrolyses ATP, PhoU represses PhoR. Two possibilities of how this may be accomplished have been discussed (Gardner *et al.*, 2014): If the complex between the 2CS, PhoU and PstSCAB<sub>2</sub> is stable regardless of the phosphate concentration, then PhoU may have the ability to cause PhoR to switch between active and inactive states depending on PstSCAB<sub>2</sub> activity. Alternatively, the

complex may dissociate when the transporter is inactive to allow the kinase to adopt its default active state.

Interestingly, it appears that PhoU plays a second important role in controlling not only the start of the Pho response, but also its termination (Fig. 5C). When a low-phosphate adapted cell returns to phosphate-replete conditions, repression of PhoR-PhoB has to be restored to terminate the response, as discussed above. The high levels of PstSCAB<sub>2</sub> and PhoU that were produced during the phosphate-limited period ensure that the 2CS is quickly returned to its repressed state. However, the presence of high transporter levels also poses a risk to the cell, as it could lead to the accumulation of toxic intracellular phosphate concentrations (Rice *et al.*, 2009). This appears to be prevented by PhoU, which has the ability to inhibit phosphate uptake by PstSCAB<sub>2</sub> when intracellular phosphate concentrations are high (Rice *et al.*, 2009). Similar negative effects of PhoU on phosphate uptake have also been observed in *Pseudomonas aeruginosa* (de Almeida *et al.*, 2015) and *Caulobacter crescentus* (Lubin *et al.*, 2016). This second regulatory function of PhoU thus constitutes an elegant mechanism to immediately curb uptake by the transporter and thereby prevent accumulation of toxic intracellular phosphate when the external availability of phosphate suddenly increases. Detailed investigations of the multiple activities of this enigmatic hub-protein will be essential to fully understand how phosphate transport connects to signalling and how these processes are embedded in the physiology of the cell.

### Transporters involved in signal integration

In the systems discussed above, a unique stimulus is responsible for sensing and signalling. Either the transporter level, the transporter activity (flux) or the 'result' of transport, namely the internal substrate, is detected. Yet many microbial adaptation processes not only rely

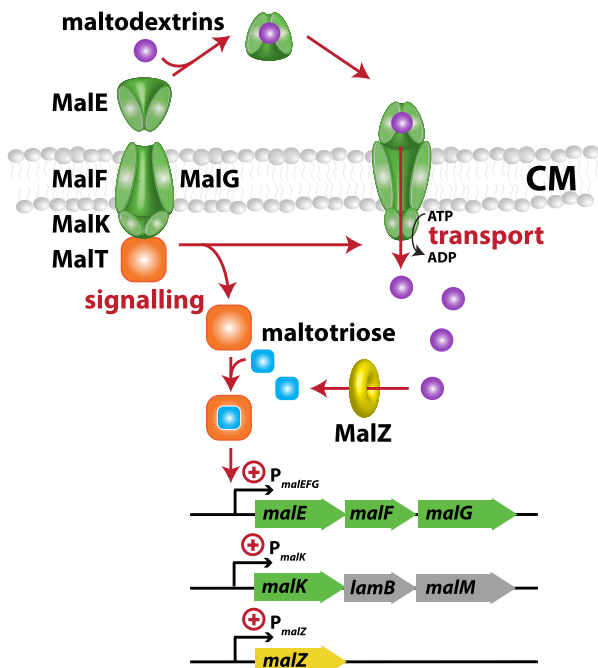


**Fig. 6.** The maltose transporter MalEFGK<sub>2</sub> of *E. coli* sequesters the transcriptional regulator MalT at low transport flux. In the maltose uptake system of *E. coli*, maltodextrins (purple) are imported via the ABC transporter MalEFGK<sub>2</sub> (green). In the absence of external maltodextrins, the inactive MalEFGK<sub>2</sub> transporter sequesters the transcriptional activator MalT to the membrane (left). Upon maltodextrin import by MalEFGK<sub>2</sub>, MalT is released to the cytoplasm, where it is activated by binding of maltotriose (light blue) – a by-product of maltodextrin metabolism produced by MalZ (yellow). Hence, after complete activation by two signals – maltodextrin influx and internal maltotriose – MalT up-regulates the expression of the transporter genes and others involved in maltodextrin metabolism.

on a single source of environmental information, but instead require the combinatorial integration of multiple external and internal cues. However, the sensors involved in stimulus perception are subject to biochemical constraints, which limit the number of cues that can be detected by a single protein. Signal integration is therefore often achieved by interactions between multiple sensory systems, which can also incorporate transporters as sensors of substrate availability and/or reporters of transport flux.

One of the best-studied systems that integrates two sources of input information is the Mal-system required for maltose-uptake in *E. coli* (Fig. 6). Here, the import of maltose and maltodextrins depends on the ABC-transporter MalEFGK<sub>2</sub>, which is genetically organized in two operons, *malEFG* and *malK-lamB-malM* [reviewed, for example, in (Boos and Shuman, 1998)]. Both operons are regulated by the transcriptional activator MalT (Hofnung, 1974; Hofnung *et al.*, 1974). Interestingly, activation of MalT itself depends on two distinct inputs. First, in the absence of external maltodextrins the ATP

binding subunits of the transporter, MalK<sub>2</sub>, sequester MalT into an inactive (ADP-bound) form (Schreiber *et al.*, 2000; Joly *et al.*, 2004) and thereby prevent its activation (Panagiotidis *et al.*, 1998). Only if MalEFGK<sub>2</sub> actively imports maltodextrins into the cell, ATP hydrolysis by MalK<sub>2</sub> triggers release of MalT and allows the latter to assume its active, ATP-bound form (Panagiotidis *et al.*, 1998; Schreiber *et al.*, 2000). Second, ATP-bound MalT is then further stabilized by internal maltotriose – an intermediate product of maltodextrin metabolism (Raibaud and Richet, 1987) – which triggers full activation of MalT (Schreiber *et al.*, 2000; Joly *et al.*, 2004). Of note, this second mode of sensing is very similar to internal substrate sensing in the Lac-system of *E. coli*, in which allolactose – an intermediate product of lactose metabolism – is detected by the *lac* repressor LacI (Müller-Hill, 1996).

By using such a dual-input sensory strategy, the cell up-regulates the production of maltose transporters only if (i) there is a sufficient flux of maltodextrins into the cell and if (ii) internal substrate has accumulated to significant levels. Using such an AND gate, the cell asserts that physiological levels of endogenously produced maltotriose, for example during metabolism of glycogen (Ehrmann and Boos, 1987), do not cause the futile production of transporters in the absence of external substrate. This raises the question as to why MalT should act as an internal sensor of maltotriose at all, considering that the sequestration of MalT by inactive transporters already appears to act as a functional flux sensor reporting on external maltose availability. One potential benefit of this dual mode of sensing might be that internal substrate sensing can easily implement a positive feedback loop on regulation: increased production of transporters raises the rate of substrate accumulation, which in turn further up-regulates transporter production. In the classical lactose and arabinose utilization systems, this positive feedback was shown to trigger switch-like ‘all-or-none’ behaviour at intermediate inducer concentrations, with one subpopulation of cells fully committing to sugar utilization and a second subpopulation not investing into costly synthesis of the associated metabolic program at all (Ozbudak *et al.*, 2004; Megerle *et al.*, 2008; Fritz *et al.*, 2014). Such a diversification of a phenotypic trait within a genetically identical population may serve as a ‘bet-hedging’ strategy in fluctuating environments, in which sugars may come and go at unpredictable times (Veening *et al.*, 2008). Nevertheless, in theory, a similar positive feedback could be implemented with a flux-sensor alone, if for instance the regulator MalT were to be up-regulated in response to influx of maltose, leading to an increase in free, that is, active pool of MalT. However, *malT* is not subject to positive autoregulation (Debarbouille and Schwartz, 1979;

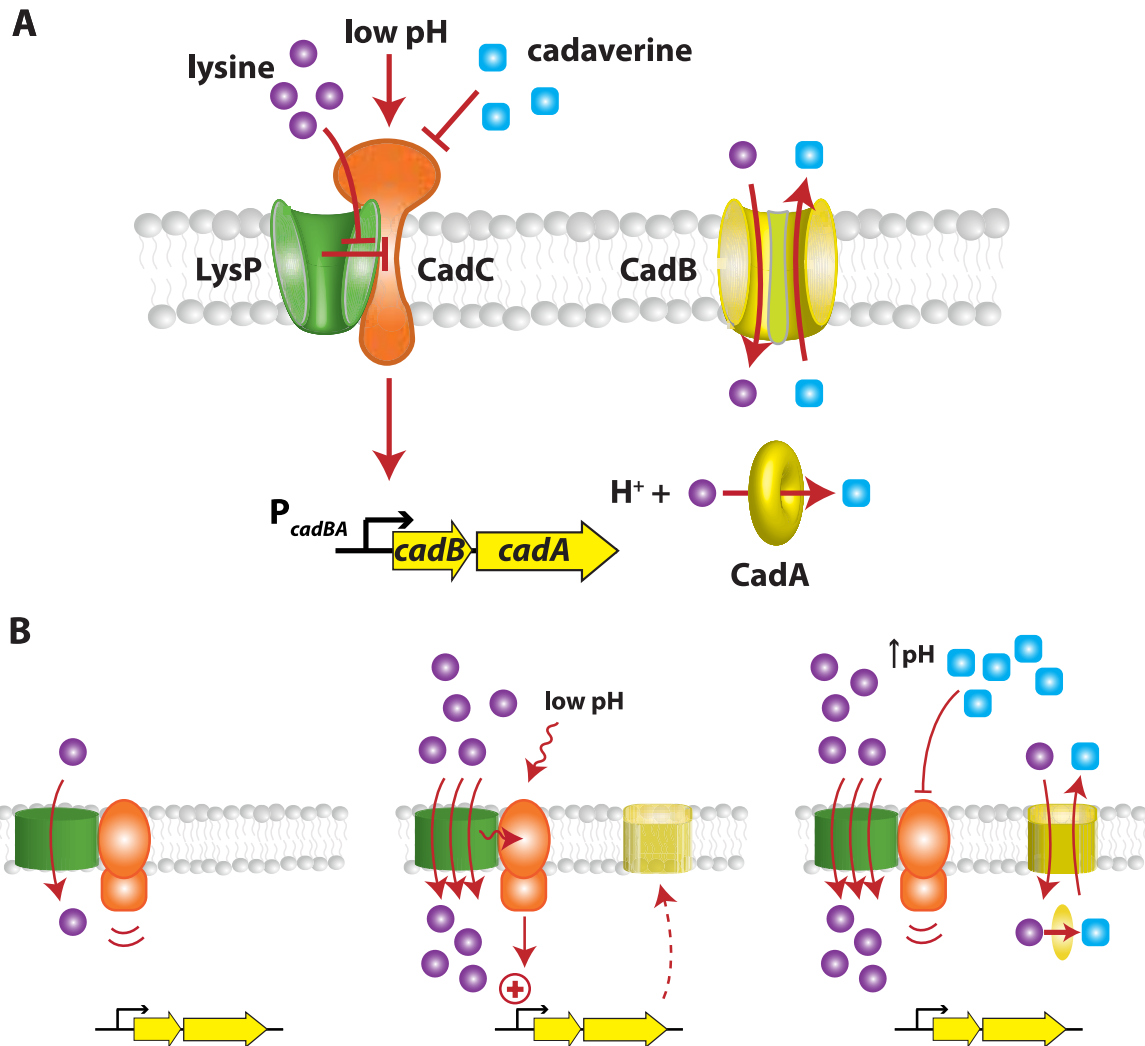


**Fig. 7.** In the acid stress response of *E. coli*, the lysine importer LysP interacts with the one-component system CadC to integrate three external signals.

**A.** The acid stress response system Cad of *E. coli* consists of the lysine decarboxylase CadA, the lysine/cadaverine antiporter CadB (both yellow) and the membrane-associated 1CS CadC (orange), which activates the expression of the *cadBA* operon at low pH, if simultaneously the lysine concentration is high and the cadaverine concentration is low. While CadC is able to sense the external pH and cadaverine directly via its periplasmic domain, the perception of external lysine relies on the interaction with the secondary lysine/ $H^+$  symporter LysP (green). **B.** Schematic illustration of the Cad-response to acid stress. In the absence of lysine (left panel), LysP inhibits the activation of CadC via intramembrane and membrane-peripheral contacts. Under increased lysine levels and at low external pH (middle panel), high lysine influx via LysP releases this inhibition of CadC and allows the latter to be activated by low pH, resulting in the induction of *cadBA* expression. After the production of sufficiently high CadA and CadB levels (right panel), cadaverine is produced and excreted to the medium, where it increases the external pH and inhibits CadC, thereby terminating the Cad response.

Chapon, 1982; Decker *et al.*, 1998), suggesting that this hypothetical scenario is not implemented in the Mal-system. Thus, it seems likely that the need for positive feedback-induced heterogeneity cannot be the only factor that shaped the evolution of this dual mode of sensing. Further quantitative experimental and theoretical work is needed to shed light on the precise response-dynamics of this system.

A remarkable example for a system integrating three physiological stimuli is the Cad system, which is

involved in the acid tolerance response of *E. coli* (Foster, 2004) (Fig. 7A). Upon exposure to acidic pH and in the presence of lysine, *E. coli* strongly up-regulates the expression of the *cadBA* operon, encoding the lysine decarboxylase CadA and the lysine/cadaverine antiporter CadB (Meng and Bennett, 1992) (Fig. 7B). Together, they increase both the intra- and extracellular pH via consumption of a cytoplasmic proton during the decarboxylation of lysine to cadaverine, followed by the excretion of the more basic cadaverine in exchange for a lysine

molecule. Ultimately, the accumulation of external cadaverine turns off the expression of *cadBA*, leading to a transient Cad response (Neely and Olson, 1996; Fritz *et al.*, 2009) (Fig. 7B).

Interestingly, signal integration is achieved by the membrane-integrated ToxR-like 1CS CadC, which is able to sense low pH (Tetsch *et al.*, 2011; Buchner *et al.*, 2015) and high cadaverine levels (Eichinger *et al.*, 2011; Haneburger *et al.*, 2012) via its periplasmic domain, while its cytoplasmic domain directly binds to and activates the *cadBA* promoter (Kuper and Jung, 2005). However, CadC cannot directly sense the presence of lysine (Tetsch *et al.*, 2008), and instead relies on the secondary lysine/H<sup>+</sup> symporter LysP, which is required for lysine uptake from the growth medium. Early experiments showed that *lysP* mutants lead to lysine-independent *cadBA* expression (Popkin and Maas, 1980), while LysP overproduction caused repressed *cadBA* activity (Neely *et al.*, 1994), suggesting that LysP is a negative regulator of CadC activity in the absence of lysine. Recently, it was shown that at low external lysine concentrations LysP indeed forms a complex with CadC via intramembrane and periplasmic contacts (Rauschmeier *et al.*, 2014), which keep CadC in an inactive state – regardless of external pH. Only if LysP imports lysine at sufficiently high rates, lysine-dependent conformational changes in LysP transduce the lysine signal via a direct conformational coupling to CadC without resolving the interaction completely (Rauschmeier *et al.*, 2014). Hence, by integrating the transport activity of LysP into the decision for activating the Cad response, the cell asserts that the acid defence via lysine decarboxylation is only activated if the substrate for the reaction – lysine – is actually present in the environment.

### Concluding remarks

During the course of evolution bacterial transporters developed into sophisticated molecular machines with exquisite abilities to bind their cognate substrates. As highlighted in this review, this not only enables efficient substrate translocation, but can also be used to provide the cell with important information about its extracellular and/or intracellular state. This is achieved via direct or indirect contacts between the transporter and a membrane-associated signalling protein. Depending on the regulatory logic of these interactions, a vast range of physiological responses can be implemented, ranging from activity switches, positive and negative flux sensors to multi-input signalling hubs. While the mechanistic details of signal transfer at the interface between transporter and signalling protein are just beginning to be

revealed, in many systems the transporter regions or even specific amino acids involved in transport are distinct from those used for information transfer. Given such a modular structure, it seems likely that these two traits either evolved independently of each other, or at least functionally diverged over the course of evolutionary time. This, together with the large diversity of implemented signalling behaviours, provokes the question as to why transporters are not observed more commonly as (co-)sensors in nature. One potential reason for this might be that the key experiments revealing transporters as essential for stimulus perception are in fact not necessarily intuitive. They require the activity of a target promoter under investigation to be monitored in a transport-deficient mutant – a scenario that is not routinely assayed when characterising a transporter or signalling system. Therefore, one might speculate that regulatory roles of transporters are far more common than currently known. As the existence and physiological relevance of information-processing transporters is becoming increasingly recognised, systematic screens should help identify other examples. Subsequent quantitative characterisation in conjunction with mathematical modelling can then reveal the actual logic implemented in each respective system and may even lead to the discovery of further regulatory complexity and novel signalling strategies in bacteria.

### Acknowledgements

To all colleagues in the field whose relevant papers we did not cite owing to space constraints, we would like to apologise. HP gratefully acknowledges financial support via the Cusanuswerk scholarship programme (Germany). Work in the GF lab is supported by grants from the Deutsche Forschungsgemeinschaft (DFG, Germany; grant FR3673/1-2), the ERA-SynBio programme via the Federal Ministry of Education and Research (Germany; grant 031L0010B) and the LOEWE programme of the State of Hesse (Germany). Work in the SG lab is supported by a grant from the Biotechnology and Biological Sciences Research Council (BBSRC, UK; grant BB/M029255/1).

### References

- de Almeida, L.G., Ortiz, J.H., Schneider, R.P., and Spira, B. (2015) *phoU* inactivation in *Pseudomonas aeruginosa* enhances accumulation of ppGpp and polyphosphate. *Appl Environ Microbiol* **81**: 3006–3015.
- Antoine, R., Jacob-Dubuisson, F., Drobecq, H., Willery, E., Lesjean, S., and Loch, C. (2003) Overrepresentation of a gene family encoding extracytoplasmic solute receptors in *Bordetella*. *J Bacteriol* **185**: 1470–1474.
- Antoine, R., Huvent, I., Chemlal, K., Deray, I., Raze, D., Loch, C., and Jacob-Dubuisson, F. (2005) The



- periplasmic binding protein of a tripartite tricarboxylate transporter is involved in signal transduction. *J Mol Biol* **351**: 799–809.
- Boos, W., and Shuman, H. (1998) Maltose/maltodextrin system of *Escherichia coli*: transport, metabolism, and regulation. *Microbiol Mol Biol Rev* **62**: 204–229.
- Breukink, E., and de Kruijff, B. (2006) Lipid II as a target for antibiotics. *Nat Rev Drug Discov* **5**: 321–323.
- Buchner, S., Schlundt, A., Lassak, J., Sattler, M., and Jung, K. (2015) Structural and functional analysis of the signal-transducing linker in the pH-responsive one-component system CadC of *Escherichia coli*. *J Mol Biol* **427**: 2548–2561.
- Chapon, C. (1982) Role of the catabolite activator protein in the maltose regulon of *Escherichia coli*. *J Bacteriol* **150**: 722–729.
- Cox, G.B., Webb, D., and Rosenberg, H. (1989) Specific amino acid residues in both the PstB and PstC proteins are required for phosphate transport by the *Escherichia coli* Pst system. *J Bacteriol* **171**: 1531–1534.
- Daruwalla, K.R., Paxton, A.T., and Henderson, P.J. (1981) Energization of the transport systems for arabinose and comparison with galactose transport in *Escherichia coli*. *Biochem J* **200**: 611–627.
- Debarbouille, M., and Schwartz, M. (1979) The use of gene fusions to study the expression of *malT* the positive regulator gene of the maltose regulon. *J Mol Biol* **132**: 521–534.
- Decker, K., Plumbridge, J., and Boos, W. (1998) Negative transcriptional regulation of a positive regulator: the expression of *malT*, encoding the transcriptional activator of the maltose regulon of *Escherichia coli*, is negatively controlled by Mlc. *Mol Microbiol* **27**: 381–390.
- Dintner, S., Staroń, A., Berchtold, E., Petri, T., Mascher, T., and Gebhard, S. (2011) Coevolution of ABC transporters and two-component regulatory systems as resistance modules against antimicrobial peptides in Firmicutes bacteria. *J Bacteriol* **193**: 3851–3862.
- Dintner, S., Heermann, R., Fang, C., Jung, K., and Gebhard, S. (2014) A sensory complex consisting of an ATP-binding cassette transporter and a two-component regulatory system controls bacitracin resistance in *Bacillus subtilis*. *J Biol Chem* **289**: 27899–27910.
- Economou, N.J., Cocklin, S., and Loll, P.J. (2013) High-resolution crystal structure reveals molecular details of target recognition by bacitracin. *Proc Natl Acad Sci USA* **110**: 14207–14212.
- Ehrmann, M., and Boos, W. (1987) Identification of endogenous inducers of the *mal* regulon in *Escherichia coli*. *J Bacteriol* **169**: 3539–3545.
- Eichinger, A., Haneburger, I., Koller, C., Jung, K., and Skerra, A. (2011) Crystal structure of the sensory domain of *Escherichia coli* CadC, a member of the ToxR-like protein family. *Protein Sci* **20**: 656–669.
- Falord, M., Karimova, G., Hiron, A., and Msadek, T. (2012) GraXSR proteins interact with the VraFG ABC transporter to form a five-component system required for cationic antimicrobial peptide sensing and resistance in *Staphylococcus aureus*. *Antimicrob Agents Chemother* **56**: 1047–1058.
- Foster, J.W. (2004) *Escherichia coli* acid resistance: tales of an amateur acidophile. *Nat Rev Microbiol* **2**: 898–907.
- Fritz, G., Buchler, N.E., Hwa, T., and Gerland, U. (2007) Designing sequential transcription logic: a simple genetic circuit for conditional memory. *Syst Synth Biol* **1**: 89–98.
- Fritz, G., Koller, C., Burdack, K., Tetsch, L., Haneburger, I., Jung, K., and Gerland, U. (2009) Induction kinetics of a conditional pH stress response system in *Escherichia coli*. *J Mol Biol* **393**: 272–286.
- Fritz, G., Megerle, J.A., Westermayer, S.A., Brick, D., Heermann, R., Jung, K., et al. (2014) Single cell kinetics of phenotypic switching in the arabinose utilization system of *E. coli*. *PLoS One* **9**: e89532.
- Fritz, G., Dintner, S., Treichel, N.S., Radeck, J., Gerland, U., Mascher, T., and Gebhard, S. (2015) A new way of sensing: need-based activation of antibiotic resistance by a flux-sensing mechanism. *mBio* **6**: e00975–e00915.
- Gardner, S.G., Johns, K.D., Tanner, R., and McCleary, W.R. (2014) The PhoU protein from *Escherichia coli* interacts with PhoR, PstB, and metals to form a phosphate-signaling complex at the membrane. *J Bacteriol* **196**: 1741–1752.
- Gardner, S.G., Miller, J.B., Dean, T., Robinson, T., Erickson, M., Ridge, P.G., and McCleary, W.R. (2015) Genetic analysis, structural modeling, and direct coupling analysis suggest a mechanism for phosphate signaling in *Escherichia coli*. *BMC Genet* **16**: S2.
- Gebhard, S. (2012) ABC transporters of antimicrobial peptides in Firmicutes bacteria—phylogeny, function and regulation. *Mol Microbiol* **86**: 1295–1317.
- Gebhard, S., and Cook, G.M. (2008) Differential regulation of high-affinity phosphate transport systems of *Mycobacterium smegmatis*: identification of PhnF, a repressor of the *phnDCE* operon. *J Bacteriol* **190**: 1335–1343.
- Gebhard, S., and Mascher, T. (2011) Antimicrobial peptide sensing and detoxification modules: unravelling the regulatory circuitry of *Staphylococcus aureus*. *Mol Microbiol* **81**: 581–587.
- Gebhard, S., Fang, C., Shaaly, A., Leslie, D.J., Weimar, M.R., Kalamorz, F., et al. (2014) Identification and characterisation of a bacitracin resistance network in *Enterococcus faecalis*. *Antimicrob Agents Chemother* **58**: 1425–1433.
- Haneburger, I., Fritz, G., Jurkschat, N., Tetsch, L., Eichinger, A., Skerra, A., et al. (2012) Deactivation of the *E. coli* pH stress sensor CadC by cadaverine. *J Mol Biol* **424**: 15–27.
- Hazelbauer, G.L. (1975) Maltose chemoreceptor of *Escherichia coli*. *J Bacteriol* **122**: 206–214.
- Hiron, A., Falord, M., Valle, J., Débarbouillé, M., and Msadek, T. (2011) Bacitracin and nisin resistance in *Staphylococcus aureus*: a novel pathway involving the BraS/BraR two-component system (SA2417/SA2418) and both the BraD/BraE and VraD/VraE ABC transporters. *Mol Microbiol* **81**: 602–622.
- Hoffer, S.M., Westerhoff, H.V., Hellingwerf, K.J., Postma, P.W., and Tommassen, J. (2001) Autoamplification of a two-component regulatory system results in “learning” behavior. *J Bacteriol* **183**: 4914–4917.
- Hofnung, M. (1974) Divergent operons and the genetic structure of the maltose B region in *Escherichia coli* K12. *Genetics* **76**: 169–184.

- Hofnung, M., Hatfield, D., and Schwartz, M. (1974) *malB* Region in *Escherichia coli* K-12: characterization of New Mutations. *J Bacteriol* **117**: 40–47.
- Hsieh, Y.J., and Wanner, B.L. (2010) Global regulation by the seven-component P<sub>i</sub> signaling system. *Curr Opin Microbiol* **13**: 198–203.
- Hu, X., Zhao, J., DeGrado, W.F., and Binns, A.N. (2013) *Agrobacterium tumefaciens* recognizes its host environment using ChvE to bind diverse plant sugars as virulence signals. *Proc Natl Acad Sci USA* **110**: 678–683.
- Island, M.D., and Kadner, R.J. (1993) Interplay between the membrane-associated UhpB and UhpC regulatory proteins. *J Bacteriol* **175**: 5028–5034.
- Joly, N., Bohm, A., Boos, W., and Richet, E. (2004) MalK, the ATP-binding cassette component of the *Escherichia coli* maltodextrin transporter, inhibits the transcriptional activator MalT by antagonizing inducer binding. *J Biol Chem* **279**: 33123–33130.
- Joseph, P., Fichant, G., Quentin, Y., and Denizot, F. (2002) Regulatory relationship of two-component and ABC transport systems and clustering of their genes in the *Bacillus/Clostridium* group, suggest a functional link between them. *J Mol Microbiol Biotechnol* **4**: 503–513.
- Kallenberg, F., Dintner, S., Schmitz, R., and Gebhard, S. (2013) Identification of regions important for resistance and signalling within the antimicrobial peptide transporter BceAB of *Bacillus subtilis*. *J Bacteriol* **195**: 3287–3297.
- Kay, W.W., and Kornberg, H.L. (1971) The uptake of C<sub>4</sub>-dicarboxylic acids by *Escherichia coli*. *Eur J Biochem* **18**: 274–281.
- Kleefeld, A., Ackermann, B., Bauer, J., Krämer, J., and Unden, G. (2009) The fumarate/succinate antiporter DcuB of *Escherichia coli* is a bifunctional protein with sites for regulation of DcuS-dependent gene expression. *J Biol Chem* **284**: 265–275.
- Kneuper, H., Janausch, I.G., Vijayan, V., Zweckstetter, M., Bock, V., Griesinger, C., and Unden, G. (2005) The nature of the stimulus and of the fumarate binding site of the fumarate sensor DcuS of *Escherichia coli*. *J Biol Chem* **280**: 20596–20603.
- Kuper, C., and Jung, K. (2005) CadC-mediated activation of the *cadBA* promoter in *Escherichia coli*. *J Mol Microbiol Biotechnol* **10**: 26–39.
- Lambert, G., Kussell, E., and Kussel, E. (2014) Memory and fitness optimization of bacteria under fluctuating environments. *PLoS Genet* **10**: e1004556.
- Lubin, E.A., Henry, J.T., Fiebig, A., Crosson, S., and Laub, M.T. (2016) Identification of the PhoB regulon and role of PhoU in the phosphate starvation response of *Caulobacter crescentus*. *J Bacteriol* **198**: 187–200.
- Megerle, J.A., Fritz, G., Gerland, U., Jung, K., and Rädler, J.O. (2008) Timing and dynamics of single cell gene expression in the arabinose utilization system. *Biophys J* **95**: 2103–2115.
- Meng, S.Y., and Bennett, G.N. (1992) Regulation of the *Escherichia coli cad* operon: location of a site required for acid induction. *J Bacteriol* **174**: 2670–2678.
- Monzel, C., and Unden, G. (2015) Transmembrane signaling in the sensor kinase DcuS of *Escherichia coli*: a long-range piston-type displacement of transmembrane helix 2. *Proc Natl Acad Sci USA* **112**: 11042–11047.
- Müller-Hill, B. (1996) *The Lac Operon*. Berlin: Walter de Gruyter.
- Neely, M.N., and Olson, E.R. (1996) Kinetics of expression of the *Escherichia coli cad* operon as a function of pH and lysine. *J Bacteriol* **178**: 5522–5528.
- Neely, M.N., Dell, C.L., and Olson, E.R. (1994) Roles of LysP and CadC in mediating the lysine requirement for acid induction of the *Escherichia coli cad* operon. *J Bacteriol* **176**: 3278–3285.
- Ohki, R., Giyanto, Tateno, K., Masuyama, W., Moriya, S., Kobayashi, K., and Ogasawara, N. (2003) The BceRS two-component regulatory system induces expression of the bacitracin transporter, BceAB, in *Bacillus subtilis*. *Mol Microbiol* **49**: 1135–1144.
- Okuda, K., Aso, Y., Nakayama, J., and Sonomoto, K. (2008) Cooperative transport between NukFEG and NukH in immunity against the lantibiotic nukacin ISK-1 produced by *Staphylococcus warneri* ISK-1. *J Bacteriol* **190**: 356–362.
- Ozbudak, E.M., Thattai, M., Lim, H.N., Shraiman, B.I., and Van Oudenaarden, A. (2004) Multistability in the lactose utilization network of *Escherichia coli*. *Nature* **427**: 737–740.
- Padan, E. (2009) Bacterial membrane transport: superfamilies of transport proteins. In *Encyclopedia of Life Sciences (ELS)*. Chichester: John Wiley & Sons.
- Panagiotidis, C.H., Boos, W., and Shuman, H.A. (1998) The ATP-binding cassette subunit of the maltose transporter MalK antagonizes MalT, the activator of the *Escherichia coli mal* regulon. *Mol Microbiol* **30**: 535–546.
- Popkin, P.S., and Maas, W.K. (1980) *Escherichia coli* regulatory mutation affecting lysine transport and lysine decarboxylase. *J Bacteriol* **141**: 485–492.
- Qi, Y., Kobayashi, Y., and Hulett, F.M. (1997) The *pst* operon of *Bacillus subtilis* has a phosphate-regulated promoter and is involved in phosphate transport but not in regulation of the *pho* regulon. *J Bacteriol* **179**: 2534–2539.
- Raibaud, O., and Richet, E. (1987) Maltotriose is the inducer of the maltose regulon of *Escherichia coli*. *J Bacteriol* **169**: 3059–3061.
- Rauschmeier, M., Schüppel, V., Tetsch, L., and Jung, K. (2014) New insights into the interplay between the lysine transporter LysP and the pH sensor CadC in *Escherichia coli*. *J Mol Biol* **426**: 215–229.
- Revilla-Guarinos, A., Gebhard, S., Alcántara, C., Staroń, A., Mascher, T., and Zúñiga, M. (2013) Characterization of a regulatory network of peptide antibiotic detoxification modules in *Lactobacillus casei* BL23. *Appl Environ Microbiol* **79**: 3160–3170.
- Revilla-Guarinos, A., Gebhard, S., Mascher, T., and Zúñiga, M. (2014) Defence against antimicrobial peptides: different strategies in Firmicutes. *Environ Microbiol* **16**: 1225–1237.
- Rice, C.D., Pollard, J.E., Lewis, Z.T., and McCleary, W.R. (2009) Employment of a promoter-swapping technique shows that PhoU modulates the activity of the PstSCAB<sub>2</sub> ABC transporter in *Escherichia coli*. *Appl Environ Microbiol* **75**: 573–582.

- Rietkötter, E., Hoyer, D., and Mascher, T. (2008) Bacitracin sensing in *Bacillus subtilis*. *Mol Microbiol* **68**: 768–785.
- Scheu, P.D., Witan, J., Rauschmeier, M., Graf, S., Liao, Y.F., Ebert-Jung, A., *et al.* (2012) CitA/CitB two-component system regulating citrate fermentation in *Escherichia coli* and its relation to the DcuS/DcuR system *in vivo*. *J Bacteriol* **194**: 636–645.
- Schleif, R. (2000) Regulation of the L-arabinose operon of *Escherichia coli*. *Trends Genet* **16**: 559–565.
- Schreiber, V., Steegborn, C., Clausen, T., Boos, W., and Richet, E. (2000) A new mechanism for the control of a prokaryotic transcriptional regulator: antagonistic binding of positive and negative effectors. *Mol Microbiol* **35**: 765–776.
- Schwöppe, C., Winkler, H.H., and Neuhaus, H.E. (2003) Connection of transport and sensing by UhpC, the sensor for external glucose-6-phosphate in *Escherichia coli*. *Eur J Biochem* **270**: 1450–1457.
- Stein, T., Heinzmann, S., Solovieva, I., and Entian, K.D. (2003) Function of *Lactococcus lactis* nisin immunity genes *nisl* and *nisFEG* after coordinated expression in the surrogate host *Bacillus subtilis*. *J Biol Chem* **278**: 89–94.
- Steinmetz, P.A., Wörner, S., and Unden, G. (2014) Differentiation of DctA and DcuS function in the DctA/DcuS sensor complex of *Escherichia coli*: function of DctA as an activity switch and of DcuS as the C<sub>4</sub>-dicarboxylate sensor. *Mol Microbiol* **94**: 218–229.
- Tetsch, L., and Jung, K. (2009) The regulatory interplay between membrane-integrated sensors and transport proteins in bacteria. *Mol Microbiol* **73**: 982–991.
- Tetsch, L., Koller, C., Haneburger, I., and Jung, K. (2008) The membrane-integrated transcriptional activator CadC of *Escherichia coli* senses lysine indirectly via the interaction with the lysine permease LysP. *Mol Microbiol* **67**: 570–583.
- Tetsch, L., Koller, C., Dönhöfer, A., and Jung, K. (2011) Detection and function of an intramolecular disulfide bond in the pH-responsive CadC of *Escherichia coli*. *BMC Microbiol* **11**: 74.
- Unden, G., Wörner, S., and Monzel, C. (2016) Cooperation of secondary transporters and sensor kinases in transmembrane signalling: the DctA/DcuS and DcuB/DcuS sensor complexes of *Escherichia coli*. *Adv Microb Physiol* **68**: 139–167.
- van Veen, H.W. (1997) Phosphate transport in prokaryotes: molecules, mediators and mechanisms. *Antonie Van Leeuwenhoek* **72**: 299–315.
- Veening, J.W., Smits, W.K., and Kuipers, O.P. (2008) Bistability, epigenetics, and bet-hedging in bacteria. *Annu Rev Microbiol* **62**: 193–210.
- Wang, B., Dukarevich, M., Sun, E.I., Yen, M.R., and Saier, M.H. (2009) Membrane porters of ATP-binding cassette transport systems are polyphyletic. *J Membrane Biol* **231**: 1–10.
- Wanner, B.L. (1993) Gene regulation by phosphate in enteric bacteria. *J Cell Biochem* **51**: 47–54.
- Widenhorn, K.A., Somers, J.M., and Kay, W.W. (1989) Genetic regulation of the tricarboxylate transport operon (*tctI*) of *Salmonella typhimurium*. *J Bacteriol* **171**: 4436–4441.
- Winnen, B., Hvorup, R.N., and Saier, M.H. (2003) The tripartite tricarboxylate transporter (TTT) family. *Res Microbiol* **154**: 457–465.
- Witan, J., Bauer, J., Wittig, I., Steinmetz, P.A., Erker, W., and Unden, G. (2012) Interaction of the *Escherichia coli* transporter DctA with the sensor kinase DcuS: presence of functional DctA/DcuS sensor units. *Mol Microbiol* **85**: 846–861.
- Wörner, S., Strecker, A., Monzel, C., Zeltner, M., Witan, J., Ebert-Jung, A., and Unden, G. (2016) Conversion of the sensor kinase DcuS of *Escherichia coli* of the DcuB/DcuS sensor complex to the C<sub>4</sub>-dicarboxylate responsive form by the transporter DcuB. *Environ Microbiol* **18**: 4920–4930.
- Yuan, Z.C., Zaheer, R., and Finan, T.M. (2006) Regulation and properties of PstSCAB, a high-affinity, high-velocity phosphate transport system of *Sinorhizobium meliloti*. *J Bacteriol* **188**: 1089–1102.
- Zhang, Y., Gardina, P.J., Kuebler, A.S., Kang, H.S., Christopher, J.A., and Manson, M.D. (1999) Model of maltose-binding protein/chemoreceptor complex supports intrasubunit signaling mechanism. *Proc Natl Acad Sci USA* **96**: 939–944.

## Acknowledgements

An dieser Stelle möchte ich ein paar Menschen danken, ohne deren Unterstützung diese Dissertation nicht möglich gewesen wäre.

Zunächst geht mein Dank an Dr. Georg Fritz, der mir die Möglichkeit zum Quereinstieg in die Wissenschaft gegeben hat. Ich danke dir, dass ich in meiner Zeit in deiner Gruppe an vielen spannenden und aktuellen Fragenstellungen arbeiten durfte und dabei meine beiden Interessensgebiete, die Biologie und die Mathematik, miteinander verbinden konnte. Danke für die zahlreichen (teilweise stundenlangen) interessanten Diskussionen, dein stetiges Interesse an meiner Arbeit und die Unterstützung, die ich von dir erfahren habe. Deine Bürotür hat mir immer offen gestanden! Ich wünsche dir und deiner Familie einen guten Start in Perth!

Prof. Dr. Torsten Waldminghaus danke ich für die Übernahme des Zweitgutachtens. Weiterhin möchte ich den restlichen Mitgliedern meines Prüfungskomitees, Prof. Dr. Peter Lenz und Prof. Dr. Martin Thanbichler meinen Dank aussprechen.

Mein Dank gilt außerdem unseren Kollaborationspartnern Prof. Dr. Julia Frunzke und Dr. Marc Keppel für die fruchtbare Zusammenarbeit.

Weiter möchte ich an dieser Stelle allen derzeitigen und ehemaligen Mitgliedern der AG Fritz danken. Jede/Jeder von euch hat auf ihre/seine eigene Art dazu beigetragen, dass ich mich in der Arbeitsgruppe immer wohlfühlt habe und ich bin euch sehr dankbar für die vielen schönen Stunden im Büro.

Für die kritische Durchsicht dieser Arbeit danke ich Andre Sim, Anna Faber und Frau Dr. Julia Foerster.

Ich möchte mich an dieser Stelle auch bei dem Cusanuswerk bedanken, welches meine Promotion finanziell gefördert und meine Promotionszeit durch zahlreiche Bildungsangebote sehr bereichert hat.

Ein besonderer Dank gilt meiner Familie. Ich danke meinen Eltern Hedwig und Bernd und meinen Schwestern Sarah und Louisa. Danke für euren stetigen Zuspruch und dafür, dass ihr immer ein offenes Ohr für mich hattet, wenn ich am Zweifeln war. Ihr habt stets die richtigen Worte gefunden, die mir das Vertrauen in mich selbst zurückgegeben haben. Eure bedingungslose Unterstützung während meiner Promotion, aber vor allen Dingen auch mein ganzes Leben hindurch, ermöglicht es mir, meinen Weg zu gehen und dafür bin ich euch unbeschreiblich dankbar!

Mein letzter und ebenso besonderer Dank geht an Christian. Danke für jedes aufmunternde Wort in den letzten 3,5 Jahren, für deine grenzenlose Zuversicht, für deine Geduld und Rücksichtnahme in stressigen Zeiten, und dafür, dass du mich auch in den schwierigsten Phasen immer wieder zum Lachen bringst. Du hast immer an mich geglaubt und nie daran gezweifelt, dass ich es schaffen werde. Mit dir unsere gemeinsame Zukunft zu planen hat mir viel Kraft für die Gegenwart gegeben und mich motiviert, nicht aufzugeben. Ich bin sehr dankbar, dich an meiner Seite zu haben!

# Eidesstattliche Erklärung

Hiermit erkläre ich, dass die vorliegende Dissertation:

**„Regulatory Mechanisms of Bacterial Stress Responses“**

von mir selbstständig und ohne unerlaubte Hilfsmittel angefertigt wurde. Es wurden keine anderen als die von mir angegebenen Quellen verwendet.

Zudem versichere ich, dass die Dissertation in dieser oder ähnlicher Form noch bei keiner anderen Hochschule eingereicht wurde.

Marburg, den

---

Hannah Piepenbreier